**Brain Connectivity Modeling in Soldiers with Mild-Traumatic Brain Injury
and Posttraumatic Stress Disorder**

by

Rangaprakash Deshpande

A dissertation submitted to the Graduate Faculty of
Auburn University
in partial fulfillment of the
requirements for the Degree of
Doctor of Philosophy

Auburn, Alabama
August 6, 2016

Keywords: Functional Magnetic Resonance Imaging, Functional connectivity, Effective
connectivity, Dynamic connectivity, Complex network modeling, Hemodynamic variability

Approved by

Thomas S. Denney Jr., Committee Chair, Director, Auburn University MRI Research Center
Stanley J. Reeves, Professor, Dept. of Electrical and Computer Engineering, Auburn University
Jeffrey S. Katz, Alumni Professor, Department of Psychology, Auburn University
Jennifer L. Robinson, Assistant Professor, Department of Psychology, Auburn University

Abstract

Functional magnetic resonance imaging (fMRI) has been increasingly used for understanding cognitive processes in both healthy and clinical populations. In this work, we employed various computational approaches in studying brain alterations in U.S. Army soldiers with posttraumatic stress disorder (PTSD) and mild-traumatic brain injury (mTBI). PTSD and mTBI share largely similar symptoms, and have high comorbidity in military populations, with 7% of war veterans acquiring both disorders. Despite such high prevalence, the neural underpinnings of PTSD as well as comorbid PTSD and mTBI remain poorly understood. We employ multiple approaches, including functional connectivity (FC) modeling, effective connectivity (EC) modeling and complex network analysis, to investigate brain disruptions in these disorders. Notably, we used dynamic connectivity in all our analyses for characterizing variability of connectivity over time, in addition to traditionally used static connectivity measures.

Using resting-state fMRI, we first employed static and time-varying FC to identify significantly altered co-activation patterns which exhibit temporally "frozen" hyper-connected profile in the disorders. Using whole-brain connectivity in a data-driven manner without the imposition of any priors or assumptions, we identified only the hippocampus-striatum path to be significantly altered in the disorders, which likely represents habit-like response associated with traumatic memories. This path also had high behavioral relevance. Using machine learning classification, we showed that this path is a potential imaging biomarker of PTSD and mTBI.

Next, we performed EC analysis using Granger causality for identifying sources of network disturbances in PTSD and mTBI. Causality, or directional connectivity quantified using EC, is characteristically different from co-activation or FC. While EC gives connections between regions, the source of disruption should be a region, not connection. We thus employed a probabilistic framework to identify the source region(s) of disruption using a novel framework. We found that the middle frontal gyrus is the source of disruptions, whose dysregulation causes overdrive in subcortical regions, leading to heightened emotional response to traumatic memories. The identified paths also had high behavioral relevance and diagnostic ability.

Though the results obtained from EC analyses were informative, we recognized that connectivity modeling of individual paths does not capture alterations in network architecture which are critical for producing complex behaviors. We thus employed complex network analysis to study network-level alterations in the disorders using EC networks. We studied specialized processing (segregation) and efficient communication (integration), as well as their variability using time-varying network dynamics technique developed by us. We identified network-level markers which help in distinguishing between PTSD and comorbid conditions, a vexed problem whose solution has been elusive in current literature. We found alterations of network architecture in two sub-networks, fronto-visual and fronto-subcortical, with disruption primarily originating in prefrontal areas of cognitive control. Taken together, FC and EC analyses provided novel insights into the underlying network structure, the flow of information and the foci of disruption in these disorders, which might help in developing objective diagnosis and treatments for these disorders.

Next, using fMRI during an emotion regulation task, we studied the network of cognitive emotion regulation in healthy adults and its dysregulation in comorbid PTSD and mTBI. This was important since emotion dysregulation is seen as the major cause of symptoms observed in

disorders like these. We identified activated regions using GLM analysis. We performed EC analysis using the timeseries obtained from the identified regions, which provided the network of emotion regulation and dysregulation while actively engaged in an emotion regulation task as opposed to resting-state.

With all the aforementioned analyses, one aspect which needs mentioning is that fMRI is not a direct measure of neural activity. It measures blood oxygenation which is an indirect measure, hence susceptible to sources of variability which are non-neural in origin. The transfer function between neural activity and fMRI, called the hemodynamic response function (HRF), is known to vary across the brain in the same subject, and across subjects. We obtained the HRF at every voxel using blind deconvolution. We hypothesized that there are group-wise differences in HRF and that they may drive connectivity differences if HRF variability is not removed from the data. We found significant HRF differences between the groups mainly in posterior cingulate, precuneus and secondary visual areas. We performed seed-based connectivity using them, and found that ignoring HRF variability during connectivity analysis leads to possible false positive and false negative connectivities.

In summary, we propose and test a comprehensive mechanistic model of brain alterations in soldiers with PTSD and mTBI, and illustrate the precautions to be followed during fMRI analysis to reliably characterize brain functioning in these disorders. We hope that this work contributes towards the development of effective diagnoses and treatments for PTSD and mTBI. Finally, the tenets of the proposed analyses framework is agnostic and generally applicable for characterizing brain alterations underlying various mental disorders and cognitive domains using neuroimaging.

Acknowledgments

I express deep sense of gratitude towards Dr. Thomas Denney for his guidance and support during the course of this work. He has not only been a source of inspiration and motivation to me but also been instrumental in kindling my interest in conducting scientific research.

I sincerely thank the MRI Center faculty for insightful discussions, invigorating courses and all the technical and moral support provided by them. In particular, I thank Dr. Gopikrishna Deshpande for his exceptional support throughout the work; and also thank Dr. Jeffrey Katz, Dr. Jennifer Robinson and Dr. Stanley Reeves for their unconditional help and support to me both as a student in their courses and outside of it. Their spirit of scientific inquiry and constant belief in my abilities has contributed towards shaping me as a researcher. The freedom of thought and work environment at the MRI Center helped me harvest my humble abilities to develop as a researcher.

I thank my PhD committee members for all their cooperation, support and insightful suggestions towards this work. I thank Auburn University, as well as Dr. Mark Nelms, the Chair of the Department of Electrical and Computer Engineering, and Dr. Thomas Denney, the Director of the AU MRI Research Center for providing world-class facilities for my work. I also thank my friends at the MRI Center and in the Auburn community for their guidance, support and camaraderie throughout my stay. I am deeply indebted to all those who helped me directly and indirectly in successfully completing my work, as well as those who shaped me as an individual throughout my life, without whose help and support this work would not have attained its present form.

I am deeply indebted to my parents, wife, brother and sister-in-law for their constant love, encouragement and support. My doctoral education was made possible through these individuals, without whose all-encompassing support, this work would not have been half of what it is today. I also thank my extended family and my little nephews for shaping my character and keeping my spirits high.

Above all, my gratitude to Almighty God, the Universal Scientist, Engineer and beyond, for His divine grace and blessings towards me in all walks of my life.

Table of Contents

List of Tables

List of Figures

List of Abbreviations

ACC   Anterior Cingulate Cortex

ADF   Augmented Dickey-Fuller test

AG   Angular Gyrus

ALE   Activation Likelihood Estimation

BOLD   Blood Oxygenation Level Dependent signal

CC   Clustering Coefficient

Cd   Cohen's d

CKF-S   Cubature Kalman filter and Smoother

CNS-VS   CNS-Vital Signs®

CPGC   Correlation Purged Granger Causality

CSF   Cerebrospinal Fluid

DC   Dynamic Connectivity

DCM   Dynamic Causal Modeling

DEC   Dynamic Effective Connectivity

DFC   Dynamic Functional Connectivity

DGC   Dynamic Granger Causality

DLPFC   Dorsolateral Prefrontal Cortex

DMN   Default Mode Network

dMVAR   Dynamic Multivariate Vector Autoregressive model

DTI   Diffusion Tensor Imaging

EB   Edge Betweenness

EC   Effective Connectivity

EffLoc   Local Efficiency

EffGlob   Global Efficiency

FC   Functional Connectivity

FDR   False Discovery Rate

fMRI   Functional Magnetic Resonance Imaging

FWHM   Full-Width at Half-Max

GABA   Gamma-Amino Butyric Acid

GC   Granger Causality

GLM   General Linear Model

GSR   Global Mean Signal Regression

HRF   Hemodynamic Response Function

M   Mean

MFG   Middle Frontal Gyrus

MNI   Montreal Neurological Institute atlas

MRI   Magnetic Resonance Imaging

mTBI   Mild-Traumatic Brain Injury

MVAR   Multivariate Vector Autoregressive model

NCI   Neurocognitive Composite Index

NDC   Data pre-processed without deconvolution

NIFC   Neurobiologically-Informed Feature Space

NIM   Non-Imaging Measure

NMDA   N-methyl-D-aspartate

NSI   Neurobehavioral Symptom Inventory

OFC   Orbito-Frontal Cortex

PCC   Posterior Cingulate Cortex

PCL5   PTSD Checklist-5 score

PCS   Post-Concussion Syndrome

PCS+PTSDComorbid PCS and PTSD (subjects with both these disorders)

PLSR   Partial Least Squares Regression

PTSD   Posttraumatic Stress Disorder

R   Correlation value

RCE   Recursive Cluster Elimination

RCE-SVM Recursive Cluster Elimination based Support Vector Machine classifier

RDoC   Research Domain Criteria

RH   Response Height

ROI   Region of Interest

RS-fMRI   Resting-State fMRI

rTMS   Repetitive Transcranial Magnetic Stimulation

SD   Standard Deviation

SEC   Static Effective Connectivity

SFC   Static Functional Connectivity

SMA   Supplementary Motor Area

SPL   Shortest Path Length

CHAPTER 1

Introduction

1.1. Motivation

Military service members put their lives at risk to protect their country. Unfortunately, a large percentage of those who return from wars develop brain-related complications, since they are constantly exposed to life-threatening circumstances and explosions. They often develop posttraumatic stress disorder (PTSD), a consequence of psychological trauma, and mild-traumatic brain injury (mTBI), a consequence of physical trauma to the head. In the U.S. alone, more than 2.7 million soldiers served in Iraq and Afghanistan, with about 20% acquiring PTSD, 19% acquiring mTBI and 7% acquiring both [1]. As of today, a thorough mechanistic understanding of their underlying brain mechanisms has not emerged, amid considerable efforts in that direction over the years. We attempt to advance human knowledge in this direction.

PTSD is characterized by high anxiety, re-experiencing traumatic memories, hypervigilance and hyperarousal. In combat veterans, PTSD has high co-morbidity with mTBI [2, 3] due to the risk of being exposed to improvised-explosive-devices (IEDs) and non-blast events. Significant percentage of those who sustain mTBI suffer chronic symptoms or post-concussion syndrome (PCS) [4]. With current diagnostic procedures and treatments centering on subjective assessments, a thorough understanding of the mechanistic basis for PTSD and PCS is essential for accurate diagnosis, targeted treatment and for making return-to-duty decisions. Due to largely overlapping symptomatology between PTSD and PCS [5], it is necessary to identify and validate objective

markers of the respective neurologic and neuropsychiatric conditions to improve clinical evaluation and, ultimately, treatment outcomes. In this work, we take a step in that direction.

There are several possible choices of modalities in studying brain functioning. Positron emission tomography (PET), functional magnetic resonance imaging (fMRI), functional near infrared spectroscopy (FNIRS), electroencephalogram (EEG) and magnetoencephalogram (MEG) are the most predominant modalities used to obtain brain signals. Among them, we use fMRI which provides the optimal tradeoff between spatial and temporal resolution with minimal risk to the subjects.

There are several ways in which fMRI can be used to infer brain functioning. In the design of the experiments itself, data can be obtained with subjects being in "resting-state", wherein they are asked to keep their eyes open, let their thoughts wander and lie still in the scanner. It is now established that the resting state of the brain acts as a baseline state, which influences the performance and outcome when the individual engages in tasks [6]. The pattern of brain activity during rest largely resembles the pattern of activity when the individual performs tasks. For this reason, resting-state fMRI (RS-fMRI) has gained enormous momentum in the past decade. RS-fMRI is not task dependent, hence free of variability in task performance across subjects. Additionally, RS-fMRI findings are not stereotypical to any particular task, hence they have better generalizability. An alternate approach is to have the subjects perform certain tasks inside the MRI scanner, which are carefully designed controlled experiments aimed at capturing certain specific mental processes. Task fMRI (T-fMRI) thus provides information on brain functioning when the particular task of interest is being performed, and hence is highly informative as well as highly stereotypical to the task under consideration. In this work, we employ RS-fMRI to discover

baseline alterations in soldiers with PTSD and mTBI, as well as T-fMRI to discover specific alterations during an emotion regulation task.

Two approaches are popular in fMRI data processing: activation analysis and connectivity analysis. Activation analysis aims at identifying brain regions which are "activated" or utilized while a particular task is performed, as compared to a baseline condition. It provides information on specific brain regions required for specific processes associated with the task under consideration. However, brain's functioning relies on communication between regions and not the isolated activation of the regions themselves. Its power lies in its interconnectedness. Connectivity analysis aims to model interrelationship between brain regions. In this work, we employed various connectivity techniques in understanding brain networks associated with PTSD and mTBI.

Interrelationship between brain regions is thought to be of two types: co-activation and causality. Co-activation refers to simultaneous activity of two brain regions, which indicates that both the regions under consideration are acting together to enable certain cognitive process. Co-activation is modeled using functional connectivity (FC) [6]. Causality, on the other hand, refers to "cause-effect" relationship between two regions, with one region being the source/cause and the other being the destination/effect. It indicates that brain activity changes in one regions is, in effect, causing altered activity in another region. It is modeled using effective connectivity (EC) [7]. FC and EC provide fundamentally different information on interrelationships in the brain. In this work we employ both FC and EC to understand brain network alterations in PTSD and mTBI.

While connectivity provides valuable information not available through activation analysis, connectivity findings are harder to interpret since our understanding of brain functioning is based on brain regions, and not connections. Hence it would be useful to identify altered regions in the disorders using connectivity data. Moreover, we recognize that most abnormalities in natural

3

systems are characterized by certain source(s), and that identifying and rectifying such source(s) could automatically rectify rest of the abnormal effects. Hence we sought to identify the source(s) of the disorders from EC networks. We employed a novel probabilistic framework to identify such disease foci.

As noted earlier, FC and EC model the interrelationship between two brain regions. This formulation is in itself imperfect, because brain operates through simultaneous interrelationship between all the regions, not just pairs of them. So, finding pairwise connectivity, as done in FC and EC, leads to an inadequate and incomplete representation of the ground-truth, wherein the importance of a particular connection in relation to the rest of the connections is ignored. It is thus imperative to study the brain as an ensemble of connections, instead of bivariate connections assessed separately. Similarly it is important to study an ensemble of nodes/regions, instead of studying aggregate connectivity profile of each node/region in isolation. To this effect, we employ complex network analysis using graph-theoretic techniques [8] to study network-level directional connectivity alterations in PTSD and mTBI. At the network-level (meaning ensemble of connections), functional segregation is a property which quantifies the ability for specialized local processing to occur in densely connected sub-networks, while functional integration quantifies the ability for efficient communication between such segregated sub-networks. It is now established that an optimal balance between segregation and integration is a characteristic of the healthy brain [8]. We study alterations in network segregation and integration in PTSD and mTBI.

Traditionally, FC and EC analysis implicitly refers to static measures of connectivity, wherein one single connectivity value is computed for the entire lengths of the timeseries. However, such a formulation seems intuitively incomplete, because the state of the brain is changing every moment, the subjects are changing every moment, and so are the mental processes. It seems

4

impossible that the brain remains in the same state for the entire duration of the scan, which typically lasts for several minutes. Dynamic connectivity (DC) captures the time-varying nature of connectivity. In DC, connectivity is continuously evaluated over time, thus giving a series of connectivity values over time. Temporal variability of connectivity can be derived from DC. Surprisingly, DC is yet to be extensively used in fMRI. There have been no works on PTSD or mTBI which have employed DC. In this work, we employed both static and dynamic FC and EC in novel frameworks, which provides unique characterizations not seen before in literature.

Having identified baseline alterations in PTSD and mTBI using FC and EC, it would be beneficial to model brain network alterations while a specific task is being performed. Given that emotion dysregulation is seen as one of the prime causes of several symptoms in PTSD and mTBI [9], we studied the brain network of altered emotion regulation in healthy adults and its dysregulation in comorbid PTSD and mTBI using effective connectivity.

A key aspect which cannot be ignored in all these analyses is that fMRI is not a direct measure of neural activity. When there is neural activity in a particular locality, the increased metabolism causes demand for oxygen, which results in increased local blood flow in the capillaries, which is captured by fMRI. Hence, all processes which happen between the firing neurons and the hemoglobin in the blood could cause changes in the fMRI signal which do not correspond to neural activity. This transfer function is called the hemodynamic response function (HRF). The HRF is known to vary across different brain regions in the same subject, and also vary across subjects [10]. Thus, HRF variability could cause connectivity differences between subjects, as well as between groups. One way to overcome the issue, at least in part, is to perform deconvolution on fMRI data to obtain latent neural signals. Deconvolution typically involves estimating the underlying HRF and then performing using it to obtain the neural signal. In this work, we

performed deconvolution to remove HRF variability, thus minimizing its impact on the data. Lastly, we sought to identify brain regions which showed HRF differences between the disorder groups and healthy controls. The motivation was to identify the regions showing altered HRF in the disorders, so that fMRI studies could exercise caution while interpreting their results if HRF variability is not removed. Additionally we found that such HRF alterations lead to possible false positives and false negatives in connectivity findings if HRF variability is not removed from the data.

In summary, we study alterations in co-activation and causality networks in the brains of soldiers with PTSD and mTBI, which might provide novel characterizations that could enhance clinical diagnosis and treatment. Ultimately, it could improve the lives of those who give their lives for their country.

1.2. This Work in Relation to Prior Literature

There has been considerable progress towards understanding the brain mechanisms of PTSD and mTBI. Several activation studies and subsequent meta-analyses have identified key cortical and subcortical areas as being involved in these disorders [11, 12, 13], which largely overlapped with the regions identified in this work. Several connectivity studies have also inconsistently identified certain connections to be affected in the disorders [14, 15, 16]. However, a comprehensive understanding of the underlying network structure, their causal relationships and information flow has not emerged from the studies. The findings have been inconsistent to some extent, and a mechanistic understanding of the underlying disruption leading to the symptoms has not emerged. We attempt to fill that gap in this work.

Additionally none of the prior studies have utilized dynamic connectivity information in characterizing these disorders. Dynamic connectivity has been shown to carry behaviorally more relevant information than static connectivity, and is also shown to have better predictive ability than static connectivity [17]. That being the case, we feel that our analysis has a distinct novelty over prior works.

It is also surprising that there have not been any studies which have utilized effective connectivity (EC) modeling to understand PTSD or mTBI. Given that these disorders are primarily seen as frontal dysregulation disorders, EC is ideally suited to characterize the underlying causal relationships arising in the prefrontal cortex and targeted towards subcortical and parietal regions, causing dysregulation. With the combination of EC and dynamic connectivity in novel frameworks, we believe that our work provides unique insights into the brain alterations in PTSD and mTBI not available till now in literature.

While the brain regions involved in cognitive emotion regulation have been studied [18], the interrelationship between them and their network structure has not been identified. Emotion regulation is key to several cognitive control processes, and emotion dysregulation is thus common to several important disorders. Prior works have speculated on the network of emotion regulation and proposed hypothetical networks [18], but none of them have been proved with evidence. We intend to identify the network of cognitive emotion regulation and dysregulation, and contribute to the field in that direction.

While progress has been made towards understanding HRF variability in fMRI and its impact on data analysis [10], there have been no prior works which have studied group differences in HRF variability and its impact on connectivity modeling. Additionally, HRF variability in PTSD or mTBI have not been studied. We attempt to contribute in this direction. In summary, we contribute

along multiple dimensions towards both computational modeling approaches and in the understanding of PTSD and mTBI in this work.

1.3. Organization of the Dissertation

The dissertation is organized as follows. Chapter 2 describes certain general methods which are common to the rest of the chapters, including data acquisition and pre-processing. Chapters 3 to 7 present work on each of the distinct topics. Each chapter begins with an introduction which described the motivation for that work and the hypotheses, followed by methods specific to that chapter, results and discussion. Chapter 3 presents functional connectivity analysis, Chapter 4 presents the identification of disease foci from effective connectivity, Chapter 5 presents complex network analysis using effective connectivity networks and Chapter 6 presents HRF variability and its impact on connectivity modeling. Chapters 3-6 deal with connectivity modeling of resting-state data. We found that networks involved in emotion regulation were impaired. Therefore, in Chapter 7, we specifically investigate effective connectivity changes in the emotion regulation network when it is engaged in an emotion regulation task. Chapter 8 provides concluding remarks on this work and Chapter 9 lists peer-reviewed publications emerging from this work.

CHAPTER 2

General Methods

This chapter describes certain general methods including data acquisition and pre-processing, which are common to the rest of the chapters.

2.1. The PTSD Dataset

Recruitment

Active-duty soldiers between the ages of 18 and 50 years were recruited from Fort Rucker, AL, USA and Fort Benning, GA, USA to voluntarily participate in the current study. Recruitment utilized posters and flyers distributed and posted at local facilities including the TBI Clinic and Behavioral Health Clinics. Soldiers being treated for PCS and were referred to the study by clinicians if believed to meet eligibility criteria. Soldiers that were interested in participating called the provided phone number whereupon they were pre-screened and sent the consent form via post or email to be signed and returned. Upon receipt of the returned consent, potentially eligible participants were called to schedule their testing session at Auburn University's MRI Research Center.

The study was carried out in accordance with the latest version of the Declaration of Helsinki and the protocol and procedures were approved by Auburn University Institutional Review Board (IRB) and the Headquarters U.S. Army Medical Research and Materiel Command, IRB (HQ USAMRMC IRB).

Participants

Resting-state fMRI data: Eighty-seven male, active-duty soldiers, 17 with PTSD, 42 with both PCS and PTSD (PCS+PTSD), and 28 controls (with all three groups matched in age, race and education), all having combat experience in Iraq (Operation Iraqi Freedom, OIF) and/or Afghanistan (Operation Enduring Freedom, OEF), were enrolled in the study.

Task fMRI data: Fifty-nine male, active-duty soldiers, 36 with both PCS and PTSD (PCS+PTSD) and 23 combat controls (both groups matched in age, race and education), all having combat experience in Iraq (Operation Iraqi Freedom [OIF]) and/or Afghanistan (Operation Enduring Freedom [OEF]), were enrolled in the study.

With both resting-state and task fMRI data, subjects were grouped based on PTSD symptom severity using the PTSD Checklist-5 (PCL5) score, clinician referral, post-concussive symptoms using the Neurobehavioral Symptom Inventory (NSI) and medical history. i) Subjects with no history of mTBI in the last five years, a total score ≥ 38 on the PCL5 were grouped as posttraumatic stress group (PTSD group). ii) Subjects with a history of medically documented mTBI, post-concussive symptoms, and scores ≥ 38 on the PCL5 were grouped as the comorbid PCS+PTSD group. iii) Subjects with a score < 38 on the PCL5, no DSM-IV-TR or DSM-V diagnosis of a psychotic disorder (e.g. schizophrenia), no mTBI within the last 5 years, and no history of a moderate-to-severe TBI were grouped as combat controls. All subjects were screened for MRI contraindications. All participants reported having deployed to a combat environment. With resting-state fMRI data, the PCL5 scores were significantly different ($F(1, 172) = 20.6443$, p = 3.64×10^{-44}) between the control group and the PTSD and PCS+PTSD groups combined; also, post-concussive symptom (NSI) scores were significantly different ($F(1, 172) = 32.6878$, p = 1.32×10^{-29}) between the PCS+PTSD group and the PTSD and control groups combined. With task

fMRI data, PCL5 scores were significantly different (F(1, 57) = 9.28, p = 4.31 × 10-24) between the two groups, as also the NSI scores (F(1, 57) = 14.37, p = 7.92 × 10-17).

Measures

PTSD Checklist-5 (PCL5, [19]). The PCL5 is a 20-item self-report measure that assesses DSM-5 symptoms of PTSD. The PCL5 has a variety of purposes, including screening individuals for PTSD, making PTSD diagnoses, and monitoring symptom change during and after treatment. Items are rated using a 5-point Likert scale; 1 = "Not at all" to 5 = "Extremely." A total symptom severity score (range: 20-100) can be obtained by summing the scores for each of the 20 items with a cut score of 38 for a precursory diagnosis of PTSD [20].

*Neurobehavioral Symptom Inventory (*NSI, [21]). This 22-item self-report questionnaire is designed to assess post-concussive symptoms in individuals who have sustained a TBI. Participants rate the severity of each symptom within the past month on a 5-point Likert scale ranging from 0 (none) to 4 (very severe). A total symptom severity score (range: 0-88) can be obtained by summing the scores of the 22 items.

CNS-Vital Signs® (CNS-VS, [22]). CNS-VS is a computerized neurocognitive assessment battery. The present study used five CNS-VS sub-tests (verbal memory, symbol digit coding, Stroop test, continuous performance test, and shifting attention test). The following CNS-VS domain scores were calculated: verbal memory (VM), complex attention (CA), reaction time (RT), processing speed (PS), cognitive flexibility (CF), and executive functioning (EF). Domain scores have a mean of 100 and standard deviation of 15. Domain scores were averaged to form a single score or neurocognitive composite index (NCI) [22].

Procedures

When participants arrived at Auburn University's MRI Research Center for their scheduled testing appointment, they were re-screened for eligibility, thoroughly screened for MRI contraindications, and re-consented to ensure full comprehension of the study's procedures, benefits, and their rights. The participants underwent resting-state fMRI, emotion regulation task fMRI and DTI scans along with a standard anatomical scan.

Resting-state fMRI: Participants were scanned in a 3T MAGNETOM Verio scanner (Siemens Healthcare, Erlangen, Germany) using T2* weighted multiband echo-planar imaging (EPI) sequence in resting state (the participants were asked to keep their eyes open and fixated on a white cross displayed with dark background on the screen using an Avotec projection system and not think of anything specific), with TR=600ms, TE=30ms, FA=55˚, multiband factor=2, voxel size= $3\times3\times5$ mm^3 and 1000 volumes. Brain coverage was limited to the cerebral cortex, subcortical structures, midbrain and pons (the cerebellum was excluded). For each subject, two separate scans were performed, thus providing us 174 sessions of resting state fMRI data for the 87 subjects. Mathematically, this boosted the statistical power for our analysis beyond that would have been available from single scans from 87 subjects.

Task fMRI: FMRI data was acquired in a 3T MAGNETOM Verio scanner (Siemens Healthcare, Erlangen, Germany) using T2* weighted multiband EPI sequence, with TR=600ms, TE=30ms, FA=55˚, multiband-factor=2, voxel size= $3.5\times3.5\times5$ mm3, 680 volumes per run and 4 runs per subject. A 32-channel head coil was used.

DTI: Participants were scanned in the same 3T MAGNETOM Verio scanner (Siemens Healthcare, Erlangen, Germany) using diffusion weighted multiband EPI sequence, with TR=3600ms, TE=95ms, FA=90˚, voxel size= 1.8×1.8×3 mm^3, b=0, 1000, 25 slices acquired parallel to the AC-PC plane, matrix=128×128, field of view (FOV) = 230 mm and number of diffusion directions=20. Participants with partial brain coverage or excessive motion were excluded from analyses.

Emotion regulation task: We adopted the task design employed by Urry et al. [23] (please see Fig.2.1), which uses a block design. After a 1s fixation cross, the subjects were shown either a negative image or a neutral image (jittered 3 to 7 seconds) under the "view" condition. The negative images were supposed to arouse a negative emotion in the subjects while the neutral images were supposed to not alter the emotional state of the subject. Unlike prior studies which used the international affective picture system (IAPS), we used the military affective picture system (MAPS) developed by our group [24], which represents images for military populations relevant to experiences of operations in Iraq and Afghanistan. Next, the subjects were asked to either "enhance", or "maintain" or "suppress" their emotion (jittered 5 to 8 seconds). During "enhance" condition, the subjects were required to increase the intensity of negative emotion towards the image by either imagining that they or their loved one was experiencing the situation, or imagining a more extreme outcome than the one depicted. During "suppress" condition, the subjects were required to reduce the intensity of negative emotion towards the picture by either viewing the situation as fake or unreal, or by imagining that the situation has a better outcome than the one being depicted. This 'suppress' act requires conscious cognitive emotion regulation, so we also choose to call it the 'regulation' condition. During "maintain" condition the subjects would just maintain attention on the picture without changing their negative feelings. The subjects would

then report the success of regulation using a button press (within 5 seconds) from the following options: no emotion, not successful, somewhat successful, very successful. Each such trial lasted about 17 seconds. A total of 96 trials were performed in 4 blocks of 24 trials each. Four counterbalanced instruction conditions were employed: (i) neutral image, maintain emotion, (ii) negative image, maintain emotion, (iii) negative image, enhance emotion, and (iv) negative image, suppress emotion.
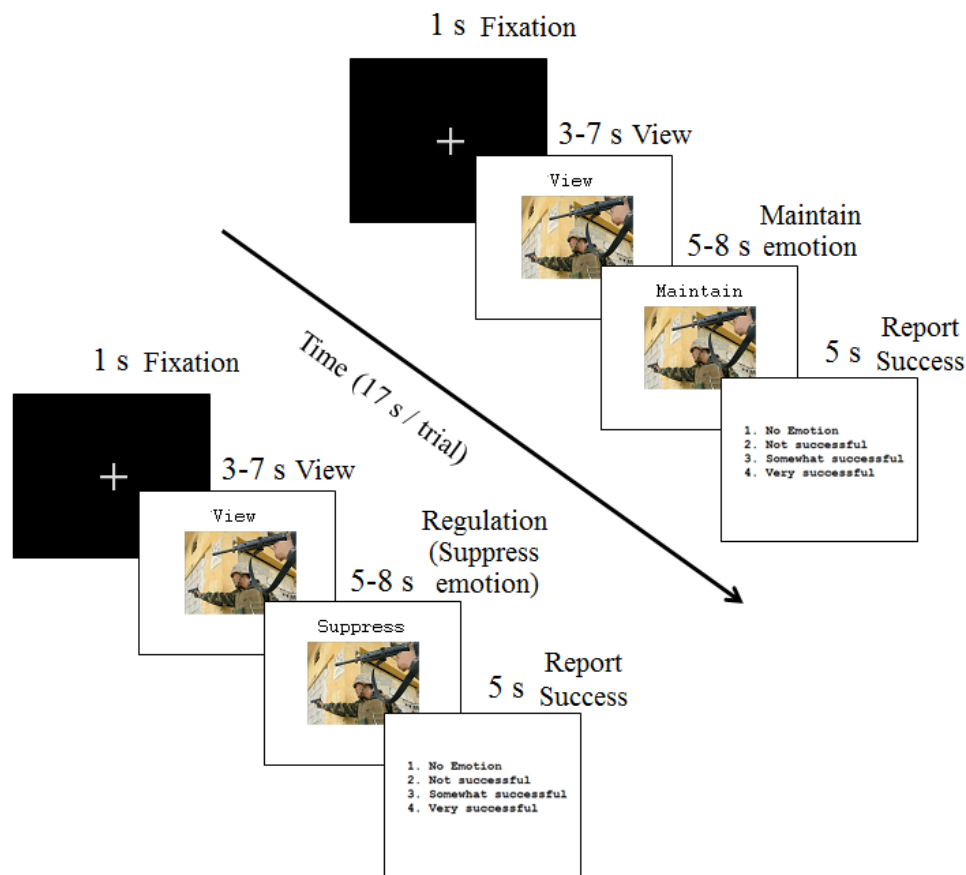
Fig.2.1. *The emotion regulation task, showing the sections relevant for this work. During 'view', the subjects would see an image arousing negative emotion. Then they would either 'maintain' the emotion (no change of emotional state), or 'suppress' the emotion (attempt to reduce negative emotion, that is, perform cognitive emotion regulation)*

2.2. FMRI Data Pre-processing

Resting-state fMRI Data Pre-processing

Standard pre-processing of resting state fMRI data was performed including realignment, normalization to MNI space, detrending and regressing out nuisance covariates such six head motion parameters, white matter (WM) signal, and cerebrospinal fluid (CSF) signal. An additional pre-processing pipeline was executed which was identical to the one described above, but with the added step of global mean signal regression (GSR) in order to examine its effects given conflicting reports about its utility [25, 26]. Pre-processing was performed using Data Processing Assistant for Resting-State fMRI (DPARSF v1.7) [27], which is based on Statistical Parametric Mapping (SPM8) [28] and Resting-State fMRI Data Analysis Toolkit [29].

The data were normalized, rendering each timeseries with zero mean and unit variance. These were then input to a blind deconvolution algorithm [30] in order to remove non-neural variability of the hemodynamic response function (HRF) and estimate latent neuronal timeseries. The deconvolution is blind since both the HRF and the underlying latent neural timeseries are estimated only from the observed fMRI data. Specifically, we used the method demonstrated by Wu et al. [30], which has gained wide acceptance and usability owing to its interpretability, robustness, simplicity, validity and an increasing awareness in the community on the necessity for deconvolution. Many recent papers have employed it (see for example [31, 32, 33]). Briefly, the approach relies on modeling resting state fMRI data as event-related data with randomly occurring events using point processes and then estimating voxel-specific HRFs using Weiner deconvolution.

Prior works show that physiologically meaningful information is contained in higher frequencies (above 0.25 Hz) in BOLD fMRI data, and that the default-mode network, for example,

can be reliably obtained using high frequencies alone [34]. It is notable that band-pass filtering was not performed during pre-processing, since deconvolution makes use of this information-carrying higher frequency components, in addition to standard lower frequencies, for reliable estimation of HRF, while discarding high-frequency noise [30].

Deconvolution was performed because confounds emerging due to inter-subject and spatial variability of the HRF [10] could give rise to a scenario wherein two fMRI timeseries have high directional connectivity while the underlying neural variables do not and vice versa (refer to Fig.2.2 for an illustration). Further, causal connections could readily switch directions if the underlying HRFs have different time-to-peak. To this effect, it has been shown that deconvolution produces improved estimation of effective connectivity [35, 36].

Given the high dimensionality of whole-brain fMRI data, mean deconvolved fMRI timeseries were obtained from 125 functionally homogeneous brain regions determined using spectral clustering (known as the cc200 template [37]). Further connectivity analysis (performed on Matlab® platform) utilized these 125 timeseries from each subject.
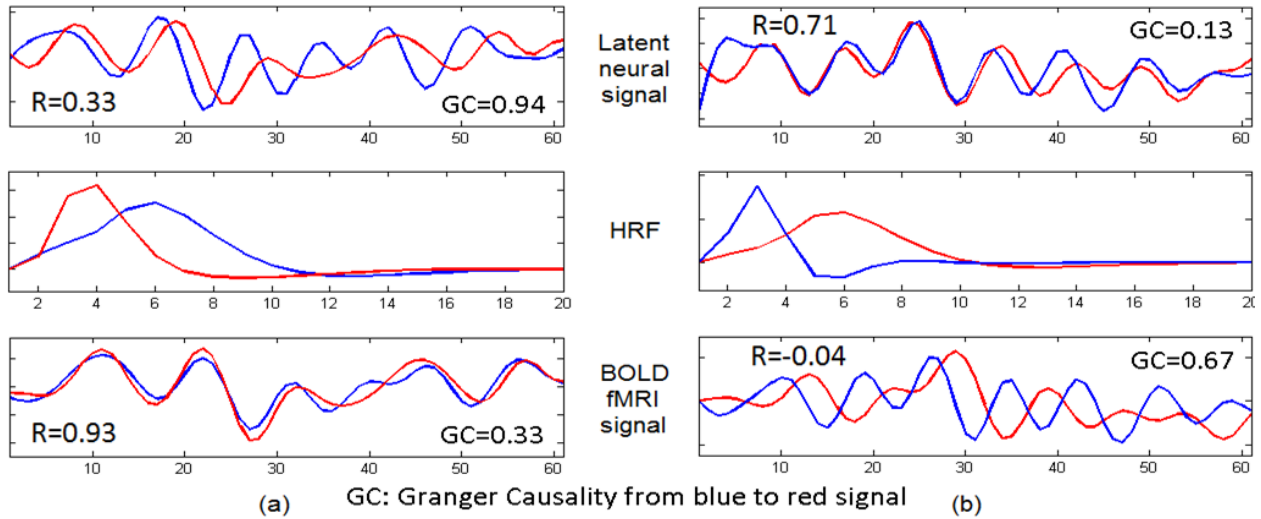
Fig.2.2. *Illustration of the importance of performing hemodynamic deconvolution, using two timeseries from real fMRI data. The latent neural signals are convolved with HRF to give BOLD fMRI timeseries. HRF variability could potentially give rise to a scenario wherein (a) the undying neural variables have true high directional connectivity (measured using Granger causality [GC] from blue to red signal) and true low correlation (R), while the BOLD fMRI timeseries show low GC and high R, and (b) the latent neural signals have true low GC and high R, while the BOLD fMRI timeseries show high GC and low R. GC and R need not necessarily have a negative relationship, though it is true in this example.*

Emotion Regulation Task fMRI Data Pre-processing

All MRI data analysis was performed on Matlab® platform. Standard pre-processing of fMRI data was carried out including de-spiking, realignment, normalization to MNI space and smoothing using an 8mm Gaussian kernel. The data was resliced to 2mm isotropic voxels. Pre-processing was performed using Statistical Parametric Mapping (SPM8) [28].

CHAPTER 3

Functional Connectivity Analysis

3.1. Introduction

About 20% of military service members develop posttraumatic stress disorder (PTSD) [38]. PTSD is characterized by high anxiety, re-experiencing traumatic memories, hypervigilance and hyperarousal. In combat veterans, PTSD has high co-morbidity with mild-traumatic brain injury (mTBI) [2, 3] due to the risk of being exposed to improvised-explosive-devices (IEDs) and non-blast events. Significant percentage of those who sustain mTBI suffer chronic symptoms or post-concussion syndrome (PCS) [4]. With current diagnostic procedures and treatments centering on subjective assessments, a thorough understanding of the mechanistic basis for PTSD and PCS is essential for accurate diagnosis, targeted treatment and for making return-to-duty decisions. Due to largely overlapping symptomatology between PTSD and PCS [5], it is necessary to identify and validate objective biomarkers of the respective neurologic and neuropsychiatric conditions to improve clinical evaluation and, ultimately, treatment outcomes.

We employed resting-state functional MRI (rs-fMRI), which avoids task dependency and subsequent performance differences. We performed connectivity-analysis on rs-fMRI data, without *a priori* assumptions concerning regions of interest (ROIs). Functional connectivity (FC) refers to measures of instantaneous correlation between fMRI signals obtained from different brain regions. There have been several recent fMRI FC studies with PTSD [38, 39, 40] and PCS [2, 5, 41]. However, very little work has been done on comorbid PTSD and PCS, even though

comorbidity is the norm rather than the exception in military populations [40]. Their findings have been mixed [39].

Hyper-connectivity is seen as a response to neurological disruption [42] and is observed in individuals with PTSD [38, 39, 43]. Most studies employ only static-FC (SFC) and ignore dynamic variation of connectivity over time or dynamic-FC (DFC). Several studies show that DFC signatures in subjects with mental disorders are different from that in healthy subjects [44, 45, 46, 47]. DFC is also related to real-world cognitive behaviors [48], which may make it a good tool for studying disorders like PTSD and PCS where cognitive functioning is compromised. SFC and DFC provide different type of information regarding connectivity between two brain regions [49]. Reduced temporal variance in DFC is associated with psychiatric disorders as well as compromised behavioral performance in healthy individuals [50, 51]. This reduction is associated with compromised ability to dynamically adjust (e.g. behavior, thoughts, etc.) to changing conditions. This phenomenon is well recognized in other biological systems such as reduced heart-rate-variability being a risk factor of cardiovascular disease [52]. Since external influences and internal body states are continually changing, a healthy biological system varies its activity in real-time to accommodate these changes. In these terms, "frozen" connectivity reflects compromised brain health. The current study uses these principles to identify functional connections in the brains of soldiers with PTSD and PCS which are in a "frozen" hyper-connected state compared to healthy soldiers.

Active-duty, U.S. Army soldiers screened positive for PTSD, both PCS and PTSD (PCS+PTSD), and healthy combat controls were recruited. We tested an overarching hypothesis that PTSD with and without PCS is associated with higher connectivity-strength (SFC) but lower connectivity-variance (variance of DFC [vDFC] calculated over time, Fig.3.2) as compared to

healthy controls (Fig.3.1a). Further, we hypothesized that connectivities would be more extreme (i.e. higher SFC and lower vDFC) in PCS+PTSD-subjects compared to PTSD-subjects, indicative of greater symptom severity. We notably tested the hypothesis on whole-brain connectivity data without imposition of any priors or assumptions.

In addition to the primary hypothesis, there were multiple corollary hypotheses addressed in this study. First, if the connectivities were indeed more extreme (i.e. higher SFC and lower vDFC) in PCS+PTSD-subjects compared to PTSD-subjects, it raises the question as to whether the PCS+PTSD group's condition is being driven by PTSD. Alternatively, is this comorbid group's state unique, potentially due to the addition of mTBI sequelae? We attempt to address this question by investigating structural alterations of white-matter tracts in all three groups with the hypothesis that changes in axonal integrity must be exclusive to the PCS+PTSD-group, likely attributed to the mTBI suffered by these subjects. MRI diffusion-tensor-imaging (DTI) tractography provides meaningful information concerning diffusion of water molecules in white-matter as a measure of tract trajectory, integrity and directionality. White-matter neuropathology can result in increased diffusivity, for example, with inflammation from demyelination [53, 54]. In a recent study involving veterans from Iraq and Afghanistan wars who were diagnosed with PCS [55], DTI showed differences in white-matter diffusivity associated with regions that also had abnormal functional connectivity. In line with this finding, we predicted that there would be congruently greater diffusivity in the tracts connecting regions with altered functional connectivity; therefore, supporting the argument that PCS+PTSD-group is etiologically different from PTSD-group.

Second, if we are successful in finding functional connections in the brain which satisfy our overarching hypothesis, it will be important to determine their relevance to behavior and clinical diagnostics. Our subjects are traditionally assigned diagnostic groups based on clinical observation

and symptom reporting. While self-report symptom scores provide quantifiable subjective assessments of severity of the disorders (i.e. psychopathology), neuroimaging data provides better characterization of underlying pathophysiology. Hence, we postulated that grouping of subjects based on significant connectivity values would be superior (in terms of how the groups map to behavioral clusters) than the traditional diagnostic grouping. Specifically, connectivities from significant paths which fit our overarching hypothesis were used to regroup the subjects, giving two distinct groups (pure-control and pure-PCS+PTSD) and an intermediate group. Indeed, this approach has been actively promoted by the National Institute of Mental Health (NIMH) in the United States by publication of "Research Domain Criteria" (RDoC, http://www.nimh.nih.gov/research-priorities/rdoc/nimh-research-domain-criteria-rdoc.shtml). RDoC is agnostic about current disorder categories, and the intent is to generate classifications in a data-driven way. The "core unit of analysis" advanced by RDoC is the "measurements of particular circuits as studied by neuroimaging techniques". In line with this ideology, a recent report demonstrates how data-driven definition of groups in psychiatric spectrum disorders can identify new groups which map better onto behavioral clusters [56]. Our regrouping strategy is inspired by these recent developments.

In order to address this secondary hypothesis, behavioral measures obtained from a neurocognitive battery were separately grouped using both conventional and proposed grouping, and their statistical separation between groups were compared for both cases. This comparison was done to test the hypothesis that the new grouping based on underlying neurobiology (as inferred from connectivity) will map better onto neurobehavior than conventional grouping based on symptom-severity scores.

Third, both our primary hypothesis and corollary hypotheses are based on an analysis framework which relies on statistical separation between groups. However, statistical separation

of between-group connectivities does not necessarily imply that they have predictive diagnostic ability [57]; that is, they may not be able to predict group membership at an individual level with reasonable accuracy. Consequently, those connectivities which are statistically significant as well as possess the discriminative power to classify subjects with high accuracy are more powerful. Several studies report that machine-learning classifiers can be successfully used on fMRI data for diagnostic prediction, including, but not limited to, major-depressive-disorder [58], Parkinson's disease [59], PTSD [60], dementia [61], autism [62] and prenatal-cocaine-exposure syndrome [57]. However, to the best of our knowledge, there are no studies which have used connectivity markers in the classification of both PTSD and PCS subjects. For neuropsychiatric disorders like PTSD and PCS, which are currently diagnosed solely through clinical observation, classification using neuroimaging signatures could be applied to obtain more accurate diagnoses in these highly comorbid conditions. Therefore, using whole-brain connectivity data we identified, in a data driven way, those features which predict the diagnostic membership of a novel subject with high accuracy. We specifically investigated whether there was an overlap between connectivity paths satisfying the overarching hypothesis and those identified as having high predictive ability. We hypothesize that these paths (i) will better predict the diagnostic membership of a novel subject than non-imaging measures, and (ii) will predict the group membership of a novel subject with significantly better accuracy for the proposed connectivity-based grouping (as elucidated in previous paragraph), as compared to conventional grouping.

Fig.3.1b illustrates the complete analysis pipeline with a hierarchical flowchart (outcomes are discussed in results section).
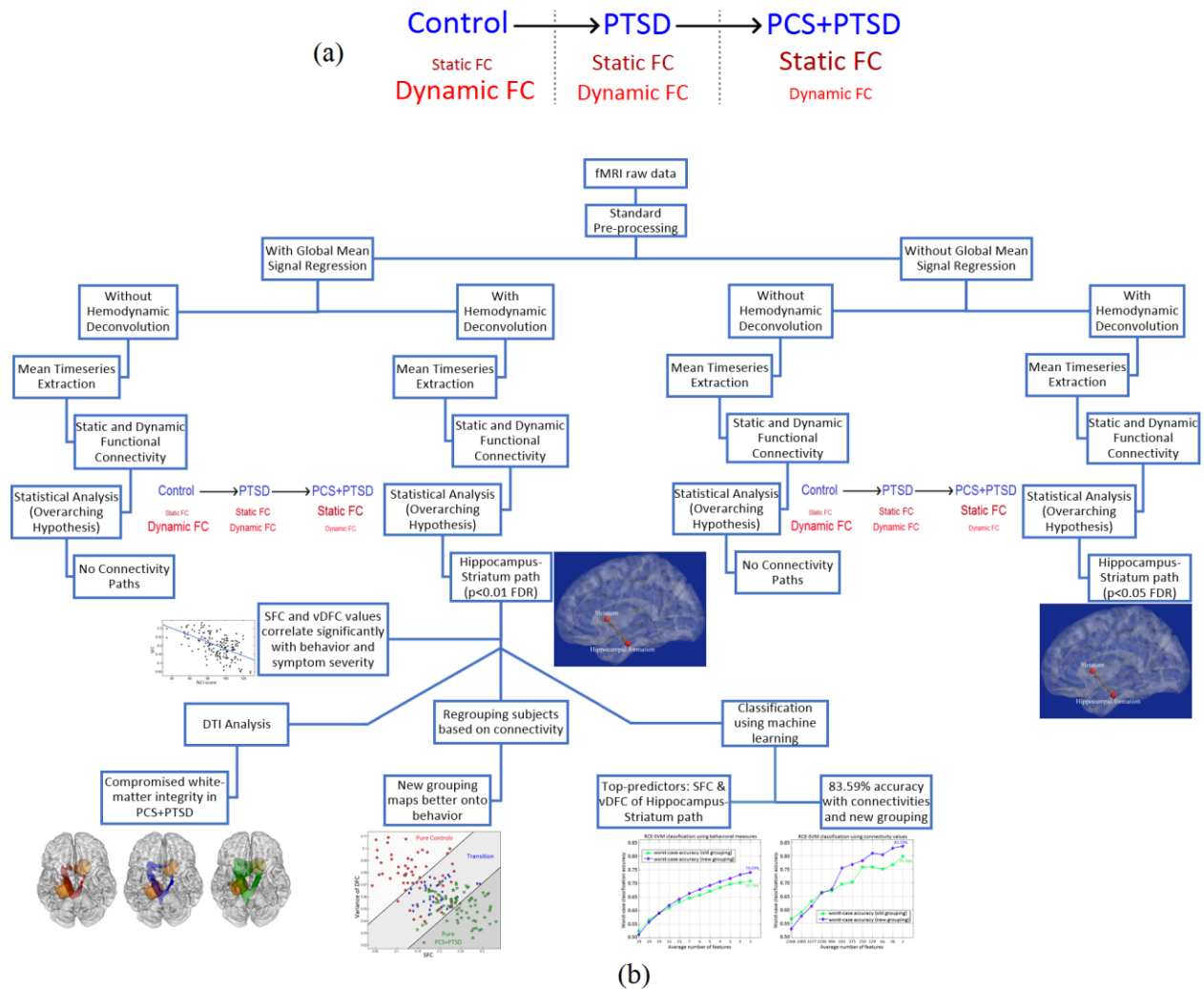
Fig.3.1 (a) *Illustration of our primary hypothesis: increasing font size of SFC implies increasing connectivity strength from controls to PTSD to PCS+PTSD. Decreasing font size of DFC implies decreasing variance of connectivity from controls to PTSD to PCS+PTSD; (b) Flowchart illustrating the analysis pipeline employed in this work*

3.2. Methods

3.2.1. *Static and Dynamic Functional Connectivity*

Most studies investigate functional connectivity (FC), a metric of synchronicity of activity in disparate brain regions, assuming connectivity to be temporally stationary. Dynamic fluctuations of connectivity are not captured when using static connectivity. It has been shown that dynamic changes in FC are relevant to neuropathology [63] as well as behavioral performance in different domains (alertness, cognition, emotion, and personality traits) in healthy individuals [17]. For a comprehensive overview of DFC of resting state fMRI see Hutchison *et al.* [64].

Previous PTSD and mTBI studies have not enumerated the utility of dynamic information in connectivity fluctuations, over and above the information obtained from conventional static connectivity, in clinical applications. In this study, we have used static as well as dynamic functional connectivity measures. SFC and DFC values were obtained between all pairs of 125 brain regions. For SFC, Pearson's correlation calculated from the entire time series was used. For DFC, we employed sliding windowed Pearson's correlation with variable window length which was determined adaptively by assessing time series stationarity through the augmented Dickey-Fuller test (ADF test), as in our recent study [17]. This procedure searches for the optimal window length within a specified range using stationarity of the signal as the criteria for optimization. We have used a liberal range of 20 to 140 data points. The justification for using this range for resting state fMRI data is provided in Jia et al. [17]. Fig. 3.2 illustrates the concept underlying SFC and DFC.
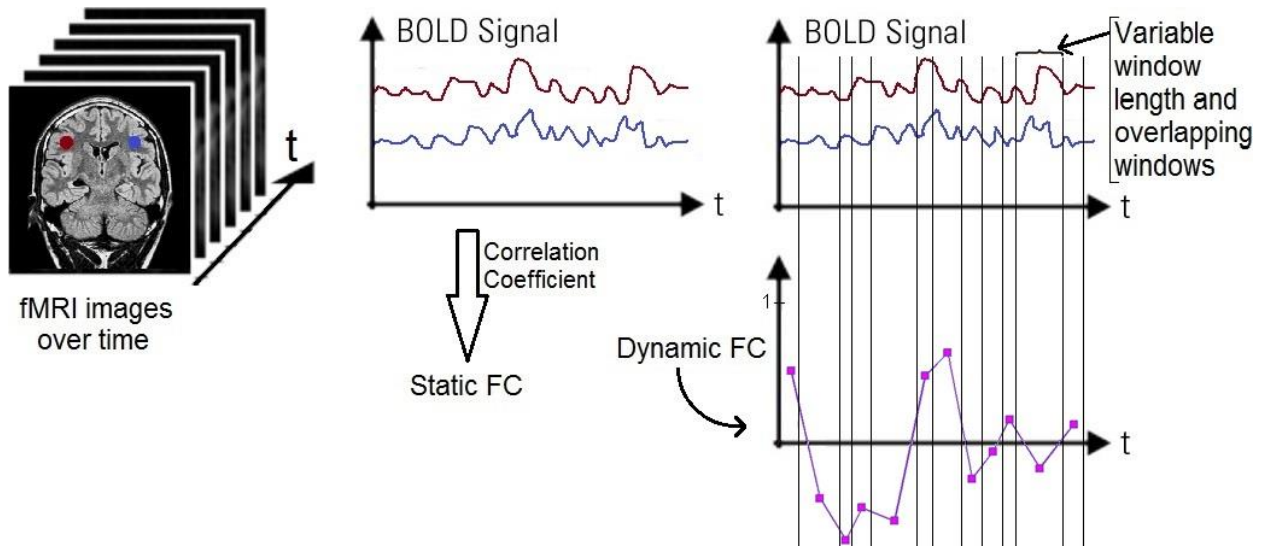
Fig. 3.2 *Illustration of the evaluation of static and dynamic functional connectivities*

SFC and DFC were obtained between all pairs of 125 regions, thus obtaining a 125×125 SFC matrix and a 125×125×1000 DFC matrix per subject (1000 being the number of time points). Variance of DFC (vDFC) values over time was evaluated to obtain a 125×125 DFC variance matrix per subject. Significant group differences in SFC (and vDFC) were obtained for all pairs of connectivity paths ($p<0.01$ FDR corrected). Multivariate N-way ANOVA (MANCOVAN) statistical test was used. Significant group differences were controlled for age, gender, race, education and head motion (using mean frame-wise displacement obtained across all brain voxels for each subject as defined by Power et al. [65]). As mentioned before, we investigated the existence of significant connectivity paths which had higher SFC but lower vDFC in disease compared to controls, with connectivities being more extreme in PCS+PTSD compared to PTSD. For the paths which fit our hypothesis, their connectivity values were also correlated with neurocognitive scores (NCI and subtests) and symptom severity in PTSD (PCL5 score) and in PCS (NSI score).

3.2.2. Regrouping subjects based on connectivities

In line with our hypothesis, we postulated the following: (i) new diagnostic groups created based on the separation of significant connectivity values would better map onto behavior, as compared to commonly used symptom severity scores (PCL5 and NSI) and (ii) PTSD and PCS are spectrum disorders wherein individuals are likely to lie on a continuum ranging from healthy controls to comorbid PCS+PTSD, rather than form distinct clusters; hence forming pure healthy and co-morbid groups (with diagnostic confidence being very high in the pure groups) and an intermediate group (low diagnostic confidence) may be clinically useful. All the control subjects also had combat experience, and hence a percentage might possess borderline neural and behavioral alterations associated with PTSD and PCS, or both. Furthermore, subjects that fall within the PCS+PTSD group might exhibit anywhere from mild-to-moderate neurocognitive decrements, making it indistinguishable from the PTSD group. With all these factors in place, it may be desirable to develop objective clinical classifications using imaging rather than symptom reporting. Hence, we propose a practical approach wherein the subjects are grouped into two extreme pure groups and an intermediate group based on imaging measures such as SFC and vDFC. This paradigm is still compatible with the fact that the groups may have significantly different means, but a large standard deviation so that they overlap. Therefore, we devised a method wherein the subjects are regrouped into the following three groups: 1) pure control, 2) intermediate group, and 3) pure PCS+PTSD. A hypothetical example is shown in Fig.3.3. Plotting the connectivity values in the two-dimensional space of SFC (x-axis) and vDFC (y-axis), we can expect to find connectivities of control subjects and PCS+PTSD subjects at opposite ends. Furthermore, we expect to see an intermediate region between these two extremes where there will be a combination of subjects that are borderline healthy, those with PTSD symptoms, and

comorbid post-concussive and PTSD symptoms. In contrast, pure controls and pure PCS+PTSD groups can be defined as subsets of subjects who fall outside this intermediate group on either side, respectively. The objective of regrouping is to maximize the heterogeneity of the intermediate group while simultaneously minimizing the heterogeneity of the pure groups.

Due to computational feasibility, a grid search was used to achieve subject grouping. Assuming that N paths satisfy our overarching hypothesis (i.e. significantly stronger SFC with lower vDFC in disease compared to healthy), the connectivity values of all the subjects were embedded in the $2N$-dimensional connectivity space (each path is associated with SFC and vDFC values, hence $2N$). In order to explain this procedure intuitively, we consider the two-dimensional example shown in Fig.3.3. Subjects in the control group were tagged as '1', PTSD group as '2' and PCS+PTSD group as '3'. We used the variance of tagged group values as a measure of heterogeneity. For example, pure control group would ideally have only control subjects (tag=1), hence the variance of the tags for the group would be zero. The intermediate group would have a mixture of all three groups (1, 2 and 3), hence it would have higher non-zero variance.
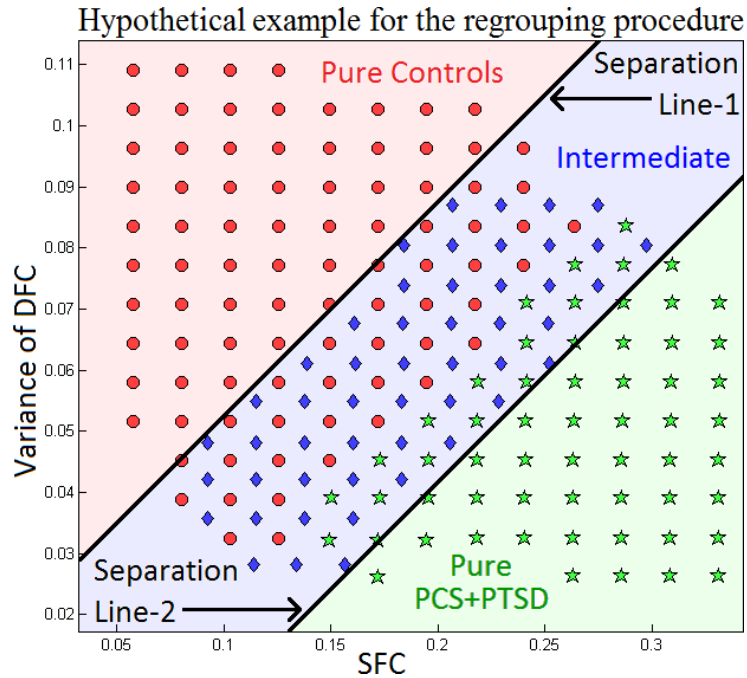
Fig.3.3. *Hypothetical example illustrating the proposed regrouping procedure using simulated data*

Two separation hyper-planes of dimension *2N-1* (lines in the two-dimensional example being considered) which were parallel to each other were arbitrarily initiated. As regards to our specific 2D example, the equation of a line in two dimensions is given by *y=mx+c*, where *y* and *x* are the variables on the y-axis and x-axis, respectively, *m* is the slope and *c* is the intercept. For a given range of *x* and *y* values, the position of the line is determined by its angle (*m*) and shift (*c*). Within the given range of SFC and vDFC values, we generated all possible pairs of parallel lines using all possible values of angle, shift, and separation between the lines. The feature space between the two separation lines was identified as the intermediate group, and the feature space outside them as the two pure groups. We evaluated the heterogeneity of each of the three groups (using variance as explained above) for all possible separation lines generated. We then searched for that pair of nearest separation hyper-planes (or lines in our 2D example), which resulted in highest variance in the intermediate group and least variance (ideally, zero) in the two pure groups. These two were

28

chosen as the final separation hyper-planes (or lines in 2D case), which were used to create the new groups based on connectivity: pure controls, intermediate, and pure PCS+PTSD.

In order to find the diversity of the intermediate group, percentage of controls in the intermediate group (say, p_c) along with the percentage of PCS+PTSD subjects (say p_{pp}) and PTSD subjects (say p_p) were obtained. If N_c is the number of control subjects in the intermediate group, N_p is the number of PTSD subjects in the intermediate group, N_{pp} is the number of PCS+PTSD subjects in the intermediate group, T_c is the total number of control subjects, T_p is the total number of PTSD subjects, and T_{pp} is the total number of PCS+PTSD subjects, then,

$$p_c = N_c/T_c \; ; \;\; p_p = N_p/T_p \; ; \;\; p_{pp} = N_{pp}/T_{pp} \tag{3.1}$$

For example, if there were 14 controls in the intermediate group (out of 56 control subjects overall) then 25% of controls ($=p_c$) would be in the intermediate group (remaining 75% would be in the pure controls group). It was important that we took the percentage mixture to calculate diversity rather than absolute numbers since the number of subjects in each group was different. We then generated a vector of ones, twos and threes in the same proportion in which we obtained the group percentages (say X_{data}), and obtained its variance (say V_{data}). Likewise, maximum possible variance was obtained with ones, twos and threes being present in equal numbers (say X_{max}, with variance V_{max}).

$$X_{data} = [1,1, \ldots N_c \; terms \quad 2,2, \ldots N_p \; terms \quad 3,3, \ldots N_{pp} \; terms]; V_{data} = Variance(X_{data}) \tag{3.2}$$

$$X_{max} = [1,1, \ldots N_m \; terms \quad 2,2, \ldots N_m \; terms \quad 3,3, \ldots N_m \; terms]; V_{max} = Variance(X_{max}) \tag{3.3}$$

Where N_m is the average number of subjects, which is the total number of subjects divided by 3 (=29 in the current study). The percentage of the ratio of variance obtained from group percentages to the maximum variance (=V_{data}/V_{max}) was used to compute the percentage diversity of the intermediate group. Obviously with this definition, the two pure groups would have 0% diversity.

$$Percentage\ Diversity = \frac{V_{data}}{V_{max}} \times 100 \tag{3.4}$$

If the new grouping maps better onto behavior than the conventional grouping (which was based on symptom screening and clinician referral), it can be postulated that the new grouping can predict PTSD and PCS sequelae better than conventional methods. In order to test this, we statistically compared subjects grouped using both the conventional grouping as well as the new grouping obtained by the proposed procedure on neurobehavioral measures (i.e., neurocognitive functioning). Corresponding mean and standard deviation (SD) values of individual groups were obtained along with the statistical significance of the differences between the groups.

3.2.3. Classification using support vector machine

Statistical separation between neural signatures (e.g. t-test) does not necessarily guarantee generalizability or predictive capacity of those signatures for diagnosis. A statistically significant connectivity path need not have high predictive ability and vice versa. Consequently those connectivity paths which are both statistically significant (according to our hypothesis) and top classifiers (high predictive ability) assume more power and, therefore, relevance. Hence, we have used machine learning methods to identify those connectivity paths (or features) which can accurately classify individuals between PTSD, PCS+PTSD, and controls. A Recursive Cluster

Elimination based Support Vector Machine (RCE-SVM) classifier [66] was used to classify the subjects based on significant SFC and vDFC values. First, significant group differences were found for all the three comparisons (control vs. PTSD, control vs. PCS+PTSD, and PTSD vs. PCS+PTSD), using a threshold of $p<0.05$ (controlled for age, race, education and head motion), for both SFC and vDFC. We used an uncorrected $p<0.05$ threshold since we wanted to be liberal about which features are input to the classifier and let the classifier choose the most predictive features. Next, we found overlapping paths between the three comparisons. The overlapping paths for SFC and vDFC were combined to provide the input features to the classifier. This initial filtering enhances the quality of classification [67], and ensures that non-discriminatory features are not fed into the classifier.

Our choice of support vector machine (SVM) [68] for classification was motivated by its wide acceptance and applicability for classification in several fields, including neuroimaging [69]. Previous studies have shown that using discriminatory features enhances classification performance of SVMs [66, 67]. Therefore, we employed recursive cluster elimination (RCE), a wrapper method which iteratively eliminates features to minimize the prediction error, where feature selection and classification steps are embedded together. The main steps involve the clustering step, the SVM scoring step and the RCE step. The features that were initially input into the classifier were divided into training and testing data sets. The classifier was trained using the training data set, while the testing data set is totally kept blinded to the classifier. Once training is complete, the testing data is input into the classifier and classification accuracy is obtained. This ensures generalizability of the results.

In the clustering step, k-means algorithm was used to cluster the training data into 'n' clusters. The number of clusters was initially set to the number of features, and then was iteratively

31

decreased by one until no empty clusters were left. The 'n' obtained by this iteration served as the initial 'n' for the RCE-SVM loop. In the SVM-scoring step, each cluster was scored based on its capacity to differentiate between the two groups by using linear SVM. In order to assess the performance of the clusters, the training data was randomly partitioned into 6 non-overlapping subsets of equal sizes (6 folds). Using 5 subsets, the SVM was trained and performance (accuracy) was computed using the remaining subset. All possible partitions were generated by repeating the clustering and cross-validation procedures 100 times. For each of these 100 repetitions, the classification accuracy was obtained using the testing data.

Using the outcome of 100 repetitions and 6 folds for each repetition, the average value of the accuracies was assigned as the cluster's score. The bottom 20% of low scoring clusters were eliminated in the RCE step. Remaining features were merged and the value of 'n' was reduced by 20%. This ensures that only certain top classifying features qualify for the next iteration. The clustering step, the SVM-scoring step and the RCE step were repeated again iteratively. After each iteration, performance of the classifier was obtained using the reduced number of features compared to the earlier iterations. Once the number of clusters reached two, the procedure was stopped. Fig.3.4 illustrates the RCE-SVM procedure using a flowchart. Complete separation of testing and training data sets in this procedure eliminates bias in the computation of classification accuracy [70]. Further, the features in the final two clusters are those with highest discriminative ability and hence carry predictive value for diagnosis. Complete details about the RCE-SVM algorithm can be obtained from previous reports [66, 71].
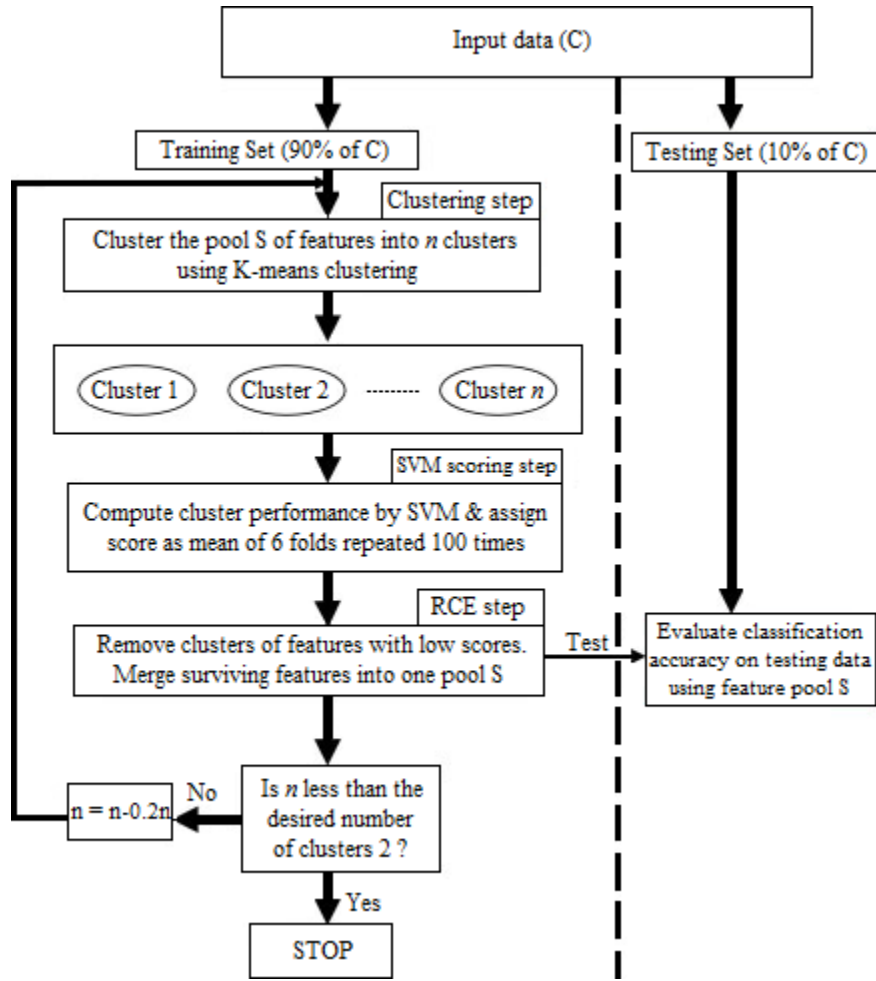
Fig.3.4 *Flowchart illustrating the RCE-SVM classification procedure*

Classification was performed separately for all the three comparisons in the conventional as well as the proposed new groupings (i.e. control vs PTSD, control vs PCS+PTSD and PTSD vs PCS+PTSD in the conventional grouping; and pure control vs intermediate, pure control vs pure PCS+PTSD and intermediate vs pure PCS+PTSD in the new grouping). For both groupings, outcome measures such as accuracy and final set of discriminative features were obtained by intersecting the results obtained by each of three individual classifiers. In order to be conservative, we obtained the worst-case classification accuracy by considering the minimum accuracy value

obtained from the test data set among all 600 iterations (100 repetitions $\times$ 6 folds). The statistical significance of accuracies was obtained by estimating the p-values using a binomial null distribution $B(\eta,\rho)$, ρ being the probability of accurate classification and η being the number of participants, as in previous studies [72]. Only those accuracies whose p-values were less than 0.05 (Bonferroni corrected) were considered as statistically significant for further processing.

We repeated the above procedure and performed classification using 32 non-imaging measures as input features instead of SFC and vDFC connectivities. The 32 measures were: (i) behavioral measures: all CNS-VS measures including the NCI score; (ii) psychological health measures: Perceived Stress Scale, Pittsburgh Sleep Quality Index, Epworth Sleepiness Scale, Zung Anxiety Scale, and Zung Depression Scale; (iii) exposure/injury descriptives: Combat Exposure Scale, lifetime concussions, and Life Events Checklist. Worst-case classification accuracies and top classifying features were obtained, as before, and these results were compared with the results obtained using connectivity values.

3.2.4. DTI Data Processing

One of the ways to find out whether increased severity in the PCS+PTSD group is due to an mTBI (structural damage) or due to the compounding effect of two disorders (PTSD and PCS) combined, is to look at structural changes using DTI. Probabilistic diffusion tractography was carried out using FSL's Diffusion Toolbox (FDT) [73, 74]. Regions of interest (ROI) which were connected by functional paths satisfying our overarching hypothesis (i.e. significantly stronger SFC and lower vDFC in disease compared to healthy) were identified as seed and target regions. Briefly, a probability density function was created at each voxel on the principal fiber direction. Connectivity probabilities were estimated between the seed and target ROIs by repeatedly

sampling connected pathways through the probability distribution function. Samples were drawn from the connectivity distribution, and the proportion of those samples that passed through both ROIs was defined as the probability of the connection between the seed and the target. For each analysis, we thresholded and binarized individual subject's results to include only those voxels with a connection probability >10%. These images were then combined to create group maps, which would help us find out whether there is any structural basis for increased severity in PCS+PTSD subjects. White matter tracts were subsequently identified using the JHU ICBM DTI 81 White Matter Label Atlas (http://www.loni.usc.edu/ICBM/Downloads/Downloads_DTI-81.shtml).

3.3. Demographics and Phenotypic Information

Demographics

The demographics for the three groups are presented in Table.3.1. There were no significant differences between the groups in age, p = .699, or education, p = .152. The results indicated that there was a difference in the frequency of reported psychotropic use between the groups, τb = .24, p = .011, with the comorbid group having the highest percentage of medicated subjects. There was a significant difference between the groups in the number of reported lifetime mTBIs, F(2) = 5.81, p = .004, specifically between control group and the PCS+PTSD group, but not the PTSD and PCS+PTSD groups or control and PTSD groups, p > .05.

Table.3.1. *Basic Demographics*

Variable		Controls	PTSD	PCS+PTSD
Age, years	Mean	32.6	32.2	33.7
	Median	31	32	33
	SD	6.7	7.6	6.8
	Range	24	24	30
Education, years	Mean	15.1	14.5	14.1
	Median	16	14	14
	SD	1.9	2.2	1.9
	Range	8	9	8
Race	White	18(66.7%)	11(64.7%)	26(66.7%)
	Black	2(7.4%)	3(17.6%)	9(22.0%)
	Hispanic	3(11.1%)	3(17.6%)	2(4.9%)
	Asian	2(7.4%)	0	1(2.4%)
	Other	0	0	1(2.4%)
Medication		2(7.4%)	4(23.5%)	13(31.7%)*
Lifetime mTBIs	Mean (Range)	0.3(2)	1.1(6)	2.5(15)*

Psychological Health and Neurocognitive Function

The results revealed significant differences between the three groups in posttraumatic symptoms (PCL5), $F_{(2, 81)} = 101.65$, $p < .001$, post-concussive symptoms (NSI), $F_{(2, 78)} = 49.79$, $p < .001$, and combat exposure (CES), $F_{(2, 79)} = 40.69$, $p < .001$. All p-values remained significant after corrections for multiple comparisons. As observed in Table.3.2, the PCS+PTSD group had the highest scores out of the three groups on these respective measures.

The results indicated that after corrections for multiple comparisons, the control group had significantly higher scores than the PCS+PTSD group on all neurocognitive measures, $p < .05$, with the exception of Reaction Time and Verbal Memory, $p > .05$. The PCS+PTSD group also had significantly lower scores in Cognitive Flexibility, Executive Functioning, and the NCI compared

to the PTSD group, p < .05. The findings suggest that both the PTSD and PCS+PTSD groups have lower scores than controls, but also, the comorbid group has greater impairments than the PTSD group (see Table.3.2).

Table.3.2 *Mean, median, and standard deviation on PCL5, NSI, CES, and CNS-VS neurocognitive measures for each of the groups*

		Controls	PTSD	PCS+PTSD
PSYCHOLOGICAL				
Traumatic Stress[a]	Mean	23.5	56.6	70.9
	Median	21.5	48.5	70.5
	SD	4.2	17.8	15.2
Post-concussive symptoms[a]	Mean	6.6	25.9	43.4
	Median	5	17.5	41.5
	SD	4.8	19.2	16.1
Combat Exposure[a]	Mean	7.2	16.7	28.6
	Median	2.5	15	29
	SD	9.8	11.2	8.6
NEUROCOGNITIVE				
Neurocognitive Composite Index[t,z]	Mean	101.2	94.3	81.7
	Median	100.7	94.6	82.2
	SD	12.9	12.5	20.7
Reaction Time	Mean	97.4	95.3	84
	Median	101	92	91
	SD	23	11.9	32.8
Complex Attention[t]	Mean	94.2	78.1	70
	Median	99.5	92	80
	SD	23.3	30.9	31.3
Cognitive Flexibility[t,z]	Mean	103.6	97.1	80.5
	Median	103	93	86
	SD	16.3	15.2	26.7
Processing Speed[t]	Mean	104.8	100.1	89.9
	Median	104	98	92
	SD	20.9	11	20.1

Executive Functioning[t,z]	Mean	106	101	84.1
	Median	104.5	104	90
	SD	13.3	13.2	24.8
Verbal Memory	Mean	99.6	92.1	83.6
	Median	106.5	103	83
	SD	12.5	9.5	13.9

[a] denotes $p<.05$, all three groups
[t] denotes $p<.05$, Controls vs. PCS+PTSD
[z] denotes $p<.05$, PTSD vs. PCS+PTSD
Note: Traumatic Stress = PCL5; Postconcussive Symptoms = NSI; Combat Exposure = CES.

3.4. Connectivity Results

3.4.1. RS-fMRI Functional Connectivity Results

In accordance with our hypothesis, the connectivity path between left striatum and right hippocampal-formation (Fig.3.5a) showed higher connectivity strength and lower connectivity variance in PCS+PTSD and PTSD groups compared to controls. This was the only path in whole-brain connectivity data to conform to our hypothesis. Striatum region mainly contained caudate head (MNI-centroid: -11.3,12.2,3.5) and hippocampal-formation contained entorhinal and perirhinal cortices, and anterior hippocampus and parahippocampal gyrus (MNI-centroid: 19.4,-12.4,-25.5).

This result was obtained with deconvolved data, pre-processed with global-mean-signal-regression (GSR). No paths were obtained in data without deconvolution, and excluding GSR did not change the current result. Figs 3.5b and 3.5c show the hippocampus-striatum path-weights being significantly different between the three groups, with decreasing vDFC and increasing SFC as we move from control to PTSD to PCS+PTSD.

(a)

(b)

(c)

White Matter Connectivity Between Hippocampus/
Parahippocampus and Caudate/Putamen

x = -50   x = -46   x = -42   x = -38   x = -34

x = -30   x = -26   x = -22   x = -18   x = -14

x = -10   x = -6   x = -2   x = 2   x = 6

x = 10   x = 14   x = 18   x = 22   x = 26

x = 30   x = 34   x = 38   x = 42   x = 46

1   27   1   15   1   40
Controls   PTSD   PCS + PTSD
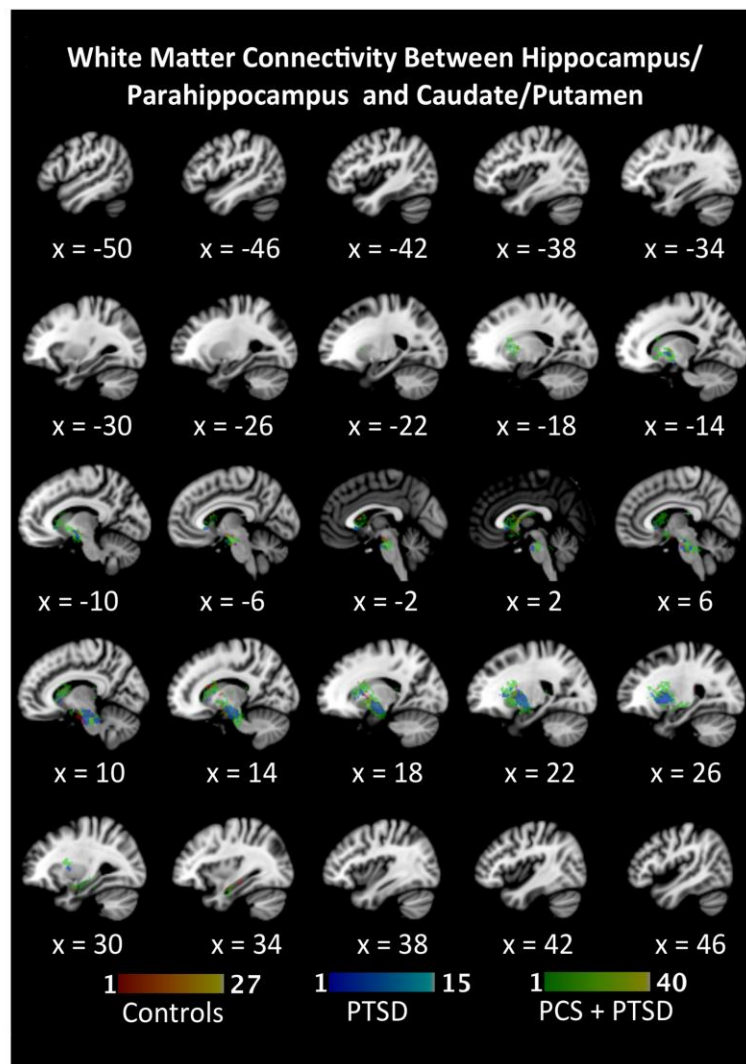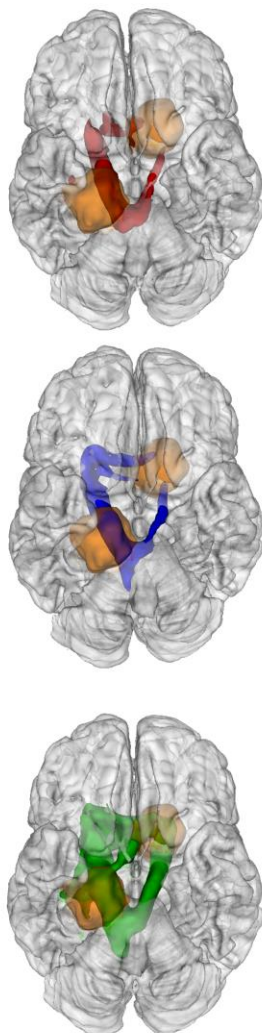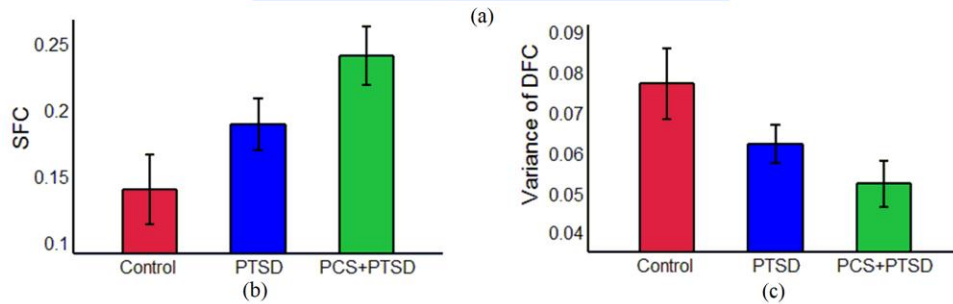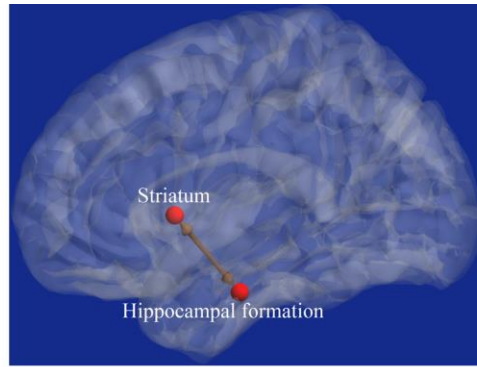
(d)

Fig.3.5 (a) *Sagittal view of brain showing the hippocampus-striatum path, (b) Variance of dynamicFC and (c) staticFC values for the three groups, (d) White-matter connectivity between striatum and hippocampal-formation: fibers connecting the two ROIs are more diffuse in PCS+PTSD-group compared to PTSD or controls.*

The aforementioned result was obtained using deconvolved data used a threshold of $p<0.01$ (FDR corrected) for testing statistical significance. Testing our hypothesis with a liberal threshold of $p<0.05$ (FDR corrected), we found two paths to be significant. In addition to the left striatum – right hippocampal formation path mentioned before, the path between left striatum and left hippocampal formation was the additional path to be found significant.

It is notable that we have used deconvolved data in our analysis. Deconvolution [30] removes HRF variability [75] in the BOLD fMRI signal and provides the latent neuronal time series. Results obtained using non-deconvolved data could potentially be influenced by HRF variability. However, we tested our hypothesis on temporally band-pass filtered (0.01-0.1Hz), preprocessed fMRI data without hemodynamic deconvolution as used in conventional resting state connectivity analyses. Notably, we did not find any significant path supporting our hypothesis, indicating the value of removing HRF variability and smoothing from fMRI time series even for functional connectivity analyses.

Though lower connectivity variance (DFC) is most likely associated with ill-health, both lower and higher connectivity strength (SFC) has been previously associated with ill-health. Specifically, previous literature has shown both stronger and weaker connectivity (SFC) in PTSD as compared to controls [76, 13, 77]. Hence, we also investigated whether paths which had significantly lower connectivity strength (SFC) and lower connectivity variance (vDFC) existed in PTSD and

PCS+PTSD groups compared to controls. However, none of the paths could fit this hypothesis using either deconvolved data or conventional non-deconvolved data.

Results were obtained with data which had undergone global mean signal regression while preprocessing the data. There has been debate in the scientific community about whether or not global mean signal should be removed [25, 26]. In fact, Power et al note that "the objections raised to global signal regression are mainly based on results from low-dimensional simulations [25], and that further work that determines the applicability of these arguments to empirical data would usefully inform decisions about using global signal regression as part of denoising strategies. In order to account for this, we also performed the same analysis on preprocessed data without global mean signal regression. We replicated the results showing that the left striatum – right hippocampal formation path was the only significant path in accordance with our hypothesis, but with reduced statistical significance ($p < 0.05$, FDR corrected). This suggests that performing global mean signal regression can improve the statistical significance of the results by removing unwanted variance from the data. Importantly, the hippocampus-striatum path remained significant despite concerns about confounds that global mean signal (or its regression) may introduce. Additionally without GSR, none of the paths fit our hypothesis with conventional non-deconvolved data. Also, no paths were found when we searched for lower SFC and lower vDFC values in PTSD and PCS+PTSD groups compared to controls, with either deconvolved data or conventional non-deconvolved data. All these results unequivocally support that the left striatum – right hippocampus path fits our hypothesis irrespective of several pre-processing choices debated lately in the scientific community.

3.4.2. DTI results

DTI results revealed greater diversity in structural connectivity between hippocampus and striatum, with white-matter fibers connecting these two ROIs being more diffuse (implying less integrity) in PCS+PTSD-group compared to PTSD and control groups (see Fig.3.5d). The profile was similar in controls and PTSD. From this we infer that compromised structural integrity, greater symptom severity and neurobehavioral impairments in individuals with PCS+PTSD could be associated with their documented mTBI, and that they are less likely just an extreme subset of PTSD.

All three groups demonstrated structural connectivity between these two regions via the following tracts: genu of the corpus callosum, bilateral cerebral peduncles, corticospinal tracts and anterior limbs of the internal capsules. It should be noted that even though these tracts were shared between groups, the comorbid group demonstrated significantly more breadth (perhaps implying less efficiency, and more diffusivity). Additionally, the PCS+PTSD group demonstrated structural connection via the pontine crossing tract (part of the middle cerebral peduncle), the right superior and anterior corona radiata, and the right superior fronto-occipital fasciculus. Both the control and comorbid group demonstrated shared structural connectivity in the fornix, the left posterior limb of the internal capsule, and the left external capsule.

3.4.3. Correlation between fMRI connectivities and non-imaging measures

Connectivity values of hippocampus-striatum path correlated significantly (see Fig.3.6) with neurocognitive functioning (neurocognitive-composite-index [NCI] and subtests) and PTSD symptoms (PCL5-score) and PCS severity (NSI-score), thus highlighting their relevance to underlying neuropathology. It was notable that correlations followed the expected trend: increase in severity and decrease in behavioral performance corresponded to higher SFC and lower vDFC.
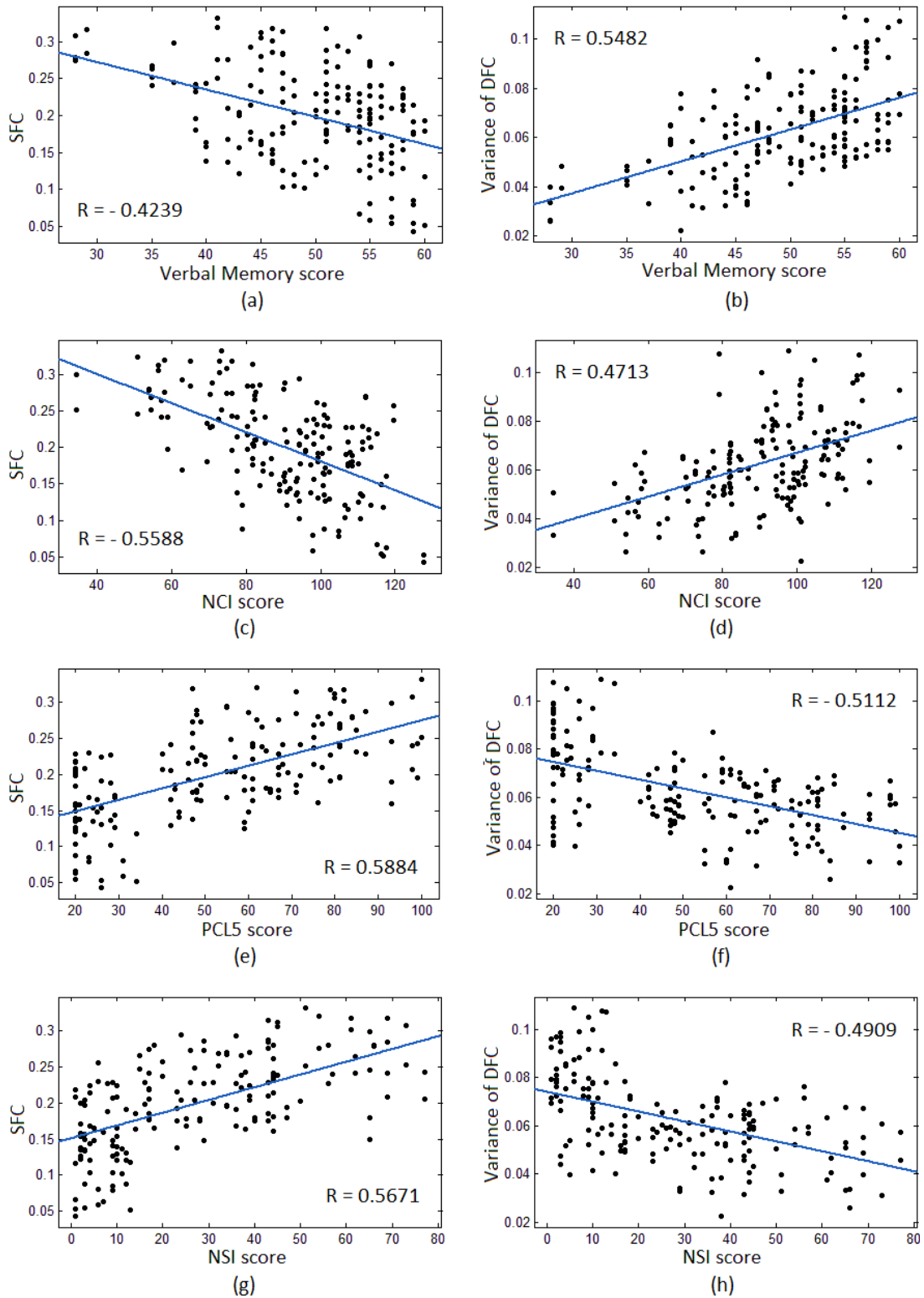
Fig.3.6 *Correlation between SFC values and (a) verbal-memory, (c) neurocognitive composite index (NCI), (e) PTSD symptom severity (PCL5) and (g) PCS symptom severity (NSI); correlation*

between variance of DFC values and (b) verbal-memory, (d) NCI, (f) PCL5 and (h) NSI. All correlations were statistically significant (numerical statistics in SI-3.3)

Here we present the correlation coefficient (R) between connectivity values and these measures, along with the p-value of correlation. We also present the mean (M), standard deviation (SD) and effect size (Cohen's d or Cd) for group-wise comparison of these measures, along with their p-values of separation. Behaviorally, the PCS+PTSD group (M = 47.26, SD = 7.88) had significantly lower scores in verbal memory compared to the PTSD group (M = 52.00, SD = 5.39; Cd = 0.65; $p = 1.76 \times 10^{-3}$); and the PTSD group (M = 52.00, SD = 5.39) had significantly lower scores in verbal memory compared to controls (M = 56.25, SD = 7.06; Cd = 0.66; $p = 3.17 \times 10^{-3}$). The PCS+PTSD group (M = 81.71, SD = 19.82) also had significantly lower scores in NCI score compared to PTSD (M = 94.33, SD = 11.50; Cd = 0.71; $p = 7.16 \times 10^{-4}$); and the PTSD group (M = 94.33, SD = 11.499) had significantly lower scores in NCI score compared to controls (M = 100.80, SD = 12.42; Cd = 0.54; p = .016).

These behavioral differences among the three groups are in accord with the pattern of neural differences in connectivity. This has significant implications that suggest a strong relationship between the clinical presentation and neurological functioning among groups (controls < PTSD < PCS+PTSD).

The PTSD and PCS+PTSD groups, when combined, showed significantly higher PCL5 scores (M = 66.31, SD = 17.10) compared to controls (M = 23.39, SD = 4.2; Cd = 3.09; $p = 3.64 \times 10^{-44}$). The PCS+PTSD group showed significantly higher scores in the NSI score (M = 43.41, SD = 15.24) compared to the PTSD and control groups combined (M = 13.11, SD = 13.7; Cd = 2.09; $p = 1.32 \times 10^{-29}$).

As mentioned before, the NCI score is an average of six behavioral measures. Table.3.3 summarizes the correlation of each of its six components with the connectivity values. We can see that the connectivities are significantly correlated with all of them.

The SFC values of hippocampus-striatum path across all subjects had significantly high negative correlations with several neurocognitive phenotypic measures, most notably with verbal memory score and NCI score. Additionally they had significantly high positive correlations with PCL5 and NSI scores. Similarly, the vDFC values had significantly high positive correlations with verbal memory and NCI scores, as well as significantly high negative correlations with PCL5 and NSI scores. Table.3.4 shows the correlation values and corresponding p-values of correlation between behavioral scores/symptom severity and connectivity values.

Table.3.3 *Correlation value (R) and corresponding p-value for the correlation of each of the six components of NCI score with SFC and variance of DFC*

Behavioral Measure	SFC		Variance of DFC	
	R	p-value	R	p-value
Reaction time	-0.2462	1.11×10^{-03}	0.1527	4.43×10^{-02}
Verbal memory	-0.4239	5.57×10^{-09}	0.5482	4.89×10^{-15}
Complex attention	-0.4415	1.07×10^{-09}	0.4017	3.93×10^{-08}
Cognitive flexibility	-0.5067	9.74×10^{-13}	0.4356	1.89×10^{-09}
Executive functioning	-0.5185	2.34×10^{-13}	0.4486	5.35×10^{-10}
Processing speed	-0.4801	2.04×10^{-11}	0.4252	4.97×10^{-09}

Table.3.4 *Correlation value (R) and corresponding p-value for the correlation of behavioral measures and symptom severity with SFC and variance of DFC*

Behavioral Measure	SFC		Variance of DFC	
	R	p-value	R	p-value
Verbal memory	-0.4239	5.57×10^{-09}	0.5482	4.89×10^{-15}
NCI score	-0.5588	1.11×10^{-15}	0.4713	5.25×10^{-11}
Symptom Severity				
PCL5 score	0.5884	1.37×10^{-17}	-0.5112	5.71×10^{-13}
NSI score	0.5671	3.43×10^{-16}	-0.4909	6.15×10^{-12}

3.4.4. Regrouping subjects based on connectivities

In line with our hypothesis, we postulated the following: (i) new diagnostic groups created based on separation of hippocampus-striatum path-weights would map better onto behavior (i.e. neurocognitive performance) as compared to original groups based on conventional diagnostic grouping and (ii) PTSD and PCS are spectrum disorders wherein symptom severity is likely to lie on a continuum, rather than forming distinct clusters; hence forming high diagnostic confidence groups (pure healthy and comorbid groups) and a low diagnostic confidence group (called intermediate group) has potential to be clinically useful. Hence, we devised a practical approach to regroup subjects into new diagnostic groups with the objective of maximizing heterogeneity of the intermediate group while simultaneously minimizing heterogeneity of pure-controls and pure-PCS+PTSD groups. This novel approach deviates from traditional ways of grouping subjects based on symptom reporting and clinical judgment.

The SFC and vDFC values of the hippocampus-striatum path showed strong statistically significant differences among the groups. In order to visualize the connectivity feature space, we

fitted a Gaussian bell-shaped surface for each group (see Fig.3.7). Connectivity values of individual subjects are embedded on the surface. It can be seen that there is a large overlap between the groups, albeit with a statistically significant mean difference between the groups. Therefore, the 2D example of the generic embedding procedure described in the methods section is directly relevant to this context, making the case for our proposed novel re-grouping procedure.
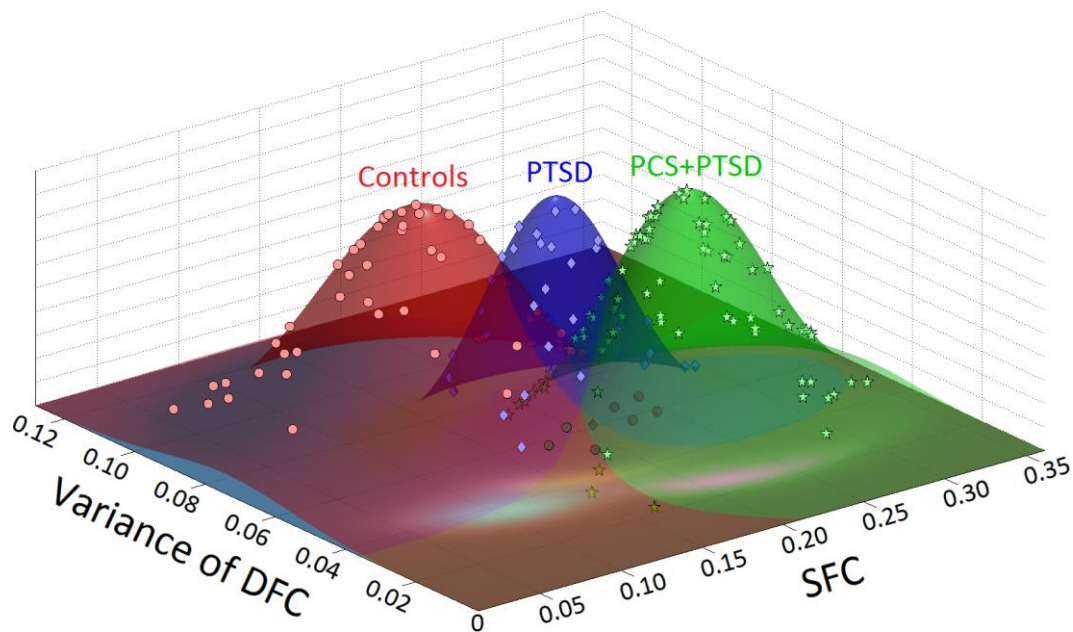
Fig.3.7 *Visualization of connectivity differences between the groups: Each group was fitted with a Gaussian bell-shaped surface using group mean and standard deviation of SFC and variance of DFC for the hippocampus-striatum path. Connectivity values of individual subjects are embedded on the surface.*

We regrouped the subjects using SFC and vDFC values of hippocampus-striatum path (see Fig.3.8a). Clearly there is a relatively narrow intermediate band where all PTSD-subjects are sandwiched along with borderline-controls and mild-PCS+PTSD subjects. Outside this band, we

find regions of the two pure groups. We observe a continuum with pure-controls merging with the narrow intermediate band, which later leads to the space of pure-PCS+PTSD.

In order to verify whether the imaging tools used for new grouping (viz. SFC and vDFC values) are a better classifier of PTSD and PCS than symptom-scores, and to assess the quality of new grouping, we compared statistical differences in the neurocognitive measures using new grouping against statistical differences obtained with conventional grouping (see Fig.3.8b). We observed that the p-values for all behavioral measures for all group-wise comparisons were consistently smaller with the new grouping. Additionally, controls (and PCS+PTSD) showed significant differences between pure group and transition group in several behavioral measures, which further supports our results. It is notable that the new grouping is based on underlying biology while conventional grouping is based on screening instruments. These findings demonstrate that the new grouping maps better onto neurobehavior than conventional grouping, indicating that SFC and vDFC values of hippocampus-striatum path may be a clinically significant marker of PTSD and PCS.

Upon regrouping the subjects based on connectivity values, we obtained a diversity of 70.1% in the intermediate group and 0% in the other two groups. PTSD subjects formed the majority in the intermediate group at 53%. Table.3.5 gives the distribution of subjects in the conventional grouping based on symptom severity scores, and the new grouping based on connectivity, along with percentage diversity for the new groups.

Table.3.5 *Distribution of subjects in the conventional grouping based on symptom severity scores and the new grouping based on connectivity: Columns 2-4 correspond to new grouping and rows 2-4 correspond to the conventional grouping. Row-5 gives the percentage diversity in the new groups.*

	Pure Controls	Intermediate	Pure PCS+PTSD
Controls	18	10	0
PTSD	0	17	0
PCS+PTSD	0	23	19
% diversity	0%	70.1 %	0%

(a)

1 = Control vs PTSD (old grouping) / Pure Control vs Intermediate (new grouping)

2 = PTSD vs PCS+PTSD (old grouping) / Intermediate vs Pure PCS+PTSD (new grouping)

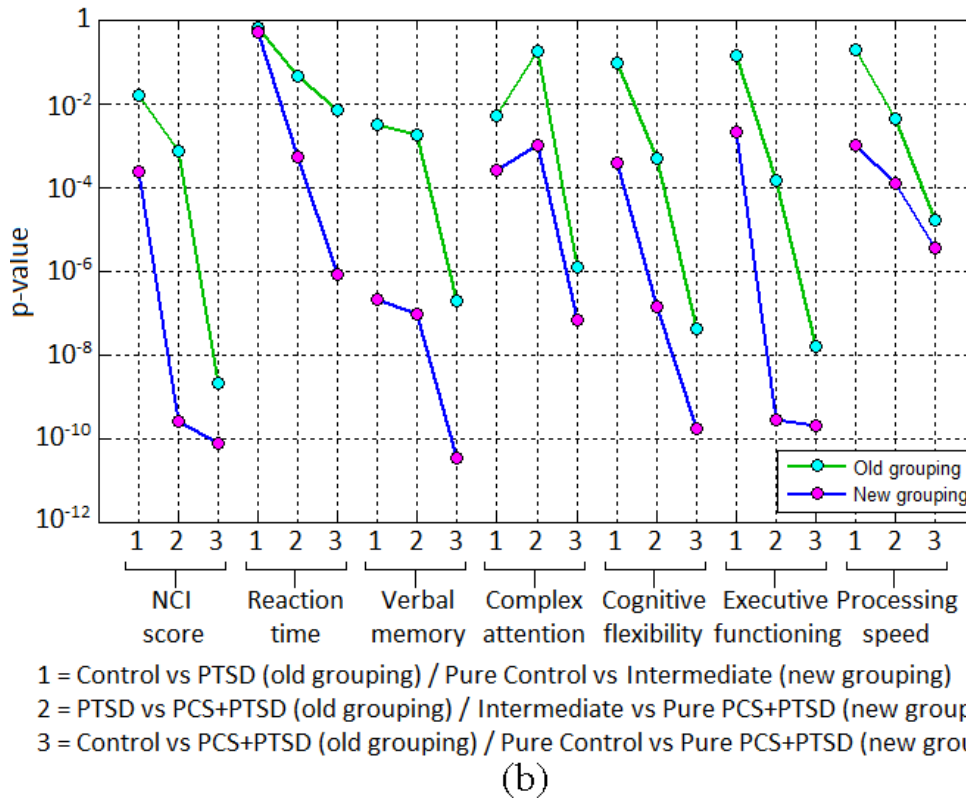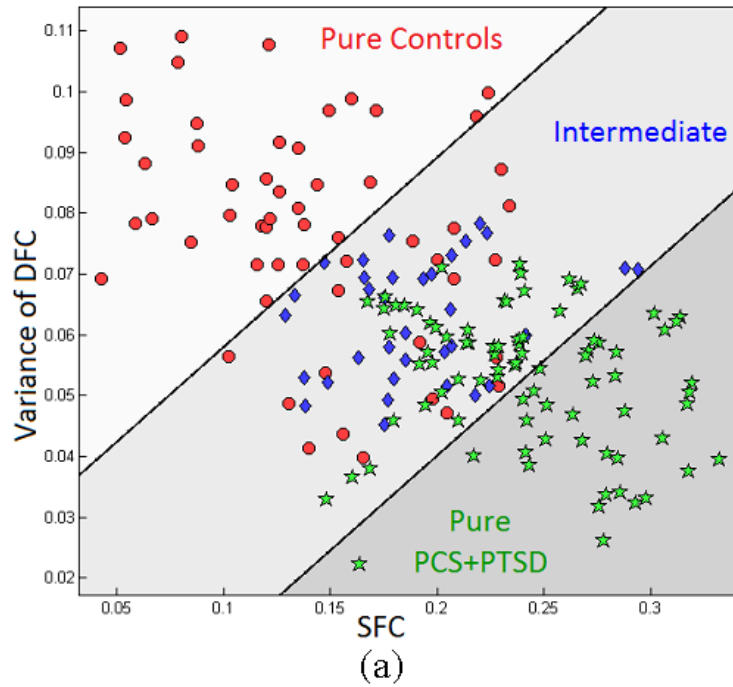3 = Control vs PCS+PTSD (old grouping) / Pure Control vs Pure PCS+PTSD (new grouping)

(b)

Fig.3.8 (a) *SFC and vDFC values of hippocampus-striatum path with new regrouping. The three new groups are shown in gray bands. Based on old grouping: red circles are controls, blue diamonds are PTSD and green stars are PCS+PTSD subjects, (b) Statistical significance (p-value)*

of behavioral measures with both conventional old-grouping and proposed new-grouping. Logarithmic scale is used for the y-axis of p-values. We observe that all behavioral measures consistently exhibit smaller p-value for all comparisons with the new grouping.

Mathematically defined regions for the new groups are as follows:

Pure Controls: $vDFC > 0.3122 \times SFC + 0.0268$

Intermediate: $0.3122 \times SFC + 0.0268 > vDFC > 0.3122 \times SFC - 0.0223$

Pure PCS+PTSD: $vDFC < 0.3122 \times SFC - 0.0223$

Fig.3.9 shows the mean and SD values of the NCI score and its components for both the conventional and the proposed groupings. This figure reiterates the findings of Fig.3.8b and shows that the new grouping resulted in important behavioral measures being separated farther apart between the groups with lesser variance.

It is also notable that control subjects in pure control and transition groups showed significant differences in several behavioral measures (see Table.3.6). A similar trend was observed between PCS+PTSD subjects in pure-PCS+PTSD and transition groups (Table.3.6). This shows that certain control subjects have behavioral and neurocognitive impairments, which puts them into the transition group, but the PCL5 symptom severity score does not diagnose them with PTSD. It is possible that the PCL5 score is not capturing those impairments in these subjects, or it is also possible that these subjects develop some other compensatory mechanism which renders them healthy, thus failing to get diagnosed with PTSD through the PCL5 score (similar logic goes with PCS+PTSD subjects).
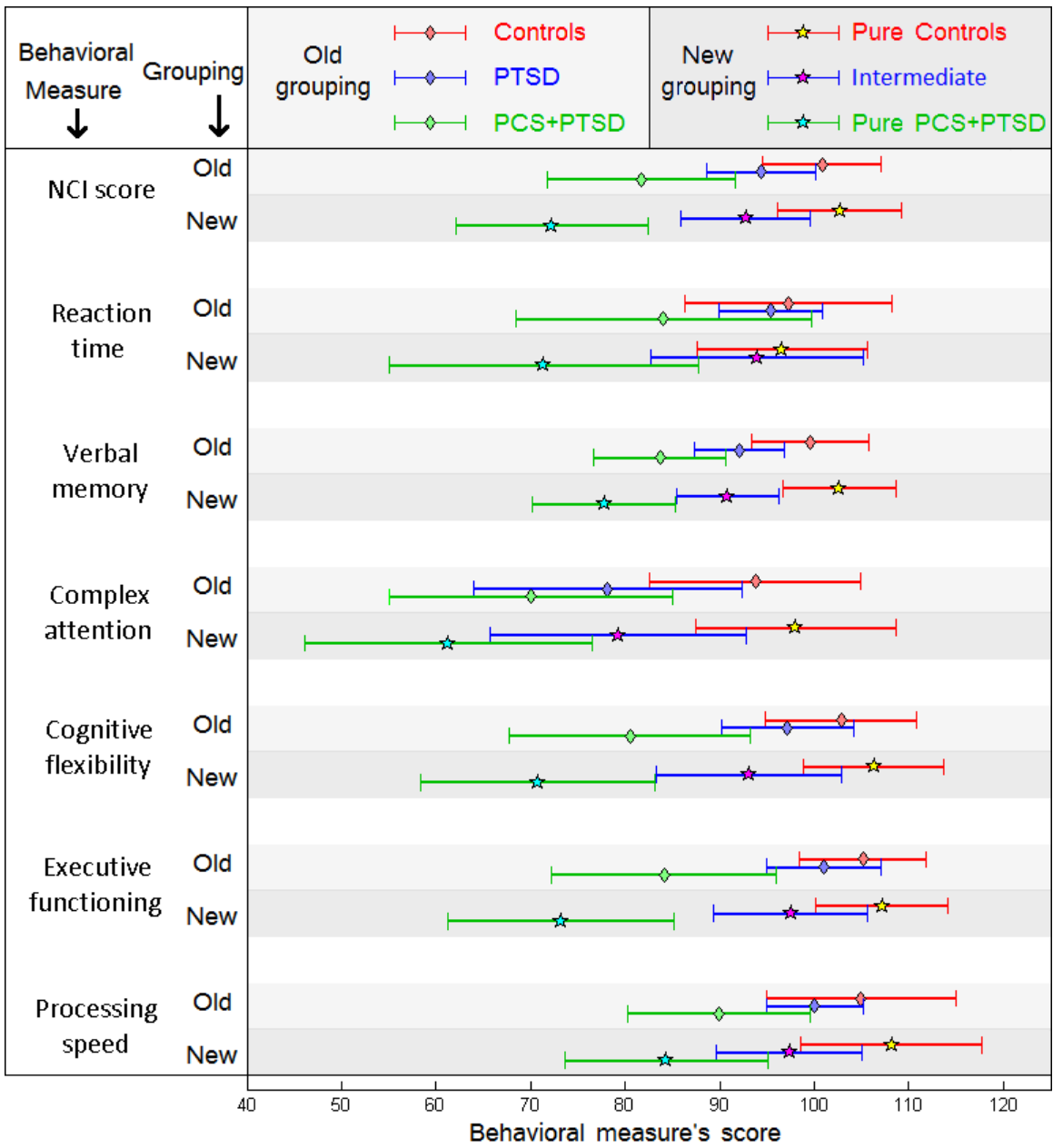
Fig.3.9 *Depiction of statistical separation of CNS-VS subtests and NCI scores for both old (conventional) grouping and new (proposed) grouping using mean and SD values*

Table.3.6 *Comparison of behavioral measures between subjects of pure group and transition group (for controls and PCS+PTSD subjects). Table provides the p-values (p<0.05) of statistical separation.*

Comparison	Non-imaging measure	p-value	Mean #1	Mean #2
Pure Controls (#1) vs. Transition Controls (#2)	Verbal memory	1.08×10^{-2}	101.67	85.70
	Complex attention	4.96×10^{-2}	98.06	86.00
	Cognitive flexibility	2.93×10^{-2}	106.28	96.60
	Epworth sleepiness scale	1.84×10^{-3}	7.06	10.10
	Zung anxiety scale	3.27×10^{-2}	27.89	31.10
	Combat exposure scale	3.32×10^{-2}	10.50	4.30
Pure PCS+PTSD (#1) vs. Transition PCS+PTSD (#2)	NSI score	7.15×10^{-3}	39.39	48.26
	NCI score	3.07×10^{-5}	89.56	72.21
	Reaction time	5.23×10^{-4}	94.57	71.37
	Verbal memory	3.68×10^{-4}	92.02	73.08
	Complex attention	1.51×10^{-2}	77.13	61.32
	Cognitive flexibility	1.07×10^{-3}	88.61	70.74
	Executive functioning	6.93×10^{-5}	93.13	73.21
	Processing speed	1.42×10^{-2}	94.57	84.32

3.4.5. Classification using support vector machine

Statistically significant neural signatures need not necessarily have generalizability or predictive ability, implying that statistically-significant (fitting our hypothesis) cum top-predictive connectivities assume higher importance. We thus used recursive cluster elimination based support vector machine (RCE-SVM) classifier [57] to identify the top-predictors.

Classification was performed for four different paradigms: classification using 32 non-imaging measures (NIMs) with i) conventional grouping, and ii) proposed grouping; classification using

whole-brain connectivities with iii) conventional grouping, and iv) proposed grouping. Table.3.7 summarizes worst-case classification accuracies along with top-predictive features. See Fig.3.10 for worst-case accuracies in every iteration. The corresponding results obtained by using average (instead of worst-case) classification accuracy are shown in Fig.3.11, which are obviously much better than the worst-case. However, in order to be conservative, we have emphasized worst-case results in this work.

Table.3.7 *Worst-case classification accuracies along with top-predictive features*

	Conventional Grouping	Proposed Grouping	p-values for column-wise comparison
Non-imaging Measures	70.79%	74.03%	5.42×10^{-11}
	Sleepiness and depression	NCI and verbal-memory	
Connectivity Values	79.78%	83.59%	1.11×10^{-13}
	SFC and vDFC values of hippocampus-striatum path		
p-values for row-wise comparison	7.12×10^{-26}	2.68×10^{-28}	

We observed that classification using connectivities provided significantly higher accuracy (about 9% more, p<0.05 Bonferroni-corrected) than classification using NIMs. This finding indicates that SFC and vDFC have better predictive ability in identifying subjects with PTSD and PCS compared to NIMs. With both NIMs and connectivities, classification with connectivity-based grouping provided higher accuracy (about 4% more, p<0.05 Bonferroni-corrected) than classification using conventional grouping. This implies that new groups derived using hippocampus-striatum path-weights not only map onto behavior better than PCL5 and NSI scores

(as shown in Fig 3.8), but also have increased predictive power to determine diagnosis of subjects irrespective of whether the features are based on connectivity or neurocognitive function.

Along with classification accuracies, the top-predictors which resulted in highest classification accuracy are also of considerable interest. The top NIMs with new grouping were the NCI-score and verbal-memory-score, which also resulted in 4% more accuracy. This further supports the notion that the connectivity-based grouping maps better onto neurobehavior and also attributes the two most important neurobehavioral measures (NCI and verbal-memory) with highest predictive ability. For classification using connectivities, SFC and vDFC values of hippocampus-striatum path were the top-predictive features. Prior to these findings, this path was attributed only with statistical significance between groups. Statistical significance does not necessarily guarantee predictive ability of connectivity features [78]. These results show that, in addition to statistical separation, this path also has the highest predictive ability, all obtained in a data-driven way from whole-brain connectivity data. For pictorial description of the entire pipeline and corresponding results, see Fig.3.1b.

(a)   (b)

Fig.3.10 *Worst-case classification accuracies obtained using recursively reducing number of discriminative features, with both old grouping (green) and new connectivity-based grouping (blue) using (a) non-imaging measures and (b) connectivity values*

(a)   (b)
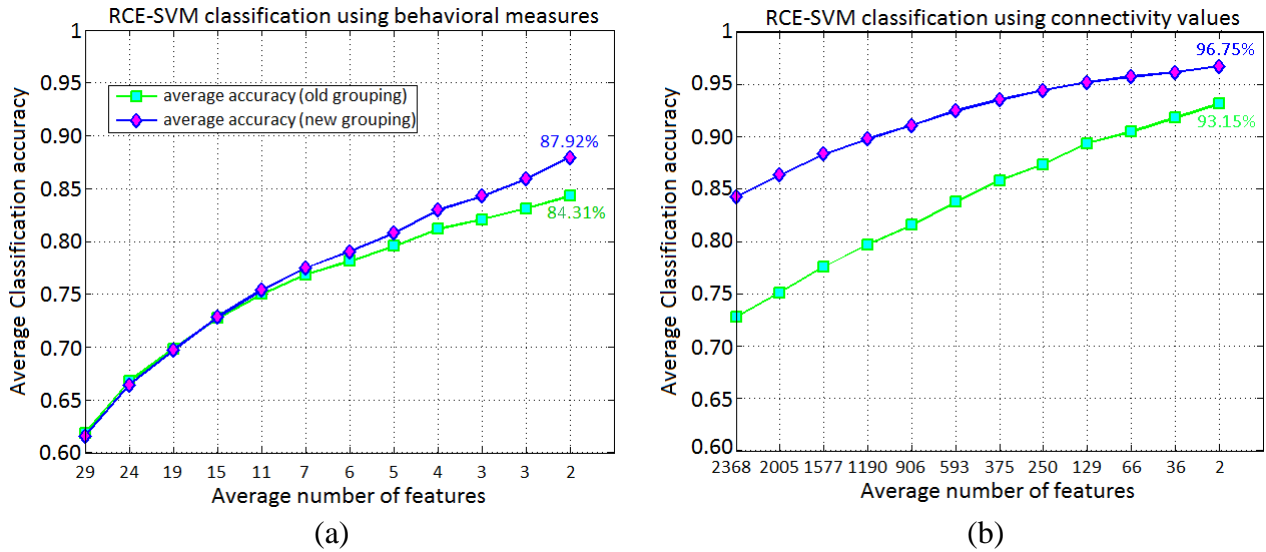
Fig.3.11 *Average classification accuracies obtained using recursively reducing number of discriminative features, with both old grouping (green) and new connectivity-based grouping (blue) using (a) non-imaging measures and (b) connectivity values*

We also performed classification by combining non-imaging measures and connectivities and using all of them as input features in the classifier. However results showed that they did not perform significantly better than classification using connectivities alone, and also the final accuracy was unchanged since the connectivities of hippocampus-striatum path remained the top classifying features (see Fig.3.12).
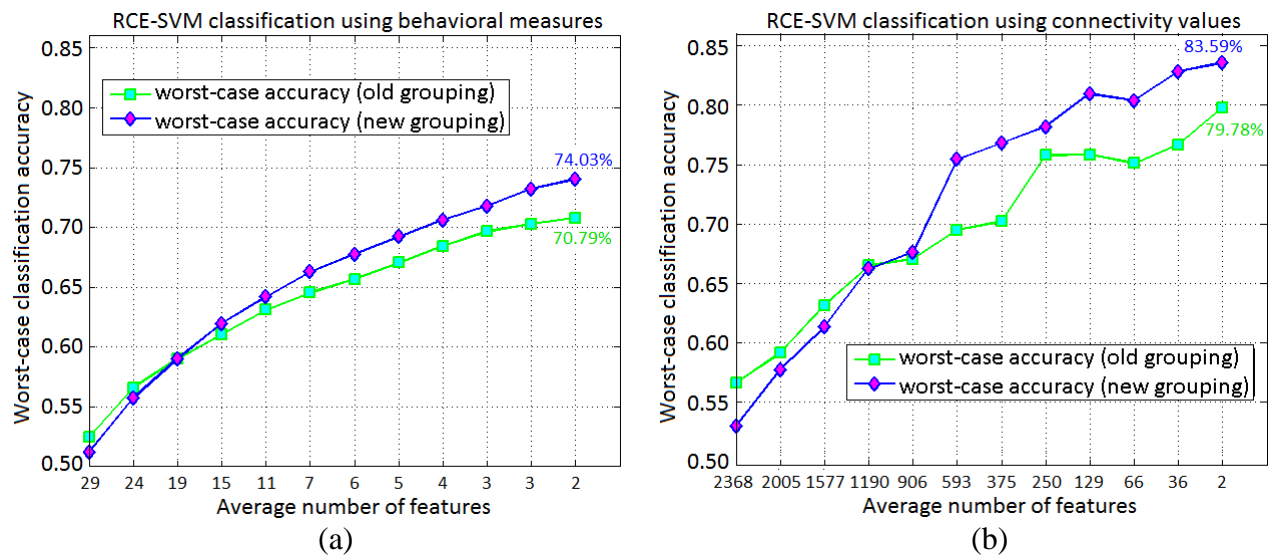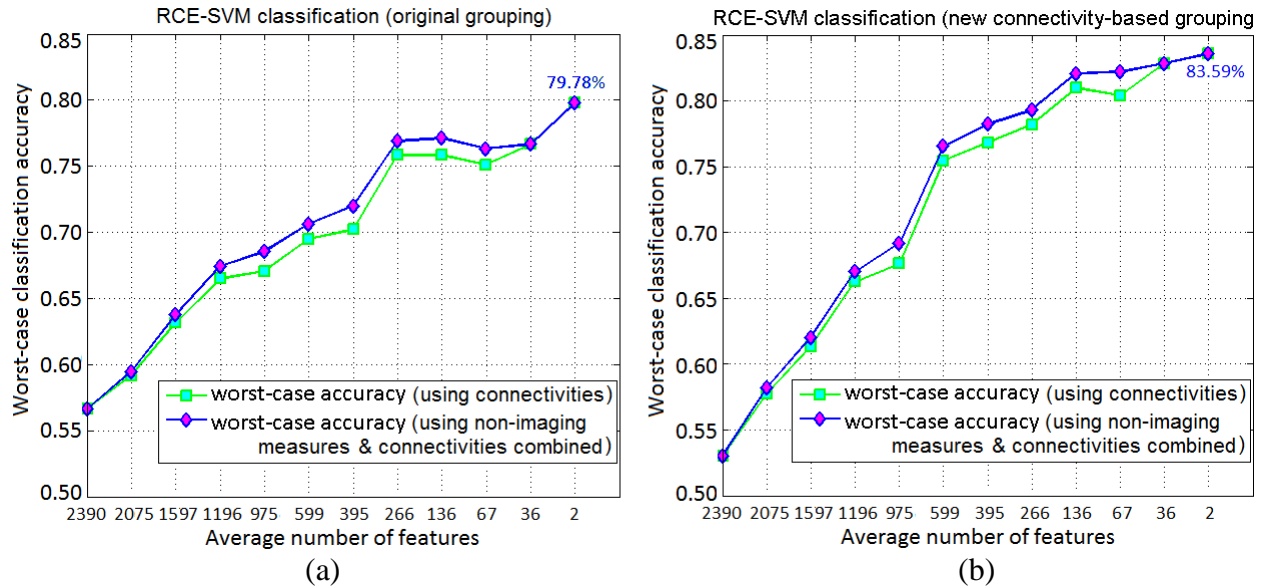
Fig.3.12 *Worst-case classification accuracies obtained using recursively reducing number of discriminative features using non-imaging measures and connectivity values combined (blue), compared with that using connectivity values alone (green), with both (a) old grouping and (b) new connectivity-based grouping*

3.5. Discussion

3.5.1. Evidence in favor of our hypotheses:

Our findings indicate perturbations in functional connectivity of hippocampal-striatal neural network associated with PTSD with/without PCS, indicative of an increased, yet less-variable drive between the regions, which supports our overarching hypothesis (Fig.3.1a). SFC and vDFC values also correlated significantly with neurocognitive measures and symptom severity. Furthermore, our results revealed directional concurrence in the differences in symptom severity, cognitive disruption, compromised connectivity, and diffusivity of related white-matter tracts between the groups, with PCS+PTSD being the most compromised, followed by PTSD then combat controls.

We also found support for three corollary hypotheses stated in the introduction. First, complementary to connectivity findings, DTI results confirmed greater diversity (hence, less integrity) of white-matter tracts between hippocampus-striatum in PCS+PTSD-group compared to both control and PTSD groups, suggesting a structural basis for PCS. Prior work shows affected white-matter integrity with left-striatum in subjects sustaining an mTBI [79]. This structural specificity implies that it is unlikely that the PCS+PTSD-group is an extreme subset of PTSD. Second, we regrouped the subjects based on SFC and vDFC of hippocampus-striatum path. We found that the p-values of separation among the three new groups were smaller for all behavioral measures for all group-wise comparisons compared to conventional grouping. Third, classification using new grouping provided significantly higher accuracy (~4% more) than conventional grouping. Further, the accuracies obtained by imaging measures were significantly higher (~9% more) than non-imaging measures for both conventional and new groupings. SFC and vDFC of hippocampus-striatum path were also the top-predictive features, in addition to being statistically significant.

3.5.2. Implications for advancing our mechanistic understanding of PTSD and PCS

Our results are interesting given that individuals with PTSD and PCS have cognitive impairments [38, 5] that reflect habit learning or procedural memory, which when impaired, is associated with perseverative thinking. While striatum is involved in this, the hippocampus is implicated in declarative memory. Both activation and connectivity studies have previously dealt with this aspect. Goodman *et.al.* [80] showed that traumatic memories relatively increase activation of striatum while decreasing activation of hippocampus, leading to a shift from declarative to habit formation. Moreover, Packard *et.al.* [81] showed that this impairing effect of

hippocampus-dependent memory effectively produces enhanced habit learning by reducing competitive interference between cognitive and habit memory systems; and this predominant use of habit memory is induced by stressful emotional states. In line with this finding, perseverative thoughts are also elicited by emotional states associated with stress in individuals with PTSD. Schwabe *et.al.* [82] showed that striatum-based procedural-memory is stress-promoted, meaning that stress induces shift from hippocampal to striatal memory. Taken together, these studies suggest that PTSD subjects perseverate on traumatic memories, more frequently and intensely than memories of other events, which leads to a habit-like response. Indeed, Spielberg *et.al.* [40] have shown that striatum is involved in re-experiencing issues seen in traumatized subjects. These observations could explain the involvement and interplay between striatum and hippocampus in PTSD-subjects. Both hippocampus and striatum have been implicated in mTBI and PTSD across several studies (see reviews [38, 5, 39, 83]). We postulate that there exists a fine balance between hippocampal and striatal activation implicated in the retrieval of memory, which determines relative emphasis placed on these memories. An imbalance in this mechanism might likely increase perseveration of intrusive memories associated with stress-related conditions [84].

Next, both structural and functional connectivity studies have investigated the memory network in PTSD and PCS. Memories of stressful negative life events, necessary for PTSD, alters the structural connectivity between striatum and hippocampus [85], which reiterates the structural basis for our findings. In support of our findings, Cisler *et.al.* [43] showed that there is increased SFC between hippocampus and striatum in PTSD-subjects during a 'repeated-exposure-to-traumatic-memory' task. However, one of our critical contributions is in showing that the hippocampus-striatum path has significantly low variability of connectivity over time in PTSD and PCS+PTSD groups. This indicates that there may be a lack of adaptability and regulation

between these regions, suggesting that PTSD is associated with a hyper-connectivity state, therefore, making it difficult to disengage from unwanted thoughts and feelings; a phenomenon which is often observed with habit formation. This mechanistic insight may be a valid explanation for clinical/behavioral manifestations in co-occurring PTSD and PCS.

In this study, we found correlations between connectivities and neurocognitive scores, as well as significant group differences in neurocognitive functioning. Looking with more statistical granularity, the greatest differences were found in Executive-Functioning (EF) and Cognitive-Flexibility (CF) indices. The EF measures performance in rapid decision management, recognizing rules and categories; and CF measures performance in adaptation to rapidly changing rules and information manipulation. As such, our results appear to be in accord with findings from Mattfeld and Stark [86, 87] which suggest functional contributions and interactions between hippocampus and striatum on tasks requiring learning of new arbitrary associations.

We have used this mechanistic understanding of altered neural circuitry to inform us about subject groupings which seem neurobiologically valid. Our regrouping strategy using connectivities has interesting implications for clinical settings wherein one could potentially obtain fMRI connectivity-values from a new subject and assign a diagnostic membership to the subject based on position of the subject's connectivities in our neurobiologically-informed-feature-space (NIFS) (see SI-3.4 for exact boundary equations). If the connectivities (SFC and vDFC of hippocampus-striatum path) are within the bounds of pure-control group in the NIFS, then the subject can be diagnosed as a control with high confidence (similar logic for pure-PCS+PTSD). If the connectivities are, however, within the intermediate group, then the subject's symptoms are likely due to PTSD. Yet further investigation is needed to validate this method. Such a classification could improve diagnostic accuracy above and beyond traditional classification.

Future studies should focus on generalizing these results by replicating it in a large sample, so that they could be used clinically as biomarkers.

Interestingly, SFC and vDFC of hippocampus-striatum path resulted in highest classification accuracy. They were also identified as the top-diagnostic features, which was determined in a data-driven way from whole-brain connectivity data. This demonstrates that they could be a better marker of neural and behavioral characteristics of PTSD and PCS than just PCL5 and NSI scores, and have potential as imaging biomarkers for these disorders. Our "potential biomarker" satisfies three of the four conditions described by Woo *et.al.* [88] to be satisfied by a good biomarker (diagnosticity, interpretability and deployability). As regards the fourth condition (generalizability), based on suggestion in Woo *et.al.*, we issue an open call for researchers having similar data to share with us so that the classifier can be tested on them.

3.5.3. Limitations and Future Work

We note a number of limitations and caveats which must be kept in mind while interpreting the results presented here, and simultaneously suggest how future studies may address those issues: (1) In accordance with our hypothesis, we observed that connectivity values were more extreme in the case of PCS+PTSD compared to PTSD alone, and that they also correlated significantly with all the behavioral/symptom severity scores. This shows that subjects who had the added burden of PCS along with PTSD had higher symptom severity than subjects with only PTSD, and also showed higher SFC and lower DFC values as compared to PTSD. Additionally, our DTI results clearly show that mTBI may lead to more severe symptomatology due to structural changes, which might explain why the PCS+PTSD group is more extreme than the PTSD group. Although

there is limited literature on comorbid imaging studies of PCS and PTSD, we speculate that: (i) the burden of a prior mTBI exacerbates PTSD-related brain alterations which were potentially already prevalent in these subjects before developing PCS or, (ii) subjects who sustain mTBI and concomitantly or subsequently had a traumatic experience will end up with greater functional neural alterations which correspond to higher symptom severity than subjects who experienced psychological trauma alone. Future experimental designs must aim to untangle the underlying causal mechanisms in comorbid PTSD and PCS in order to confirm either of the two scenarios. (2) The structural specificity for PCS in subjects who had sustained an mTBI implies that the comorbid group being an extreme subset of PTSD is unlikely. However, future studies must verify this finding in subjects with mTBI/PCS, but without PTSD. (3) Our findings were based on results obtained from military subjects with combat exposure. Having a control population with combat exposure is a unique contribution since it provides a more representative control group. Indeed, a recent study revealed differences in resting state fMRI connectivity patterns between civilian and combat controls [89] "potentially due to military training, deployment, and/or trauma exposure." Therefore, further work needs to be done to verify whether these results are applicable to non-combat-related (or civilian) PTSD and PCS. (4) Only male veterans were studied, thus our findings cannot be generalized to female soldiers. In order to ascertain diagnostic utility of the connectivity values of hippocampus-striatum path and apply these methods in clinical settings in the future, the results need to be replicated on a much larger sample size, which is more representative of the target population in terms of gender, ethnicity, etc. (5) Future studies with the targeted populations could specifically address the habit systems and declarative systems separately, with behavioral measures involving probabilistic classification (e.g., the weather prediction task) which are sensitive to such shifts [90, 91]. (6) Time since concussion for PCS subjects was not available. It

is possible that it might correlate with SFC and vDFC values. Also, the data was acquired from the subjects only on one instance. Longitudinal studies could focus on the behavior of the connectivities of hippocampus-striatum path over the advancement, recovery and rehabilitation phases of subjects with PTSD with and without PCS. This will be an appropriate test for validating striatum-hippocampus SFC and vDFC as a candidate imaging biomarker for PTSD and PCS+PTSD.

CHAPTER 4

Identifying Disease Foci from Effective Connectivity

4.1. Introduction

Brain imaging provides insight into the functional neuroarchitecture associated with neurological conditions such as mild traumatic brain injury (mTBI) and posttraumatic stress disorder (PTSD) [12], both prevalent in military service members. However, much of our understanding of the brain is organized around properties of neural regions, whereas our knowledge of the complex connections between the various regions is not as mature. Given that connectivity contains mechanistically pertinent information not available through functional Magnetic Resonance Imaging (fMRI) activation studies, attaining region-specific information from connectivity data could advance our understanding of the neural circuitry and associated brain processes. Additionally, large effects in natural systems are often caused by a few isolated sources; identifying these source(s) of disruption could greatly mitigate the distributed network abnormalities. Hence, we have developed a novel framework to identify affected pathological foci from directional brain networks, which likely represent the source(s) of dysfunction in a given disorder. We illustrate the approach with data obtained from soldiers with PTSD and post-concussion syndrome (PCS, a chronic outcome of mTBI).

Exposure to blasts and subsequent concussions result in mTBI, which has a high comorbidity with PTSD [15, 92]. As of September 2014, over 2.7 million Americans have served in Iraq and Afghanistan, of whom about 20% developed PTSD, 19% acquired TBI, and 7% acquired both [1]. With current diagnostic procedures and treatments centering on subjective assessments, a thorough

understanding of the mechanistic basis for both PTSD and PCS symptom presentation is essential for accurate diagnosis, targeted treatments, and return-to-duty decision making. Due to largely overlapping symptomatology between PCS and PTSD [11], it is imperative that objective connectivity markers of the respective neuropsychiatric and neurologic conditions are identified and validated in order to improve clinical evaluation and treatment outcomes. In this work, we study group-level differences between PTSD, PCS+PTSD (comorbid group having both PCS and PTSD) and healthy combat controls.

Several studies have identified [93] certain key frontal and subcortical areas, among others, and associated connections which are impaired in both PTSD and mTBI. However, a mechanistic explanation of the affected network architecture in PTSD with and without mTBI is still under development. Specifically, given that network disruption often arises from alterations in a few focal areas, segregation of such sources of network disruption from the connectivity changes which happen as a consequence of them, has been elusive. Since such foci are part of the affected network, the disruption is propagated to other regions connected with the foci. Therefore, we investigate the foci of network disruption, in addition to characterizing connectivity alterations associated with them.

While functional connectivity (FC) is popularly used to study brain networks, there is a need to identify networks with causal relationships rather than co-activation. Underlying network interactions could be causal in nature in addition to (or rather than) being synchronous, which are shown to exist even in fMRI timescales [94]. As such, it is important to discover causal networks in addition to co-activation networks for a more complete characterization. PTSD and mTBI are generally seen as frontal dysregulation disorders [93], in which directional (or causal) influences

originating from frontal areas are impaired. This further motivated us to employ directional connectivity based on causality.

Effective connectivity (EC) refers to directional influences among brain regions [94]. Granger causality (GC) is an exploratory technique used to quantify EC between brain regions [95]. It is the most widely used approach to quantify causal influences in natural systems [96] including, but not limited to, epidemiology, molecular biology, econometrics, evolutionary biology, climate science, computer networks, linguistics and brain science [97]. GC has the advantage that it is a data driven approach and there are no requirements for specifying connectivity priors like in dynamic causal modeling (DCM) [94, 98, 99, 100]. It would be practically impossible to build a DCM model with priors for whole-brain connectivity as it would be computationally not feasible [101]. Both recent simulations [102, 103] and experimental results [104, 35, 105] indicate that GC applied after deconvolving the HRF from fMRI data (as we have done), is reliable for making inferences about directional influences between brain regions. This method has also been employed in several recent fMRI studies [106, 107, 108, 109, 110, 111, 112, 113, 114].

Most studies investigate EC or directional brain connectivity by assuming connectivity to be temporally stationary. Dynamic fluctuations of connectivity are not captured when using static connectivity. Given that mental processes happen within a few milliseconds to seconds' time, while an fMRI scan lasts for several minutes, it is natural that connectivity fluctuates over time, and that such variations carry biologically relevant information [115], which is distinct from that represented by static connectivity [116]. Previous studies in PTSD and mTBI have not utilized dynamic connectivity information in a manner that extends our understanding based on the information obtained from conventional static connectivity. In this study, we used static EC (SEC) as well as dynamic EC (DEC) measures [106].

66

Upon obtaining these whole-brain connectivities, we used a probabilistic framework to identify affected foci, i.e. regions which could possibly be the primary sources of disruption which is then transmitted to other areas via the underlying directional network. We adopted a technique developed recently for FC data [117], and made specific modifications to the model formulation to make it suitable for both EC and dynamic connectivity data. The modifications were necessary because the probability distributions of EC and FC metrics are different, in addition to the fact that, unlike FC, EC is directional in nature. The method is based on the concept that affected foci are associated with a large number of affected connections. It identifies dysfunctional foci and also provides associated dysfunctional connections.

We constructed separate brain networks using strength (SEC) and temporal variability (variance of DEC [vDEC]) of directional connectivity, and then used them to identify diseased foci separately. The obtained foci for SEC and vDEC were then overlapped (intersection) to obtain final foci which had both altered SEC and vDEC. The dysfunctional connections associated with the foci were obtained and overlapped in a similar manner, but with certain restrictions as described next.

It has been shown that lower temporal variability of connectivity is associated with both neurologic and psychiatric conditions [116, 118, 119, 120] often presenting as a lack of cognitive flexibility. Reduced temporal variance in DFC is associated with psychiatric disorders as well as compromised behavioral performance in healthy individuals [63, 116]. This reduction is associated with compromised ability to dynamically adjust (e.g. behavior, thoughts, etc.) to changing conditions. This phenomenon is well recognized in other biological systems such as reduced heart rate variability being a marker of cardiovascular disease [121]. Since external influences and internal body states are continually changing, a healthy biological system varies its activity in real-

time to accommodate these changes. In these terms, "frozen" connectivity reflects compromised brain health. Such connectivity characterization has been employed in recent works, with higher connectomic flexibility being associated with favorable/better task performance in healthy adults [116] and psychiatric disorders [122]. In this work, we identified connections with altered SEC and lower vDEC in the disorders compared to controls.

Additionally, PCS+PTSD was a more severe group compared to the PTSD group, owing to the added burden of mTBI. It is noteworthy that mTBI is a result of pressure waves arising from a blast and PCS is a behavioral syndrome which is a consequence of that. Therefore, unlike TBI wherein the spatial location of injury can be different in different subjects, the common behavioral manifestations among subjects with PCS and mTBI suggests that it is likely to have common sources of neural network disruption in their brains. Also, evidence shows that mTBI increases the severity of PTSD [123]. Hence we looked for paths associated with the affected foci, which had reducing vDEC and altered (either monotonically reducing or monotonically increasing) SEC as we moved from Control to PTSD to PCS+PTSD. We hypothesized that PTSD with and without mTBI is characterized by certain affected regional foci, and those foci are associated with connections having altered strength and lower variability of directional brain connectivity (see Fig.4.1 for an illustration of our hypothesis). The foci were identified using whole-brain connectivity data, while the affected paths conforming to our hypothesis were restricted to those connections which were associated with the foci. Notably, we tested the hypothesis in a data-driven manner using resting-state fMRI which is not task dependent.
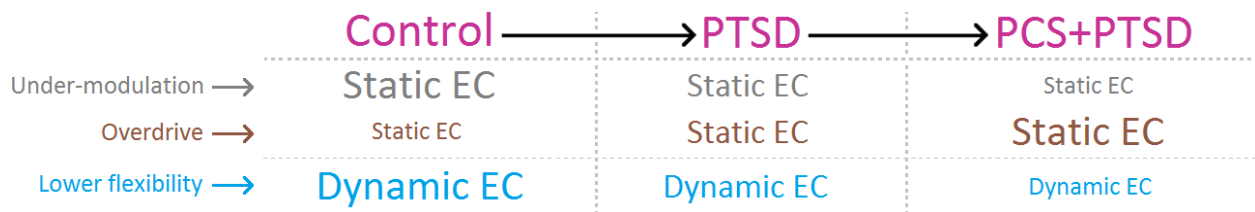
	Control ──────→	PTSD ──────→	PCS+PTSD
Under-modulation ──→	Static EC	Static EC	Static EC
Overdrive ──→	Static EC	Static EC	Static EC
Lower flexibility ──→	Dynamic EC	Dynamic EC	Dynamic EC

Fig.4.1. *Illustration of our hypothesis showing monotonically reducing variability of vDEC, and either increasing or decreasing SEC as we move from Control to PTSD to PCS+PTSD. Font sizes are symbolic of the increasing/decreasing trend.*

For the paths which fit our hypothesis, we sought to assess their behavioral relevance, hence their connectivity values were correlated with neurocognitive scores and symptom severity in PTSD and PCS.

Our hypothesis is based on an analysis framework, which relies on statistical separation between groups. However, statistical separation of between-group connectomics does not necessarily imply that they have predictive diagnostic ability [57]; that is, they may not be able to predict group membership at an individual level with reasonable accuracy. Consequently, those connections which are both statistically significant and possess the discriminative power to classify subjects with high accuracy are more powerful. Several studies report that machine-learning classifiers can be successfully used on fMRI data for diagnostic prediction, including, but not limited to, major-depressive-disorder [58], Parkinson's disease [59], PTSD [60], dementia [61], autism [62] and prenatal-cocaine-exposure syndrome [57]. However, to the best of our knowledge, there are no studies which have used connectivity markers in the classification of both PTSD and mTBI subjects. For neurological disorders like PTSD and PCS, classification using neuroimaging signatures could be applied to obtain more accurate diagnoses by assisting the clinician with additional information. Therefore, using whole-brain connectivity data we identified, in a data

driven way, those features which predict the diagnostic membership of a novel subject with high accuracy. We specifically investigated whether there was an overlap between connectivity paths satisfying the primary hypothesis (Fig.4.1) and those identified as having high predictive ability. We hypothesized that (secondary hypothesis) these paths will better predict the diagnostic membership of a novel subject than non-imaging measures (behavioral, neurocognitive and self-report measures), thus highlighting their relevance to the neuropathology of PTSD and mTBI. We lay emphasis on dysfunctional foci and their associated connections which have high statistical separation as well as high predictive ability in addition to having behavioral relevance.

4.2. Effective Connectivity Analysis

4.2.1. Granger Causality

Whole-brain SEC was obtained using Granger causality (GC) [95]. GC is an exploratory technique used to quantify directional influences between brain regions. The underlying concept is that, if past values of a timeseries "T1" can, in a mathematical sense, predict the future values of another timeseries "T2", then a causal influence from timeseries T1 to timeseries T2 is inferred [124]. GC employs a multivariate vector autoregressive (MVAR) model to quantitatively predict one timeseries using the other, which is briefly described next.

Given a system defined by k different timeseries $X(t) = [x_1(t), x_2(t), \ldots x_k(t)]$, with k being 125 ROIs in this study, the MVAR model of order p is given by:

$$X(t) = A(1)X(t-1) + A(2)X(t-2) + \cdots + A(p)X(t-p) + E(t) \tag{4.1}$$

Where *E(t)* is the model error and *A(1) ... A(p)* are the model coefficients. The coefficients were estimated through multivariate least squares estimation, which calculates the optimal set of coefficients that minimizes the model error in the least squares sense. Model order *p* must be chosen either by employing a mathematical principle such as the Bayesian Information Criterion (BIC) [100] or based on the requirements of the application under consideration. In neuroimaging, the interest is in causal relationships within neural delays of a TR [107], thus we chose a first order model. Since fMRI's temporal resolution is low, a first order model is shown to capture the most relevant causal information [94].

Coefficient *A(p)* indicates the degree to which the past *X(t-p)* can predict the present *X(t)*. Then, the sum of coefficients of all delays would represent the degree to which all the past values together can predict the present. This formulation is used to evaluate GC by predicting the present value of timeseries-2 (T2) using the past values of timeseries-1 (T1). If, for example, the sum of resulting model coefficients is large, then it implies that T1 can predict T2 very well. If T1's past can predict T2's present then that implies a causal relationship from T1 to T2. As in previous studies [125], GC was derived formally, based on the model coefficients, as:

$$GC_{ij} = \sum_{n=1}^{p} a_{ij}(n) \tag{4.2}$$

Where GC_{ij} is the SEC value from ROI *i* to ROI *j* and a_{ij} are the elements of matrix *A*. It is notable that a single coefficient matrix is obtained for the entire duration of data, and the coefficients do not vary over time. This traditional formulation of GC was slightly modified, as in earlier studies [95], to remove the effect of zero-lag cross-correlation between timeseries. For this, we included the zero-lag term in Eq.1 as shown below.

$$X(t) = A'(0)X(t) + A'(1)X(t-1) + A'(2)X(t-2) + \cdots + A'(p)X(t-p) + E(t) \qquad (4.3)$$

The diagonal elements of $A(0)$ are set to zero, such that only the instantaneous cross correlation, and not auto correlation, between the timeseries are modeled. The model coefficients obtained from Eq.3 would not be equal to those obtained from Eq.1, since the inclusion of zero-lag term affects other coefficients by removing cross-correlation effects from them. The zero-lag term is thus not used in the evaluation of GC. GC thus obtained would be free from zero-lag correlation effects and is defined as correlation-purged GC (CPGC), which has been widely used in recent times (for example, see [126, 127]). A 125×125 SEC matrix was obtained for every subject by employing CPGC.

Next, DEC was obtained using time-varying dynamic Granger causality (DGC), evaluated in a Kalman filter framework. We employed a dynamic multivariate vector autoregressive (dMVAR) model for estimating DEC [106, 109]. The model is 'dynamic' because, unlike CPGC formulation, its model coefficients vary as a function of time. Here, DEC is the time-varying physiological process, which is quantified through the DGC measure, which employs the dMVAR model solved in the Kalman filter framework. In DGC, coefficients $A'(p)$ are allowed to vary over time, thus giving coefficients $A'(p,t)$ in the dMVAR model as:

$$X(t) = A'(0,t)X(t) + A'(1,t)X(t-1) + \cdots + A'(p,t)X(t-p) + E(t) \qquad (4.4)$$

The dynamic model coefficients are estimated in a Kalman filter framework using variable parameter regression [128]. DGC is then computed as:

$$DGC_{ij}(t) = \sum_{n=1}^{p} a'_{ij}(n,t) \qquad (4.5)$$

72

Where DGC_{ij}(t) is the DEC value from ROI i to ROI j at a given timepoint t, and a'_{ij} are the elements of matrix A'. We compensated for zero-lag cross-correlation effects here also, like in CPGC. Given that our data had 1000 timepoints, we obtained a 125×125×1000 DEC matrix for every subject by employing DGC.

Recent simulations [102, 103] as well as experimental results [104, 35, 105] suggest that GC applied after deconvolving the HRF from fMRI data (as we have done), is reliable for making inferences about directional influences between brain regions. This method for obtaining SEC and DEC has also been employed in several recent fMRI studies [106, 107, 108, 109, 110, 111, 112, 113, 114]. Variance of DEC (vDEC) was taken as the measure of variability in directional connectivity over time (125×125 matrix per subject), which, along with SEC, was used further in identifying disease foci. To comprehend the idea of SEC and DEC from a neuroimaging standpoint, we provide an illustration using a simple example of a pair of real fMRI timeseries (please see Fig.4.2).
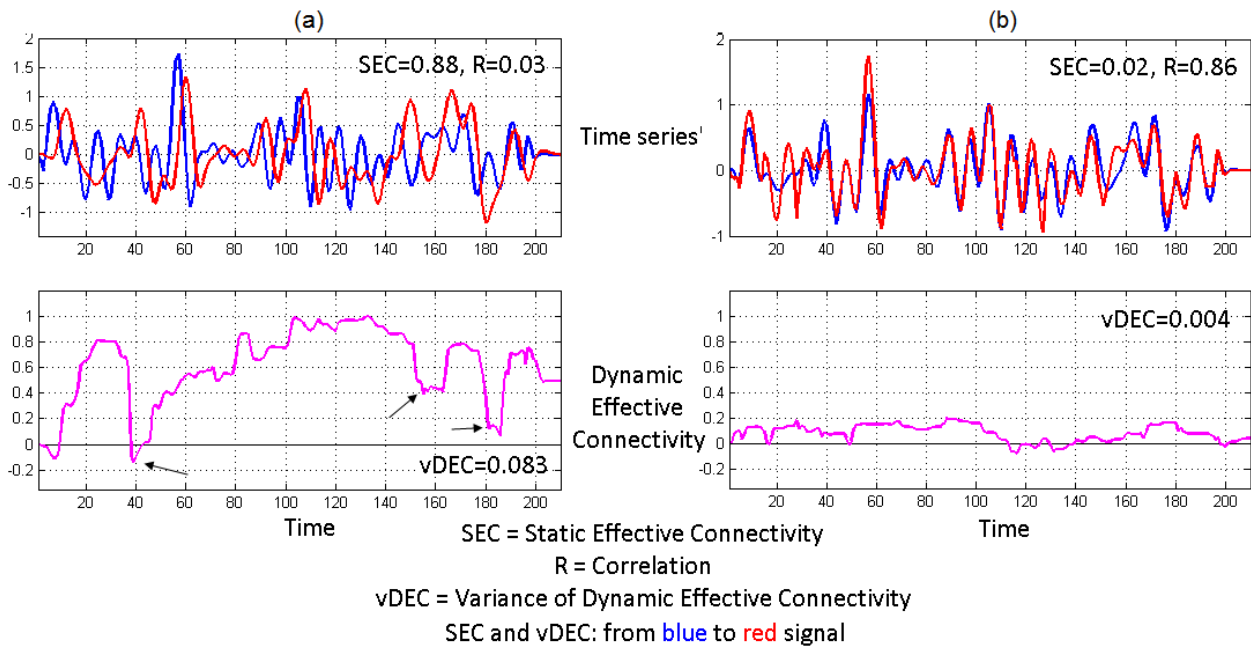
Fig.4.2. *Illustration of SEC and DEC from a neuroimaging standpoint using two real fMRI timeseries. In (a), the red timeseries consistently seems to follow after the blue timeseries, indicating that red's associated brain region activates (and deactivates) as soon as blue's region activates (and deactivates), hence a causal influence and a high SEC value (note that correlation is low). DEC provides further insight, which shows that steady causality is maintained mainly in the middle phase and that causality is lost on three brief instances (where it dips due to observable loss of causality between the timeseries' of those sections [please follow the arrows]). This variability is quantified in vDEC. In (b), the two timeseries are nearly overlapping hence highly correlated. But the variations in red timeseries do not occur after (or before) the variations in blue timeseries (and vice versa). This lack of causal relationship gives low SEC value. Correspondingly, DEC values linger around the zero-mark since causal relationship does not seem to emerge at any point in time.*

4.2.2. Identifying Disease Foci

As noted earlier, connectivity modeling identifies interrelationships through connections, while our insights on the brain center on functions of regions. Hence we sought to identify disrupted regional foci in PTSD and mTBI using EC data.

We used a Bayesian probabilistic model to identify disorder foci from connectivity data [117], which assumes that disrupted regions are associated with large number of abnormal connections. The efficacy of this method has been demonstrated earlier with simulations as well as real fMRI data, in particular using static functional connectivity (FC) [117]. However, their model made certain assumptions on the priors, which were suited for FC data's probability distribution. Here we extend this method to identify disease foci using both static and dynamic EC, albeit with certain

modifications in the model formulation given that EC matrices are not symmetric, unlike FC, and that the distributions of FC and EC data are dissimilar, and static and dynamic connectivity data have dissimilar distributions. We explain the method briefly before addressing these issues. For a detailed account of the method, please refer to Venkataraman et al. [117].

The model was developed for FC. FC is seen as a latent phenomenon with three distinct states: positive connection (+1), negative connection (-1) and no connection (0). FC obtained from fMRI is seen as a noisy measurement of the unknown latent FC. The model makes the following three assumptions: (i) a connection between two disease foci is abnormal with probability 1, (ii) a connection between two non-affected regions is normal with probability 1, and (iii) a connection between a disease focus and a non-affected region is abnormal with probability p. Upon initiating the model with standard priors, variational expectation maximization (EM) algorithm is employed to solve for the model parameters. The model produces posterior probabilities for every region and every connection, using which diseased foci and connections can be identified.

SEC's probability distribution resembled a Gaussian, similar to correlation. While correlation usually has a distribution with mean±SD of 0±0.25, SEC's distribution had mean±SD of 0±0.19, which is acceptable. But it is not a bounded measure, unlike correlation which is bounded by [-1,1]. The model assumes a tri-state distribution, with default states set to [-1,0,1]. In our entire data, we found a very small number of SEC values which were greater than 1 or smaller than -1 (0.0026%). We wanted to avoid its negative impact on model evaluation, as well as ensure reliable results. Hence, we replaced each such value (which corresponds to one connectivity path in one subject) by the group-average SEC value for that connectivity path. Similarly, in vDEC, we replaced any values not within range by the corresponding group average (0.0053% of values). With both SEC and vDEC, the connectivity matrix is asymmetric, unlike FC which is directionless.

Hence the entire matrix was fed into the model, unlike with FC where only the lower or upper triangular part would be used. Put together, these modifications allowed the model to be applied to effective connectivity as well as dynamic connectivity data.

The model was evaluated for one thousand runs and statistical significance of foci were determined based on a non-parametric permutation test. We took the entire dataset and randomly assigned groups. We then fit the model using the standard approach and extracted the posterior probabilities of each region being diseased with random group assignment. This was repeated (randomly assigning labels, fitting model, extracting posterior) for 10000 iterations to obtain the posterior null distribution for each region. The p-value for each region was then the proportion of the thousand runs for which the null posterior (i.e. random assignment) was greater than what foci posterior we had observed when we fit the model with the true labels. We thus obtained significantly affected disease foci in the disorders (p<0.05, Bonferroni corrected).

The method also provided affected connectivities associated with the disease foci, which would help in interpreting affected networks from the point of view of the dysfunctional foci. Among such connectivities, we retained only those connections which crossed our statistical significance threshold for effective connectivity values outside of the foci method, in accordance with our primary hypothesis (p<0.05, whole-brain FDR-corrected). Differences were controlled for age, race, education and head-motion (using mean frame-wise displacement obtained across all brain voxels for each subject as defined by Power et al. [65]). This was done to ensure that, irrespective of the model used by us, the significant connections which emerge in this work would have crossed whole-brain multiple comparisons corrected statistical threshold like in most studies, in addition to the fact that the model quantitatively selected these paths using the posteriors. This ensured that

our results conformed to multiple layers of verification and statistical standards, in addition to providing novel insights through the foci method.

This model is applicable only for comparison between two groups. Since we were comparing three groups, we overlapped the foci and connections obtained in the three pairwise comparisons to extract only the common foci and connections (intersection). In statistical sense, this was the most conservative approach possible. In accordance with our hypothesis, we identified those paths associated with the dysfunctional foci which exhibited altered SEC (either reducing only or increasing only) and lower vDEC as we moved from Controls to PTSD to PCS+PTSD. Such a network would disentangle the effects of PTSD as well as comorbid PTSD and mTBI, providing novel insights through directional and dynamic connectivity.

4.2.3. Behavioral Relevance of Connectivity Values

In order to assess the behavioral relevance of connectivity values, we first correlated SEC and vDEC values of each of the identified paths with symptom severity in PTSD (PCL5 score) and PCS (NSI score), and neurocognitive functioning (NCI score and subtests). Neurocognitive functioning (e.g. cognitive flexibility, executive functioning) is affected in psychiatric disorders such as PTSD and PCS, hence identifying behaviorally relevant connections carries importance. We report significant correlations, thus associating such connections with altered behaviors.

We observed that majority of the identified connections correlated well with behavior. In order to get further insight into how the ensemble of identified connections mapped onto the ensemble of behaviors, we performed partial least squares regression (PLSR) analysis [129]. Using PLSR, we tried to predict symptom severity (PCL5, NSI) and neurocognitive functioning (NCI and subtests) from SEC and vDEC connectivity values of the connections identified from prior

analysis. We report the percentage of variance in behaviors explained by the connectivities. Fig.4.3 summarizes the processing pipeline of all methods used.
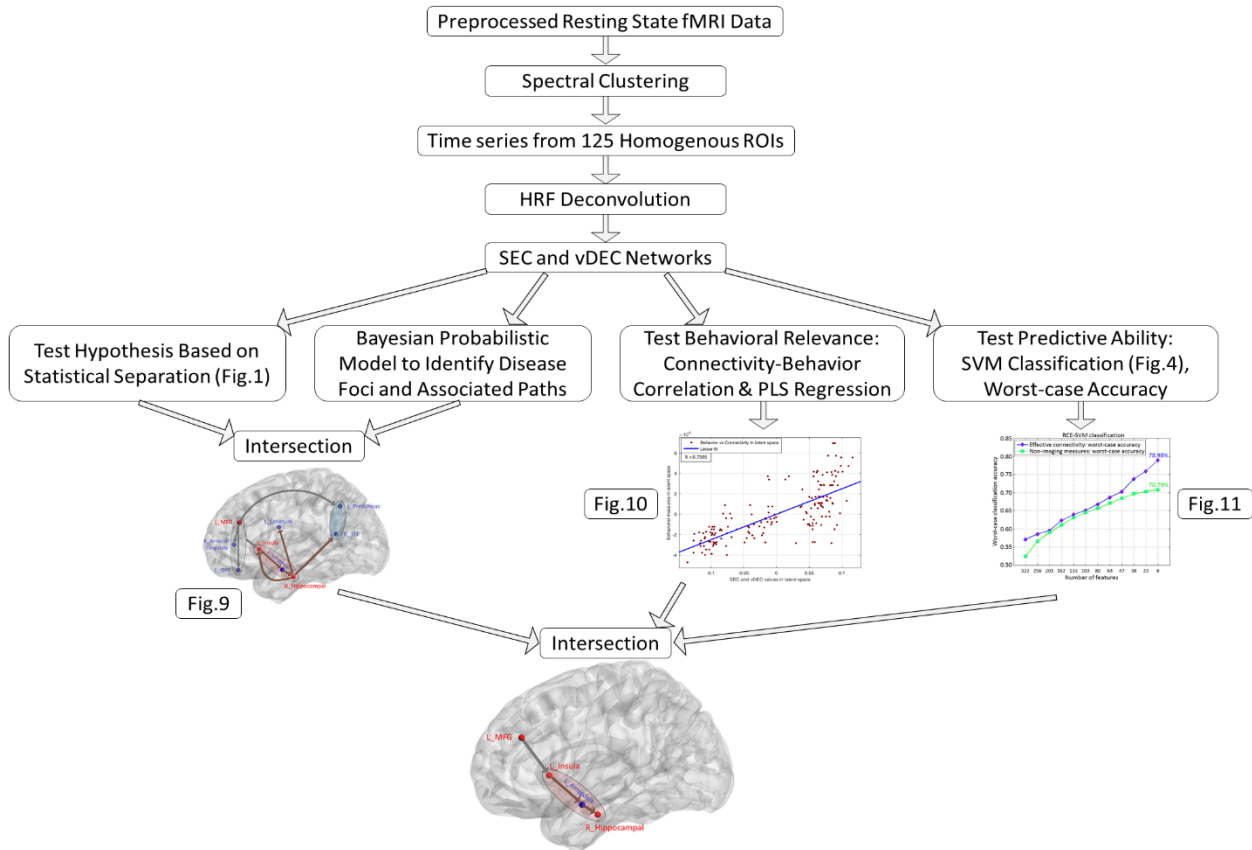
Fig.4.3. *Schematic of the entire processing pipeline*

4.3. Results

4.3.1. *FMRI Connectivity Results*

We evaluated SEC and vDEC and used that in a novel framework to identify disrupted regional foci and their associated connections in the disorders in accordance with our hypothesis. We identified three foci: (i) left middle frontal gyrus [MFG], which mainly included parts of BA9 and BA10, (ii) left anterior insula, and (iii) right hippocampal formation (included anterior parts of

hippocampus, parahippocampal gyrus, entorhinal and perirhinal cortices). These affected foci were connected to/from other brain regions which were part of the disrupted network (see Fig.4.4 for affected ROIs and Table 4.1 for affected connections with MNI coordinates).
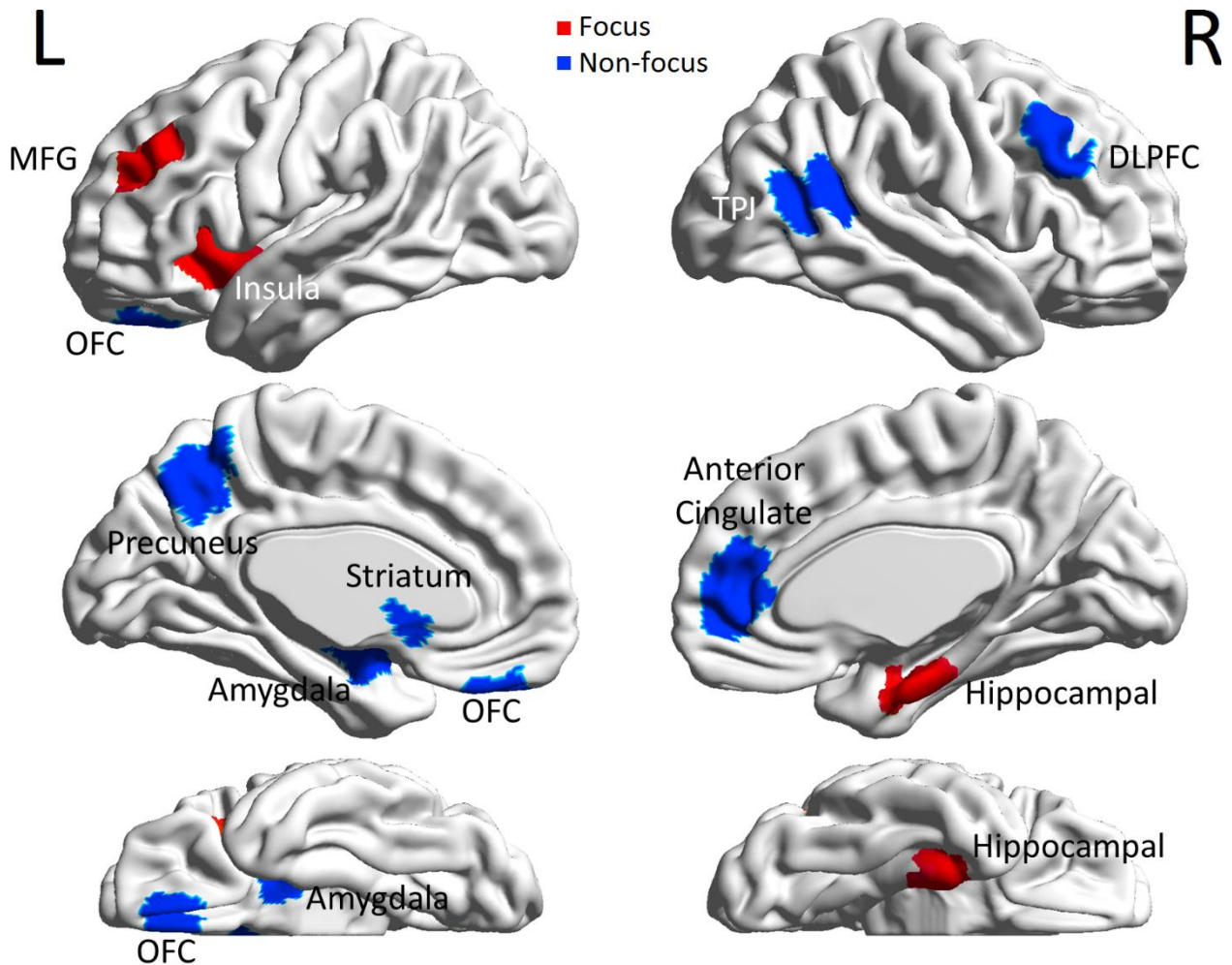

Fig.4.4. *Brain regions (with exact region boundaries) involved in the affected network. Regions in red are the affected foci and those in blue are the regions connected to/from the affected foci. MFG= middle frontal gyrus, OFC= orbito-frontal cortex, TPJ-temporo-parietal junction, DLPFC=dorsolateral prefrontal cortex.*

Table.4.1. *The 12 paths whose effective connectivity values were significantly different between the three groups: table provides the MNI coordinates for these paths. MFG=middle frontal gyrus, OFC=orbito-frontal cortex, TPJ=temporo-parietal junction, DLPFC=dorsolateral prefrontal cortex.*

Path no.	Path	MNI coordinates of centroid (x, y, z)	
		Source	Destination
1	L_MFG → L_Insula	-31.4, 39.1, 28.3	-32.9, 20.5, 1.9
2	L_Insula → L_Amygdala	-32.9, 20.5, 1.9	-23.1, -2.6, -20.5
3	L_Amyg → R_Hippocampus	-23.1, -2.6, -20.5	19.4, -12.4, -25.5
4	L_MFG → L_OFC	-31.4, 39.1, 28.3	-8.1, 40.3, -28.9
5	L_OFC → L_Insula	-8.1, 40.3, -28.9	-32.9, 20.5, 1.9
6	L_MFG → R_Ant_Cingulate	-31.4, 39.1, 28.3	10.3, 44.2, 6.5
7	R_Ant_Cingulate → L_Insula	10.3, 44.2, 6.5	-32.9, 20.5, 1.9
8	R_Hippocampus → L_Insula	19.4, -12.4, -25.5	-32.9, 20.5, 1.9
9	R_Hippocampus → L_Precuneus	19.4, -12.4, -25.5	1.23, -57.1, 44.6
10	R_Hippocampus → L_Striatum	19.4, -12.4, -25.5	-11.3, 12.2, 3.5
11	L_MFG → R_TPJ	-31.4, 39.1, 28.3	46.3, -53.4, 16.9
12	L_MFG → R_DLPFC	-31.4, 39.1, 28.3	47.1, 26.6, 37.1

Fig.4.5 shows the networks associated with each focus. It shows widespread dysregulation originating from MFG, followed by information integration from frontal and hippocampal regions relayed to the amygdala by the insula, followed by overdrive of memory retrieval regions caused by hippocampus. Further clarity was obtained by reorganizing them into three functionally separable networks (Fig.4.6): (i) frontal top-down dysregulation network steered by MFG, causing direct and indirect (through OFC and ACC) dysregulation of insula as well as parietal memory retrieval region, (ii) insula → amygdala → hippocampal loop which appears to go into a positive-

feedback loop representing unrestrained subcortical overdrive, caused due to frontal disinhibition mediated by the insula, and (iii) hippocampal memory-retrieval network which likely translates and mediates subcortical overdrive into heightened memory-retrieval through overdrive of association areas involving memory processing/retrieval. This likely leads to trauma re-experiencing, hyperarousal, flashbacks and other symptoms observed in PTSD and mTBI.
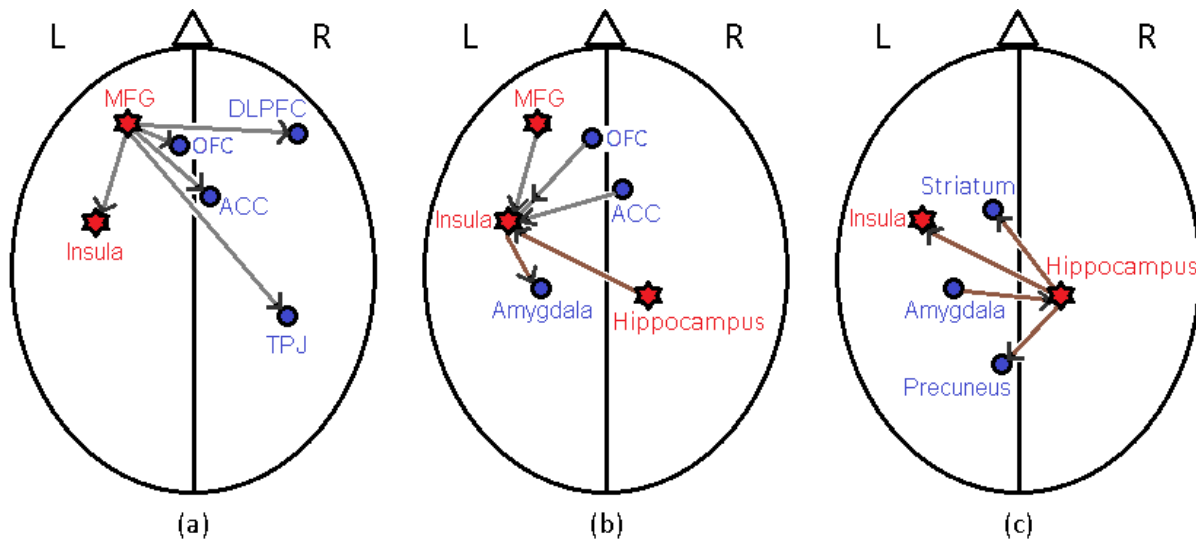
Fig.4.5. *Networks associated with the following three foci (in red): (a) left middle frontal gyrus (MFG), showing widespread dysregulation originating from this region, (b) left anterior insula, which integrates information from frontal and hippocampal regions, and relays it to the amygdala, and (c) right hippocampal formation, which relays subcortical overdrive to regions of the memory network. Gray lines correspond to connections with lower SEC (dysregulation); brown lines correspond to connections with higher SEC (overdrive). All paths followed this trend with vDEC: PCS+PTSD<PTSD<Controls.*

Fig.4.6. *Networks associated with different functions: (a) frontal top-down dysregulation network, steered by MFG, causing direct and indirect influence on insula and parietal regions, (b) insula → amygdala → hippocampal loop, which is likely a positive-feedback loop representing unrestrained subcortical overdrive, and (c) hippocampal memory-retrieval network, which likely mediates and translates subcortical overdrive into memory retrieval, leading to trauma re-experiencing, hyper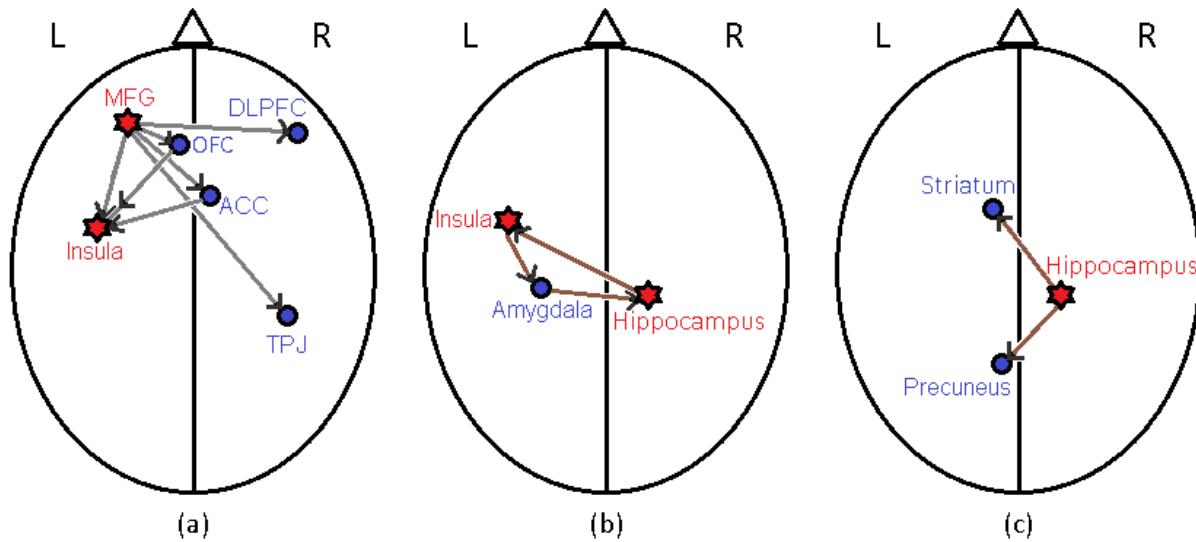arousal, flashbacks and other symptoms associated with PTSD. Gray lines correspond to connections with lower SEC (dysregulation); brown lines correspond to connections with higher SEC (overdrive). Foci are in red, non-foci are in blue.*

Taken collectively, we identified the MFG to be the pivotal source of disruption in soldiers with PTSD and comorbid PTSD and mTBI (Fig.4.7), which was further affecting other emotion and memory related processes, potentially exacerbating symptoms. This network provides a mechanistic explanation of emotion dysregulation and subsequent reoccurrence of traumatic memories associated with PTSD.
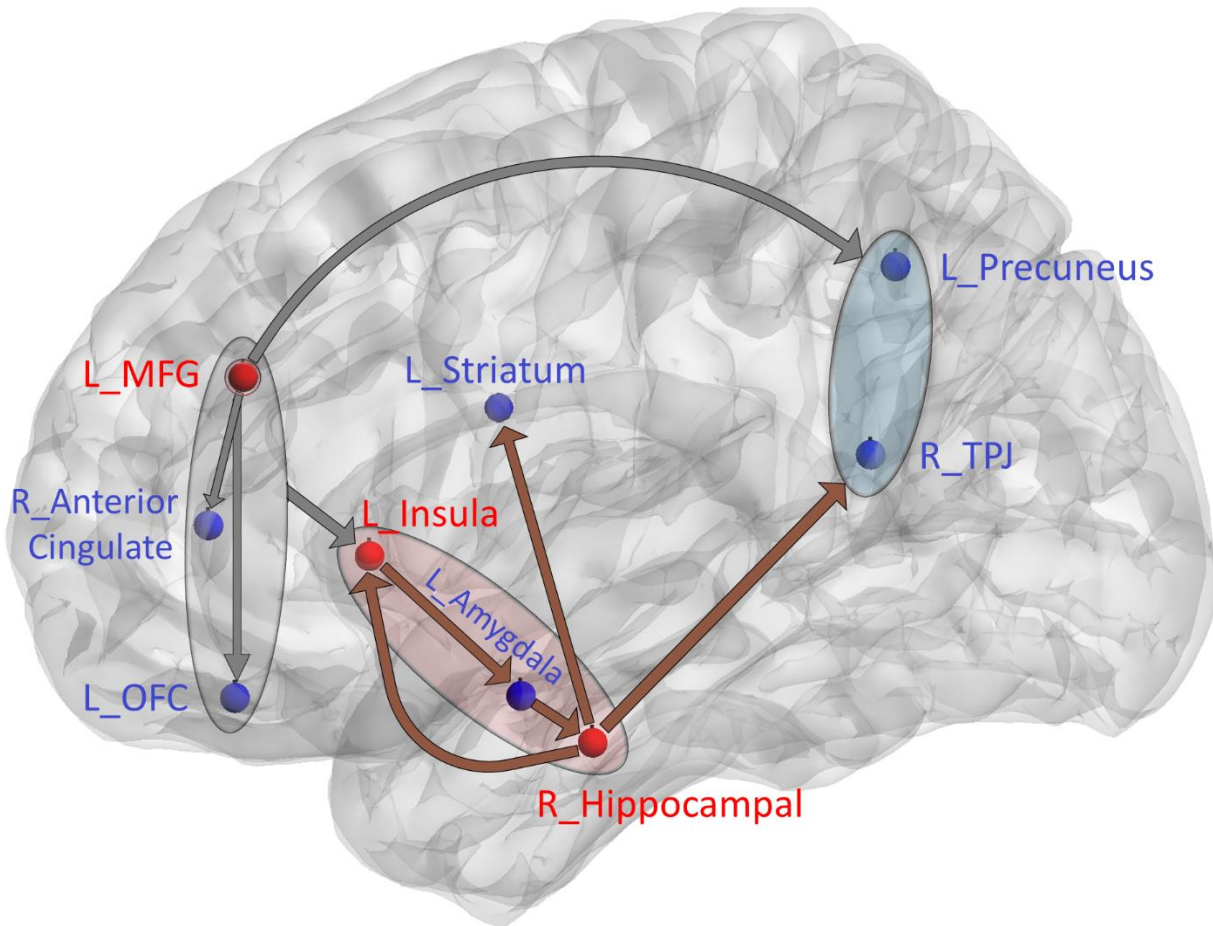
Fig.4.7. *The disrupted foci and their connections as a possible mechanistic model of neural alterations in PTSD and mTBI: The pre-frontal regions anchored by the left MFG are unable to regulate the left insula which disinhibits the subcortical regions into an overdrive. This overdrive results in heightened emotional and memory processing, culminating in overdriven parietal memory-retrieval, which causes the heightened behaviors often observed in soldiers with PTSD and mTBI. Gray lines correspond to connections with lower SEC (dysregulation); brown lines correspond to connections with higher SEC (overdrive); and all paths had lower vDEC (lower flexibility) in the disorders compared to controls (with the trend PCS+PTSD<PTSD<Controls). Foci are in red, non-foci are in blue.*

4.3.2. Behavioral Relevance of Connectivity Values

Connectivity values of three paths (paths 1-3 in Table 4.1) correlated significantly with neurocognitive functioning (neurocognitive-composite-index [NCI] and subtests) and PTSD symptoms (PCL5-score) and PCS severity (NSI-score) (see Table 4.2), thus highlighting their relevance to underlying neuropathology. Other paths also correlated with these behaviors but not as well as paths 1-3, hence not crossing the p-value threshold of 10-20 (Bonferroni corrected). It was notable that correlations followed the expected trend: increase in severity and decrease in behavioral performance corresponded to higher SEC in overdrive paths (L_Insula → L_Amygdala and L_Amyg → R_Hippocampus), lower SEC in dysregulation paths (L_MFG → L_Insula), and lower vDEC in all paths.

Table.4.2. *Correlation (R-value) of SEC and vDEC values of three pivotal connectivity paths with the NCI score and symptom severity in PTSD (PCL5 score) and PCS (NSI score). These correlations were significant with Bonferroni-corrected p-values smaller than 10^{-20}.*

Path	Symptom Severity Score		Behavioral Measure
	PCL5 score (PTSD)	*NSI score (PCS)*	*Neurocognitive Composite Index (NCI)*
SEC			
L_MFG → L_Insula	-0.6852	-0.6780	0.6229
L_Insula → L_Amygdala	0.6650	0.6816	-0.5945
L_Amyg → R_Hippocampus	0.7203	0.7022	-0.6642
vDEC			
L_MFG → L_Insula	-0.6462	-0.6544	0.6507
L_Insula → L_Amygdala	-0.6728	-0.6805	0.6462
L_Amyg → R_Hippocampus	-0.6896	-0.6981	0.6534

A majority of the 12 connections correlated significantly with a majority of behaviors (75.5% of the correlations were significant with p<0.05 Bonferroni corrected). Thereby we performed partial least squares regression (PLSR) to find the combined ability of the 12 connections to predict the set of 9 behaviors (PCL5 and NSI scores, NCI and its 6 subtests). We found that SEC values could explain 47.25% variance in the behaviors, while vDEC could explain 48.29% variance. When combined SEC and vDEC values were taken, they could explain 57.08% variance in the behaviors. A high correlation between connectivities and behavior (R=0.75, p=9.3×10-33) was found in the latent space (see Fig.4.8 for linear fit). This reiterates the fact that the 12 connectivity paths identified in this work are behaviorally relevant.
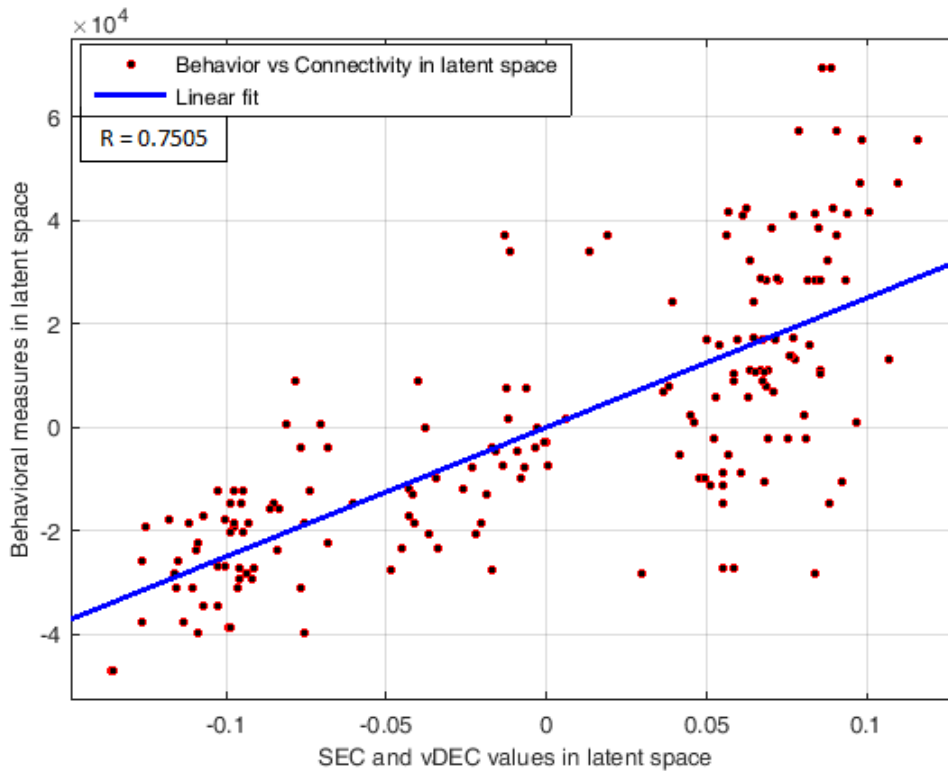

Fig.4.8. *Linear fit between SEC as well as vDEC connectivity values with behaviors in the latent space (obtained through partial least squares regression)*

4.3.3. Machine Learning Classification Results

Machine learning classification was performed as described in section 3.2.3 of this document. Statistically significant neural signatures need not necessarily have generalizability or predictive ability, implying that connections which are statistically significant, fitting our hypothesis and at the same time are also top predictors of diagnostic label, assume higher importance. We thus used recursive cluster elimination based support vector machine (RCE-SVM) classifier [57] to identify the top predictors.

Classification was performed for two different paradigms: (i) classification using 32 non-imaging measures (NIMs), and (ii) classification using connectivities from the entire brain (whole data, nothing left behind). We found that classification using connectivities provided significantly higher accuracy (about 8% more, p<0.05 Bonferroni-corrected) than classification using NIMs (see Fig.4.9). This finding indicates that SEC and vDEC have better predictive ability in identifying subjects with PTSD and PCS compared to NIMs.
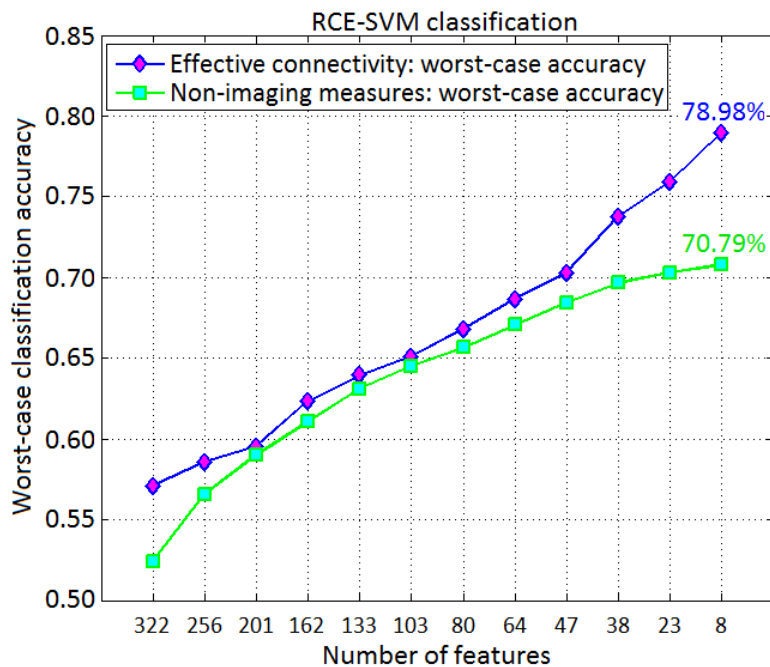

86

Fig.4.9. *Worst-case classification accuracies obtained using recursively reducing number of discriminative features, with both whole-brain effective connectivities and non-imaging measures (NIMs). We observe that connectivities consistently outperform NIMs, with 8% better performance using top-predictive connectivity features.*

Table 4.3 summarizes worst-case classification accuracies along with top-predictive features (see Fig.4.10 for average accuracy). Along with classification accuracies, the top-predictors which resulted in highest classification accuracy are also of considerable interest. For classification using connectivities, SEC and vDEC values of four paths were the top-predictive features (L_MFG→ L_Insula, L_Insula→L_Amygdala, L_Amygdala→R_Hippocampus and R_Ant_Cingulate→ R_Inferior_Frontal). The first three paths were among the twelve paths to have emerged in this study (paths 1-3 in Table.4.1), and they also correlated significantly with symptom severity and neurocognitive functioning. Prior to these findings, these paths were attributed only with statistical significance between groups and behavioral relevance. Statistical significance does not necessarily guarantee predictive ability of connectivity features [74]. These results show that, in addition to statistical separation and behavioral relevance, these paths also have the highest predictive ability, all obtained in a data-driven way from whole-brain connectivity data. Fig.4.3 summarizes the processing pipeline of our entire work, along with corresponding results.

Table.4.3. *Worst-case classification accuracies along with top-predictive features*

	Worst-case accuracy	Top-predictive features
Non-imaging measures	70.79%	Epworth sleepiness scale and Zung depression scale
Connectivity values	78.98%	SEC and vDEC of paths 1-3 (see Table.4.1) and R_Ant_Cingulate -> R_Inf_Frontal
p-value for row-wise comparison	4.48×10^{-24}	

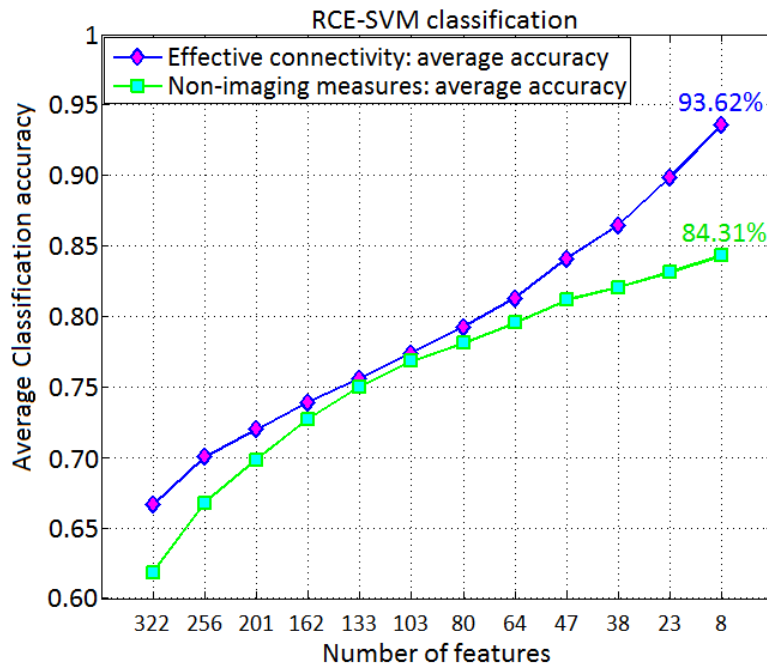**Fig.4.10.** *Average classification accuracies obtained using recursively reducing number of discriminative features, with both whole-brain effective connectivities and non-imaging measures (NIMs). We observe that connectivities consistently outperform NIMs, with 8% better performance using top-predictive connectivity features. The trend is highly similar to what was observed with worst-case accuracies.*

88

4.4. Discussion

In the current study, we sought to identify sources of abnormality from effective connectivity networks in soldiers with PTSD and mTBI. We hypothesized that these disorders are associated with dysfunctional foci which are in turn associated with affected connections that have altered SEC and lower vDEC in the disorders. We found evidence in favor of our hypothesis. We identified three dysfunctional foci (L_MFG, L_Insula and R_Hippocampus) which were significantly different between all three groups. We also identified a network of altered connections in accordance with our hypothesis. Our results showed widespread dysregulation originating from MFG. We found that the pre-frontal regions steered by MFG had reduced influence on the insula which was mediated by OFC and ACC. This resulted in insular disinhibition of amygdala and hippocampus causing an overdrive of these sub-cortical regions. This overdrive manifested through disinhibited parietal (TPJ, precuneus) and other subcortical (striatum) regions, which could be the cause for the heightened behaviors often observed in these disorders. The network was obtained from resting-state data, hence represents the differences in baseline state between the groups. Based on prior knowledge [9], we propose that this network represents prefrontal dysregulation of emotion leading to inadequate control over emotionally-intensive traumatic memories, which gives rise to trauma re-experiencing, hyperarousal, flashbacks and other symptoms in soldiers with PTSD with and without mTBI.

The MFG is known to play a key role in cognitive control [130], of which emotion regulation is a part. Although the amygdala is key to emotion generation and medial prefrontal regions are key to mediating subconscious emotion regulation such as fear conditioning [9], lateral prefrontal regions such as MFG are responsible for the initiation of conscious and cognitive emotion regulation [9]. Several studies have guessed that the MFG might be the likely source of dysfunction

in PTSD [131, 89], including a recent meta-analysis [93], although direct evidence for this hypothesis has not been provided. We provide, what we believe, to be one of the first such evidences for their hypotheses in this work. In fact, a recent meta-analysis discussed evidences from several papers that repetitive transcranial magnetic stimulation (rTMS) applied to MFG could be used as a treatment for PTSD [132]. While they do not explain the underlying mechanism, we provide the network of disturbance caused by MFG dysfunction, with MFG as the source of the disruptions. Put together, MFG's role is likely the initiation of cognitive control including emotion regulation, whose disruption could thus lead to a chain reaction of impaired cognitive control.

We observed prefrontal top-down dysregulation of the insula by MFG (both direct and indirect via OFC and ACC). OFC is considered important for social emotional processing as well as emotion regulation execution [9]. ACC plays the key role of executive functioning in cognitive control [9]. Together, OFC and ACC could be seen as the executive arm of cognitive control, which, when insufficiently driven by MFG, could dysregulate other regions such as insula.

Anterior insula is largely involved in mediating between the prefrontal cortex and subcortical regions, and is shown to be involved in emotion dysregulation [9, 133]. It is heavily connected to the amygdala through white-matter tracts [134], and plays a major role in subjective emotional experience (feelings). It integrates emotionally relevant information from multiple sources and likely represents them as of one of the several complex emotions. Dysregulation of insula from prefrontal regions likely leads to elevated amygdala activity, which then causes increased hippocampal activity. Overdrive in hippocampus, a key region for declarative memories, could indicate elevated retrieval of explicit traumatic memories. The critical role of amygdala and hippocampus in PTSD and mTBI have been well documented [93, 12]. The uniqueness of

traumatic memories is the intensity of certain negative emotions associated with them, hence emotion and memory are deeply interconnected in PTSD.

The striatum's role in generating a habit-like response to traumatic memories in PTSD has been well documented [77], and increased, but less variable drive from the hippocampus may underlie the habit-like response. The precuneus is largely responsible for generating the experience of visual memories, while the TPJ is largely responsible for higher-level audio-visual information processing and verbalization [9]. Both regions had reduced strength and variance of influence from MFG. Thus the hippocampal memory-retrieval network involving precuneus, TPJ and striatum likely translates the subcortical overdrive into heightened memory-retrieval for traumatic memories. This likely leads to trauma re-experiencing, hyperarousal, flashbacks and other symptoms observed in soldiers with PTSD and mTBI.

Taken collectively, we identified the MFG to be the pivotal source of disruption in soldiers with PTSD and mTBI (as all the connections could be traced back to this source), which was further affecting other emotion and memory processes, potentially exacerbating symptoms. The other two foci also play a key role in mediating disruption with the insula involved in subjective cognitive-emotional processing, and hippocampus involved in declarative memories. In concert, this network provides a mechanistic explanation of impaired cognitive control with emotion dysregulation and subsequent lack of control over traumatic memories, contributing to several symptoms observed in soldiers with PTSD and mTBI. Fig.4.11 summarizes the findings with a flowchart.
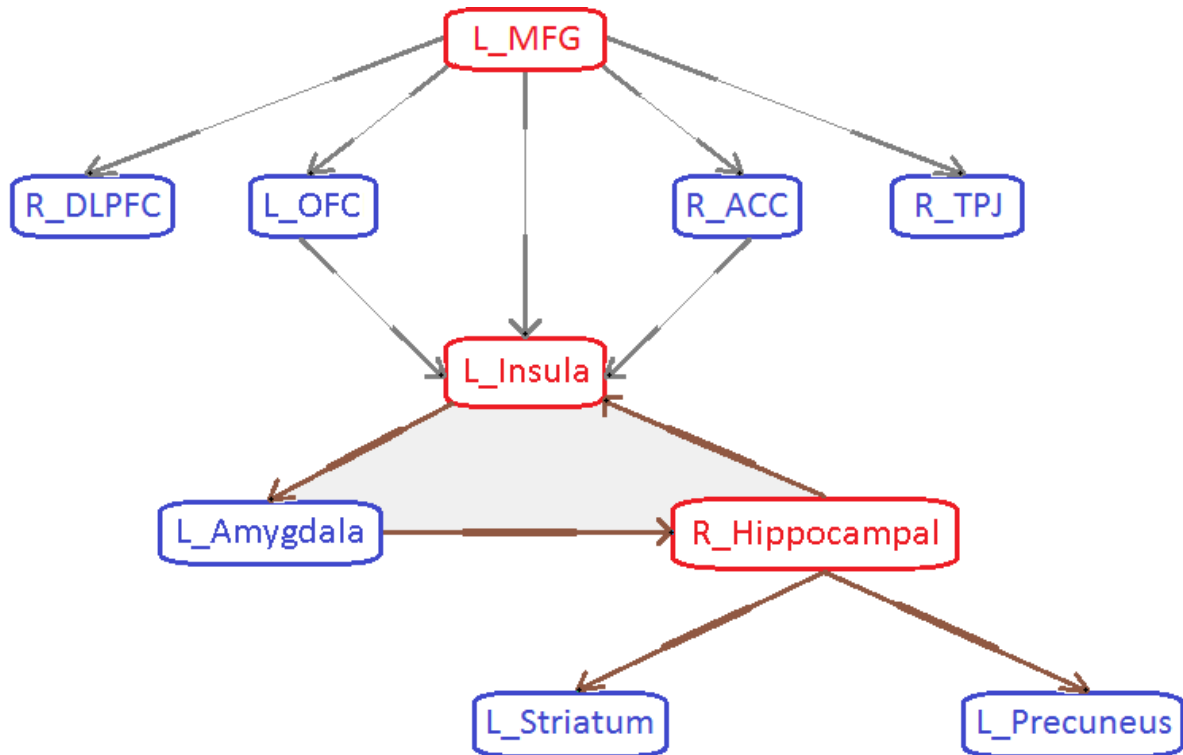
Fig.4.11. *Flowchart illustrating the effective connectivity network and affected foci obtained in this work. Paths with thin gray lines correspond to lower strength of connectivity (SEC) and lower variation in connectivity (vDEC) in patients compared to healthy controls, indicative of breakdown in top-down modulation. Paths with thick brown lines correspond to higher SEC and lower vDEC, indicative of overdrive in subcortical limbic and parietal memory-retrieval regions. Foci are in red, non-foci are in blue.*

Although progress in PTSD research seems to have arrived at some consensus on the pivotal role of MFG, our understanding of PTSD with comorbid mTBI do not seem to have progressed so far. It remains largely unclear as to what are the markers which distinguish between the two disorders [93], and what are the subtle differences which characterize the similar disorders that have dissimilar origins. But it is known that the added burden of mTBI in comorbid PCS+PTSD

causes increased symptom severity [123]. We provide a mechanistic basis for these behavioral observations, and explain network disturbance that distinguishes PTSD from comorbid PCS+PTSD.

Earlier studies have repeatedly identified these and other regions [93, 76, 11] to be involved in both PTSD and mTBI, but a precise understanding of the sources of disruption, their subsequent causal relationships and the underlying network structure has not emerged from them. Employing a novel framework involving foci identification and static/dynamic EC networks, we identified the regional foci associated with the disorders and elucidated their causal relationships. Our characterization fits well with behavioral manifestations of PTSD and PCS+PTSD, thus illustrating the utility and fidelity of our approach.

Additionally, three of the paths correlated significantly with symptom severity and neurocognitive performance (MFG→insula, insula→amygdala, amygdala→hippocampus), thus highlighting the behavioral relevance of these paths. The ensemble of connectivities could also explain about 57% variance in the behaviors in the PLS regression model. Upon performing machine learning classification, we found that the accuracies obtained using connectivities were significantly higher (~8% more) than non-imaging measures. Interestingly, we found that SEC and vDEC of these three paths (along with another path not part of the network) resulted in highest classification accuracy. They were also identified as the top predictive features of diagnostic status, in addition to being statistically significant, which was determined in a data-driven way from whole-brain connectivity data. This demonstrates that they could be a better marker of neural and behavioral characteristics of PTSD and PCS than just PCL5 and NSI scores, and have potential as imaging biomarkers for these disorders. Our connectivity features satisfy three of the four conditions described by Woo *et.al.* [88] to be satisfied by a good biomarker (diagnosticity,

interpretability and deployability). In regard to the fourth condition (generalizability), based on suggestion in Woo *et.al.*, we issue an open call for researchers having similar data to share with us so that the classifier can be tested on them.

Our novel framework used in this work is applicable to the study of any psychiatric illness or cognitive domain. We urge researchers to take advantage of this approach in identifying sources of disruption/alteration in various psychiatric illnesses and cognitive domains.

CHAPTER 5

Complex Network Analysis using Effective Connectivity

5.1. Introduction

The human brain's abilities are attributable to its highly interconnected architecture. Functional Magnetic Resonance Imaging (fMRI) connectivity modeling is popularly employed to study interrelationships between brain regions at the systems-level. However, fMRI connectivity is limited in that it can characterize only pair-wise relationships, i.e. it is bivariate. Our understanding of brain functioning suggests that mental processes are encoded through a carefully orchestrated timed pattern of connection ensembles. Hence, to characterize connection ensembles, not just connection pairs, strategies beyond traditional connectivity modeling are deemed necessary. Complex network modeling [8], using graph-theoretic measures, which can inform us on the properties of ensembles of connections, is a step in that direction. It makes use of individual connectivity weights as well as the pattern in which these connections coexist to make various inferences on the network structure.

Graph-theoretic measures are widely used in studying computer networks and internet, social networks, linguistics, biochemistry, condensed-matter physics, brain networks, among others [135]. It has been used even for pre-surgical planning [136]. Complex network modeling arises from theoretical concepts in graph theory developed originally by mathematicians and computer scientists [135]. A graph comprises of a set of nodes which are interconnected by edges. In brain networks, individual brain regions are the nodes and the connectivity weights between them represents the edges.

Rubinov and Sporns [8] illustrate the applicability and interpretation of several network measures in brain imaging. Among such network properties, functional segregation informs about dense-connectedness within separate subnetworks. It provides a measure of how well a given node is connected to its neighbors. It essentially quantifies whether the regions connected to a given node are connected among themselves, thus forming sub-networks wherein majority of the nodes are connected to every other node. High segregation is necessary for optimal specialized processing within densely-connected subnetworks. For example, during altered consciousness, segregation is reduced especially in the thalamus [137], given that certain specialized processing necessary for consciousness are impaired. In this work we used transitivity (global whole-brain-level measure), clustering coefficient and local efficiency (both local node-level measures) to quantify segregation [8].

On the other hand, functional integration captures the ease of interaction between segregated regions [8]. It is often seen as a measure of connectedness of different sub-networks, necessary for amalgamation of multiple specialized information into generalized information. For example, there is higher segregation in frontal and cerebellar subnetworks in attention-deficit hyperactivity disorder (ADHD), but lower integration between these subnetworks [138], indicative of typical timing deficits seen in ADHD. In this work we used global efficiency (global measure), shortest path length and edge betweenness (both local measures at connection-level) to quantify integration [8]. While traditional connectivity identifies standalone important connections altered between groups, these measures of integration identify those connections which are not only important by themselves but are also important for the rest of the connections in the network. The measures of segregation and integration used by us have high interpretability [8].

In general, it has been extensively demonstrated that segregation and integration are altered in psychiatric disorders (for example, see [139, 140]). Most such works report a fine balance between segregation and integration in the healthy population (called as metastability) [141], which is altered in disorders. Using resting-state fMRI, we investigated network-level alterations in the brains of soldiers diagnosed with posttraumatic stress disorder (PTSD) and post-concussion syndrome (PCS, which is an outcome of persistent symptoms after mild-traumatic brain injury [mTBI]). While we illustrate our techniques to advance our understanding of PTSD and mTBI, they are equally applicable for the study of any other cognitive domain or psychiatric disorder.

PTSD, an outcome of psychological trauma, is marked by hyper-anxiety, hyperarousal and hypervigilance. Exposure to detonating explosives often results in mTBI, which has considerable comorbidity with PTSD [15, 92]. Of the 2.7 million Americans who served in Afghanistan and Iraq until Sept'2014, 20% developed PTSD, 19% developed TBI and 7% developed both [1]. With prevailing clinical approach focusing on subjective judgments, a thorough comprehension of the mechanistic basis for PTSD and PCS is imperative for improved diagnosis and treatment, and for making return-to-duty decisions. Owing to substantially overlapping symptoms between PTSD and PCS [5], it is important to identify objective network-level markers to enhance clinical evaluation and treatment outcomes. Three groups were compared in this work: PTSD, PCS+PTSD (comorbid group sustaining both PTSD and PCS) and healthy combat controls.

For the sake of disambiguation, we call complex network modeling as 'network-level', while connectivity modeling would be called 'connectivity-level' and activation analysis would be called 'region-level'. While several studies have identified specific key prefrontal and subcortical areas, among others, along with their related connections to be altered in mTBI and PTSD [39], a thorough understanding of the alterations of directional influences and associated changes in

network structure have not emerged from them. We address these gaps by identifying network-level alterations associated PTSD only, as well as comorbid PTSD and mTBI with the hope of developing a mechanistic explanation for underlying neural alterations as well as behavioral impairments.

Brain networks are constructed using pair-wise connectivities. While functional connectivity (FC) is the popular choice, we sought directional networks with causal relationships instead of co-activation (a non-directional entity). This is because the underlying causal influence of one region over the other has not been adequately explored even though it is an equally important mechanism for network level interactions in addition to synchronization which is captured via FC. Causal influences between brain regions have been discovered even in fMRI timescales [94, 126, 100, 35, 105, 142]; signifying that identifying causal networks besides co-activation networks is important for more exhaustive characterization. Moreover, PTSD and mTBI are typically seen as prefrontal dysregulation disorders [39], meaning that causal influences emanating from prefrontal areas are defective, which motivated us further to investigate directional connectivity.

Effective connectivity (EC) deals with directional relationships among brain regions [94]. Granger causality (GC), an exploratory technique, was employed to quantify EC between brain regions [95]. It is the most prevalent technique for deriving causal relationships in natural systems [96] including, but not restricted to, molecular biology, epidemiology, econometrics, climate science, evolutionary biology, computer networks, linguistics and brain science [97]. Being a data-driven approach, GC has no requirement for the specification of connectivity priors as in dynamic causal modeling (DCM) [94, 98, 99, 100]. For whole-brain connectivity, it would be practically impossible to build a DCM model with priors since it would result in computational intractability. Recent simulations [102, 103] as well as experimental results [104, 35, 105] demonstrate that GC

used after deconvolving the hemodynamic response function (HRF) from fMRI data (as done by us), is reliable for drawing inferences regarding directional relationships between brain regions. Several recent fMRI works have also employed this method [106, 107, 108, 109, 110, 111, 112, 113, 114].

Most studies investigating EC assume connectivity to be stationary over time. Static connectivity does not capture dynamic variations of connectivity. While an fMRI scan endures for several minutes, mental processes occur within a few milliseconds to a few seconds' time. It is thus natural to note that connectivity varies over the timescales of fMRI scans, and that those variations contain biologically relevant information [115], which are different from that contained in static connectivity [116]. Therefore, we have used static EC (SEC) as well as dynamic EC (DEC) in this work.

Brain networks were constructed from strength (SEC) and temporal variability (DEC) of directional connectivity. SEC network was then used to obtain static segregation and integration measures. With DEC, we constructed a network at each timepoint and then evaluated segregation and integration measures at each timepoint to obtain timeseries of network-measure values. We then took the variance of those values, which indicated the variability of network properties over time. Such a characterization of dynamic network properties is one of the important novel contributions of this work.

A recent study reported complex network characterization in PTSD and mTBI [16]. However, they neither considered directed networks nor dynamic variations in network properties, meaning that our work is looking at a fundamentally different characterization, providing novel insights which cannot be obtained through static and non-directional connectivity. Consequently, their work also did not present a coherent and comprehensive network structure that explains PTSD and

99

mTBI symptoms, possibly because they used only global measures of integration which do not give connection-level characterization, and they did not use directional connectivity. Rather they identified certain nodes with reduced static non-directional segregation, which correlated with certain behaviors, whose usefulness and applications are different from that aimed in this work.

Lower variability of connectivity over time is associated with both psychiatric and neurologic conditions [116, 120, 119, 118], often corresponding to a lack of cognitive flexibility. Compromised behavioral performance in psychiatric disorders as well as in healthy adults is linked to reduced temporal variance of DFC [63, 116]. Such reduction is linked to impaired ability in dynamically adjusting to changing conditions (e.g. thoughts, behavior, etc.). Other biological systems exhibit such a phenomenon, for example, with reduced heart rate variability being indicative of cardiovascular disease [121]. A healthy biological system modifies its action in real-time because internal and external conditions with respect to the body are changing continuously. In those terms, "frozen" connectivity and/or complex network measures such as segregation and integration points to compromised brain health. Such a characterization has been done in recent works [116] wherein the authors showed that greater connectomic flexibility was associated with better/favorable task performance in healthy adults. In this work, we extend these concepts to the reduced temporal variability or rigidity in network properties instead of individual connection strengths. We hypothesized that PTSD and mTBI are characterized by altered strength and lower temporal variability of segregation and integration in directional brain networks. We sought to identify such networks properties which were (i) affected by PTSD but not mTBI (we call this hypothesis-1, see Fig.5.1a), and (ii) affected by PTSD as well as comorbid PTSD and mTBI (we call this hypothesis-2, see Fig.5.1b). Such dichotomy would enable us to identify both common and distinguishing network features between PTSD and mTBI, given the high comorbidity and

overlapping symptomatology between them. This would enhance our understanding of PTSD alone, as well as comorbid PTSD and mTBI. Notably, we tested the hypothesis on whole-brain data in a data-driven manner without imposition of any priors, using resting-state fMRI which is not task dependent.

(a)
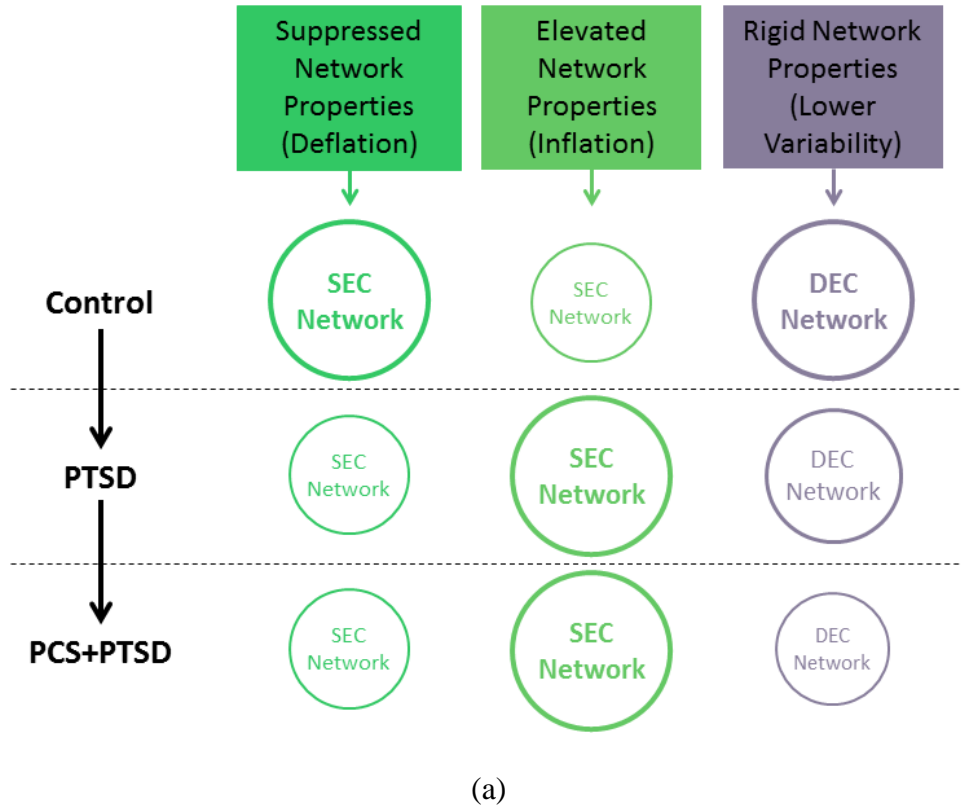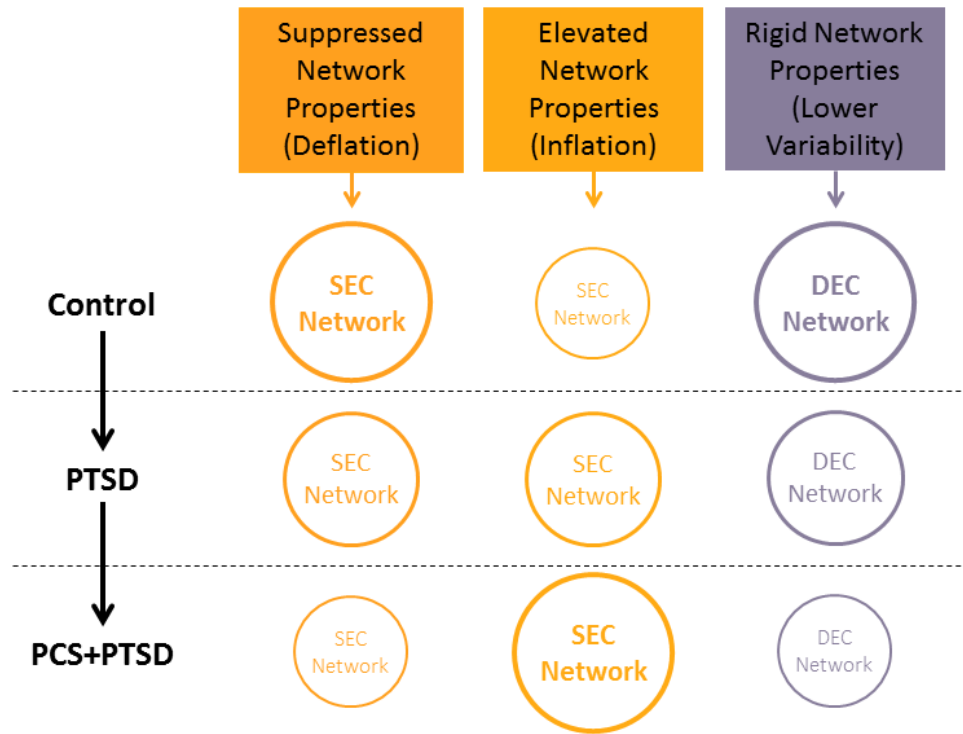
(b)

Fig.5.1. *Illustration of our hypothesis showing reducing temporal variability (i.e. rigidity) of segregation/integration, and either increasing or decreasing segregation/integration as we move from Control to PTSD to PCS+PTSD. Font and circle sizes are symbolic of the increasing/decreasing trend. (a) Some network properties would be altered only in PTSD (significant for Control vs PTSD and Control vs PCS+PTSD comparisons, but not PTSD vs PCS+PTSD comparison) (hypothesis-1). (b) Some network properties would be altered between all three groups (hypothesis-2). Note that inflation and deflation generally corresponds to elevation or suppression of network properties, respectively, and not just connection strengths of individual paths. However in the special case when local network properties of paths are considered, inflation and deflation referred to network properties as well as connection strengths of the paths under consideration*

Statistical separation between the groups is the analysis framework on which our hypothesis rests. However, statistical separation in network properties does not automatically attribute them with diagnostic predictive ability [57]; which means, they may not possess acceptable ability to predict group affiliation at the individual-subject level. As a result, those network properties are more powerful which possess statistical significance as well as discriminative ability to classify the subjects with high accuracy. Machine-learning classifiers have been successfully utilized on fMRI data for such diagnostic prediction in disorders like major-depressive-disorder [58], PTSD [60], Parkinson's disease [59], dementia [61], ADHD [143], prenatal-cocaine-exposure syndrome [57], autism [62] and many others. However, there have been no works which, to the best of our knowledge, have utilized complex network properties in the classification of PTSD and/or mTBI subjects. Given the unique high-level information contained in network properties, we expected them to possess predictive abilities. Neuropsychiatric conditions such as PCS and PTSD are currently diagnosed entirely through clinical observation, hence classification using neuroimaging-based network signatures can be useful in obtaining more accurate diagnoses in these highly comorbid conditions. Hence, by utilizing network measures derived from entire brain effective connectivity data, we found those features that predicted a novel subject's diagnostic membership with high accuracy. Specifically we sought to find an overlap between connections with network properties satisfying our primary hypotheses (Fig.5.1) and connections with network properties possessing high predictive ability. We hypothesized that (secondary hypothesis) such network properties would predict the diagnostic membership of a new subject better than non-imaging measures (neurocognitive, behavioral and self-report measures), thus underscoring their relevance to the underlying neuropathology of mTBI and PTSD. We place special emphasis on network properties having all the desirable qualities: high statistical separation, behavioral

relevance (assessed through correlation between network properties and behavioral variables) and high predictive ability.

5.2. Methods

5.2.1. Complex Network Analysis

Effective connectivity analysis using Granger causality was first performed, as described in detail in section 4.2.1 of this document. Static (SEC) and dynamic (DEC) effective connectivity matrices were then used in further complex network analysis.

We first describe the network measures of segregation and integration, and then explain how they were used in the context of this work. As noted earlier, we dealt with weighted directed networks in this work. Weighted because we did not binarize our connectivity matrices, since binarizing requires choosing an arbitrary threshold value that might bias the results in faulty ways. There are approaches to binarize reliably [8], which essentially involves using a range of arbitrary thresholds and choosing one of them based on a mathematical criteria. But given the complexity of our hypothesis, we chose to use weighted networks instead, which is equally acceptable [8].

Functional segregation was obtained using transitivity (global measure, one value for whole brain per subject), clustering coefficient and local efficiency (both local measures, one value per node/region per subject). Functional integration was obtained using global efficiency (global measure), shortest path and edge betweenness (both local measures, one value per connection per subject). We obtained source codes for these measures from the Brain Connectivity Toolbox (April 2014 release) [8], and implemented the entire pipeline in Matlab® platform through custom code. We explain each of these measures in brief here (for weighted directed networks only), while a detailed account can be found at [8].
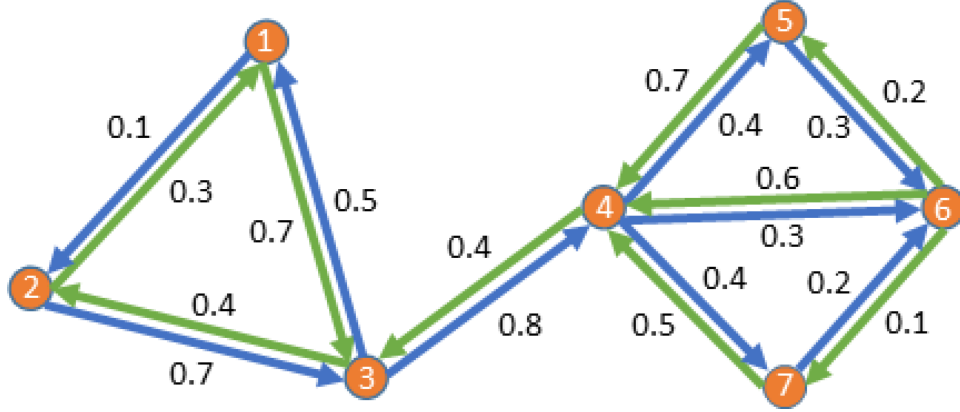
Fig.5.2. *Simplified example network used to numerically explain several complex network measures. The node numbers are marked within the node. The connectivity weight for each direction are marked next to the path. This network contains two sub-networks or modules (nodes 1,2,3 and nodes 4,5,6,7) which are connected through pivotal connections between node-3 and node-4.*

We first define certain basic network entities. All measures are numerically explained using a simplified example (see Fig.5.2). Degree of a node is the sum of all connectivity weights associated with a node. Given the set of all nodes (regions) N and connectivity weights (EC value) w_{ij} for path *(i,j)*, degree of a node is defined as,

$$Out\ degree: k_i^{out} = \sum_{j \in N} w_{ij}; \quad In\ degree: k_i^{in} = \sum_{j \in N} w_{ji} \tag{5.1}$$

In the example (Fig.5.2), the degrees for node-4 are $k_4^{in} = 2.6$, $k_4^{out} = 1.5$, while that for node-2 are $k_2^{in} = 0.5$, $k_2^{out} = 1.0$. This shows that node-4 is a strong node which is predominantly driven by other nodes while node-2 is a weak node which predominantly drives other nodes. The

weight of a "no connection" is taken as zero. The number of triangles around a node is the basis for measuring segregation, which informs about how well the neighbors of a node are neighbors themselves. This characterizes how well-connected a sub-network is. It is defined as the geometric mean of the triangles around node i as,

$$t_i = \frac{1}{2}\sum_{j,h \in N}\left[(w_{ij} + w_{ji})(w_{ih} + w_{hi})(w_{jh} + w_{hj})\right]^{1/3} \tag{5.2}$$

In the example (subscripts indicate node number), $t_3 = 0.4$, $t_6 = 1.3$. If the connection between nodes 4 and 5 is removed and inserted as the connection between nodes 4 and 1, we get $t_3 = 1.6$, $t_6 = 0.5$. We see a reversal in this case.

The shortest path length (SPL) is a basis for measuring integration, which indicates the smallest sum of inverse path-weights from node i to j. It is a measure of how easy it is to reach node j from node i. The shortest path $g_{i \to j}$ is usually determined using Dijkstra's algorithm. The shortest path length is then determined as,

$$d_{ij} = \sum_{w_{uv} \in g_{i \to j}} 1/w_{uv} \tag{5.3}$$

In the example (Fig.5.2), $d_{1 \to 7} = 5.2$, $d_{7 \to 1} = 6.5$, indicating that it is shorter (easier) to communicate from node 1 to 7 than from node 7 to 1. The SPL is very important, and is analogous to meta-connectivity, because it represents indirect connections between regions which are originally not connected (or weakly connected). For example nodes 1 and 7 are not directly

connected, but SPL makes it possible to quantify indirect influences between them through other regions.

Measures of segregation

Transitivity is a global measure indicating the average percentage of triangles (clusters) in the nodes compared to the total strength of all connections. It is a global measure of overall efficiency of local processing in the brain, which is defined as,

$$T = \frac{\sum_{i \in N} t_i}{\sum_{i \in N}\left[\left(k_i^{in} + k_i^{out}\right)\left(k_i^{in} + k_i^{out} - 1\right) - 2\sum_{j \in N} w_{ij}w_{ji}\right]} \tag{5.4}$$

In the example, simple computation yields T=0.22. If nodes 4 to 7 were to be removed, we get T=0.39 since nodes 1-3 form neat triangles. If nodes 1 to 3 were to be removed, we get T=0.28; lower since nodes 5 and 7 are not connected. The entire network has a smaller value since the connection from nodes 3 to 4 is not part of any triangle/cluster.

Clustering coefficient (CC, a local measure) gives a transitivity-type characterization for every node. It is the ratio of all triangles around a node to the total sum of all paths associated with the node.

$$CC_i = \frac{t_i}{\left[\left(k_i^{in} + k_i^{out}\right)\left(k_i^{in} + k_i^{out} - 1\right) - 2\sum_{j \in N} w_{ij}w_{ji}\right]} \tag{5.5}$$

In the example, $CC_3 = 0.13,\ CC_5 = 0.45$, because 33% of node-3's connections do not form a triangle at all, while all of node-5's connections form triangles and with high strengths. Clearly node-5 is associated with specialized processing.

Local efficiency (*EffLoc*, a local measure) is closely related to *CC*. Essentially, if a given node has powerful neighbors which are involved in several shortest paths then the node has high *EffLoc*, indicating that the node is important in the sub-network for specialized processing.

$$EffLoc_i = \frac{\sum_{j,h \in N, j \neq i}\left[(w_{ij} + w_{ji})(w_{ih} + w_{hi})([d_{jh}(N_i)]^{-1} + [d_{hj}(N_i)]^{-1})\right]}{\left[(k_i^{in} + k_i^{out})(k_i^{in} + k_i^{out} - 1) - 2\sum_{j \in N} w_{ij}w_{ji}\right]} \tag{5.6}$$

Where $d_{jh}(N_i)$ is the shortest path length between *j* and *h* which contains only the neighbors of node *i*. In the example, $EffLoc_3 = 0.15$, $EffLoc_5 = 0.45$. While *CC* and *EffLoc* usually give similar (but not same) results, their interpretations are different. In this work, along with transitivity as the global measure, we employed both *CC* and *EffLoc* as local measures, which are the two popularly used local measures of segregation. We took an overlap (intersection) of the final significant group differences for the two measures, so that affected nodes had differences in both measures, thus providing conservative results.

Measures of integration

Global efficiency (*EffGlob*) is a global measure indicating the aggregate ease of communication in the entire network. It is defined as the average inverse shortest path length of the complete network. That means, if the shortest paths in the network are shorter (easier to communicate) on average then we get larger global efficiency.

$$EffGlob = \frac{1}{n}\sum_{i \in N} \frac{\sum_{j \in N, j \neq i}(d_{ij})^{-1}}{n - 1} \tag{5.7}$$

Where *n* is the total number of nodes in the network. In the example shown in Fig.5.2, *EffGlob*=0.32. Now if we removed the connections between nodes 1 and 2, we get *EffGlob*=0.32 (unchanged), because it is a local connection that does not have much role in information integration. However if we remove the connections between nodes 3 and 4, which is the key link between the two sub-networks, we get *EffGlob*=0.18.

Edge betweenness (*EB*) is a local measure obtained for each path. For a given path, it measures the fraction of all shortest paths in the entire network that contain the given path. That means, if the path is an important link in the network, then a large portion of shortest paths would go through it, giving a high value of *EB*. It is evaluated through a variant of Dijkshra's algorithm. In our example, $EB_{1\rightarrow2} = 0$, $EB_{4\rightarrow6} = 4$, $EB_{6\rightarrow4} = 6$, $EB_{3\rightarrow4} = 12$. These values are intuitive since path 1→2 has little role in rest of the network, while the paths between nodes 4 and 6 have a role restricted within the sub-network (with 6→4 being stronger than 4→6). The path between nodes 3 and 4, however, is pivotal to the efficient communication between the sub-networks and integration of information, which is why we get highest *EB* for that path.

Like shortest path length, *EB* is a very important measure because it characterizes the importance of a connectivity path not only through its connectivity value but also through the significance of the path for other connectivity paths present in the network. If a path matters a lot for other paths, i.e. for communication between various other nodes, then the given path would have high integration ability (i.e. *SPL* and *EB*). Such a characterization can be obtained only through complex network modeling since traditional connectivity informs us about the strength of interaction only between two regions.

In this work we employed both *EffGlob* as the global measure and *SPL* and *EB* as local measures of integration. As with segregation, we took an overlap (intersection) of the final significant group

differences in the two local measures, so that affected paths had differences in both measures, thus providing conservative, but potentially more reliable, results.

Next, we describe how these six network measures were used in the context of this work. SEC and DEC connectivities were used separately to construct static and time-varying networks with brain regions as nodes and connectivity strengths between them as the weighted directed edges of the network graphs. With SEC, a single network was constructed for the entire duration of data, giving a "connectivity strength" network, which was used to obtain each one of the six complex network measures for every run of every subject. With DEC, we considered every timepoint as a network snapshot, and computed network measures by treating each timepoint like a SEC matrix. Accordingly, we obtained network measures at each timepoint, which, when computed at every timepoint successively, resulted in a timeseries of network properties that captures network dynamics. Then, for each network measure, we computed the variance of the network measure timeseries to obtain a single value for entire duration of the experiment, thus giving a "connectivity variation" network for every measure for every run of every subject, similar to SEC.

Statistically significant differences in these strength and variation networks were obtained, in accordance with our hypothesis ($p<0.05$, FDR corrected). Differences were controlled for age, race, education and head-motion (using mean frame-wise displacement obtained across all brain voxels for each subject as defined by Power et al. [65]). That is, we found significant group differences with both SEC and DEC network measures separately for these three pairwise comparisons (thus giving a total of six comparisons per network measure): Control vs PTSD, Control vs PCS+PTSD, PTSD vs PCS+PTSD. We then identified the common network measures among four of these comparisons (hypothesis-1) which excluded PTSD vs PCS+PTSD comparison, and we also identified common network measures among all the six comparisons

(intersection, hypothesis-2), all of which also fit our hypothesis, that is, conformed to the increasing/decreasing trend as we moved from Control to PTSD to PCS+PTSD.

It is notable that we have taken a conservative approach in this work. We opted to look for common differences in pair-wise statistical comparisons, rather than performing a single 3-way statistical comparison which is less conservative. We obtained common differences in static as well as dynamic network measures, and we also constrained the differences to conform to a trend as per our hypothesis. Additionally, we computed two local measures in segregation as well as integration, and considered only common differences in them, which added another level of constraints to our results. In addition to these, we notably discarded any paths which had significant network-level differences in local measures of integration (i.e. SPL and EB), but not significant pair-wise connectivity differences themselves. That is, we included only those paths which had significantly different SEC and variance of DEC in accordance with the trend set out in our hypothesis ($p<0.05$, FDR corrected, controlled for age, race, education and head-motion), in addition to having significantly different local measures of integration (i.e. SPL and EB). This was done to ensure that, irrespective of network-level disturbance, the significant connections which emerged in this work would have cleared whole-brain multiple-comparisons-corrected statistical threshold like in most other studies. This reassured that our results conformed to multiple layers of validation, verification and statistical standards, and that evidence of network disruption were obtained via multiple analysis approaches, in addition to providing novel insights through network characterization.

111

5.2.2. Behavioral Relevance of Network Properties

In an effort to assess the behavioral relevance of complex network measures, we first correlated the strength and variability of complex network measures (only those which fit our hypothesis) with symptom severity in PCS (NSI score) and PTSD (PCL5 score), as well as neurocognitive functioning (NCI score and subtests). Neurocognitive functioning (e.g. executive functioning, cognitive flexibility) is impaired in psychiatric disorders such as PTSD and PCS, hence identifying such behaviorally relevant network properties is important. We report significant correlations, and associate corresponding complex network properties with altered behaviors.

We observed that several complex network properties had considerable correlations with behavior. In an effort to obtain better insight into how network properties of the ensemble of identified connections mapped on to the ensemble of behaviors, we performed partial least squares regression (PLSR) analysis [129], which we employed to predict neurocognitive functioning (NCI and subtests) and symptom severity (PCL5, NSI) from strength and variability of network measures obtained from our prior analysis. We present the percentage variance in behaviors explained by the complex network measures. Fig.5.3 summarizes the processing pipeline of all the methods.
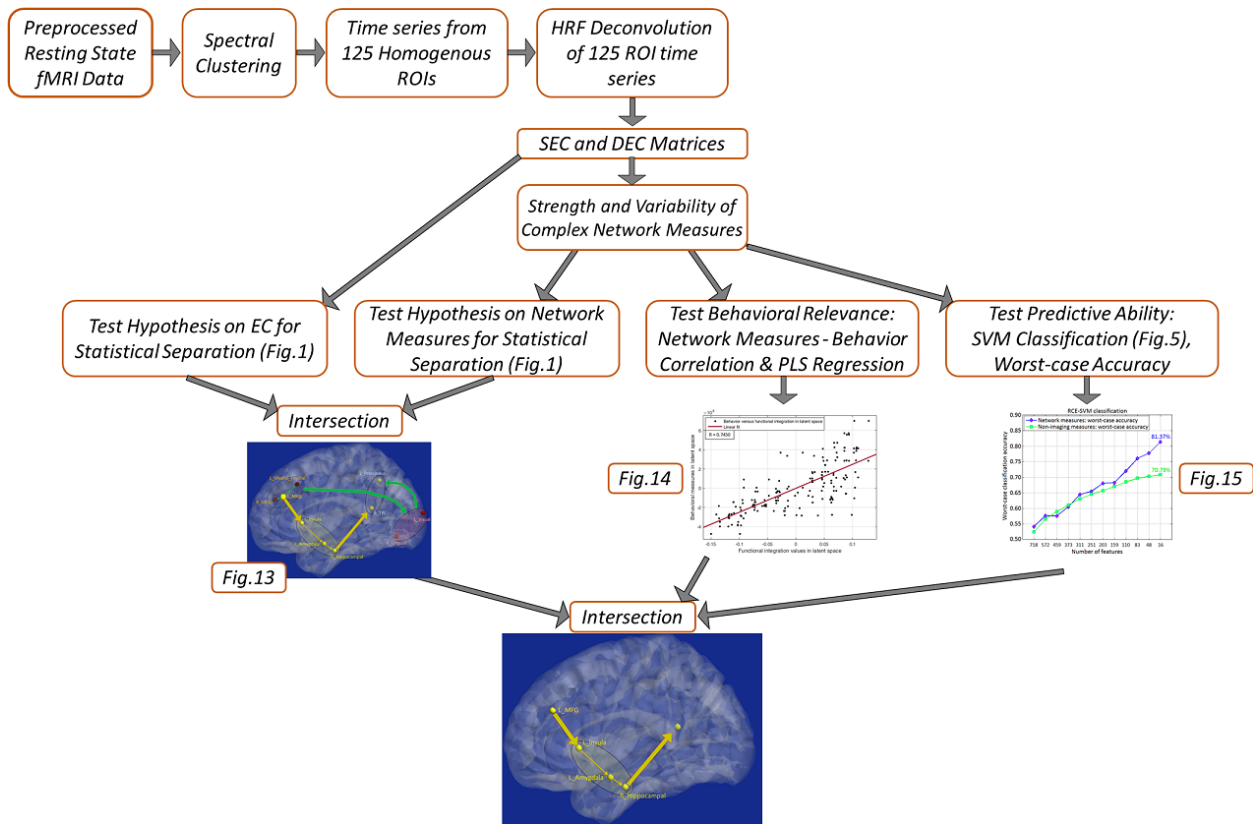
Fig.5.3. *Schematic of the complete processing pipeline*

5.3. Results

5.3.1. Complex Network Analysis Results

We used SEC and DEC connectivities to compute six complex network measures (two global and four local measures). With global measures (see Table 5.1), we found significantly reduced strength and variability of both segregation and integration in PTSD and PCS+PTSD compared to controls. Our finding indicates that both specialized processing and efficient communication are affected in the disorders at the whole brain level. However, no significant differences were found between PTSD and PCS+PTSD groups, indicating that PTSD might contribute to global alterations whereas the effect of mTBI might be more localized.

Table 5.1. *Significance of group differences for the two global measures obtained from both SEC and vDEC. We observe that whole-brain differences are driven by PTSD while mTBI likely causes local changes*

Measure	Connectivity metric	p-value of comparison		
		Controls vs. PTSD	Controls vs. PCSPTSD	PTSD vs. PCSPTSD
Transitivity (segregation)	SEC	0.0088	0.0154	0.4974
	vDEC	0.0076	0.0041	0.5891
Global Efficiency (integration)	SEC	0.0104	0.0236	0.4291
	vDEC	0.0081	0.0047	0.5827

Further granularity was obtained with local measures. Altered segregation was mainly observed in frontal and occipital regions (Figs 5.4 and 5.5). All occipital regions were not different between PTSD and PCS+PTSD, while most of the remaining regions were different. While these results were obtained using a strict statistical threshold, we noticed that when a liberal threshold (not shown here) was used, more frontal nodes were affected compared to parietal/occipital, and they were all characterized by lower segregation. This might explain why we observed lower transitivity (global segregation) in PTSD and PCS+PTSD compared to controls.
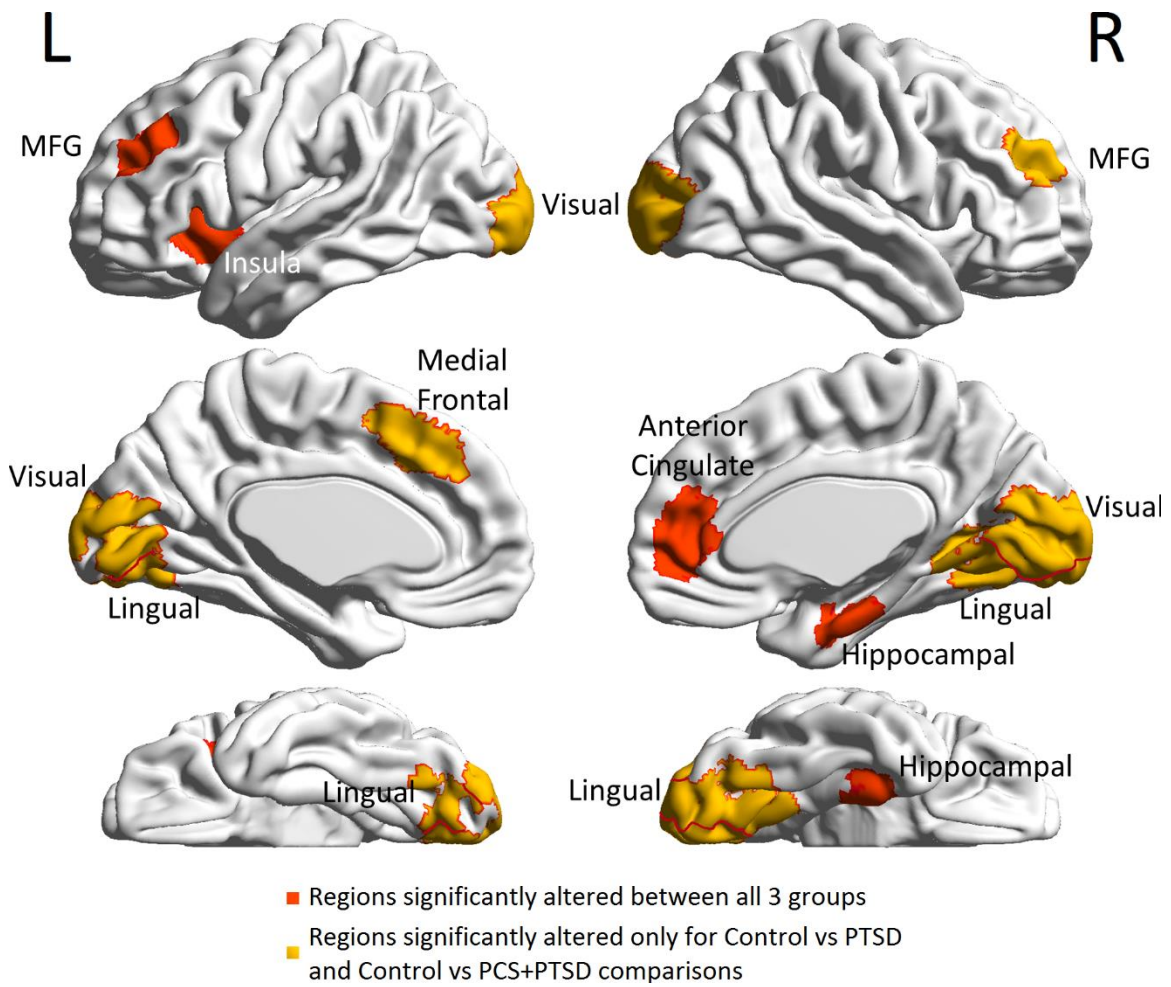
Fig.5.4. *ROIs associated with significantly altered functional segregation*
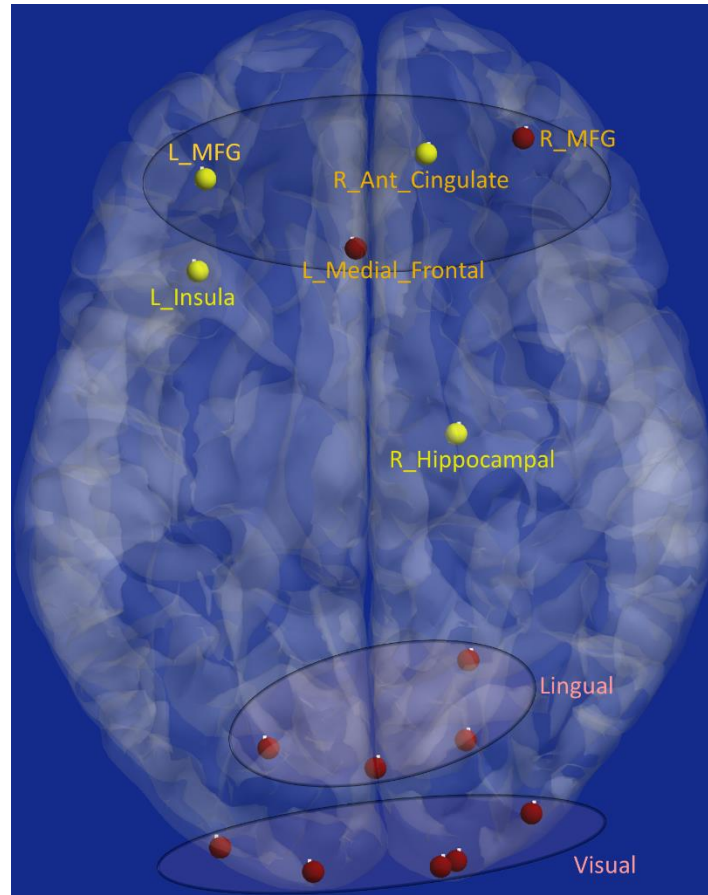
Fig.5.5. *Nodes which had altered functional segregation and lower variation of segregation over time in the disorders compared to controls. Red nodes were statistically significant only for control vs PTSD and Control vs PCS+PTSD comparisons (but not PTSD vs PCS+PTSD comparison). Yellow nodes were significantly different between all three groups. Additionally, all occipital regions plus insula and hippocampus showed higher segregation, while all frontal regions showed lower segregation (this observation is not color-coded).*

We wish to clarify the meaning of terms 'inflation' and 'deflation' which we have used in our hypotheses (Fig.5.1) as well as in the description of results and discussions in the following sections. Generally they correspond to elevation (increased value) or suppression (decreased

116

value) of static network properties, respectively, and not just connection strengths of individual paths. Similarly, 'rigidity' generally corresponds to lower temporal variability of dynamic network properties. However in the special case when local network properties of paths (i.e. integration) were considered, these terms referred to network properties as well as connection strengths of the paths under consideration.

Next, altered local measures of integration were found along two distinct pathways (see Fig.5.6 for the affected ROIs), which we present as two subnetworks for clarity: (i) fronto-visual subnetwork (Fig.5.7), and (ii) parietal-inflation subnetwork (Fig.5.8). The fronto-visual subnetwork showed frontal deflation of secondary visual areas and lingual gyrus, i.e. lower strength/variance of network properties (SPL and EB) of paths connecting frontal areas to visual areas. This subnetwork was, however, not different between PTSD and PCS+PTSD, indicating that it might not be affected by mTBI (since one difference between these groups is history of significant prior mTBI(s) in the PCS+PTSD group). Notably, all paths here had lower SEC/vDEC connectivity values in addition to lower strength and variability of integration.
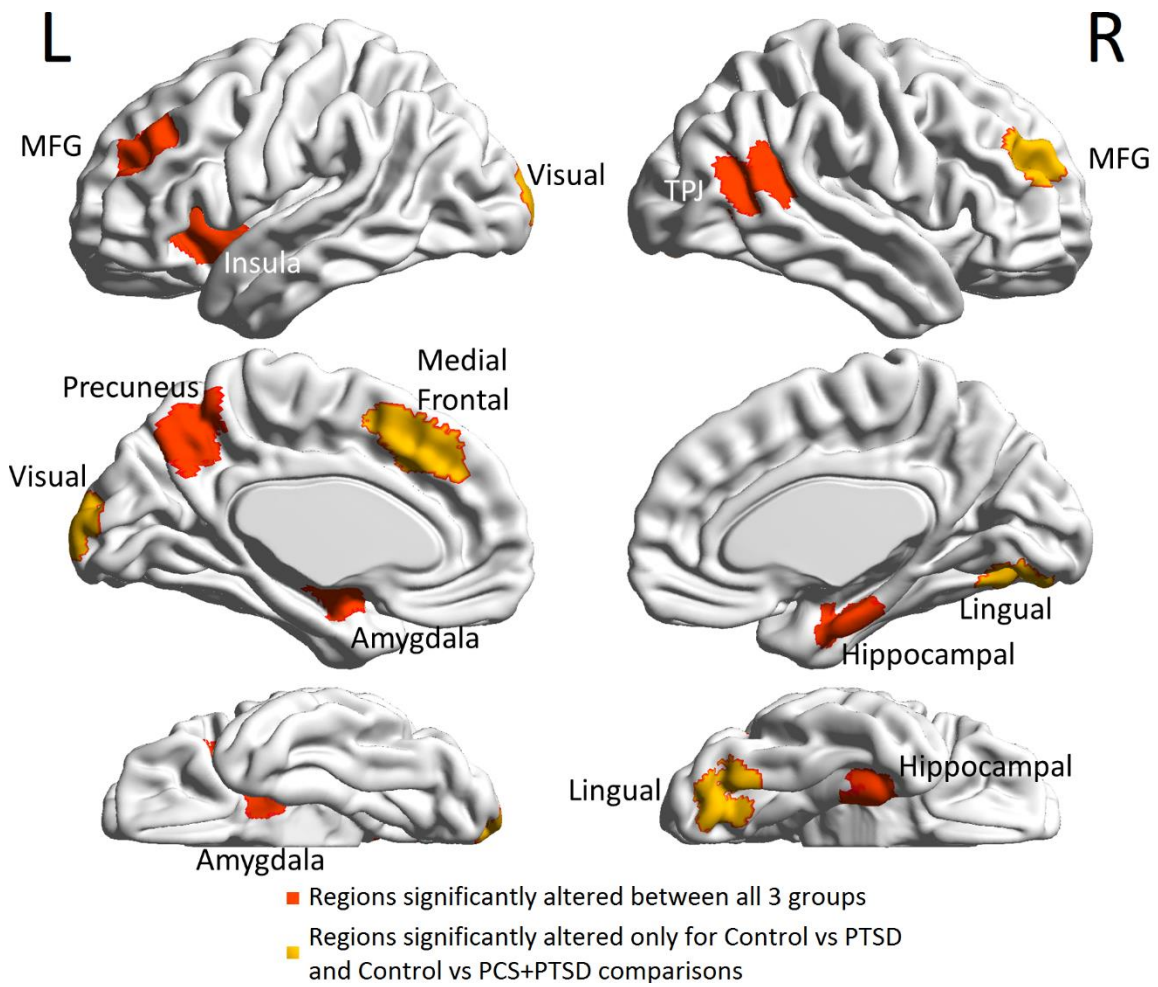
Fig.5.6. *ROIs associated with significantly altered functional integration*
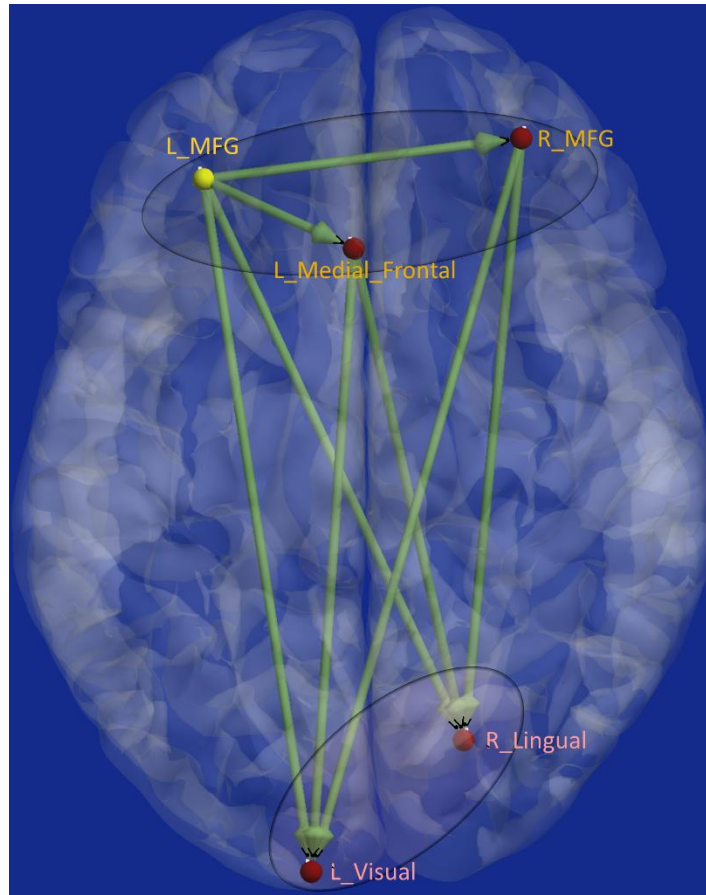
Fig.5.7. *The fronto-visual sub-network which had lower functional integration and lower temporal variation of integration, which was significant for control vs PTSD and control vs PCS+PTSD comparisons (but not PTSD vs PCS+PTSD comparison). The yellow node had altered segregation between all three groups, while the red nodes were altered except for the PTSD vs PCS+PTSD comparison. This sub-network likely represents reduced frontal inhibition of visual memory processing and retrieval.*

The parietal-inflation subnetwork (see Fig.5.8) showed that the visual areas affected in the fronto-visual subnetwork were driving two key parietal regions (precuneus, temporo-parietal-junction [TPJ]). Additionally there was fronto-subcortical disinhibition resulting in inflation

(increased strength but lower variance of network properties SPL and EB) of key subcortical areas (amygdala, hippocampus) and anterior insula, which then resulted in inflation of the same key parietal regions. Interestingly, this fronto-subcortical-parietal subnetwork was significantly altered between all groups, indicating that both PTSD and mTBI affect this subnetwork, while the occipital part was not altered between PTSD and PCS+PTSD (see Fig.5.9).
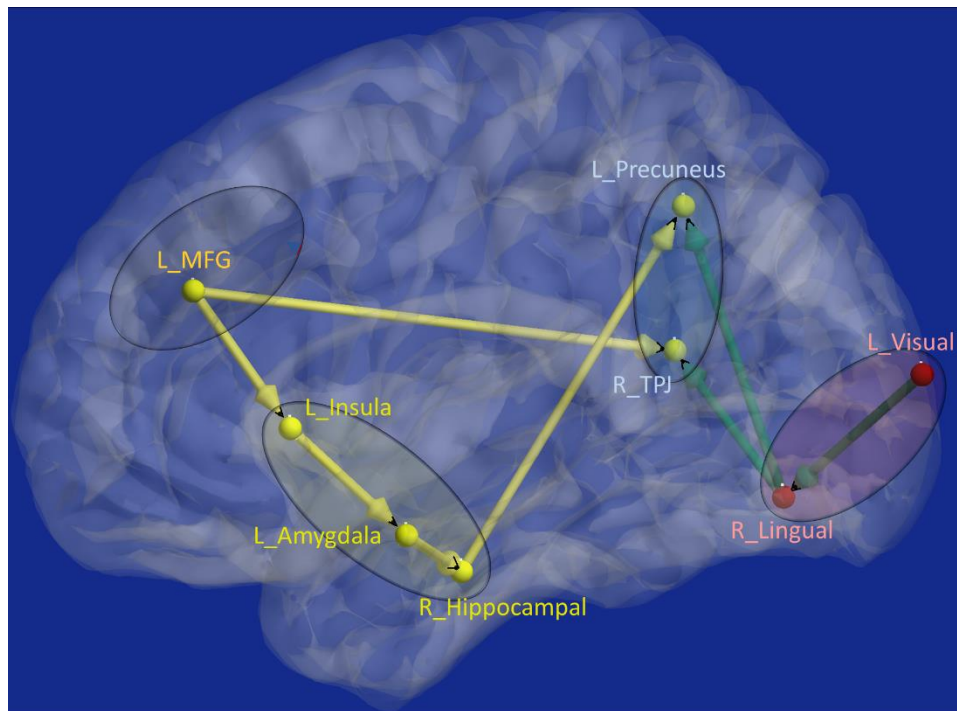
Fig.5.8. *Parietal inflation sub-network which had altered integration and lower temporal variation of integration. Yellow paths were significantly different for all group-wise comparisons. Green paths were altered except for the PTSD vs PCS+PTSD comparison. The yellow nodes had altered segregation between all three groups, while the red nodes were altered except for the PTSD vs PCS+PTSD comparison. This sub-network showed parietal-inflation caused by subcortical and visual network disruptions, which were in-turn caused by left MFG*
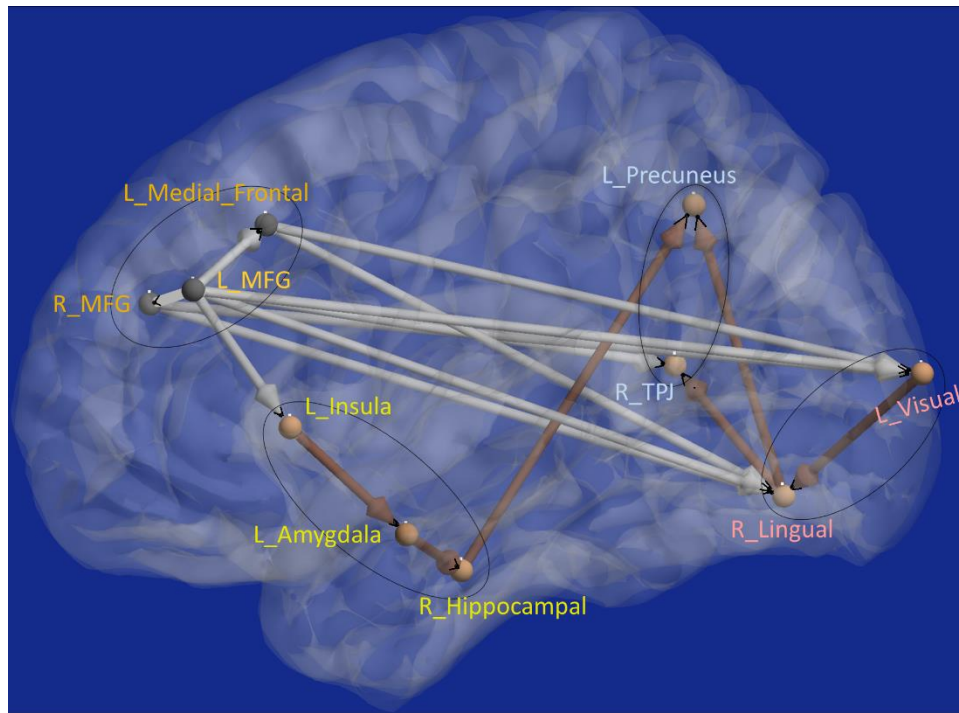
Fig.5.9. *The entire network showing nodes/paths in gray which were on a deflated regime (lower strength and temporal variability of integration, as well as lower SEC and vDEC), and nodes/paths in brown, which were on an inflation regime (higher strength of integration and lower variation of integration over time, as well as higher SEC and lower vDEC). All prefrontal nodes and originating paths exhibit a deflated regime, while the rest exhibit an inflated regime. It is clearly observable that the deflation originates in the pre-frontal cortex, which further results in inflation of parietal regions through two routes, subcortical and visual.*

Schematic of the entire network (Fig.5.10) shows that the left middle frontal gyrus (MFG), also known as dorsolateral prefrontal cortex (DLPFC), is the likely source of the network-level disruption, whose deflation (suppressed network properties) results in inflation (elevated network properties) of downstream subcortical and visual pathways, culminating in a parietal inflation.
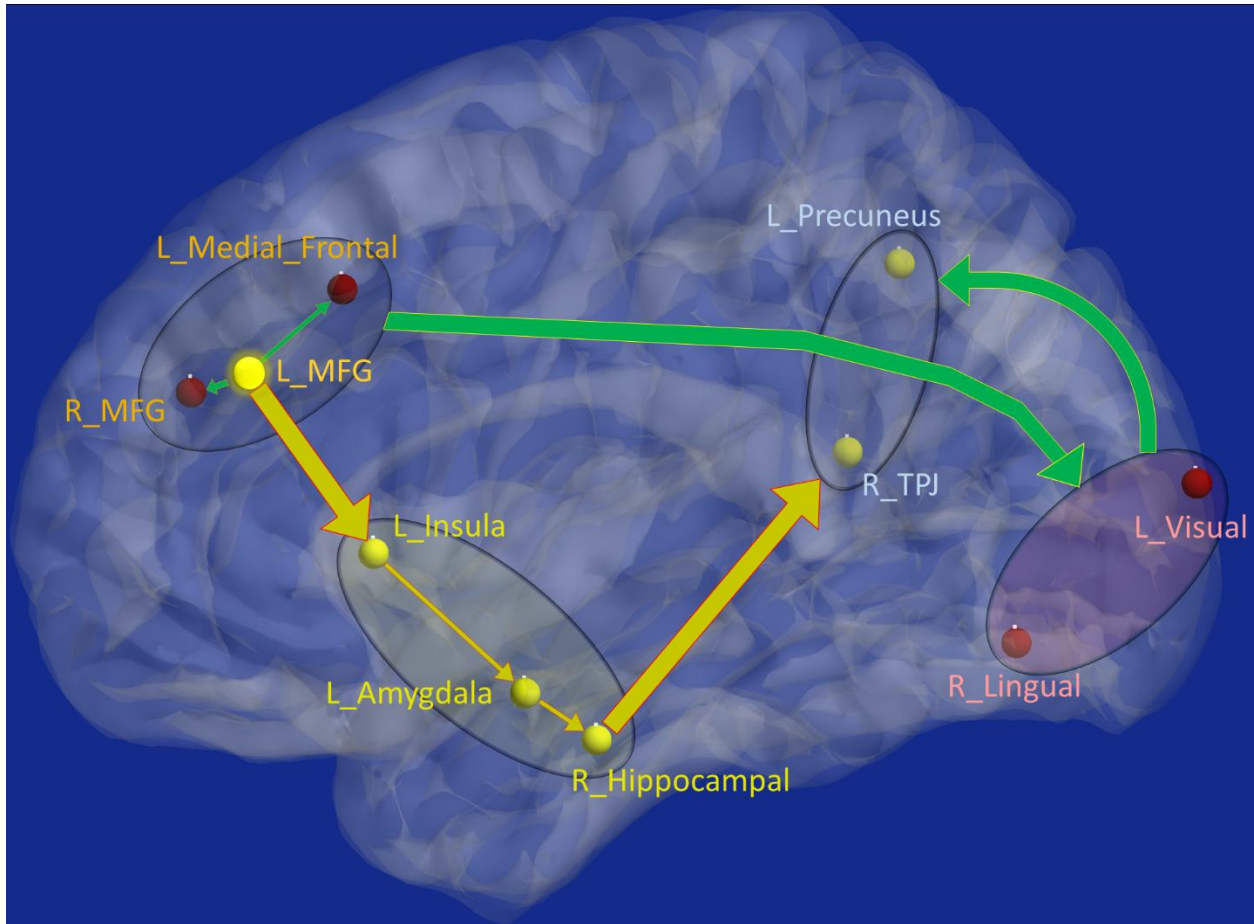
Fig.5.10. *Schematic of the entire network: Yellow nodes/paths were significantly altered for all three comparisons. Green paths (and red nodes) were altered except for PTSD vs PCS+PTSD comparison. Thick lines correspond to connections between major sub-networks while thin lines correspond to connections within sub-networks. The frontal sub-network consisted of MFG and medial frontal, the parietal sub-network consisted of TPJ and Precuneus, the visual sub-network consisted of lingual and primary visual areas while the emotion-memory sub-network consisted of sub-cortical regions such as Amygdala and hippocampus and cortical regions such as Insula. Disrupted Left-MFG causes deflation of emotion-memory regions and visual memory-retrieval regions, culminating in parietal-inflation causing heightened symptoms.*

5.3.2. Behavioral Relevance of Network Properties

Strength and temporal variability of functional integration values of four paths which were altered among all three groups (the yellow connections in Fig.5.10), as well as the strength and temporal variability of functional segregation of MFG and Insula (Fig.5.5) correlated significantly (p<0.05 Bonferroni corrected) with neurocognitive functioning (neurocognitive-composite-index [NCI]) and symptom severity in PTSD (PCL5-score) and PCS (NSI-score), thus highlighting their relevance to underlying neuropathology (see Table 5.2). Notably the correlations followed the expected trend: increase in severity and decrease in behavioral performance corresponded to higher static functional integration in inflated paths and lower in deflated paths, and lower variability (i.e. rigidity) in dynamic functional integration in all paths (similarly with segregation). However those connections which were not different between PTSD and PCS+PTSD (green paths in Fig.5.10), as well as other nodes in Fig.5.5 and global complex network measures had no significant correlations with behavior.

Table 5.2. *Correlation (R-value) of strength and variability of complex network measures with the NCI score and symptom severity in PTSD (PCL5 score) and PCS (NSI score). These correlations were significant with p<0.05 Bonferroni corrected.*

Complex Network Measure	Path (Integration) or Node (Segregation)	Symptom Severity Score		Behavioral Measure
		PCL5 score (PTSD)	*NSI score (PCS)*	*Neurocognitive Composite Index (NCI)*
Static Functional Integration Measures				
Shortest Path Length	L_MFG → L_Insula	-0.6902	-0.6756	0.6589
	L_Insula → L_Amygdala	0.6822	0.6759	-0.6298
	L_Amyg → R_Hippocampus	0.6535	0.6930	-0.6389

	R_Hippocampus → L_Precuneus	0.6990	0.6580	-0.3545
Edge Betweenness	L_MFG → L_Insula	-0.6704	-0.6853	0.5871
	L_Insula → L_Amygdala	0.7370	0.6868	-0.5303
	L_Amyg → R_Hippocampus	0.7080	0.6372	-0.3956
	R_Hippocampus → L_Precuneus	0.7156	0.6669	-0.4193
Variance of Dynamic Functional Integration				
Shortest Path Length	L_MFG → L_Insula	-0.7532	-0.7327	0.6704
	L_Insula → L_Amygdala	-0.7579	-0.7382	0.6748
	L_Amyg → R_Hippocampus	-0.7541	-0.7358	0.6709
	R_Hippocampus → L_Precuneus	-0.8520	-0.7737	0.4579
Edge Betweenness	L_MFG → L_Insula	-0.7330	-0.7287	0.6672
	L_Insula → L_Amygdala	-0.7358	-0.7260	0.6586
	L_Amyg → R_Hippocampus	-0.7326	-0.7264	0.6590
	R_Hippocampus → L_Precuneus	-0.8513	-0.7776	0.4619
Static Functional Segregation Measures				
Clustering Coefficient	L_MFG	-0.6859	-0.6685	0.6245
Local Efficiency	L_MFG	-0.7013	-0.6990	0.6826
	L_Insula	0.6527	0.6550	-0.6290
Dynamic Functional Segregation Measures				
Clustering Coefficient	L_MFG	-0.7478	-0.7271	0.6538
	L_Insula	-0.7412	-0.7204	0.6533
Local Efficiency	L_MFG	-0.7524	-0.7324	0.6692

Since multitude of network paths and nodes had relevant correlations with multitude of behaviors, it would be interesting to see how much variance in behaviors could be collectively explained by those network measures. We thus performed partial least squares regression (PLSR) [129] to find the combined ability of the strength and variability of functional integration of the 4

connections and functional segregation of 2 nodes to predict the set of 9 behaviors (PCL5 and NSI scores, NCI and its 6 subtests). We found that the strength of network measures could explain 48.95% variance in the behaviors, while the temporal variability of network measures could explain 57.17% variance. When both were combined, they could explain 61.74% variance in the behaviors. A high correlation between these network measures and behavior (R=0.746, p=3.5×10^{-32}) was found in the latent space (see Fig.5.11 for linear fit). This reiterates that the strength and variability of functional integration of the four paths and that of segregation of the two nodes identified in this work are behaviorally relevant.
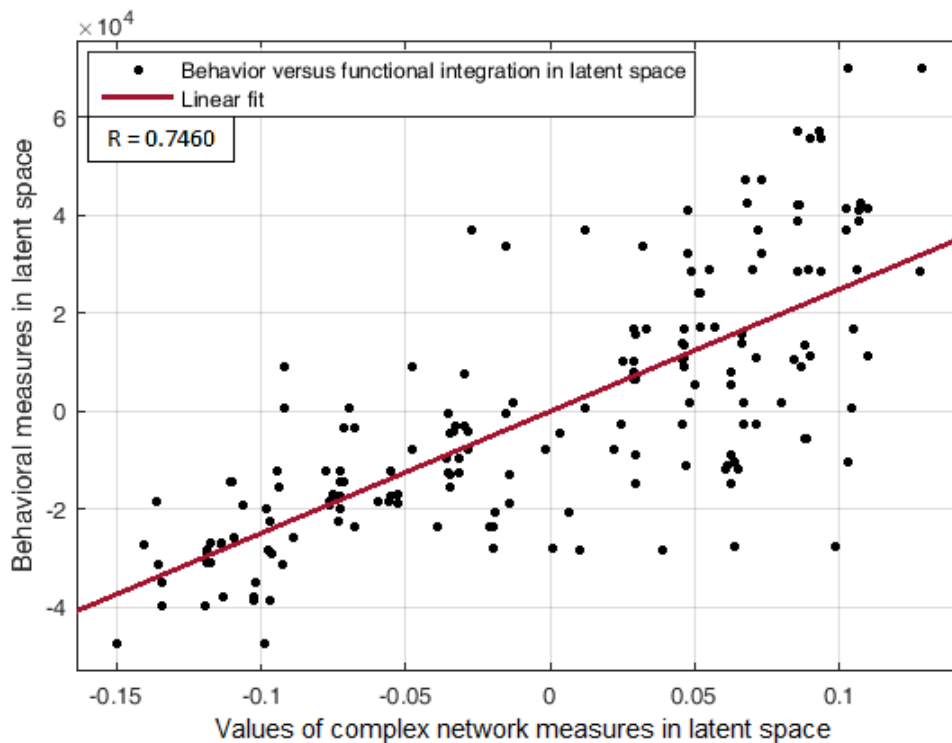

Fig.5.11. *Linear fit between strength and temporal variability of functional integration of the 4 connections (MFG→Insula, Insula→Amygdala, Amygdala→Hippocampus, Hippocampus→Precuneus) and functional segregation of 2 nodes (MFG, Insula), and behaviors in latent space*

5.3.3. Machine Learning Classification Results

Machine learning classification was performed as described in section 3.2.3 of this document. Statistically significant differences between groups for a specific neural signature may not necessarily imply that it is generalizable to a larger population and/or can predict the clinical diagnosis of an unseen subject. That means, statistically significant (conforming to our hypothesis) cum top-predictive features assume higher importance. Thus, to identify the top-predictors, we used recursive cluster elimination based support vector machine (RCE-SVM) classifier [57].

Classification was done with two different paradigms: (i) classification using the 32 non-imaging measures (NIMs), and (ii) classification using strength and temporal variability of network measures taken from the entire brain (all data, nothing left out). Results showed that classification using network measures provided significantly better accuracy (approximately 10% more, $p < 0.05$ Bonferroni-corrected) than classification using NIMs (Fig.5.12). This result indicates that network measures have superior predictive ability in identifying individuals with PCS and PTSD as compared to NIMs.
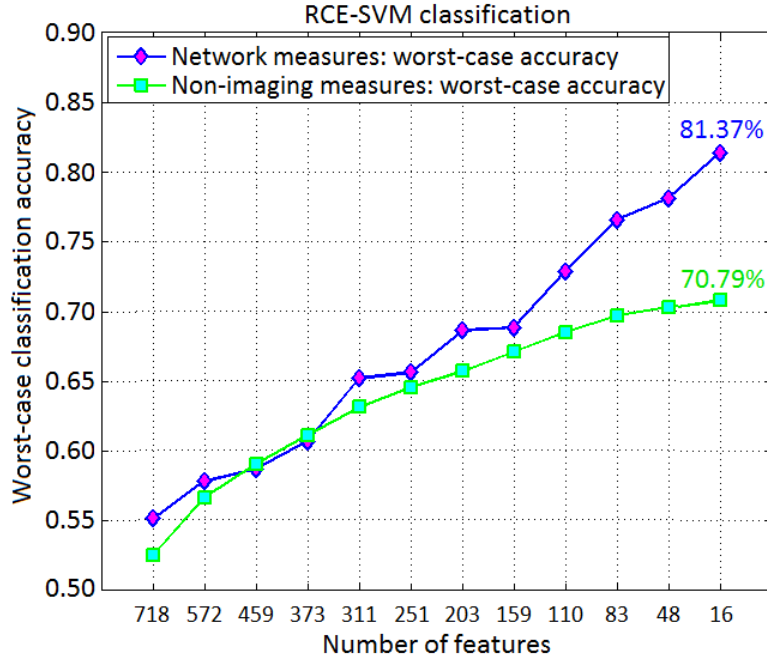
Fig.5.12. *Worst-case classification accuracies obtained using recursively reducing number of discriminative features, with both complex network measures obtained from the entire brain and non-imaging measures (NIMs). We observe that network measures outperforms NIMs, with approximately 10% superior performance using top-predictive features of network measures.*

Table 5.3 shows the worst-case accuracies and top predictive features (for average accuracy, please see Fig.5.13). Also of considerable interest are the top-predictors that resulted in highest classification accuracy. For classification using network measures, strength and temporal variability of functional integration of the following four paths were the top predictive features: L_MFG→L_Insula, L_Insula→L_Amygdala, L_Amygdala→R_Hippocampus and R_Hippocampus→L_Precuneus). Coincidentally all these four paths also showed statistically significant differences in network properties (the yellow paths in Fig.5.10, which were significantly different between all three groups). Also coincidentally, these were the same four paths whose network measures had significant correlations with neurocognitive functioning and

symptom severity. Statistical significance does not necessarily guarantee predictive ability of network measures [78]. Our findings elucidate that, in addition to behavioral relevance and statistical separation, these paths also possess the highest predictive ability, all obtained in a data-driven fashion from whole-brain complex-network data. Fig.5.3 summarizes the processing pipeline of our entire work, along with corresponding results.

Table 5.3. *Worst-case classification accuracies along with top-predictive features*

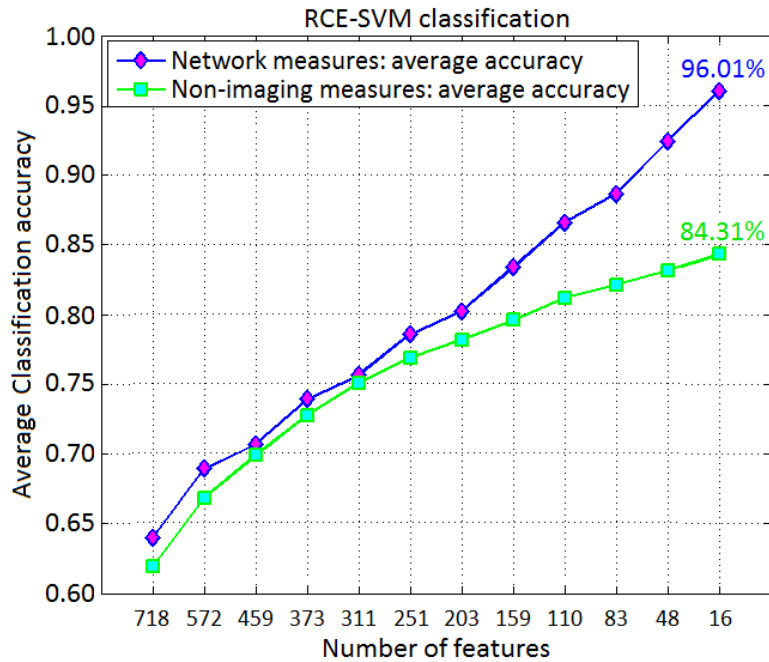|	**Worst-case accuracy**	**Top-predictive features**
Non-imaging measures	70.79%	Epworth sleepiness scale and Zung depression scale
Complex network measures of integration	81.37%	Strength and variability of functional integration of the 4 yellow paths in Fig.12
p-value for row-wise comparison	7.81×10^{-28}	

Fig.5.13. *Average classification accuracies obtained using recursively reducing number of discriminative features, with both whole-brain network measures and non-imaging measures. The trend is highly similar to what was observed with worst-case accuracies.*

5.4. Discussion

We employed complex network modeling in this work, in an effort to understand network-level characteristics of directional brain networks and associated impaired network architectures in PTSD with and without mTBI. With the evidence that the healthy brain is characterized by a balance between functional segregation and integration, we sought to identify alterations in segregation and integration in these disorders. We hypothesized that PTSD and mTBI are characterized by altered strength (either inflated or deflated network properties) and lower temporal variability (i.e. rigidity) of segregation and integration in directional brain networks. We sought to identify such networks which were affected by PTSD but not mTBI (hypothesis-1), as well as those affected by both PTSD and PCS+PTSD (hypothesis-2). We found evidence for our hypotheses, in that we identified certain nodes/paths which had altered segregation/integrations as discussed below.

First with global measures, we found that segregation and integration were significantly altered for control vs PTSD and control vs PCS+PTSD comparisons only, implying that the disorder groups have whole-brain-level alterations compared to controls but the PTSD and comorbid groups do not exhibit any whole-brain-level differences between themselves, suggesting rather more localized differences in them. To get further insight, we studied local measures of segregation and integration

With local segregation measures, we observed a clear dichotomy between prefrontal and occipital regions, with all identified prefrontal nodes having lower segregation and all identified occipital and subcortical nodes having higher segregation. This indicates disrupted local processing in the prefrontal cortex, especially in the MFG and medial prefrontal regions. This disruption seems to have a negative relationship with the occipital and subcortical nodes which showed increased local processing. Also, all alterations in occipital nodes were not different between PTSD and PCS+PTSD implying that those regions might not have a role to play in differentiating between PTSD and PCS+PTSD.

With local integration measures, we found a clear dichotomy along two distinct pathways. The fronto-visual-parietal pathway (Fig.10) was not altered between PTSD and PCS+PTSD groups, indicating that an mTBI likely does not have an impact on this part of the network. Since none of these paths or the associated occipital regions (either connectivities or network measures) had any significant correlation with symptom severity (PCL5, NSI), we inferred that this part of the network does not play a significant role in symptom generation, but might act as a supportive backend for other processes generating the symptoms. The other pathway (fronto-subcortical-parietal, Fig.5.7) was significantly altered between all three groups, and network properties of the paths also correlated significantly with symptom severity and neurocognitive functioning. We thus inferred that this part of the network plays a considerable role in symptom generation, and thus highly important for PTSD and mTBI pathology. This dichotomy provides novel insights into our understanding of both common and distinguishing network characteristics in PTSD and mTBI, which has largely plagued the field, given the high comorbidity and overlapping symptomatology between them [13].

Another clear dichotomy arises in the strength of network properties across groups. All prefrontal nodes and the paths associated with them had lower segregation/integration in PTSD and PCS+PTSD compared to controls, vividly indicative of the strong effect of disruption arising from the prefrontal cortex. All the subcortical, parietal and occipital nodes had higher segregation, and all paths associated with them not involving prefrontal regions had higher integration in PTSD and PCS+PTSD compared to controls, clearly indicative of inflation in these regions. Notably these trends exhibited by network measures were also exactly replicated in the raw effective connectivity values. Such unambiguous dichotomy clearly delineates the distinct functionality between the prefrontal cortex and the rest of the brain, and its relevance to PTSD and mTBI.

However such a dichotomy did not exist in variance of network properties, with all nodes/paths having lower variance, indicative of a pathological "frozen" state (in accordance with our hypothesis). That is, paths with lower strength of network properties (deflation) tended to remain in that state over the duration of the scan, indicating that they could not get out of the deflated state most of the time. Similarly paths with higher strength of network properties (inflation) tended to remain inflated, indicating that they were stuck in that state most of the time. In total, we identified 15 nodes (segregation) and 16 paths (integration) which were altered in the Control vs PTSD and Control vs PCS+PTSD comparisons, while only 4 nodes and 5 paths were altered across all three groups. It is noteworthy that, except amygdala and parietal regions, all other nodes involved in affected connections with functional integration also had altered segregation, implying that such regions exhibited a clear segregation-integration imbalance.

The networks were obtained with resting-state data, hence signifies the baseline state difference between groups. We propose, based on prior knowledge [9], that this network corresponds to lack of prefrontal control over the emotion-generation system, leading to an insufficient control over

emotionally-intensive traumatic memories, which leads to trauma re-experiencing, flashbacks, hyperarousal and other symptoms in soldiers with PTSD and PCS+PTSD.

Functions of the individual nodes/regions identified with alterations of complex network properties provides interesting insights into the neuropathology underlying PTSD and mTBI. The MFG is a known key player in cognitive control [130], which includes emotion regulation. It has a pivotal role in the initiation of conscious cognitive emotion regulation [9]. On the other hand, amygdala is necessary for emotion generation, and medial prefrontal regions mediate subconscious emotion regulation like fear conditioning [9]. All of the network-level alterations in our results could be traced back to the MFG, leading us to conclude that MFG is the origin of dysfunction in these disorders. Many earlier works have speculated about MFG to be the likely origin of dysfunction in PTSD [131, 89], including in a recent meta-analysis [93], while direct evidence for such a hypothesis has not been found. We provide one of the first evidence in that direction. In fact, a recent ALE meta-analysis work presented evidences from numerous findings that repetitive transcranial magnetic stimulation (rTMS) applied to the MFG could potentially be employed for the treatment of PTSD [132], though they do not elucidate the underlying mechanisms. We discovered the network of disturbance possibly caused by dysfunctionality of MFG, wherein MFG is the source of disruptions. Taken together, MFG likely plays a key role in the initiation of cognitive control which includes emotion regulation, whose disruption likely leads to a chain-reaction of impaired cognitive control.

We noticed prefrontal top-down deflation of functional integration driven by MFG, resulting in the inflation of functional integration in sub-cortical structures via insula as well as parietal memory-retrieval and sensory association regions. Anterior insula plays a major role in mediating prefrontal control over subcortical areas, and is thus found to be involved in emotion regulation

and dysregulation [9, 133]. It is structurally well connected with amygdala through white-matter tracts [134], and also plays a key role in subjective emotional experiences (feelings), integrating emotionally relevant information through multiple sources, and possibly representing them as one of the many complex emotions. We found that prefrontal deflation of insula causes inflated functional integration in amygdala, which then results in inflated local functional integration in hippocampus. Inflation of hippocampus, a prime region involved in declarative memories, might imply elevated explicit traumatic memory retrieval. It is well documented that hippocampus and amygdala play a vital role in mTBI and PTSD [93, 12]. Traumatic memories are unique in the intensity of associated negative emotions, so emotion and memory share deep interconnection in PTSD.

Precuneus plays a key role in the generation of the experience of visual memories, whereas TPJ is critical for higher-level audio-visual verbalization and information processing [9]. The path from MFG leading to these regions was characterized by reduced strength and variance of functional integration. Thus the memory-retrieval and sensory association network comprising the precuneus and TPJ seems to translate the subcortical inflation and lack of frontal control into elevated retrieval of traumatic memories. This likely leads to trauma re-experiencing, flashbacks, hyperarousal and such symptoms observed in soldiers with mTBI and PTSD.

There is a large presence of occipital regions in our results. While majority of nodes and paths were associated with it, none of them were different between PTSD and PCS+PTSD groups, and none of them had behavioral relevance (through correlations with symptom severity and neurocognitive performance). Hence we inferred that this part of the network does not play a significant role in symptom generation, but might act as a supportive backend for the other fronto-subcortical-parietal processes which generate the symptoms. This inference is justifiable since

visual imagery aspect of traumatic memories dominates the experience of flashbacks, re-experiencing and other symptoms in these disorders. It is known that secondary visual areas including lingual gyrus largely enable visual imagery [144]. Also the degree of activation in visual areas during imagery is directly proportional to the visual intensity of the object being imagined [145]. Hence, it is possible that the visual intensity of the traumatic memories (vividness or strength of the visual content) is not different between PTSD and PCS+PTSD groups, but is different in these disorder groups compared to controls (because PTSD and PCS+PTSD groups suffered posttraumatic stress due to trauma, while controls did not). This could provide substantiation for our inference that the occipital part of the network might be a backend process providing 'imagery' support. The severity of symptoms could thus be directly proportional to the inflation in subcortical regions and their origins in MFG, which is substantiated by the fact that their network properties correlated significantly with neurocognitive performance and symptom severity.

Our understanding of comorbid PTSD and mTBI does not appear to have progressed far in the past. However it remains to be known that the additional burden of an mTBI in comorbid PCS+PTSD results in increased symptom severity [123]. We provide a mechanistic explanation for these behavioral observations, and also explain the network of disturbance that distinguishes between PTSD and comorbid PTSD/mTBI.

Collectively taken, we identified the MFG to be pivotal to disruption in soldiers with mTBI and PTSD (since all network-level disturbances could be traced back to this region), which further affected other emotion and memory processes, potentially exacerbating symptoms. This network provides a mechanistic explanation of impaired cognitive control with emotion dysregulation, and

subsequent inability to control traumatic memories, contributing to many symptoms observed in soldiers with mTBI and PTSD. Fig.5.14 summarizes our findings with a flowchart.
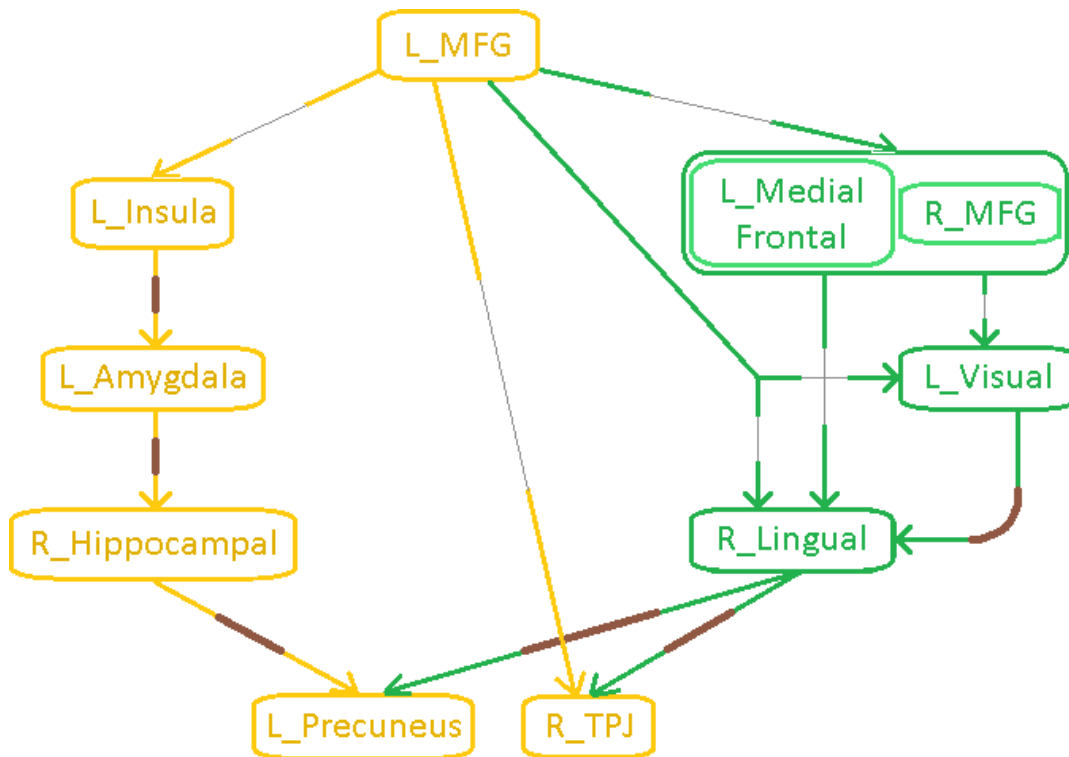
Fig.5.14. *Flowchart illustrating an integrated model of connectivity and network level alterations in PTSD and mTBI. Paths with thin gray lines correspond to lower strength of network properties and connectivity (SEC) and lower temporal variability of network properties (i.e. rigidity) and connectivity (vDEC) in patients compared to healthy controls, indicative of breakdown in frontal top-down modulation. Paths with thick brown lines correspond to higher strength and lower temporal variability (i.e. rigidity) of network properties and connectivity, indicative of inflation in subcortical limbic and parietal memory-retrieval regions. Yellow paths were significantly different between all three groups, while the green paths were different for all comparisons except the PTSD vs PCS+PTSD comparison.*

Our results are significant given that regions affected here have been implicated (inconsistently) in earlier studies [93, 76, 11] to be involved in both PTSD and mTBI, but a precise understanding of the underlying mechanisms, network structure and their subsequent causal relationships has not emerged from them. With the help of a novel framework involving complex network modeling with static and dynamic EC networks, we identified the nodes and network paths associated with the disorders, and detailed their directional relationships. We also highlighted the commonalities and differences in PTSD and PCS+PTSD networks. Our characterization corroborates with behavioral manifestations of PTSD and PCS+PTSD, thus substantiating the utility and fidelity of our approach.

Additionally, functional integration of four paths had significant correlations with neurocognitive performance and symptom severity (MFG→insula, insula→amygdala, amygdala→hippocampus, hippocampus→precuneus), as also did functional segregation of two nodes (MFG and insula), highlighting their behavioral relevance. These paths and nodes were also those which were significantly altered between all three groups. In the PLS regression model, the aforementioned network measures taken together could also explain about 62% variance in the behaviors.

Upon performing machine learning classification, it was found that accuracies obtained using network measures were significantly higher (~10% more) than non-imaging measures. Interestingly, we found that it were the network measures of the same four aforementioned paths that resulted in the highest classification accuracy. They were thus identified to be the top predictive features of diagnostic ability, along with being statistically significant and behaviorally relevant, which were all determined in a data-driven fashion from network properties of the entire brain. This demonstrates that these network-level markers could be high-quality indicators of

neural and behavioral characteristics of PTSD and PCS, and have potential as imaging biomarkers for these disorders. Our network-level features satisfy three out of four conditions enumerated by Woo *et.al.* [88] to be fulfilled by a good biomarker (diagnosticity, deployability and interpretability). With regard to the fourth condition (generalizability), based on suggestions by Woo *et.al.*, we issue an open call for researchers possessing similar data to share them with us, in order for our classifier be tested on them.

Our novel framework is relevant to the study of any psychiatric condition or cognitive domain. We urge researchers to employ this framework for better understanding other disorders and cognitive domains.

CHAPTER 6

Hemodynamic Variability and its Impact on Connectivity Modeling

6.1. Introduction

Functional MRI (fMRI) is used extensively for studying neural correlates of brain functioning. FMRI is an indirect measure of neural activity as it measures changes in blood oxygenation level. Blood oxygenation is impacted by neural activity, the neurochemical signals which couple neural activity with blood flow, the properties of blood flow and the biochemistry of blood's response to oxygen demand from the neurons. The non-neural components of the hemodynamic response vary across brain regions, which are in turn variable across individuals [10, 146]. With neural activity being the subject of interest in fMRI studies, interpretation of results are often less reliable due to the aforementioned non-neural sources of variability in fMRI.

The mathematical transfer function between local neural activity and corresponding blood oxygenation level dependent (BOLD) fMRI signal is called the hemodynamic response function (HRF). Most fMRI studies assume a standard canonical HRF (usually made up of two gamma functions) during analysis. However, prior works show variability in HRF for different brain regions across subjects [10, 146]. This challenges the interpretation of fMRI results since it is unclear if observed changes are due to neural activity or HRF variability. There are three main dimensions of variability in HRF: (i) intra-subject spatial variability (the HRF being different in different brain regions of the same individual), (ii) inter-subject intra-group variability (for a given location in the brain, the HRF being different across different healthy individuals), and (iii) inter-

138

group variability (for a given location in the brain, the HRF being different between a healthy group and a pathological group, arising in part from neurochemical disturbances due to pathology). Each of these dimensions can lead to misleading results during fMRI data analysis.

Intra-subject variability, for example, could lead to detection of false activations or mistaken strong connectivities, as well as missed true activations or mistaken weak connectivities. Inter-subject variability can lead to noisy variations in variables of interest, thus reducing the statistical significance of true effects, while attributing higher significance to false effects. Inter-group variability causes detection of wrong group differences in activations or connectivities, as well as missed detection of true effects. The effect of HRF variability on activation analysis can be alleviated, in part, by using time and dispersion derivatives in the general linear model [147]. Much attention has also been received on the effect of HRF variability on lag-based connectivity models [148]. However, its effects on zero-lag connectivity models based on Pearson's correlation have not been explored. In this work, we address this issue by investigating the effect of inter-group HRF variability on zero-lag functional connectivity differences between the groups. In order to do so, we considered the case of soldiers with posttraumatic stress disorder (PTSD) and post-concussion syndrome (PCS) [4], a chronic outcome associated with mild traumatic brain injury [mTBI]).

PTSD and mTBI arising from combat exposure are highly relevant to the society, with large percentage of soldiers acquiring them during warfare. In the U.S. alone, more than 2.7 million soldiers served in Iraq and Afghanistan, with about 20% acquiring PTSD, 19% acquiring mTBI and 7% acquiring both [1]. PTSD has high comorbidity with mTBI [2], added to the fact that they have similar symptomatology [5]. Recent evidences using Doppler ultrasound and infrared spectroscopy suggested alterations in cerebrovascular reactivity in mTBI [149]. Neurochemical

alterations in PTSD are well established [150], though it is important to explore if these changes affect cerebrovascular reactivity. We hypothesized that the HRF, which depends on cerebrovascular reactivity and neurovascular coupling, may be altered in PTSD and mTBI. We then tested this primary hypothesis by obtaining significant group differences in voxel-specific HRF parameters which were estimated by performing blind hemodynamic deconvolution of resting-state fMRI data obtained from these populations. As a corollary, we also tested the hypothesis (=secondary hypothesis) that functional connectivity differences between groups are at least partially driven by HRF differences, if HRF variability is not removed through deconvolution.

The HRF is characterized by three main parameters [10, 146] (see Fig.6.1): (i) response height (RH), (ii) time-to-peak (TTP), and (iii) full-width at half-max (FWHM). Recent works have shown that reduced TTP and FWHM as well as increased RH are attributable to disruption in metabolism and microvasculature associated with brain pathology [151]. Additionally aging causes reduction in TTP/FWHM and increase in RH [152]. Taken together, this profile of HRF alterations could be indicative of degraded neurochemical metabolism in the brain. With our primary hypothesis, we predicted that the HRF in PTSD and mTBI would be taller (RH), quicker (TTP) and narrower (FWHM) as compared to healthy combat controls in certain affected regions.
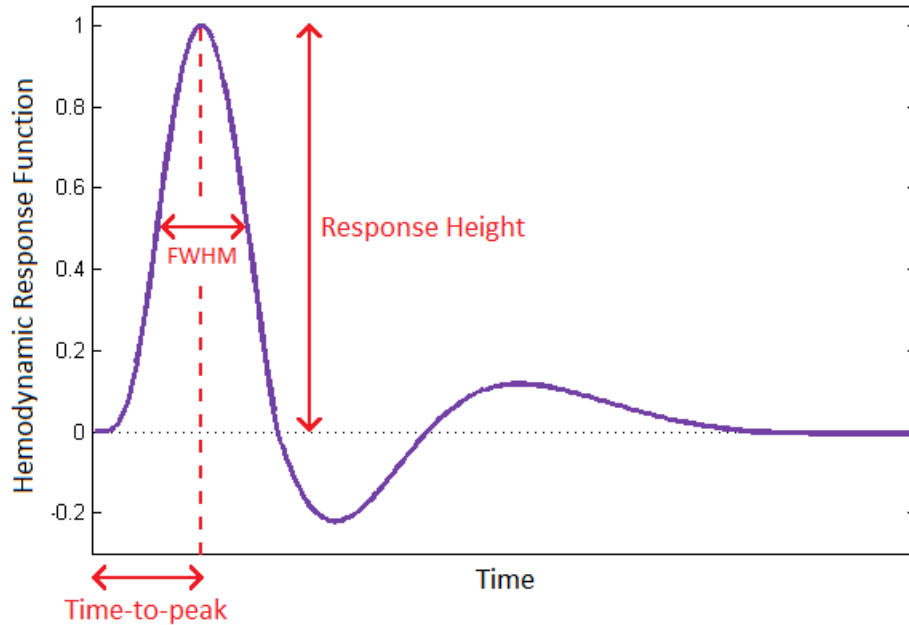
Fig.6.1. *Typical HRF with its three characteristic parameters. FWHM = full-width at half max.*

Upon identifying HRF differences between the groups, it would be necessary to elucidate its impact on fMRI data analysis and subsequent inferences. This would impact fMRI analysis at large, as well as studies on PTSD and mTBI. In this work, we consider the impact of HRF variability on functional connectivity (FC) analysis. Specifically, we investigate the negative effects of HRF variability on group-wise connectivity differences.

We elucidate two possible negative effects using example time series from experimental resting state fMRI data (please refer to Fig.2.2 in Chapter 2): (i) there exists no correlation between latent neural signals, but BOLD fMRI time series show high correlation, and (ii) there is true high correlation between latent neural signals, but BOLD fMRI time series show no correlation. The former leads to possible false positives while the latter leads to possible false negatives in traditional fMRI FC analysis that does not remove HRF variability. Since the ground-truth HRF is not known, and the HRF is being estimated from a blind deconvolution approach, we do not take

141

the leap of calling them false positives or negatives. Instead they are likely false positives and false negatives, or what we term as pseudo-positives and pseudo-negatives respectively.

In this work, we identified the cluster(s) which showed significant differences in HRF between the groups (our primary hypothesis), and performed seed-based connectivity using the cluster(s) as seed(s). Similar to the example, we hoped to identify pseudo-positives and pseudo-negatives arising from traditional connectivity analysis, which ignores HRF variability, given the fact that those seeds have different HRF profiles across the groups. Significant group differences in connectivity were obtained. This procedure was performed for two separate pipelines: (i) data pre-processed without hemodynamic deconvolution, (ii) data pre-processed with hemodynamic deconvolution. Deconvolution minimizes HRF variability from BOLD fMRI, giving latent neural variables. We then compared the group differences in connectivity for the two pipelines. We hypothesized that (=secondary hypothesis), owing to HRF variability, data without deconvolution would show misleading connectivity differences (both pseudo-positives and pseudo-negatives) as compared to the data with deconvolution.

6.2. Methods

6.2.1. HRF Analysis

HRF analysis began with the preprocessed (and deconvolved) resting-state fMRI data, along with the HRF parameters obtained as a by-product of deconvolution. Deconvolution provided the estimated HRF at each voxel in each subject, which was characterized by three parameters – response height (RH), time-to-peak (TTP), and full-width at half-wax (FWHM), as illustrated earlier. Tests for statistical significance were performed separately on each of the three parameters to obtain group-wise voxel-specific differences in HRF parameters ($p<0.05$, cluster-level

thresholded, controlled for age, race, education and head-motion). This was done separately for the three pairwise comparisons between groups, that is, Control vs PTSD, Control vs PCS+PTSD and PTSD vs PCS+PTSD. We thus obtained nine maps: three comparisons with three parameters each.

These maps were then used to obtain the following final overlapped (intersection) maps of interest. (i) O-1: Overlap between Control vs PTSD and Control vs PCS+PTSD maps (we call this control vs disease comparison), for each of the three HRF parameters separately. This would elucidate HRF differences in disease compared to healthy controls, which would directly validate or invalidate our primary hypothesis. (ii) O-2: Overlap between all the three HRF parameters' maps obtained from both Control vs PTSD and Control vs PCS+PTSD comparisons (i.e. control vs disease). These differences would obviously be a subset of the first case, but would identify those regions with alteration of all HRF parameters in PTSD and mTBI. (iii) O-3: Overlap between all three group-wise comparisons for each of the three HRF parameters separately. This would illustrate those HRF differences which were altered in all the groups. These differences would naturally be a subset of the first case. These differences represent important information regarding PTSD and mTBI since identifying commonalities and differences between them are of deep interest, given that the two disorders have high comorbidity and similar symptomatology [5]. In all cases, the overlapped maps were obtained by finding the common regions in the maps being considered (i.e. intersection), which had a cluster size of at least $50mm^3$ in the overlapped map (to eliminate false positives).

6.2.2. Seed-Based Functional Connectivity Analysis

The overlapped maps obtained from the second and third cases mentioned above were used in further seed-based functional connectivity (FC) analysis, with the identified cluster(s) being chosen as the regions of interest (ROIs). The time series from all the voxels in each ROI were averaged to obtain a single time series per ROI. Seed-based connectivity was performed by evaluating Pearson's correlation coefficient between mean time series from the seed ROI and rest of the voxels in the brain. Significant group differences in FC were obtained between all groups (p<0.05, FDR corrected, controlled for age, race, education and mean head-motion). This pipeline was implemented separately for two cases: (i) NDC: data pre-processed without deconvolution, and (ii) DC: data pre-processed with deconvolution. The NDC case, which is the traditional approach in most studies, contains data contaminated by HRF variability. As hypothesized by us (secondary hypothesis), we expected to see pseudo-positives and pseudo-negatives in the connectivity map obtained from NDC data as compared to the DC data. The pseudo-positives were obtained from final NDC and DC maps as "NDC > DC". Similarly pseudo-negatives were obtained as "NDC < DC". We tested our secondary hypothesis through these two maps.

6.3. Results

6.3.1. Inter-Group HRF Differences

As mentioned earlier, pair-wise group differences in voxel-wise values of each of the three HRF parameters were obtained, and three categories of overlapped maps were derived from them. In all the regions with altered HRF, we found that RH increased in the disorders compared to controls, while TTP and FWHM decreased in the disorders. We first elucidate the differences for Control vs Disease comparison, which refers to an overlap of Control vs PTSD and Control vs PCS+PTSD

144

comparisons (overlap O-1 mentioned earlier). Differences in RH were found in (see Fig.6.2) thalamus, midbrain, precuneus, posterior cingulate cortex (PCC), secondary visual areas and parts of insula (anterior and posterior). Further, alterations in TTP (Fig.6.3) and FWHM (Fig.6.4) were largely similar, with key default-mode network (DMN) regions being disrupted (PCC and precuneus) along with secondary visual areas.
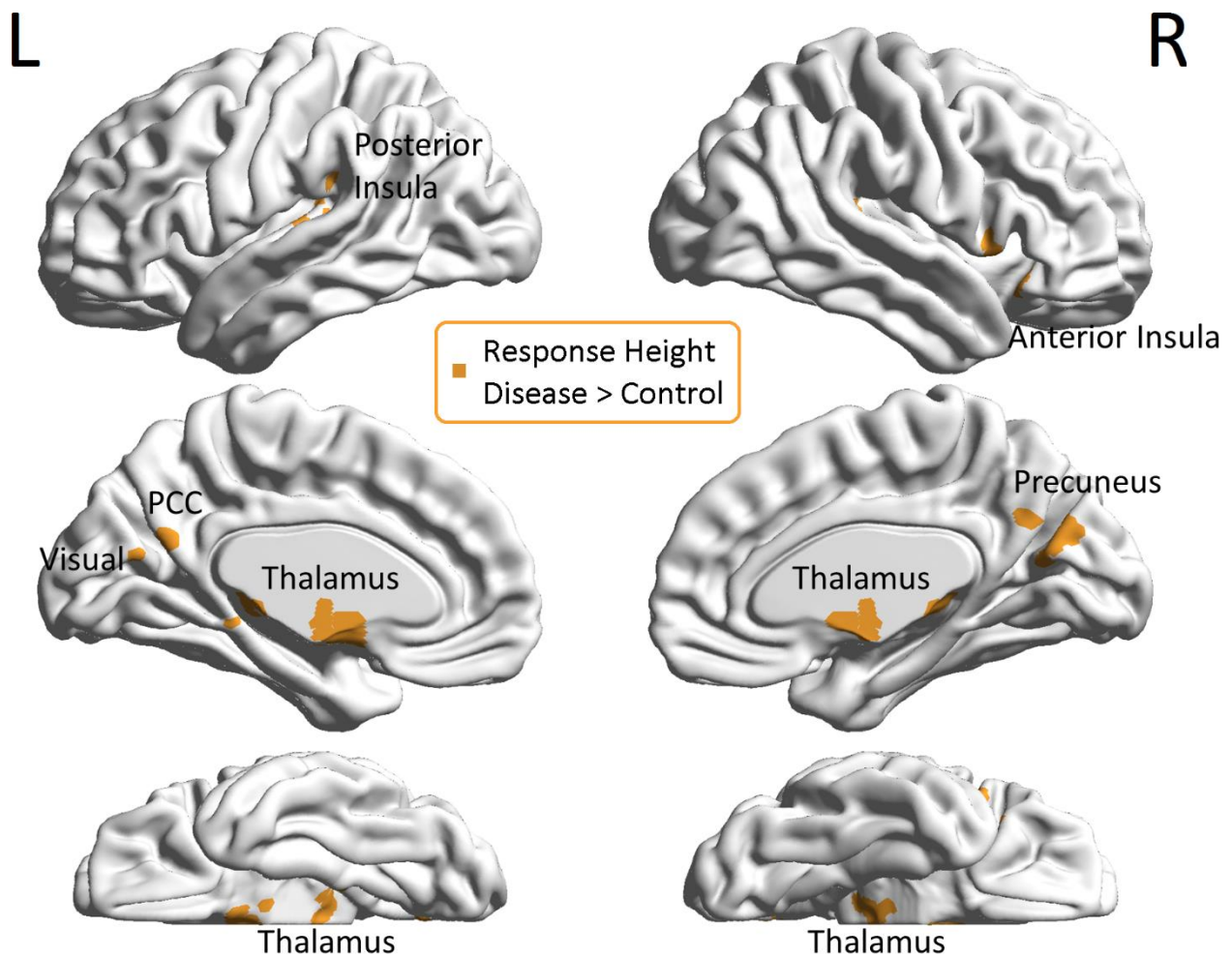
Fig.6.2. *Regions with significantly altered response height (RH) in hemodynamic response function, HRF. They were significant for PTSD > Control and PCS+PTSD > Control*

comparisons. Thalamus, midbrain, insula, visual and default-mode network regions were altered.

PCC = posterior-cingulate cortex. Please refer to Appendix A, Table A1 for further details.
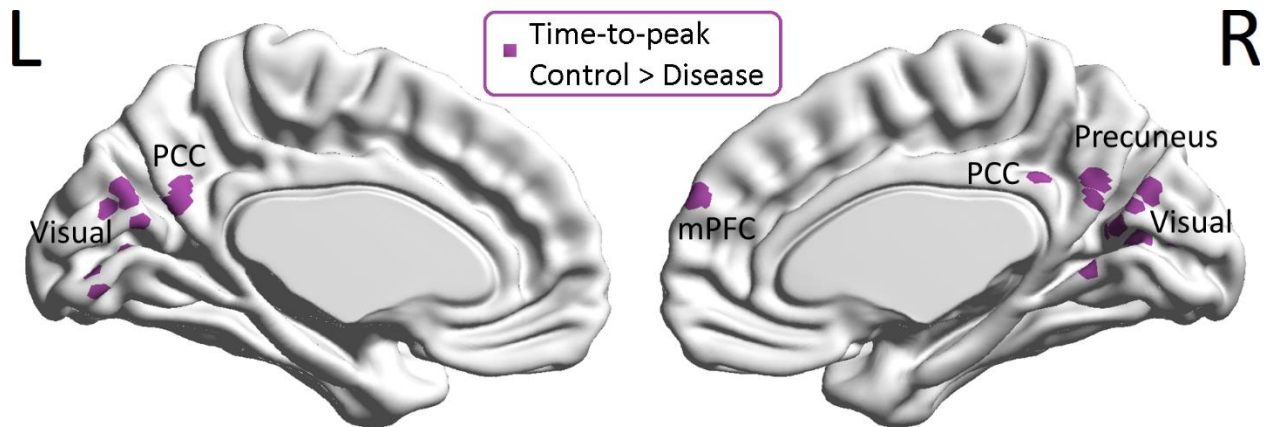
Fig.6.3. *Regions with significantly altered time-to-peak in HRF. They were significant for Control > PTSD and Control > PCS+PTSD comparisons. Visual and default-mode network regions were altered. PCC = Posterior-cingulate cortex. Please refer to Appendix A, Table A2 for further details.*
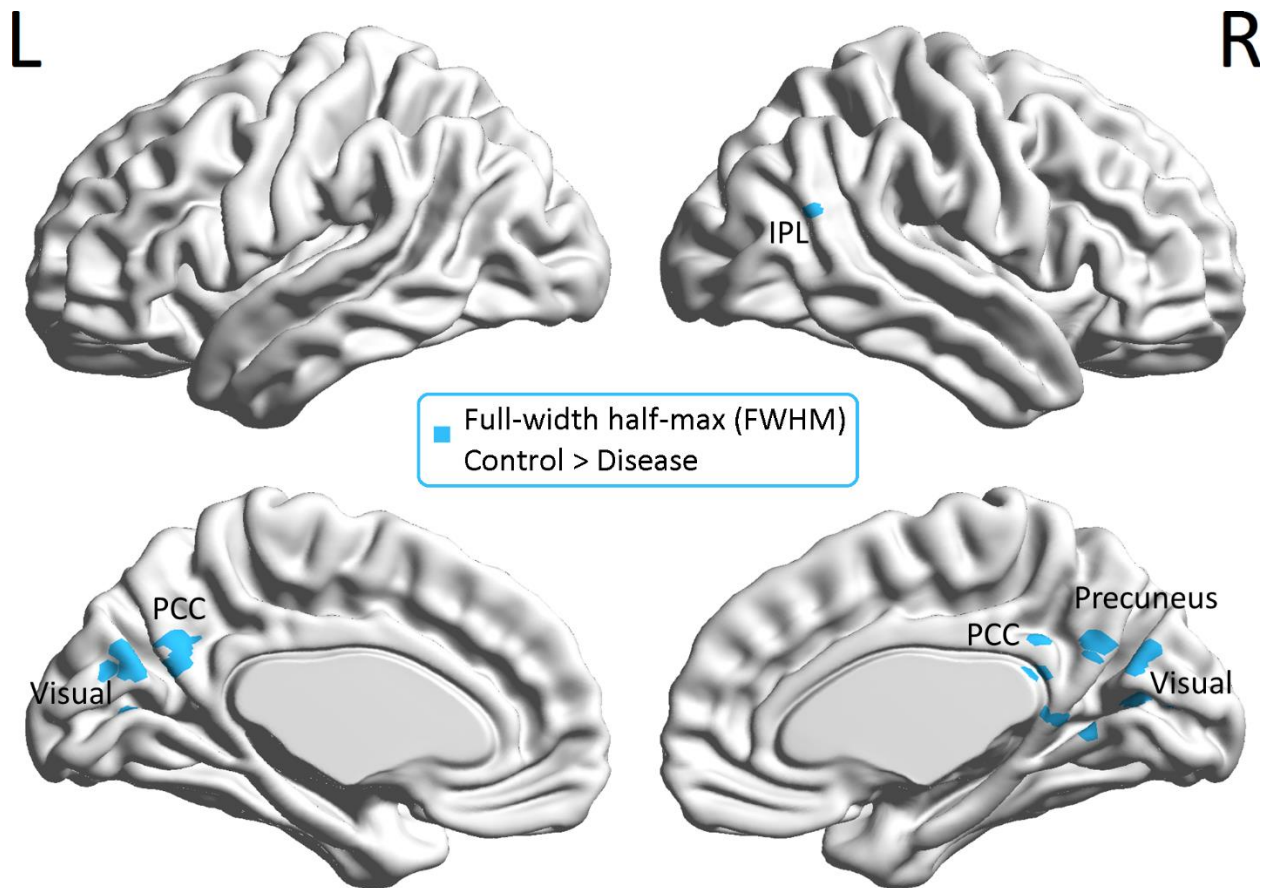
Fig.6.4. *Regions with significantly altered FWHM in HRF. They were significant for Control > PTSD and Control > PCS+PTSD comparisons. Visual and default-mode network regions were altered. PCC = Posterior-cingulate cortex; IPL = inferior parietal lobule (angular gyrus). Please refer to Appendix A, Table A3 for further details.*

Next, we present the results for overlap between RH, TTP and FWHM for Control vs Disease (overlap O-2 mentioned earlier). We found the common regions to be left PCC and right precuneus (see Fig.6.5). Then, identifying those differences which were significantly different between all three groups (overlap O-3), we found FWHM to be significantly different between all three groups in left PCC and right precuneus again (see Fig.6.6, note: RH and TTP did not show differences).
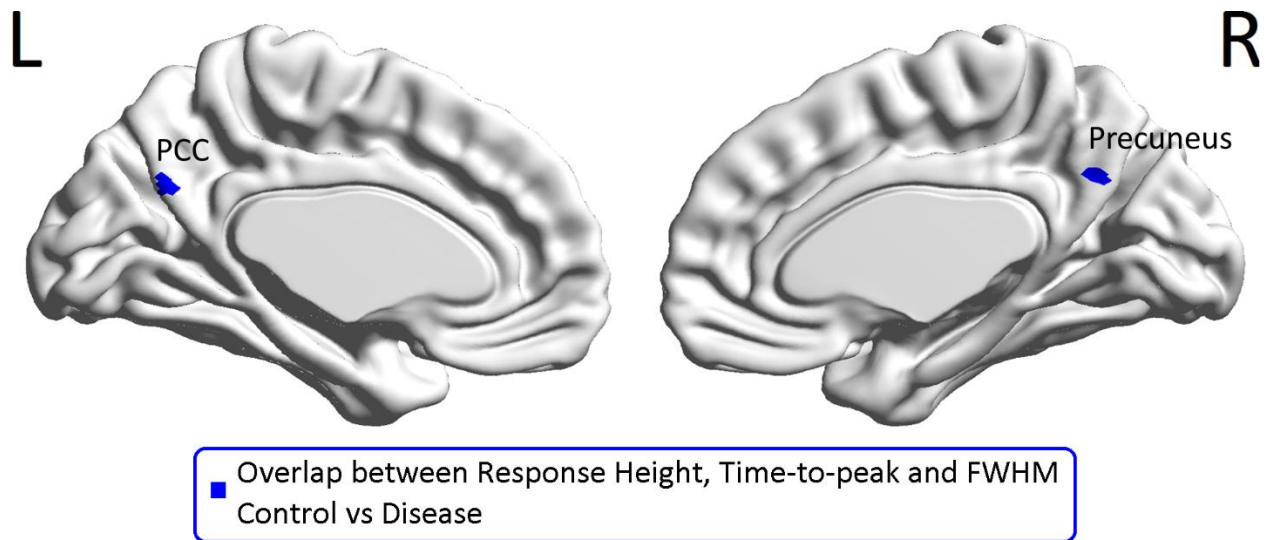
Fig.6.5. *Regions which had significant alterations in all three HRF parameters. They were significant for Control > PTSD and Control > PCS+PTSD comparisons. Posterior-cingulate cortex (PCC) and precuneus were identified. Please refer to Appendix A, Table A4 for further details.*
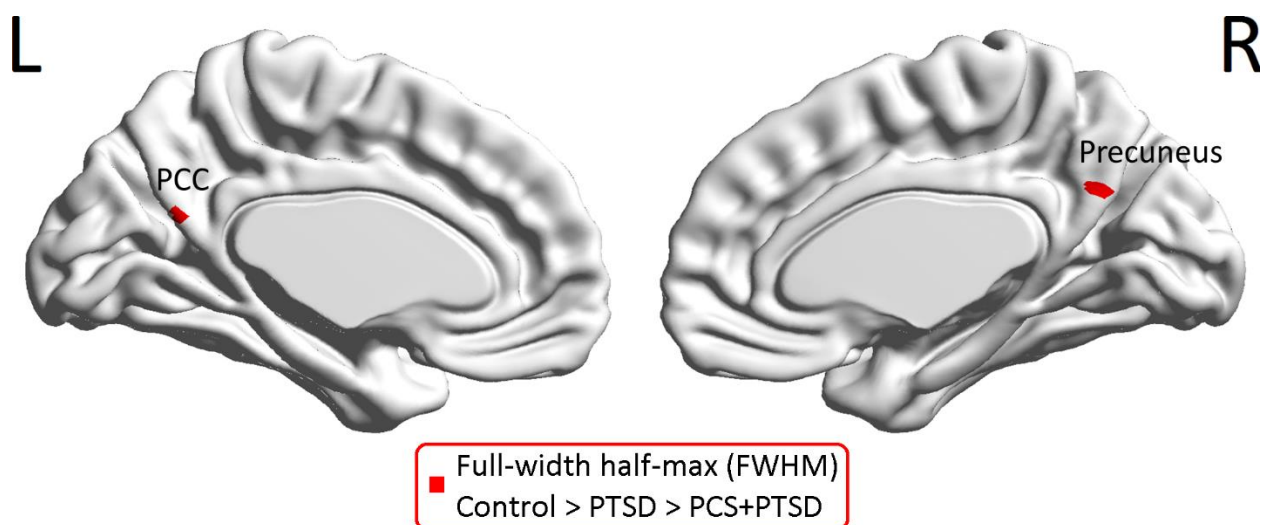
Fig.6.6. *Regions which were significantly different between all three groups, implying that both PTSD and mTBI caused alterations in them. This difference was observed only with FWHM.*

Posterior-cingulate cortex (PCC) and precuneus were identified. Please refer to Appendix A, Table A5 for further details.

6.3.2. Seed-Based Functional Connectivity Analysis

In accordance with our secondary hypothesis, we performed seed-based FC analysis using left PCC (as well as right precuneus, independently) as the seeds, thus obtaining two separate set of connectivity maps, one for each seed. Group differences in FC were then obtained for each seed. We performed this procedure for two separate pipelines: (i) NDC: data pre-processed without deconvolution, and (ii) DC: data pre-processed with deconvolution. Results from the two pipelines were then compared, with the hope of identifying pseudo-positives (connectivities which are not significantly different [or considerably less statistically significant] after removal of HRF variability, but are significantly different in NDC case), and pseudo-negatives (connectivities significantly different in DC case but not (or less) in NDC case). Pseudo-positives were obtained as: NDC map > DC map, and pseudo-negatives as: NDC map < DC map. Here we present the results for the PCC ROI, while results for the precuneus ROI can be found in Appendix A, since the latter also leads to the same conclusion as the former (Figs A1 through A4 and Tables A10 through A13).

Group differences for the NDC (Fig.6.7) and DC (Fig.6.8) pipelines clearly show that the identified significant alterations in PTSD and mTBI differ appreciably between the two pipelines. This translates to providing us the evidence that HRF variability drives a sizeable portion of group differences reported in fMRI studies ignoring such HRF variability. We also notice that there are more number of pseudo-positives (Fig.6.9) than pseudo-negatives (Fig.6.10), which is especially

undesirable since false activations are more detrimental than missed detections. These observations are formally presented in Table 6.1.

Significant group differences in seed-based correlation for the L_PCC ROI
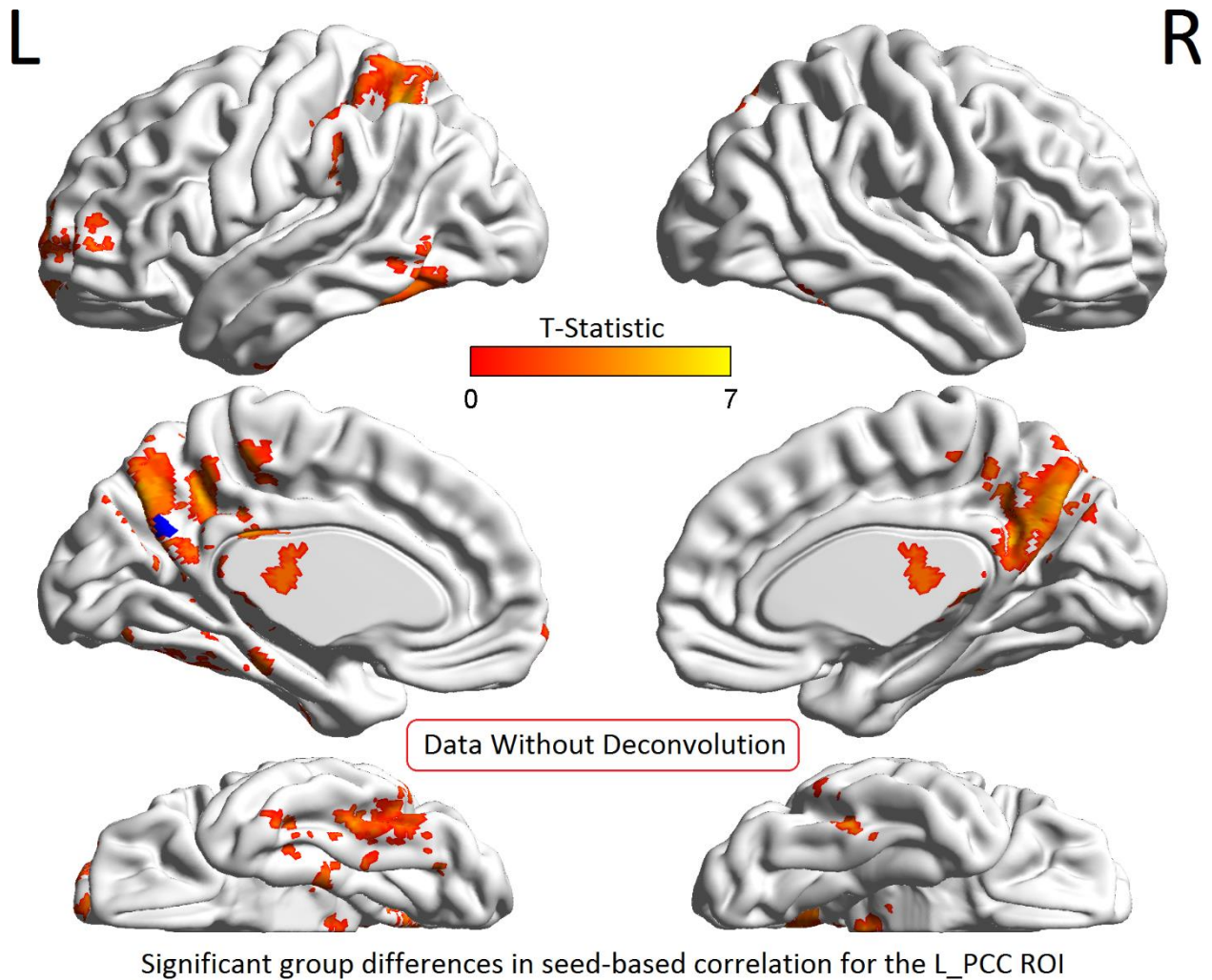
Fig.6.7. *Brain regions whose functional connectivity with the left posterior cingulate (L_PCC) seed ROI (marked blue region) was significantly different between the groups for data **without** hemodynamic deconvolution. Please refer to Appendix A, Table A6 for further details.*

Significant group differences in seed-based correlation for the L_PCC ROI
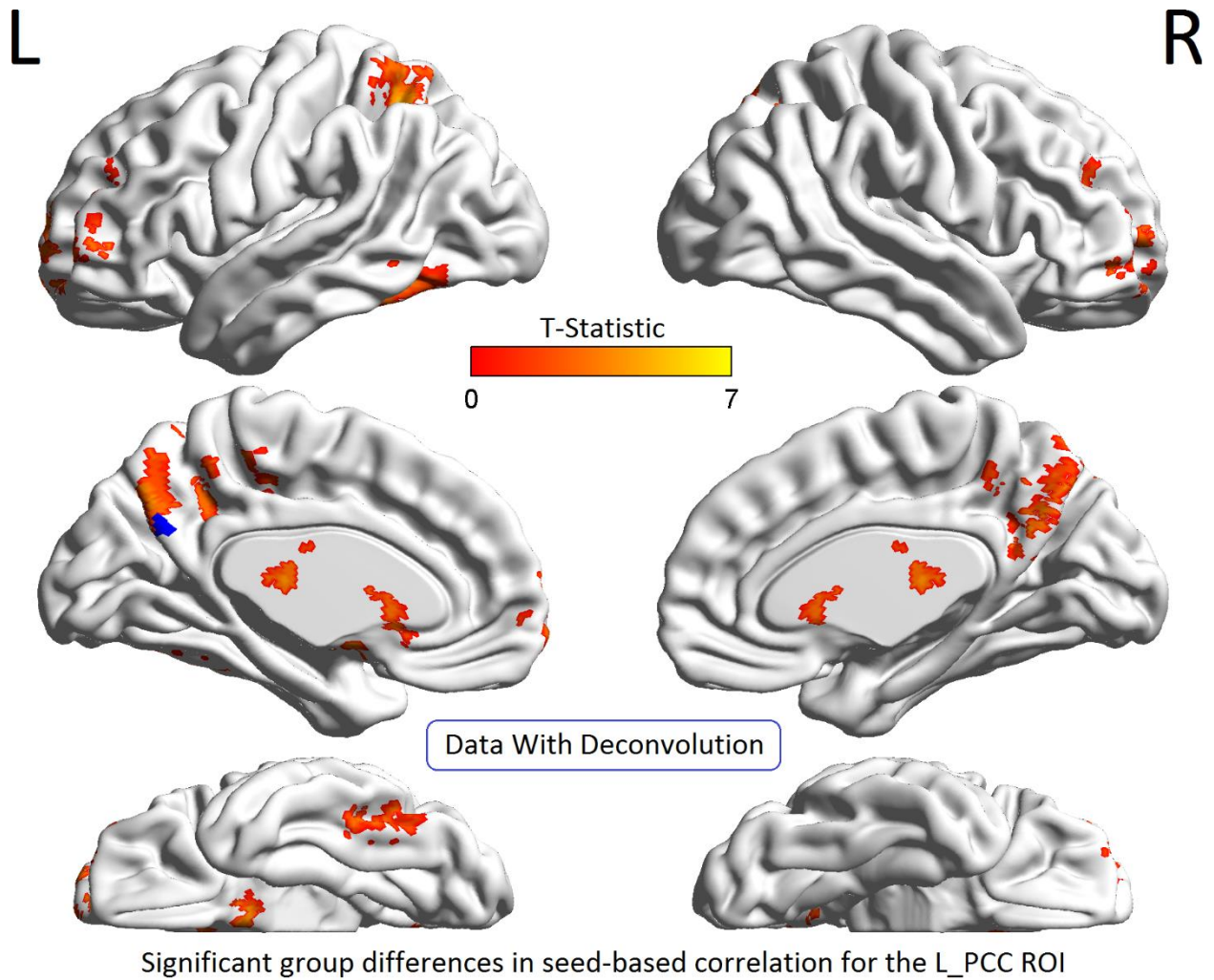
Fig.6.8. *Brain regions whose functional connectivity with the left posterior cingulate (L_PCC) seed ROI (marked blue region) was significantly different between the groups for data* **with** *hemodynamic deconvolution.. Please refer to Appendix A, Table A7 for further details.*

L_PCC ROI T-Statistic Map: Without Deconvolution > With Deconvolution
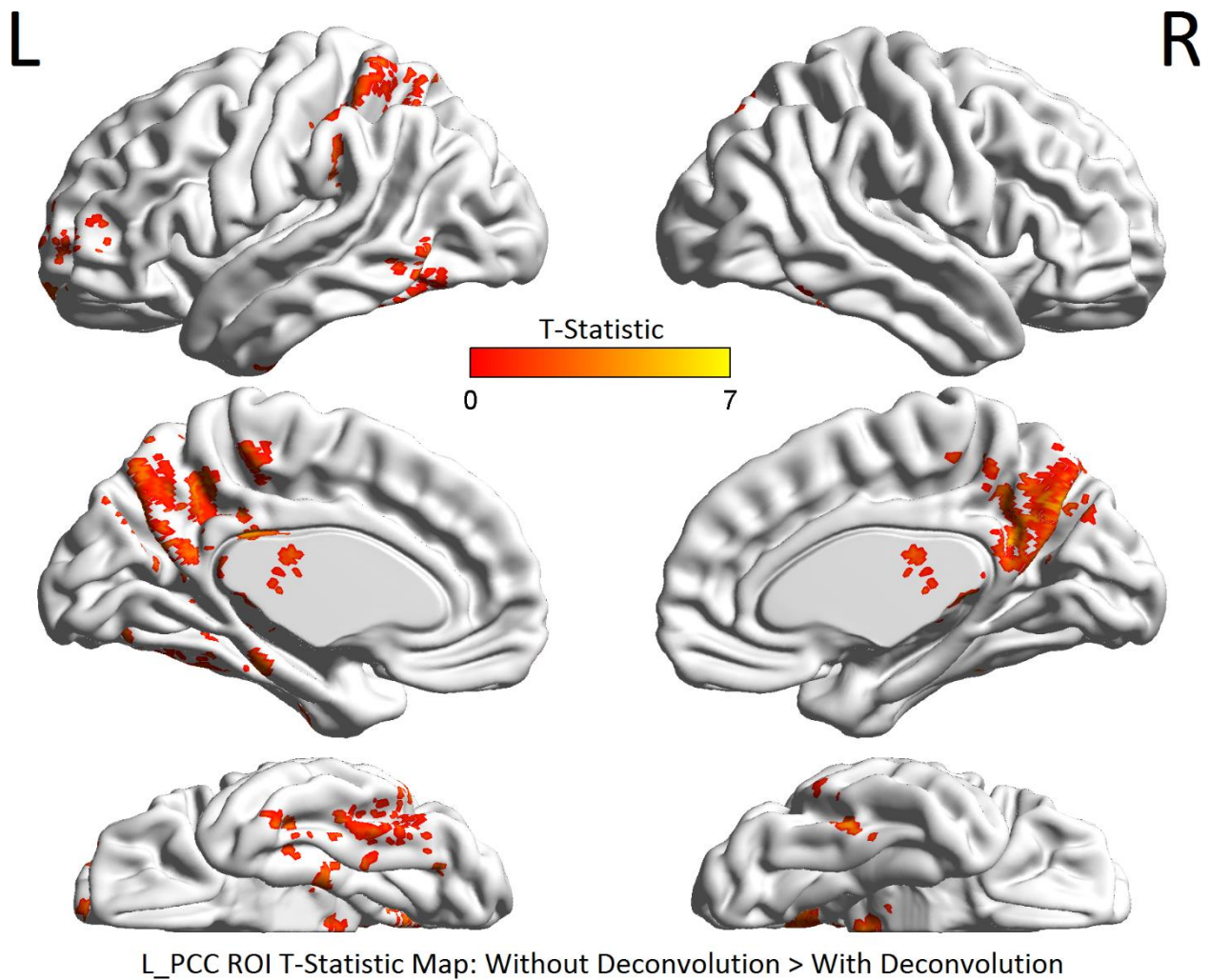
Fig.6.9. *Pseudo-positives, that is, functional connectivity group differences which were greater (higher T-value) in data without deconvolution as compared to that with deconvolution performed (for the left posterior cingulate [L_PCC] seed ROI). Please refer to Appendix A, Table A8 for further details.*

L_PCC ROI T-Statistic Map: With Deconvolution > Without Deconvolution
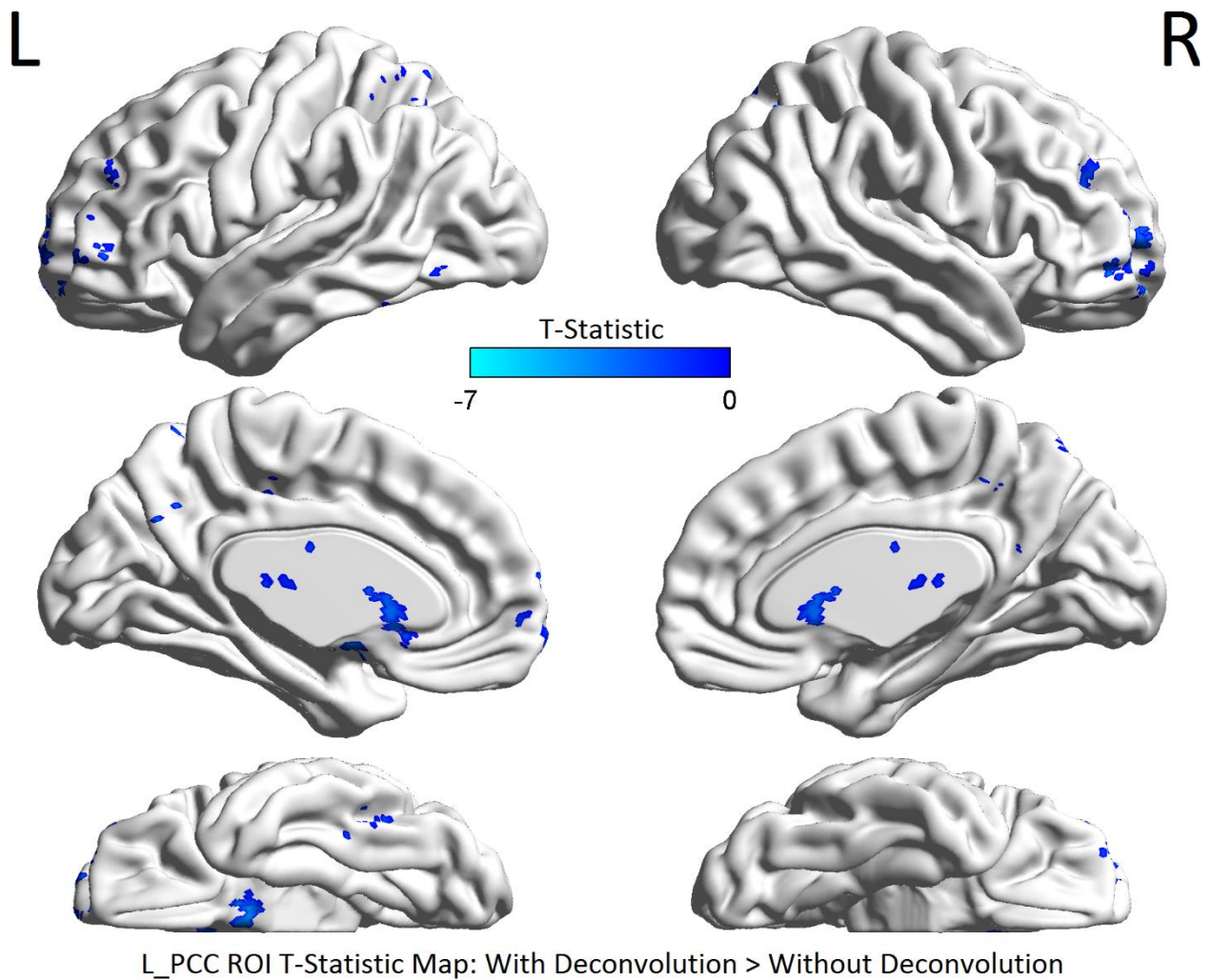
Fig.6.10. *Pseudo-negatives, that is, functional connectivity group differences which were smaller (lower T-value) in data without deconvolution as compared to that with deconvolution performed (for the left posterior cingulate [L_PCC] seed ROI). Please refer to Appendix A, Table A9 for further details.*

Table 6.1. *Number of non-zero voxels in the thresholded T-maps and its derivatives (please refer to Figs 6.7 through 6.10 for L_PCC ROI and Figs A1 through A4 for R_Prec ROI). There are notable differences in the significance maps (as seen in figures) as well as corresponding notable differences in the number of voxels between non-deconvolved and deconvolved data, and their comparisons. Further details are available in Appendix A, Tables A6 through A13.*

Seed ROI	No. of significant voxels		No. of voxels	
	Data Without Deconvolution	*Data With Deconvolution*	*Without Deconv > With Deconv*	*With Deconv > Without Deconv*
L_PCC	11599	5141	9968	2526
R_Prec	6407	5828	4753	3814

6.4. Discussion

In this work, we tested two hypotheses. First, we hypothesized that the HRF, which depends on cerebrovascular reactivity and neurovascular coupling, may be altered in PTSD and mTBI. We then tested this primary hypothesis by obtaining significant group differences in voxel-specific HRF parameters which were estimated by performing blind hemodynamic deconvolution of resting-state fMRI data obtained from these populations. Second, we also tested the hypothesis that functional connectivity differences between groups are at least partially driven by HRF differences, if HRF variability is not removed through deconvolution.

We found substantial evidence to support our hypotheses. First, we found altered HRF parameters in disease groups combined compared to controls in subcortical and DMN regions. We also found a subset of these alterations to be significantly different between all three groups, which characterized HRF differences between PTSD and mTBI. In all the regions with altered HRF, we found that RH increased in the disorders compared to controls, while TTP and FWHM decreased

in the disorders. Throughout, control vs disorder refers to an overlap of control vs PTSD and control vs PCS+PTSD comparisons. This finding conforms to our prediction made earlier that HRF in PTSD and mTBI would be taller, quicker and narrower compared to controls. This profile of HRF alteration has been attributed to disrupted metabolism and microvasculature associated with brain disorders, for example in mTBI [151]. Additionally, Thompson et al. [153] showed that there is a negative relationship between RH and TTP/FWHM, that is, whenever the height of HRF increases, it is highly likely that the ascent and descent are quicker. We observed the same in our results also.

For Control vs Disease comparison, we found RH differences mainly in thalamus, midbrain, default-mode regions (PCC, precuneus) and secondary visual areas. Alterations in TTP and FWHM, which were largely similar, were found in default-mode regions (PCC, precuneus) and secondary visual areas. Prior work showed abnormal GABAergic and glutamatergic neurotransmitter systems related to anxiety disorders such as PTSD [154]. Neuromodulators released by glutamatergic and GABAergic interneurons are known to directly modulate local cerebral blood flow [155], and thus the HRF [156]. Glutamate acts on N-methyl-D-aspartate (NMDA) receptors, which causes dilation of blood vessels associated with activated brain regions [157], thus impacting the HRF. Importantly, lower gamma-Amino butyric acid (GABA) concentration is shown to result in taller, quicker and narrower HRFs [158], as observed by us in PTSD and mTBI. Thus, at least part of the HRF alterations observed by us could be attributed to lower GABA concentration (as also suggested in [158]). GABA being an inhibitory neurotransmitter, lower GABA levels indicate lack of inhibition in affected brain regions found to have HRF alterations. This provides a potential neurochemical basis for HRF alterations observed by us.

The thalamus, identified with altered RH, is necessary for the production of anxiety, in addition to the fact that it is anatomically well situated, mediating pre-frontal activity with subcortical and midbrain structures, to produce the experience of anxiety [159]. Additionally, serotonin (5-hydroxytryptamine) in the midbrain is known to play a key role in anxiety disorders [160]. Serotonin is a vasoconstrictor, providing blood-brain barrier permeability, which modulates neurovascular coupling, and thus the HRF, via the neuronal-astrocytic-vascular tripartite functional unit [161].

Earlier studies have reported neurochemical alterations in key areas of the DMN and in insula in PTSD. Using PET imaging, Ramage et al. [162] found heightened glucose metabolism in precuneus in PTSD compared to combat controls, which correlated with PTSD symptom severity (PCL-S score). Using magnetic resonance spectroscopy, Rosso et al. [163] found decreased GABA in the insula in PTSD, which correlated with anxiety levels. Taken together, these findings provide substantiation for neurochemical and vascular alterations, and thus HRF differences, in brain regions found to be significantly different between healthy controls and disease groups in this work.

Interestingly, findings of higher brain activation [5] as well as hyper-connectivity [13, 77, 122] in PTSD and mTBI, owing to reduced inhibition, also corroborates with the regions identified with altered HRF in this work. We thus noticed from prior literature discussed above that reduced GABA likely causes both reduced neural inhibition and altered HRF; and the HRF alterations identified in this work largely overlapped with neural alterations identified in prior works (PCC, precuneus, secondary visual and thalamus). This observation conforms to prior studies that attribute part of HRF variability to neural activity differences [10], which might be an indirect relationship mediated by neurotransmitters like GABA [158], as noted earlier. These findings raise

important considerations. If group-differences in HRF parameters and neural activity are indeed largely similar, owing to underlying neurochemistry, then interpretation of findings from fMRI studies which ignore HRF variability would not be straightforward.

Next, for the overlap between RH, TTP and FWHM for Control vs Disease (overlap O-2 mentioned earlier), we identified the common regions to be left PCC and right precuneus. Additionally, significant differences between all the three groups (overlap O-3) were also found in left PCC and right precuneus (with FWHM). This shows that the hemodynamic response in PCC and precuneus were possibly affected by both PTSD and mTBI. These regions were naturally a subset of the regions identified in overlap O-1. Previous studies have reported neurochemical alterations in these key areas in soldiers affected by trauma [162, 163]. These regions have also been largely implicated in PTSD [13] and mTBI [5] studies. This is a substantial finding given that neural underpinnings of comorbid PTSD and mTBI are poorly understood [13]. PCC and precuneus showed altered HRF between all three groups with all the three HRF parameters.

We also found strong evidence in support of our secondary hypothesis. Seed-based functional connectivity analysis with the PCC and precuneus ROIs revealed perceptible distinction in group differences obtained from data without deconvolution as compared to data with deconvolution. This implies that part of the functional connectivity group differences reported in fMRI studies (which do not perform deconvolution) could potentially be attributable to non-neural HRF variability. Several previous works have speculated on this aspect [10, 146, 148], since BOLD fMRI is not a direct measure of neural activity. We provide quantitative formal evidence for the impact of hemodynamic variability on group differences in fMRI-derived measures like functional connectivity. In view of this, we urge the community to employ deconvolution in their pre-processing pipeline to remove/reduce HRF variability. Researchers must exercise caution in

interpreting their results when the effect of HRF variability has not been accounted for in their resting state functional connectivity analysis, more so when dealing with PTSD and mTBI populations. Future studies could also investigate the effect of HRF variability on functional connectivity measures in other clinical populations.

In summary, we showed that PTSD and mTBI cause overlapping and distinct HRF alterations in subcortical structures and the DMN. Our findings also corroborate with prior findings, in addition to providing new insights and directions. Given these findings, future studies on PTSD and mTBI, and fMRI studies in general, must practice prudence in reporting and interpreting results obtained from resting-state functional connectivity analysis of non-deconvolved BOLD fMRI data, especially if they assume a fixed canonical HRF. Though only a handful to regions showed HRF alterations in this work, it does not imply that HRF variability between groups does not exist elsewhere, because we used a conservative statistical threshold which might have ignored smaller effects. We encourage researchers to employ hemodynamic deconvolution during data pre-processing to mitigate the issue.

CHAPTER 7

Brain Network of Emotion Regulation and Dysregulation

7.1. Introduction

Emotions play an important role in the overall functioning of the human organism. Emotions arise when the brain judges a situation from the point of view of its goals. Obviously several situations are not favorable to the goals, which leads to negative emotions. The brain has natural mechanisms for manipulating such emotions, which is termed as emotion regulation.

Emotion Regulation can be achieved through several strategies. Gross [9] illustrates the "Process Model" wherein emotion regulation can be achieved through situation selection, situation modification, attention deployment, cognitive re-appraisal or response suppression. Like most studies, we concentrate here on antecedent-focused conscious cognitive emotion regulation, which is achieved through cognitive re-appraisal of the imminent situation. That is, the subject consciously reinterprets the meaning of the situation, leading to a modified emotional response and thus emotion regulation.

Several functional Magnetic Resonance Imaging (fMRI) works have studied brain activation during emotion regulation [18], which primarily identify the following regions activated during cognitive emotion regulation: middle frontal gyrus (MFG) also referred to as dorsolateral prefrontal cortex (DLPFC), insula, anterior cingulate cortex (ACC), supplementary motor area (SMA), angular gyrus (AG), superior temporal gyrus (STG) and amygdala. However, activation studies cannot explain the interrelationship between brain regions involved in emotion regulation. Connectivity modeling is thus popularly used to assess co-activation and causality between brain

regions, which can provide a mechanistic insight into the underlying neural networks. Such a brain network of emotion regulation has been elusive. In this work, we obtained the network of emotion regulation in healthy adults from fMRI data obtained during an emotion regulation task, all obtained in a data-driven fashion.

Kohn et al. [18], in their meta-analysis on emotion regulation, identify several brain regions to be involved in emotion regulation, as mentioned earlier. They suggest a heuristically hypothesized network of emotion regulation involving these regions. We compared our emotion regulation network with their hypothetical network (see Fig.7.1).

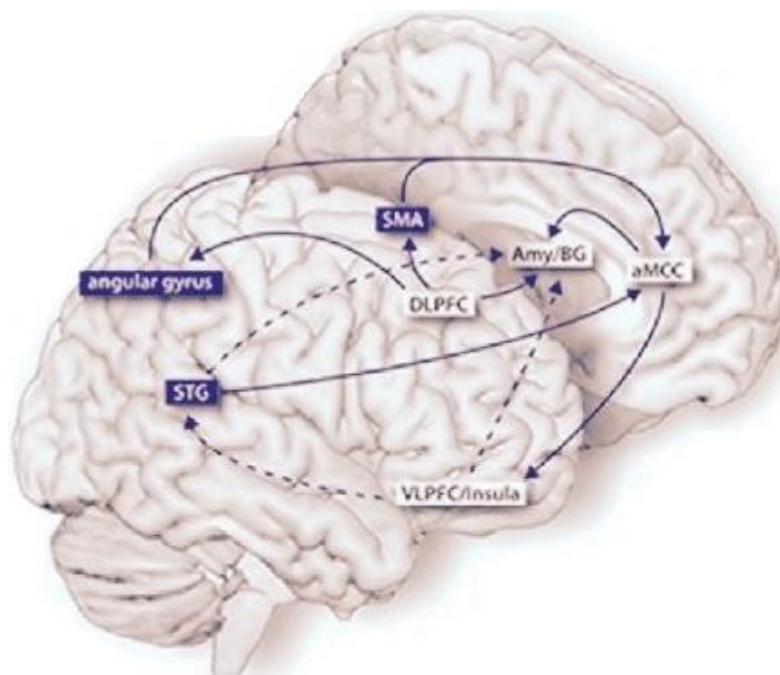**Fig.7.1.** *Reproduced from Kohn et al.* [18] *(With permission), the figure shows their heuristically hypothesized emotion regulation model. We test their hypothesis in this work. This model relates to the modal model of emotion* [9]. *Here, DLPFC performs emotion regulation, and its feedforward signal to angular gyrus, STG, SMA, basal ganglia and amygdala result in a regulated emotional state.*

Emotion regulation is the successful modification of the generated emotion. However several psychiatric disorders are characterized by symptoms which reflect an inability to effectively manage one's negative emotions. In such cases, emotion dysregulation is said to have occurred. Posttraumatic stress disorder (PTSD) and mild-traumatic brain injury (mTBI) are such disorders with high comorbidity [164], characterized by symptoms like flashbacks, hyperarousal and trauma re-experiencing, which are a consequence of emotion dysregulation. In this work, we identify the underlying brain networks responsible for impaired emotion regulation in soldiers with comorbid PTSD and post-concussion syndrome (PCS, a chronic aftermath of mTBI).

U.S. Army soldiers with comorbid PCS and PTSD (PCS+PTSD) and matched healthy combat controls performed an emotion regulation task. We first performed activation analysis to identify significantly activated regions during the emotion regulation condition compared to a control condition. These activations were almost identical to the findings from the meta-analysis by Kohn et al. [18]. Given that the emotion regulation model proposed by Kohn et al. is comprised of causal/directional relationships between brain regions, and that emotion regulation is itself a top-down process, we employed effective connectivity (EC) modeling to assess directional causal relationships between identified regions. We employed the widely used Granger causality (GC) [95] to quantify EC. Recent GC investigations with experimental applications [104] as well as simulations [102] have shown its advantages and validity for assessing EC, especially after performing hemodynamic deconvolution [165, 105]. Several recent works have also employed this approach [106, 107, 108, 109, 110, 111, 112, 113, 114]. We performed EC analysis to obtain subject-wise directional connectivities between the regions, which were then used to obtain the network of emotion regulation in healthy brains and its impairment in PCS+PTSD. For the first

time, we provide evidence for the brain networks of cognitive emotion regulation and dysregulation.

7.2. Methods

7.2.1. GLM Analysis

Pre-processed data was used to perform activation analysis in SPM8 in the general linear model (GLM) framework [28]. SPM's canonical double-gamma HRF was used to model the BOLD fMRI timeseries. Two contrasts were used in first-level modeling: (i) negative image, suppress emotion, and (ii) negative image, maintain emotion, both against fixation. Six head motion parameters, white matter (WM) signal and cerebrospinal fluid (CSF) signal were used as regressors of no interest. The second level maps were obtained for the two conditions, by collapsing all the subjects of both groups into one group and comparing the following conditions against fixation: (i) negative maintain, (ii) negative suppress. Age, race and education were used as regressors of no interest. The final second-level contrast which captured emotion regulation was derived as thus: negative suppress > negative maintain (assuming that emotion suppression requires cognitive emotion regulation). Between group activation contrasts were not performed because we did not want to bias the selected ROIs with between-group differences.

We thresholded this emotion regulation map at $p < 0.05$ (FDR corrected). For extracting fMRI timeseries representing each ROI for connectivity modeling, we wanted to ensure that the selected voxels were within the ROIs obtained from a meta-analysis of emotion regulation as reported by Kohn et al. [18], were significantly activated at the group level using GLM analysis on our experimental data, as well as activated in each of the individual subjects at an uncorrected threshold of $p < 0.05$ (please see Fig.7.2). Upon obtaining voxels satisfying these criteria, we determined the

162

centroid of every cluster and drew spheres of radius 'R' at each centroid such that the sphere encompasses only activated voxels satisfying our criteria. We chose this strategy as opposed to the alternative strategy of averaging the timeseries from the entire clusters since this would have resulted in spheres of varying radii, which would have resulted in different signal-to-noise ratios in the resulting timeseries across different clusters. This might have resulted in false connectivity differences driven by SNR differences. Hence we chose the final sphere radius as the smallest radius among all clusters, thus having the same sphere volume for every cluster. Averaged timeseries were then extracted from each of the distinct regions of interest (ROIs), which were then used in effective connectivity analysis.
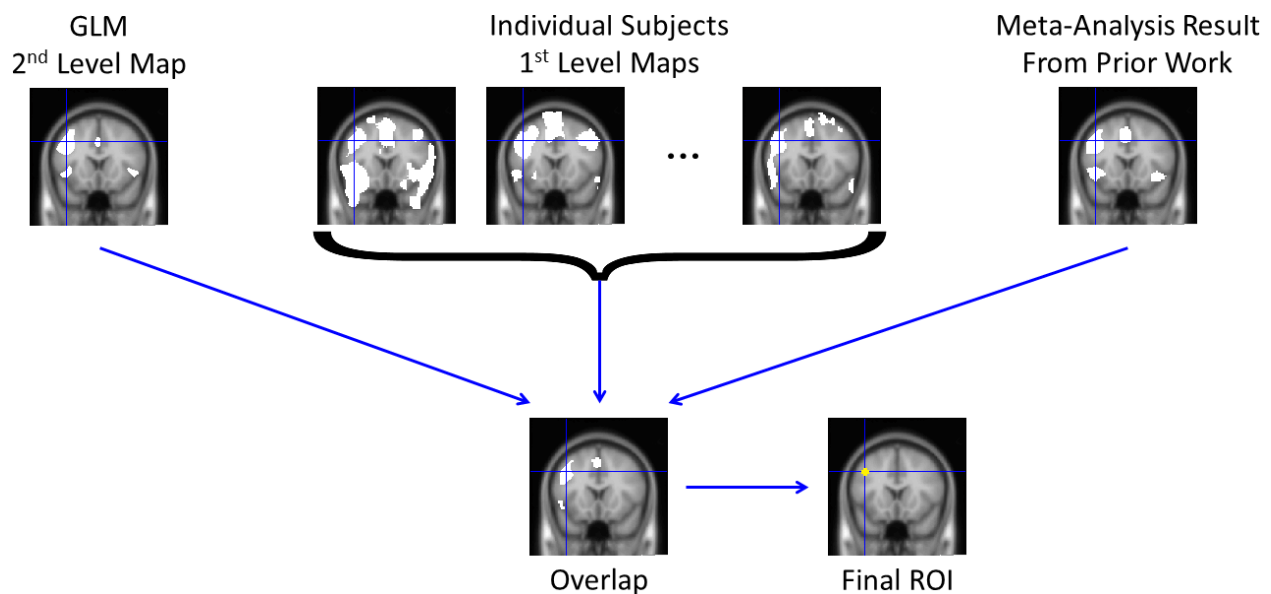
Fig.7.2. *Schematic explaining the ROI extraction procedure employed in this work. The second level map representing activations during emotion regulation (suppress>maintain in all subjects taken together, p<0.05 FDR corrected) was overlapped with (i.e. intersection) first level maps of each of the subjects ('suppress' condition, p<0.05 uncorrected), which was then overlapped with the activation likelihood estimate (ALE) map obtained from an earlier meta-analysis work* [18].

These overlapped voxels have the property that they were activated in each individual subject as well as at the group level, as also corroborated with meta-analysis findings. Spheres were drawn around the centroids of each of the identified ROIs. The smallest sphere among all ROI spheres was taken as the final ROI size for all the ROIs.

7.2.2. Effective Connectivity Analysis

The averaged ROI timeseries obtained from GLM analysis were normalized separately for each of the four runs and each participant by making it have zero mean and unit variance. These were then deconvolved to obtain latent neuronal variables using a popular method [166]. This blind deconvolution algorithm based on the Cubature Kalman filter and Smoother (CKF-S) [108, 106] jointly estimates latent neuronal timeseries as well as ROI-specific hemodynamic response function (HRF). Such hemodynamic deconvolution minimizes the smoothing effect of HRF, as also its inter-regional and inter-subject variability [10], resulting in improved effective connectivity estimation [165, 36], and avoiding potential confounds arising from HRF variability across the brain within and between individuals (whether pathologic or normal). Further, the CKF-S algorithm has been shown to recover underlying latent neural variables with high fidelity. Since the model is formulated in continuous time, the latent neural time series can be evaluated at time steps of TR/10, thereby improving the temporal fidelity of the estimated latent neural time series. Recently, it was also shown that the CKF-S deconvolution model does not overfit, even though it is highly parameterized [167]. The estimated latent neural time series from each ROI were then used for the evaluation of Dynamic Effective Connectivity (DEC).

DEC was obtained for all pairs of connections between the ROIs for all the subjects, as described in section 4.2.1 of Chapter 4. From the DEC timeseries of each connection, the time

164

points associated with those trials in the 'regulate' condition ('suppress' emotion) were identified and the EC values corresponding to those periods were extracted from the DEC timeseries (for each path) and pooled into 'regulate' connectivity samples for all subjects. It is notable that the length of DEC is same as the number of time points in the fMRI data. EC values for the 'maintain' condition (no regulation) were similarly extracted for all subjects.

The network of emotion regulation in healthy adults was obtained by comparing EC between regulate (i.e. 'suppress') and 'maintain' conditions in the control group. We drew similarities and differences of this network with the hypothetical network proposed by Kohn et al. [18]. Similarity between our network and Kohn et al.'s hypothetical network was quantified as the ratio of total number of overlapping connections to the total number of connections. Formally,

$$Similarity\ between\ connectivity\ matrices = \frac{2S}{N_1 + N_2} \tag{7.1}$$

Where S is the number of connections common between the two connectivity matrices, N_1 and N_2 are the total number of connections in each of the networks respectively. We present similarity values in percentage by multiplying this number by 100. When there is complete overlap between the networks, similarity is equal to 100% and it is 0% in case of no overlapping paths between the two networks. The network of emotion dysregulation in PCS+PTSD was obtained by comparing EC between PCS+PTSD and control groups for the regulate (i.e. 'suppress') condition, which would possibly highlight parts of the emotion regulation network whose dysfunction causes the dysregulation. Like before, similarity between the regulation and dysregulation networks was quantified. For both cases, significant differences in EC values were obtained (p<0.001, Bonferroni corrected), with differences being controlled for age, race, education and head-motion (mean frame-wise displacement [65]). Fig.7.3 illustrates our methodology
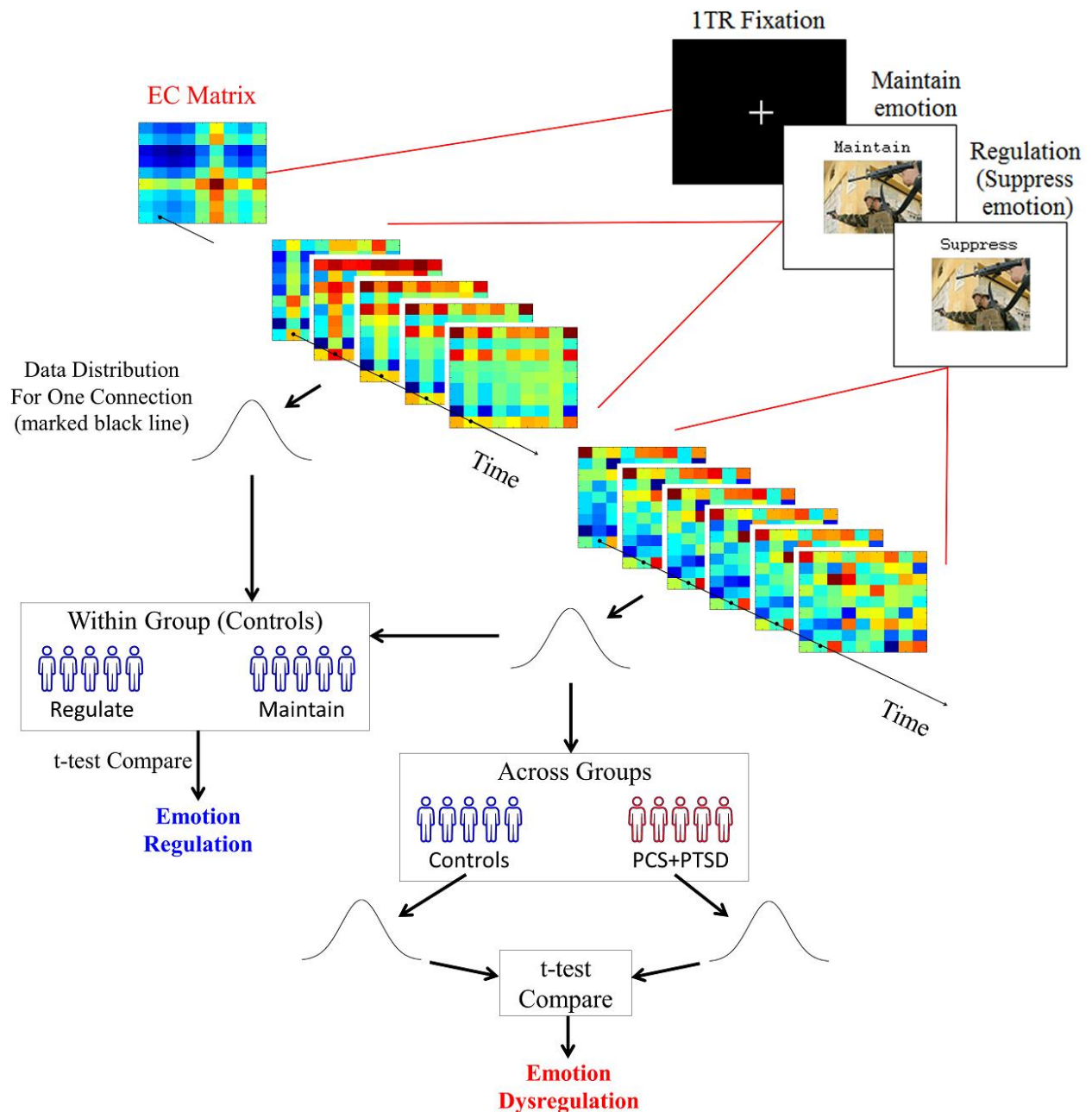
Fig.7.3. *Schematic illustrating the effective connectivity analysis performed to obtain the networks of emotion regulation and dysregulation using our emotion regulation task. EC matrices were obtained for every time point in the fMRI data. For a given connection, EC values corresponding to a task of interest were extracted from the respective TRs, and subsequent statistical tests were done for appropriate comparisons to obtain the networks of emotion regulation and dysregulation*

7.3. Results

7.3.1. Activation Results

Upon performing GLM analysis and evaluating the common regions between the group-level map and individual-subject-level maps (obtained from all subjects in both groups), we found nine regions to be significantly activated and satisfying our criteria listed in the previous section (see Table 7.1 and Fig.7.4). The minimum radius 'R' of the sphere which encompassed activated voxels in all the ROI clusters was found to be 5mm. We found that these final regions were within the boundary of activated voxels reported in the meta-analysis on emotion regulation [18]. This was important because, in this work, we were testing their heuristically hypothesized model of emotion regulation.

Table.7.1. *Regions which were significantly activated at the group level as well as in individual subjects (obtained from all subjects in both groups), with a sphere of 5mm radius drawn around the below mentioned centroids. MFG = middle frontal gyrus, ACC = anterior cingulate cortex, SMA = supplementary motor area, AG = angular gyrus, STG = superior temporal gyrus*

Region	MNI coordinates of centroid			Max T-value
	X	y	z	
MFG_L	-42	16	38	4.5281
Insula_L	-38	20	-6	6.6924
Insula_R	44	22	-8	6.0205
ACC_L	-2	22	33	4.1216
SMA_L	-2	14	51	5.4965
Amygdala_L	-22	-4	-20	5.4417
Amygdala_R	24	-2	-20	5.7578
AG_L	-44	-57	40	4.1826
STG_L	-58	-38	14	5.1881
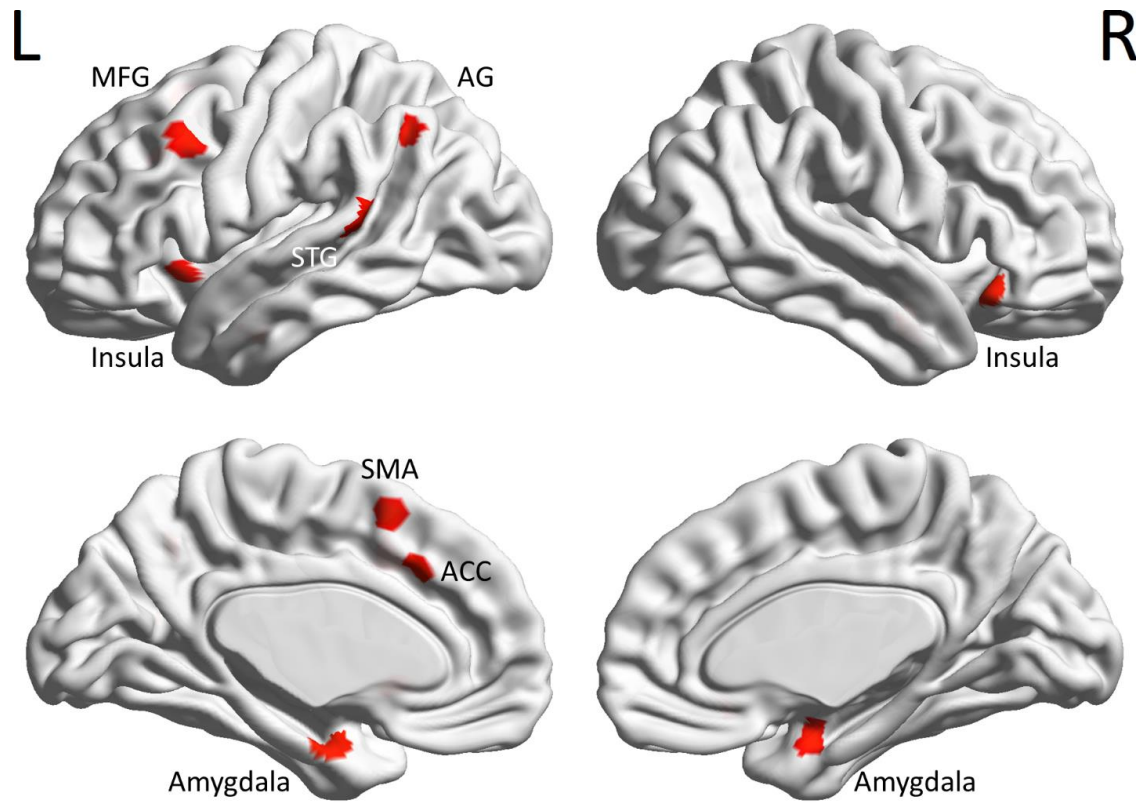
Fig.7.4. *Regions significantly activated at group level as well as in individual subjects (obtained from all subjects in both groups). Further, these voxels also belonged to ROIs identified as being involved in emotion regulation using a previously published meta-analysis* [18]. *A 5mm-radius sphere was drawn at the centroid of each of these regions and mean timeseries were extracted from each of them. These were deconvolved and the resulting latent neural signals were used in effective connectivity analysis. Please refer to Table 7.1 for expanded abbreviations of region names.*

7.3.2. Effective Connectivity Results

We performed effective connectivity analysis using the fMRI timeseries obtained from the 9 identified regions responsible for emotion regulation (please refer to Table 7.1 and Fig.7.4 for the identified regions). Using directional connectivity derived for all pairwise connections between the 9 regions, we obtained the networks of emotion regulation in healthy controls and dysregulation in soldiers with trauma. The regulation network was also compared with the hypothetical emotion regulation model proposed by Kohn et al. [18], simultaneously providing first evidence for the network of emotion regulation and dysregulation. The regulation network was obtained in healthy controls by comparing connectivity in 'regulation' condition as compared to 'maintain' condition (no regulation). The dysregulation network was obtained by comparing connectivity in only the regulation condition in PCS+PTSD group compared to healthy controls.

Table 7.2 provides the T-values of the comparison for the emotion regulation network (regulate>maintain in controls), and Table 7.3 provides the same for the emotion dysregulation network (regulate PCS+PTSD>controls). Fig.7.5 provides the expected connectivity pattern as hypothesized by Kohn et al. [18] (also refer to Fig.7.1). Fig.7.6 provides the emotion regulation connectivity pattern comprising T-values (plotted using Table 7.2); Fig.7.7 provides the same for emotion dysregulation (plotted using Table 7.3).

Table 7.2. *T-values of comparison for the emotion regulation network (regulate>maintain in controls). Values in bold font correspond to significant connections. Rows represent connections emanating 'from' the corresponding region, while columns represent connections terminating 'into' the corresponding region (this is indicated by the red arrow).*

	MFG_L	Insula_L	Insula_R	ACC_L	SMA_L	Amyg_L	Amyg_R	AG_L	STG_L
MFG_L	0	**17.62**	-2.45	**18.94**	**17.25**	**19.05**	**19.88**	**14.88**	-3.98
Insula_L	2.95	0	1.98	1.79	3.08	**10.89**	**13.68**	**19.92**	**8.82**
Insula_R	2.14	**16.20**	0	2.04	**11.84**	**12.33**	0.29	**17.08**	**10.87**
ACC_L	-3.49	**15.49**	-3.96	0	-3.76	**17.31**	-2.77	**13.86**	0.20
SMA_L	-0.91	**13.14**	-1.99	**14.89**	0	-2.01	-3.06	-0.28	-1.85
Amyg_L	-0.97	-3.24	-1.10	-2.21	0.53	0	-0.19	**10.44**	**8.02**
Amyg_R	1.59	2.44	0.09	**10.02**	3.21	-1.92	0	0.25	2.45
AG_L	0.49	**9.65**	**12.01**	0.85	-0.14	-2.55	0.56	0	1.14
STG_L	0.61	2.81	1.55	1.84	0.21	**11.19**	0.93	2.63	0

Table 7.3. *T-values of comparison for the emotion **dysregulation network** (regulate PCS+PTSD>controls). Values in **bold** font correspond to significant connections. Rows represent connections emanating 'from' the corresponding region, while columns represent connections terminating 'into' the corresponding region.*

	MFG_L	Insula_L	Insula_R	ACC_L	SMA_L	Amyg_L	Amyg_R	AG_L	STG_L
MFG_L	0	**-6.71**	-1.33	-2.07	**-5.09**	**-7.00**	**-6.11**	-1.31	-2.41
Insula_L	2.29	0	2.58	1.96	2.91	**7.74**	**7.11**	**8.05**	**4.83**
Insula_R	1.97	**6.74**	0	1.44	**5.64**	-0.30	0.21	**7.17**	**5.81**
ACC_L	-1.02	0.62	-2.72	0	-1.56	-2.25	-1.05	**-5.02**	0.93
SMA_L	-0.31	-0.56	-0.93	**-5.32**	0	-0.78	-1.36	-0.08	-0.88
Amyg_L	0.08	-1.24	0.31	-0.82	0.98	0	0.73	**5.15**	**4.45**
Amyg_R	1.45	1.87	0.17	**4.88**	2.44	-0.60	0	1.42	2.41
AG_L	1.32	**4.60**	**6.66**	1.28	1.03	-0.61	1.46	0	1.04
STG_L	0.66	2.71	2.07	1.64	0.40	**6.07**	1.33	2.49	0
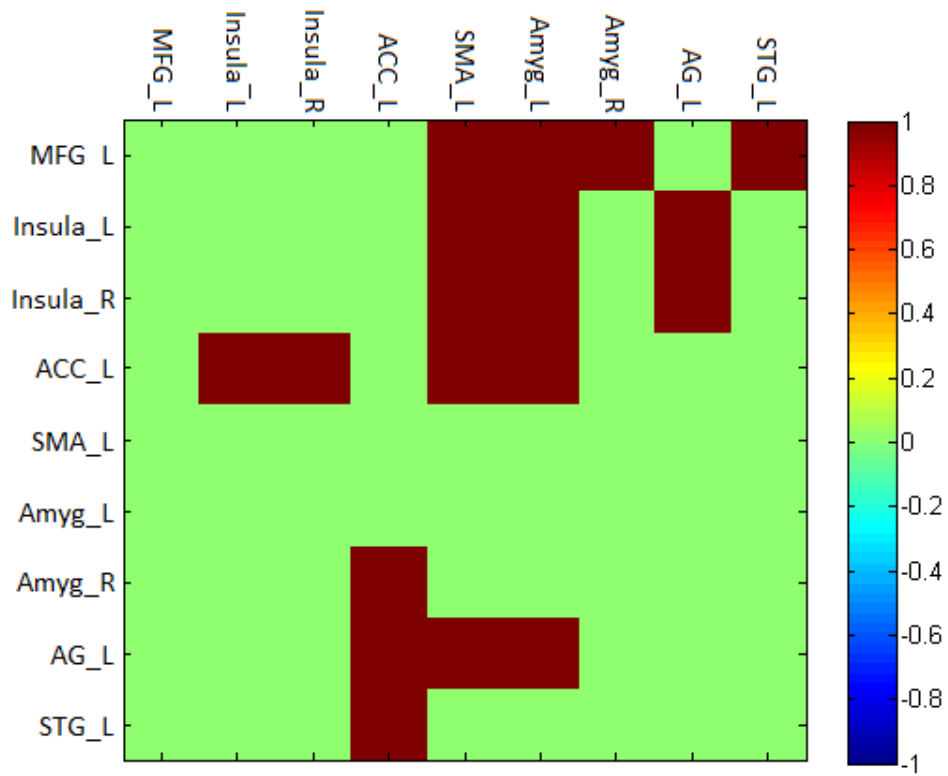
Fig.7.5. *Image showing the expected network structure for the hypothetical network of emotion regulation proposed by Kohn et al.* [18].
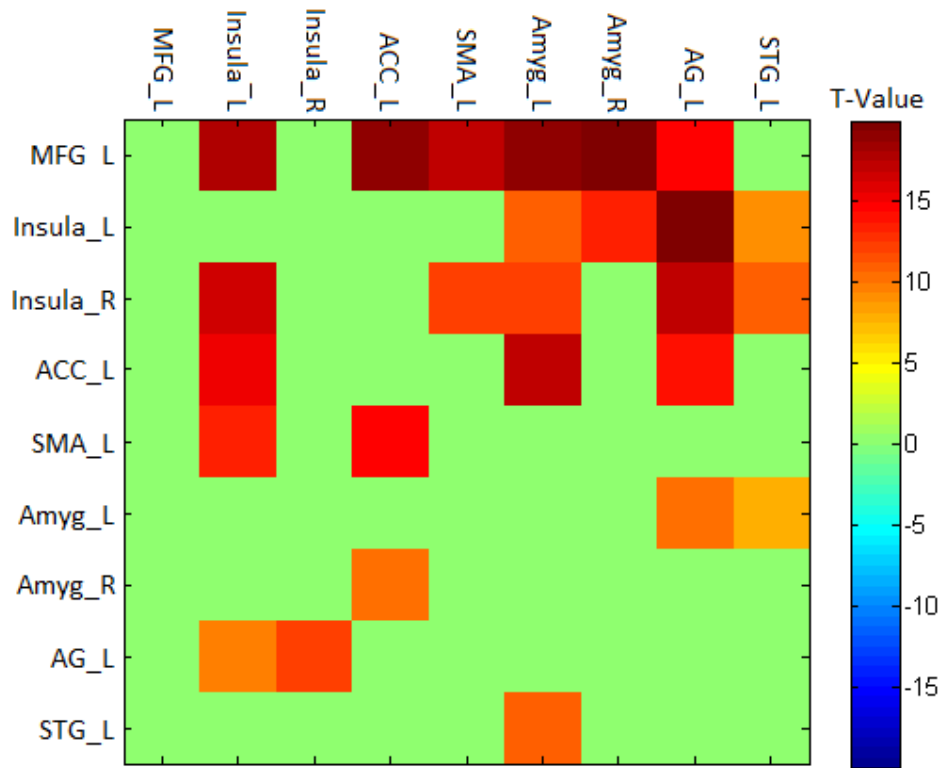
Fig.7.6. *Image showing T-values of comparison for the emotion **regulation network** (regulate>maintain in controls). Rows represent connections emanating 'from' the corresponding region, while columns represent connections terminating 'into' the corresponding region. Non-significant connections are shown as zero. A similarity of 50.1% was obtained between our data-driven result and Kohn et al.'s hypothetical network.*
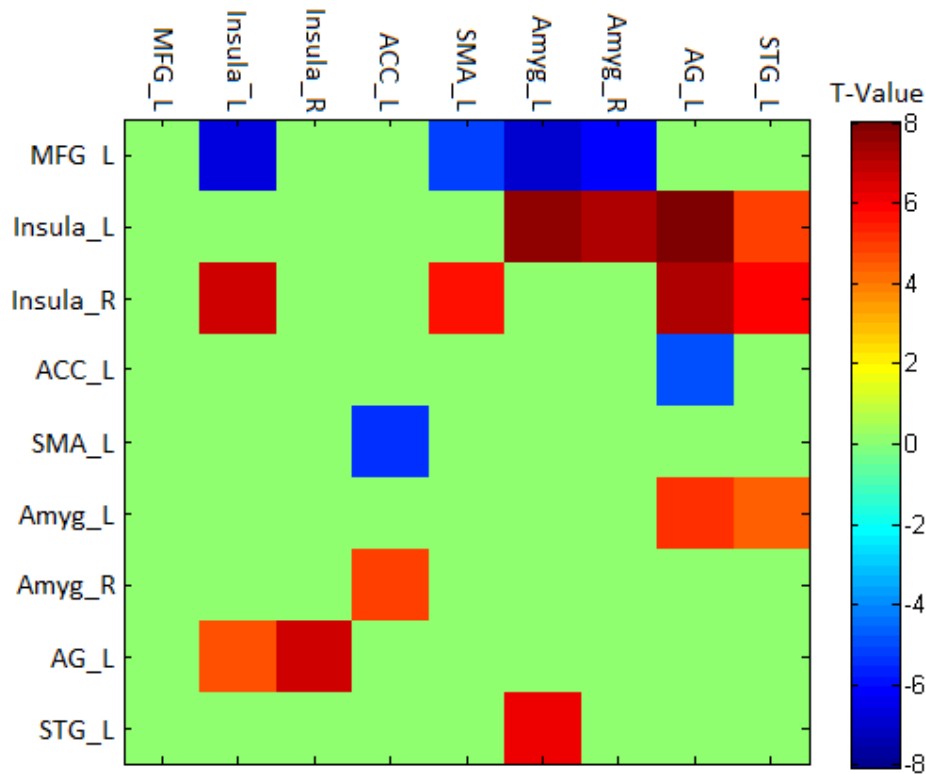
Fig.7.7. *Image showing T-values of comparison for the emotion **dysregulation network** (regulate PCS+PTSD>controls). Rows represent connections emanating 'from' the corresponding region, while columns represent connections terminating 'into' the corresponding region. Non-significant connections are shown as zero. A similarity of 88.5% was obtained between the regulation and dysregulation networks.*

Several observations can be made from Figs 7.5, 7.6 and 7.7. The regulation network obtained from imaging data by us is not identical to the network hypothesized by Kohn et al, (50.1% similarity), though the differences are not major in principle. While a 50% similarity may seem low, it is not unexpected given that their network was hypothetical.

The dysregulation network is a complete subset of the regulation network, all obtained in a data-driven manner (88.5% similarity). This is an impressive result which shows that dysregulation

arises entirely from an imbalance in the native regulation network (since the former is a complete subset of the latter), and that any other cognitive process not involved in regulation (i.e. not part of regulation network) does not take part during the dysregulation phenomenon.

While the regulation network weights (Fig.7.6) show the strength of directional connections during the process of cognitive emotion regulation, the dysregulation network weights (Fig.7.7) do not correspond to absolute strength of directional connections. Rather, they refer to the strength of imbalance caused in dysregulation as compared to regulation. It quantifies the degree by which a given connection deviates from the expected normal connectivity value for regulation. In these terms, connections from left MFG and connections to left insula seem to be maximally altered in dysregulation.

Comparing the T-values of significance, we notice that the regulation network has T-values about twice that of the dysregulation network, implying that the change in connectivity strengths owing to dysregulation is only a fraction of the absolute connectivity strengths during regulation (average connectivity strength in dysregulation across all significant paths was just about 42.8% of that in regulation), signifying a modest disturbance of the native regulation network, nonetheless with severe consequences.

We attempt to provide lucidity by presenting network schematics for emotion regulation (Fig.7.8) and dysregulation (Fig.7.9). The network of emotion regulation can be broken down into three distinct parts: there is a direct influence from MFG on amygdala and angular gyrus (Fig.7.8a), then there is the network originating from MFG causing a hierarchical downward influence through ACC, SMA and insula onto amygdala and angular gyrus (Fig.7.8b), and finally there is the secondary influence from insula onto STG (Fig.7.8c).

The network of emotion dysregulation clearly shows connections from prefrontal regions being weaker during dysregulation, while the rest being stronger. It resembles the regulation network, and can be broken down into three distinct parts: there is impaired direct influence from MFG on amygdala (Fig.7.9a), then we observe the impaired top-down network of MFG wherein the direct pathway to left insula is impaired, which leads to disinhibition of amygdala and subsequently lateral parietal regions (Fig.7.9b), and finally elevated secondary influence is observed from insula to STG (Fig.7.9c).

In summary, the regulation network exhibits a typical top-down architecture driven by MFG which influences amygdala and parietal memory retrieval and association-related regions, mediated by insula and medial prefrontal regions. The dysregulation network exhibits reduced influence from prefrontal regions leading to disinhibition of subcortical and lateral parietal regions.
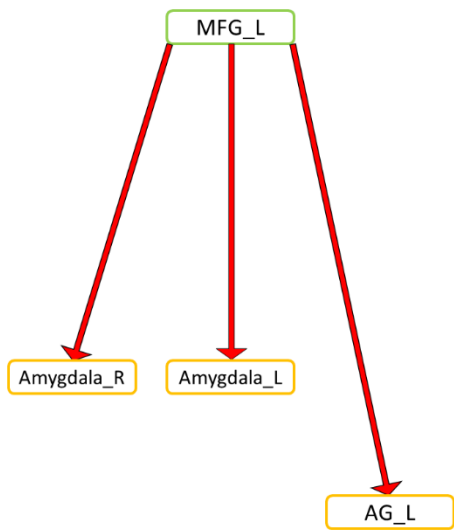
7.8(a)
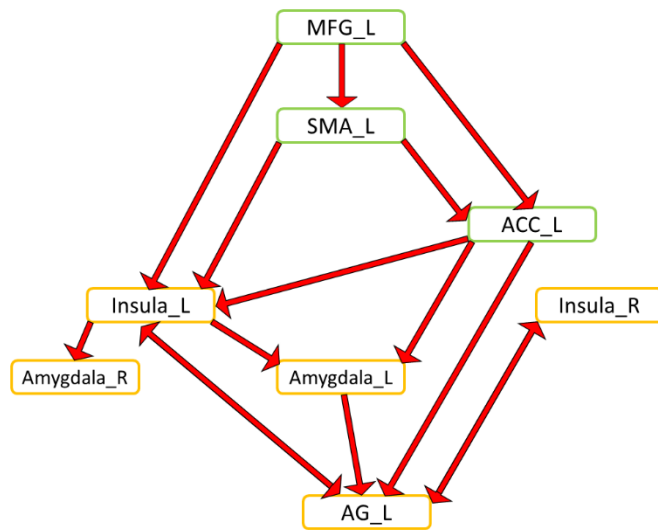
7.8(b)
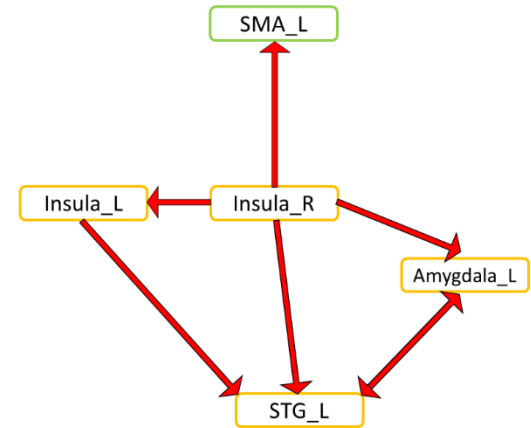
7.8(c)
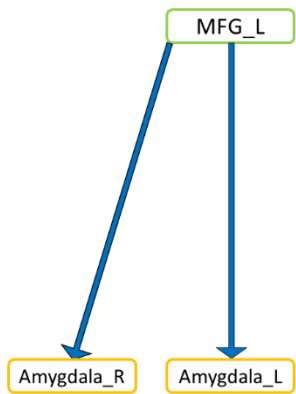
7.9(a)
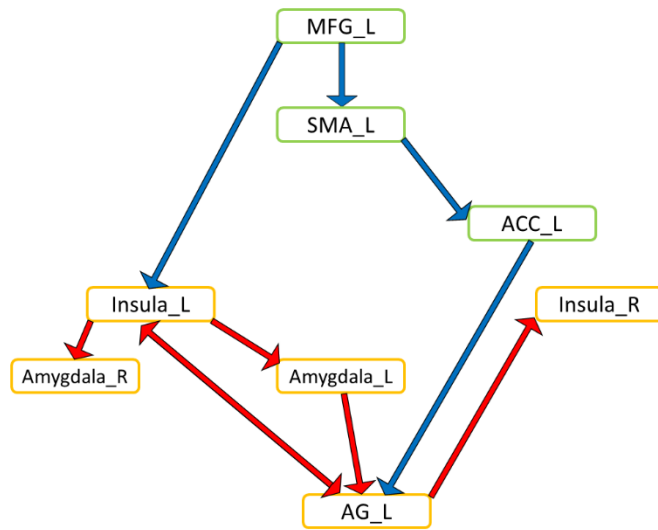
7.9(b)
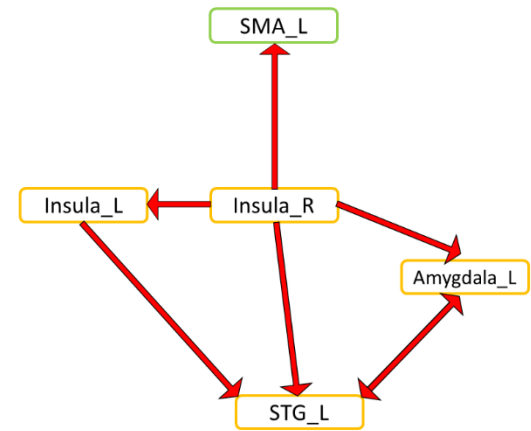
7.9(c)

Fig.7.8. Network *schematic of **emotion regulation*** *derived from Fig.7.6. Prefrontal regions are in green boxes while the rest are in orange ones. Red connections signify higher connectivity during 'regulation' compared to 'maintain' condition. The network is broken down into three distinct parts: (a) direct influence of MFG on amygdala and angular gyrus, (b) top-down network of direct and indirect influence from MFG through ACC, SMA and insula, (c) secondary influence from insula to STG. Double arrows imply two-way relationship.*

Fig.7.9. Network *schematic of **emotion dysregulation*** *derived from Fig.7.7. Prefrontal regions are in green boxes while the rest are in orange ones. Red connections signify higher connectivity and blue ones signify lower connectivity in PCS+PTSD compared to controls. Clearly, connections from prefrontal regions go weaker during dysregulation, while the rest go stronger. The network is broken down into three distinct parts: (a) impaired direct influence of MFG on amygdala, (b) impaired top-down network of MFG: direct pathway to left insula is impaired, which causes disinhibition of amygdala and thus lateral parietal regions, (c) elevated secondary influence from insula to STG. Double arrows imply two-way relationship.*

7.4. Discussion

In this work, we investigated brain networks of emotion regulation in healthy adults and their dysregulation in comorbid PTSD and mTBI. We identified regions activated during an emotion regulation task, and defined ROIs around the centroid of each of the nine identified clusters. Effective connectivity was estimated between all pairs of nine connections during 'regulate' (suppress) and 'maintain' conditions. Network of emotion regulation consisted of paths which were stronger during 'regulate' as compared to 'maintain' in healthy controls, while that of

dysregulation was the difference between PCS+PTSD and controls during the 'regulate' condition. We then identified the regulation network as having a top-down architecture with the MFG driving the rest of the network (insula, medial prefrontal regions, amygdala and lateral parietal regions). During dysregulation this network was imbalanced with reduction in prefrontal connectivity and elevation of subcortical and lateral parietal connectivity.

Our network of emotion regulation fits well with findings from prior studies [9, 18, 168], which have identified the pivotal role of MFG in the initiation of emotion regulation, and also identify the subsequent role of medial prefrontal regions, insula, amygdala and lateral parietal regions. MFG plays an important role in cognitive control [130], which includes emotion regulation. While amygdala is involved in emotion generation, and medial prefrontal regions enable subconscious emotion regulation like fear conditioning [9], the MFG initiates conscious cognitive emotion regulation (also referred to as cognitive reappraisal) [9]. All the directional connections are traceable to the MFG in our network, thus concluding that MFG is the source of emotion regulation, which corroborates with prior findings.

With dysregulation, MFG emerged as the key source of dysfunction as well. All connections emerging from MFG exhibited reduced connectivity during dysregulation, which seemed to have a ripple-effect with reduced connectivity from medial prefrontal regions and enhanced connectivity (disinhibition) from insula and amygdala. Several prior works have speculated that MFG could be the cause of dysfunction in PTSD [131, 89], including in a recent meta-analysis [93], while direct evidence has not been found for such a hypothesis (to the best of our knowledge). We provide one of the first evidences in that direction. A recent ALE meta-analysis paper showed evidences from several findings that repetitive transcranial magnetic stimulation (rTMS) applied on MFG could be employed for a potential treatment of PTSD [132], though they did not explain

the underlying mechanisms. In summary, MFG plays a pivotal role in the initiation of cognitive emotion regulation, whose disruption likely leads to a ripple-effect of impaired emotion regulation, which fits well with behavioral manifestations arising from emotion dysregulation.

We noticed strong connectivity to insula, amygdala and lateral parietal regions from MFG in regulation, and its impairment in dysregulation. Anterior insula, a key player in a large number of psychiatric disorders [169], is known to mediate prefrontal control over subcortical regions, and is thus known to be involved in emotion regulation as well as dysregulation [9, 133]. It has good white-matter connectivity with amygdala [134], and is important for subjective emotional experiences or feelings, integrating emotionally relevant information from multiple sources and representing them as one of the many complex emotions. We found that prefrontal regulation of insula drives the amygdala, a region critical for emotion generation. Larger downward connectivity from prefrontal regions to amygdala signifies the enforcement of regulation on amygdala, seen as an effort to minimize the intensity of emotion generated by it [12]. Consequently in dysregulation, such an effect from prefrontal regions is minimized, shifting the balance and causing a disinhibited amygdala, which in effect leads to several symptoms of uncontrolled emotions in conditions like comorbid PTSD and mTBI [93].

In the regulation network, prefrontal regulation of amygdala was followed by an increased connectivity of amygdala with angular gyrus (AG) and superior temporal gyrus (STG). Along with this indirect pathway from MFG to these regions, there were direct pathways of increased connectivity from MFG and insula to both AG and STG. AG and STG are crucial for higher-level audio-visual processing [9], which means they facilitate audio-visual memory retrieval, imagery and perception, which enables the final audio-visual "experience" of an external sensory input or past memory. STG is also involved in processing emotions [170]. AG and STG connectivity thus

179

seem to suggest manipulation of the intensity and content of audio-visual perception and memory retrieval following influence from amygdala, which is necessary for emotion regulation. Consequently during dysregulation, amygdala disinhibition and prefrontal dysregulation of AG and STG translates into enhanced retrieval of undesirable audio-visual memories, which, in disorders like PTSD and mTBI, leads to symptoms such as flashbacks, trauma re-experiencing, hyperarousal and such other symptoms. This explanation fits well with behavioral manifestations of these conditions [164].

Next, the network of regulation obtained by us was not identical to the network hypothesized by Kohn et al. [18] (50.1% similarity). This was not unexpected since their network was hypothetical and not backed by imaging data. However certain key aspects of their network were found to be true with our network also, like the pivotal role of MFG, control over amygdala and its projection onto AG and STG, but their hypothetical network primarily seems to underplay the projections into left insula and overstate the projections from AG.

Our dysregulation network was a complete subset of the regulation network (with a high similarity of 88.5% between them), that is, all dysregulation paths existed in the regulation network also, but some regulation paths did not exist in the dysregulation network. This implied that dysregulation arose entirely from disruption in majority of the regulation network paths, and that other paths not involved in regulation did not play a role in dysregulation.

One strange observation was that, in the regulation network, statistical significance was highest, on average, with connections emanating from prefrontal regions, while significance seemed to reduce with caudal/ventral parts of the network involving amygdala, AG and STG. Even in the dysregulation network, prefrontal regions and insula seemed to be maximally involved. One possible explanation, though hypothetical, is that prefrontal regions and associated connections are

the core 'workhorse' of the networks, while alterations in subcortical and lateral parietal regions are merely a consequence or ripple-effect of that. Often ripple-effects are lower in magnitude than the primary effects themselves. There is preliminary evidence to support such a hypothesis [171].

While the regulation network weights (Fig.7.6) provide the strength of directional connections during the process of emotion regulation, the dysregulation network weights (Fig.7.7) do not correspond to absolute strength of directional connections. Instead they refer to the strength of imbalance caused during dysregulation in comparison with regulation. It quantifies the magnitude by which a given connection deviates from the expected normal connectivity value for regulation. In these terms, connections from left MFG and connections to left insula seemed to be maximally altered in dysregulation. This highlights an important aspect that emotion regulation requires a network of regions to work together in a particular fashion compared to baseline involving no regulation, while dysregulation results due to an imbalance in such a network. As such, the connectivity pattern we observed in regulation had a particular pattern of connection strengths, while in dysregulation the connection pattern did not change drastically (88.5% similarity), but the connection weights and thus the balance was altered, leading to dysregulation.

One of the limitations of this work is that our control group comprised of healthy soldiers and not healthy civilians. Though this enhances the credibility of our dysregulation network (where we compare combat controls and PCS+PTSD), it restricts the interpretability of our regulation network to combat controls. Future works could replicate our analysis on a population of healthy civilian adults, which could not only bring out the regulation network in civilians but also provide a comparison between healthy civilians and healthy veterans in their ability to perform emotion regulation.

In summary, we identified the MFG to be pivotal for emotion regulation in healthy adults and also for dysregulation in soldiers with comorbid PTSD and mTBI (since all connections could be traced back to this region), which further modulated amygdala and lateral parietal memory retrieval and sensory association regions through the insula and medial prefrontal regions. This network provides a mechanistic explanation of emotion regulation in healthy individuals and its impairment in comorbid PTSD and mTBI, causing an inability to control traumatic memories, contributing to several symptoms. Our results are significant given that the regions affected here are implicated in prior activation studies [93, 76, 11, 18], but a precise understanding of the underlying network structure and their causal relationships had not emerged so far.

CHAPTER 8

Conclusions

The purpose of this work was to identify brain network alterations in soldiers with posttraumatic stress disorder (PTSD) and mild-traumatic brain injury (mTBI). We employed multiple approaches to successfully achieve this end.

Here we summarize the contributions of this work:

1. Using static and time-varying functional connectivity modeling, we identified the hippocampus-striatum path to be significantly altered in the disorders, all obtained in a data-driven manner from whole-brain connectivity data without assumptions. We showed that the connectivities of this path had high behavioral relevance, and that they have better diagnostic ability than conventional clinical measures. We demonstrated that they are a potential imaging biomarker of PTSD and mTBI.

2. Using static and time-varying effective connectivity modeling, we identified dysfunctional regional foci and their associated dysfunctional connections in the disorders. We identified the middle frontal gyrus (MFG) to be the source of dysfunction in these disorders. Prior works have largely speculated that MFG might be the source of dysfunctional cognitive control in these disorders. In addition to providing evidence for those speculations, we elucidated the entire dysfunctional network and explained how the dysfunctional MFG causes cascading effects leading to heightened emotional response for traumatic memories, giving rise to several symptoms observed in PTSD and mTBI. For the first time in this field, a lucid mechanistic explanation of the underlying causal relationships and information flow has emerged.

3. Recognizing the fact that connectivity modeling is bivariate and that it does not capture the interrelationship among connections, we employed complex network analysis to study network-level alterations in PTSD and mTBI. We found altered segregation and integration along two distinct pathways. We showed that these pathways explained the commonalities and differences in PTSD and comorbid PTSD/mTBI. We also showed how widespread deflation in prefrontal regions leads to inflation of subcortical, visual and parietal regions. Neither effective connectivity nor complex network modeling have been used in prior works to study PTSD or mTBI. We demonstrated the utility of these approaches and provided novel insights into network alterations in PTSD and mTBI.

4. In all these works, we employed dynamic connectivity in addition to conventional static connectivity, and demonstrated its utility. Dynamic connectivity has not been used before to study PTSD or mTBI, despite the fact that it has high behavioral relevance, predictive ability and unique information not available through static connectivity.

5. Despite overlapping symptomatology and high comorbidity between PTSD and mTBI, a clear understanding of the similarities and differences in their associated brain networks has not emerged in the literature. Using effective connectivity modeling, we discovered brain alterations common to PTSD and PCS+PTSD, as well as those which distinguish the two, thus contributing tremendously towards advancement of knowledge in the field.

6. Given that fMRI is an indirect measure of neural activity, it was imperative that we identified the impact of hemodynamic (HRF) variability on connectivity modeling. We found significant differences in the HRF among the groups in key areas like precuneus and posterior cingulate. Seed-based whole-brain functional connectivity associated with these regions was found to be corrupted by HRF variability if the analysis ignored HRF differences among groups, thus

showing that all fMRI studies, not just specific to PTSD or mTBI, need to consider the impact of HRF variability while interpreting their connectivity results.

7. We performed effective connectivity analysis on emotion regulation task fMRI and identified, for the first time in literature, the brain network of emotion regulation in healthy adults and its dysregulation in comorbid PTSD and mTBI. While brain regions involved in emotion regulation and dysregulation are well identified, their interactions and causal relationships have remained elusive. Prior works developed hypothetical networks of emotion regulation, but we provided evidence for the networks of emotion regulation and dysregulation, which is important for the understanding of several psychiatric disorders including PTSD and mTBI.

8. Though our focus was on the understanding of PTSD and mTBI, this work was intensive on computational modeling. We developed several new frameworks, approaches and techniques. We devised a novel approach to combine static and dynamic connectivities to characterize strength and variability of connectivity simultaneously. We developed a novel regrouping procedure to form new diagnostic groups using connectivities, which map better onto behavior than conventional grouping. We developed a modified probabilistic framework to identify disease foci from effective connectivity as well as dynamic connectivity data. We developed a technique for obtaining variability in complex network properties using dynamic connectivity data. All these methodological innovations emerged for the first time, including the study of inter-group differences in HRF. Put together, our work has made significant contributions towards the advancement of computational modeling and analysis methodology in fMRI. We thus feel that the outcome of this work goes beyond the boundaries of PTSD and mTBI, as we urge researchers to take advantage of the various methodological innovations of this work in understanding other psychiatric disorders and cognitive domains.

CHAPTER 9

Information on Peer-Reviewed Publications

9.1. Peer-reviewed *Journal* publications

<u>Under second-round review:</u>

i. *D Rangaprakash*, Gopikrishna Deshpande, Thomas A Daniel, Adam Goodman, Jennifer L. Robinson, Nouha Salibi, Jeffrey S Katz, Thomas S Denney Jr. and Michael N Dretsch, "*Compromised Hippocampus-Striatum Pathway as a Potential Imaging Biomarker of Mild Traumatic Brain Injury and Posttraumatic Stress Disorder*", Human Brain Mapping, 2016 (*revisions awaited*)
(From Chapter-3)

<u>For review:</u>

i. *D Rangaprakash*, Michael N Dretsch, Archana Venkataraman, Jeffrey S Katz, Thomas S Denney Jr. and Gopikrishna Deshpande, "*Identifying Disease Foci from Static and Dynamic Effective Connectivity Networks: Illustration in Soldiers with Trauma*", NeuroImage, 2016
(From Chapter-4)

ii. *D Rangaprakash*, Michael N Dretsch, Jeffrey S Katz, Thomas S Denney Jr. and Gopikrishna Deshpande, "*Dynamics of Segregation and Integration in Directional Brain Networks: Demonstration in Soldiers with Trauma*", Human Brain Mapping, 2016
(From Chapter-5)

iii. *D Rangaprakash*, Michael N Dretsch, Wenjing Yan, Jeffrey S Katz, Thomas S Denney and Gopikrishna Deshpande, "*Hemodynamic Variability in Soldiers with Trauma: Implications for fMRI Studies*", Cerebral Cortex, 2016
(From Chapter-6)

iv. *D Rangaprakash*, Michael N Dretsch, Thomas A. Daniel, Jeffrey S Katz, Thomas S Denney Jr. and Gopikrishna Deshpande, "*Brain Network of Emotion Regulation in Healthy Adults And its Impairment in Soldiers with Trauma*", Journal of Neuroscience, 2016
(From Chapter-7)

9.2. Peer-reviewed *Conference* proceedings (published):

i. *D Rangaprakash*, Gopikrishna Deshpande, Archana Venkataraman, Jeffrey S Katz, Thomas S Denney Jr. and Michael N Dretsch, "*Identifying Foci of Brain Disorders from Effective Connectivity Networks*", Proceedings of the Annual Meeting of the International Society for Magnetic Resonance in Medicine, ISMRM 2016, pp. 3740, vol. 24, Singapore, May 2016
    (2016 ISMRM Magna Cum Laude Merit Award)
    (From Chapter-4)

ii. *D Rangaprakash*, Gopikrishna Deshpande, Jeffrey S Katz, Thomas S Denney Jr. and Michael N Dretsch, "*Brain Network Segregation and Integration is altered in Soldiers with Post-traumatic Stress Disorder and Mild Traumatic Brain Injury*", Proceedings of the Annual Meeting of the International Society for Magnetic Resonance in Medicine, ISMRM 2016, pp. 1733, vol. 24, Singapore, May 2016
    (From Chapter-5)

iii. Gopikrishna Deshpande, *D Rangaprakash*, Wenjing Yan, Jeffrey S Katz, Thomas S Denney Jr. and Michael N Dretsch, "*Hemodynamic Alterations in Post-traumatic Stress Disorder and Mild Traumatic Brain Injury*", Proceedings of the Annual Meeting of the International Society for Magnetic Resonance in Medicine, ISMRM 2016, pp. 0222, vol. 24, Singapore, May 2016
    (From Chapter-6)

iv. *D Rangaprakash*, Gopikrishna Deshpande, Thomas A Daniel, Adam Goodman, Jeffrey S Katz, Nouha Salibi, Thomas S Denney Jr. and MAJ Michael N Dretsch, "*Static and Dynamic Functional Connectivity Impairments in Concussed Soldiers with and without PTSD*", Proceedings of the Annual Meeting of the International Society for Magnetic Resonance in Medicine, ISMRM 2015, pp.4402, 23, Toronto, ON, Canada, May 2015
    (2015 ISMRM Magna Cum Laude Merit Award)
    (From Chapter-3)

v. *D Rangaprakash*, Gopikrishna Deshpande, D Narayana Dutt, Thomas A Daniel, Adam Goodman, Jeffrey S Katz, Nouha Salibi, Thomas S Denney Jr. and MAJ Michael N Dretsch, "*Global Brain Network Alterations in Post-Traumatic Stress Disorder and Post-Concussion Syndrome*", Proceedings of the International Society for Magnetic Resonance in Medicine, ISMRM 2015, pp.1357, 23, Toronto, ON, Canada, May 2015
    (From Chapter-5)

9.3. Author contributions

Author abbreviations:

D.R.   D Rangaprakash
T.S.D.   Thomas S Denney Jr.
G.D.   Gopikrishna Deshpande
M.N.D.   Michael N Dretsch
J.S.K.   Jeffrey S Katz
J.L.R.   Jennifer L Robinson
S.J.R.   Stanley J Reeves
T.A.D.   Thomas A Daniel
A.G.   Adam Goodman

Contributions:

PTSD Project Conceptualization:	M.N.D., T.S.D., J.S.K. and G.D.
Funding Acquisition:	M.N.D. and T.S.D.
Data Acquisition:	T.A.D. and A.G.
Resting-state fMRI Data Pre-processing:	**D.R.**
Task fMRI Data Pre-processing:	T.A.D. and **D.R.**
Imaging Data Analysis Methodology:	G.D. and **D.R.**
Resting-state and Task fMRI Data Analysis:	**D.R.**
Diffusion MRI Data Analysis:	J.L.R.
Investigation:	**D.R.,** G.D., M.N.D., J.S.K. and J.L.R.
Primary Manuscript Preparation:	**D.R.**
Writing:	**D.R.**, G.D., M.N.D., J.S.K., J.L.R. and T.S.D.
Resources:	T.S.D. and G.D.
Supervision:	G.D., T.S.D., M.N.D., J.S.K., J.L.R and S.J.R

BIBLIOGRAPHY

[1] "Veterans statistics: PTSD, Depression, TBI, Suicide," [Online]. Available: http://www.veteransandptsd.com/PTSD-statistics.html. [Accessed November 2015].

[2] Hoge.C.W, Castro.C, Messer.S.C and et.al., "Mild traumatic brain injury in U.S. soldiers returning from Iraq," *The New England Journal of Medicine,* vol. 358, p. 453−463, 2008.

[3] Hoge.C.W, Goldberg.H.M and Castro.C.A, "Care of war veterans with mild traumatic brain injury: Flawed perspectives," *The New England Journal of Medicine,* vol. 360, no. 16, p. 1588−1591, 2009.

[4] Cicerone.K.D and Kalmar.K, "Persistent postconcussion syndrome: The structure of subjective complaints after mild traumatic brain injury," *The Journal of head trauma rehabilitation,* vol. 10, no. 3, pp. 1-17, 1995.

[5] Eierud.C, Craddock.R.C and Fletcher.S, "Neuroimaging after mild traumatic brain injury: Review and meta-analysis," *NeuroImage Clinical,* vol. 4, pp. 283-294, 2014.

[6] J. D. Power, B. L. Schlaggar and S. E. Petersen, "Studying brain organization via spontaneous fMRI signal," *Neuron,* vol. 84, no. 4, pp. 681-96, 2014.

[7] G. Deshpande and X. Hu, "Investigating effective brain connectivity from fMRI data: past findings and current issues with reference to Granger causality analysis.," *Brain Connectivity,* vol. 2, no. 5, pp. 235-245, 2012.

[8] M. Rubinov and O. Sporns, "Complex network measures of brain connectivity: uses and interpretations," *Neuroimage,* vol. 52, no. 3, pp. 1059-69, 2010.

[9] J. J. Gross, Handbook of Emotion Regulation, Ney York: The Guilford Press, 2014.

[10] D. A. Handwerker, J. M. Ollinger and M. D'Esposito, "Variation of BOLD hemodynamic responses across subjects and brain regions and their effects on statistical analyses," *Neuroimage,* vol. 21, no. 4, pp. 1639-51, 2004.

[11] C. Eierud, R. C. Craddock, S. Fletcher, M. Aulakh, B. King-Casas, D. Kuehl and S. M. LaConte, "Neuroimaging after mild traumatic brain injury: Review and meta-analysis," *NeuroImage Clinical,* vol. 4, pp. 283-294, 2014.

[12] M. E. Costanzo, Y. Y. Chou, S. Leaman, D. L. Pham, D. Keyser, D. E. Nathan, M. Coughlin, P. Rapp and M. J. Roy, "Connecting combat-related mild traumatic brain injury with posttraumatic stress disorder symptoms through brain imaging," *Neuroscience Letters,* vol. 577, pp. 11-15, 2014.

[13] A. N. Simmons and S. C. Matthews, "Neural circuitry of PTSD with or without mild traumatic brain injury: a meta-analysis," *Neuropharmacology,* vol. 62, no. 2, pp. 598-606, 2012.

[14] J. Cisler, J. Steele, J. Lenow, S. Smitherman, B. Everett, E. Messias and C. Kilts, "Functional reorganization of neural networks during repeated exposure to the traumatic memory in posttraumatic stress disorder: an exploratory fMRI study.," *Journal of Psychiatric Research,* vol. 48, no. 1, pp. 47-55, 2014.

[15] C. W. Hoge, C. Castro, S. C. Messer, D. McGurk, D. I. Cotting and R. L. Koffman, "Mild traumatic brain injury in U.S. soldiers returning from Iraq," *The New England Journal of Medicine,* vol. 358, p. 453−463, 2008.

[16] J. M. Spielberg, R. E. McGlinchey, W. P. Milberg and D. H. Salat, "Brain network disturbance related to posttraumatic stress and traumatic brain injury in veterans," *Biological Psychiatry,* vol. 78, no. 3, pp. 210-6, 2015.

[17] H. Jia, X. Hu and G. Deshpande, "Behavioral relevance of the dynamics of the functional brain connectome," *Brain Connectivity,* vol. 4, no. 9, pp. 741-59, 2014.

[18] N. Kohn, S. B. Eickhoff, M. Scheller, A. R. Laird, P. T. Fox and U. Habel, "Neural network of cognitive emotion regulation--an ALE meta-analysis and MACM analysis," *Neuroimage,* vol. 87, pp. 345-55, 2014.

[19] B. D. Dickstein, F. W. Weathers, A. C. Angkaw, C. M. Nievergelt, K. Yurgil, W. P. Nash, D. G. Baker, B. T. Litz and the Marine Resiliency Study Team, "Diagnostic Utility of the Posttraumatic Stress Disorder (PTSD) Checklist for Identifying Full and Partial PTSD in Active-Duty Military," *Assessment,* p. pii: 1073191114548683, 2014.

[20] F. W. Weathers, B. T. Litz, T. M. Keane, P. A. Palmieri, B. P. Marx and P. P. Schnurr, "The PTSD Checklist for DSM-5 (PCL-5)," 01 05 2015. [Online]. Available: Scale available from the National Center for PTSD at www.ptsd.va.gov. [Accessed 01 05 2015].

[21] K. D. Cicerone and K. Kalmar, "Persistent postconcussion syndrome: The structure of subjective complaints after mild traumatic brain injury," *The Journal of head trauma rehabilitation,* vol. 10, no. 3, pp. 1-17, 1995.

[22] C. T. Gualtieri and L. G. Johnson, "Reliability and validity of a computerized neurocognitive test battery, CNS Vital Signs," *Archives of Clinical Neuropsychology,* vol. 21, no. 7, pp. 623-43, 2006.

[23] H. L. Urry, C. M. van Reekum, T. Johnstone, N. H. Kalin, M. E. Thurow, H. S. Schaefer, C. A. Jackson, C. J. Frye, L. L. Greischar, A. L. Alexander and R. J. Davidson, "Amygdala and Ventromedial Prefrontal Cortex Are Inversely Coupled during Regulation of Negative Affect and Predict the Diurnal Pattern of Cortisol Secretion among Older Adults," *The Journal of Neuroscience,* vol. 26, no. 16, pp. 4415-4425, 2006.

[24] A. M. Goodman, J. S. Katz and M. N. Dretsch, "Military Affective Picture System (MAPS): A new emotion-based stimuli set for assessing emotional processing in military populations," *Journal of Behavior Therapy and Experimental Psychiatry,* vol. 50, pp. 152-161, 2015.

[25] Z. S. Saad, S. J. Gotts, K. Murphy, G. Chen, H. J. Jo, A. Martin and R. W. Cox, "Trouble at rest: how correlation patterns and group differences become distorted after global signal regression," *Brain Connectivity,* vol. 2, no. 1, pp. 25-32, 2012.

[26] J. D. Power, B. L. Schlaggar and S. E. Petersen, "Recent progress and outstanding issues in motion correction in resting state fMRI," *Neuroimage,* vol. 105, pp. 536-51, 2015.

[27] Y. Chao-Gan and Z. Yu-Feng, "DPARSF: a MATLAB toolbox for "pipeline" data analysis of resting-state fMRI," *Frontiers in Systems Neuroscience,* vol. 4, no. 13, 2010.

[28] K. J. Friston, J. Ashburner, S. J. Kiebel, T. E. Nichols and W. D. Penny, Statistical Parametric Mapping: The Analysis of Functional Brain Images, Academic Press, 2007.

[29] X. W. Song, Z. Y. Dong, X. Y. Long, S. F. Li, X. N. Zuo, C. Z. Zhu, Y. He, C. G. Yan and Y. F. Zang, "REST: A Toolkit for Resting-State Functional Magnetic Resonance Imaging Data Processing," *PLoS One,* vol. 6, p. e25031, 2011.

[30] G. Wu, W. Liao, S. Stramaglia, J. Ding, H. Chen and D. Marinazzo, "A blind deconvolution approach to recover effective connectivity brain networks from resting state fMRI data," *Med Image Anal. ,* vol. 17, no. 3, pp. 365-374, 2013.

[31] M. Boly, S. Sasai, O. Gosseries, M. Oizumi, A. Casali, M. Massimini and G. Tononi, "Stimulus set meaningfulness and neurophysiological differentiation: a functional magnetic resonance imaging study," *PLoS One,* vol. 10, no. 5, p. e0125337, 2015.

[32] B. Lamichhane, B. M. Adhikari, S. F. Brosnan and M. Dhamala, "The neural basis of perceived unfairness in economic exchanges," *Brain Connectivity,* vol. 4, no. 8, pp. 619-30, 2014.

[33] E. Amico, F. Gomez, C. Di Perri, A. Vanhaudenhuyse, D. Lesenfants, P. Boveroux, V. Bonhomme, J. F. Brichant, D. Marinazzo and S. Laureys, "Posterior cingulate cortex-related co-activation patterns: a resting state FMRI study in propofol-induced loss of consciousness," *PLoS One,* vol. 9, no. 6, p. e100012, 2014.

[34] R. N. Boubela, K. Kalcher, W. Huf, C. Kronnerwetter, P. Filzmoser and E. Moser, "Beyond Noise: Using Temporal ICA to Extract Meaningful Information from High-Frequency fMRI Signal Fluctuations during Rest," *Frontiers in Human Neuroscience,* p. 7:168, 2013.

[35] O. David, I. Guillemain, S. Saillet, S. Reyt, S. Deransart, C. Segebarth and A. Depaulis, "Identifying neural drivers with functional MRI: an electrophysiological validation," *PLoS Biology,* vol. 23, no. 6, pp. 2683-97, 2008.

[36] S. Ryali, T. Chen, K. Supekar and V. Menon, "Estimation of functional connectivity in fMRI data using stability selection-based sparse partial correlation with elastic net penalty," *Neuroimage,* vol. 59, no. 4, pp. 3852-61, 2012.

[37] R. C. Craddock, G. A. James, P. E. I. Holtzheimer, X. P. Hu and H. S. Mayberg, "A whole brain fMRI atlas generated via spatially constrained spectral clustering," *Human Brain Mapping,* vol. 33, p. 1914–28, 2012.

[38] Hayes.J.P, Vanelzakker.M.B and Shin.L.M, "Emotion and cognition interactions in PTSD: a review of neurocognitive and neuroimaging studies," *Frontiers in Integrated Neuroscience,* vol. 6, p. 89, 2012.

[39] Simmons.A.N and Matthews.S.C, "Neural circuitry of PTSD with or without mild traumatic brain injury: a meta-analysis," *Neuropharmacology,* vol. 62, no. 2, pp. 598-606, 2012.

[40] Spielberg.J.M, McGlinchey.R.E, Milberg.W.P and Salat.D.H., "Brain Network Disturbance Related to Posttraumatic Stress and Traumatic Brain Injury in Veterans," *Biological Psychiatry,* pp. pii: S0006-3223(15)00123-7, 2015.

[41] Costanzo.M.E, Chou.Y.Y, Leaman.S and et.al., "Connecting combat-related mild traumatic brain injury with posttraumatic stress disorder symptoms through brain imaging," *Neuroscience Letters,* vol. 577, pp. 11-15, 2014.

[42] Hillary.F.G, Roman.C.A, Venkatesan.U and et.al, "Hyperconnectivity is a fundamental response to neurological disruption," *Neuropsychology,* vol. 29, no. 1, pp. 59-75, 2015.

[43] Cisler.J.M, Steele.J.S, Lenow.J.K and et.al, "Functional reorganization of neural networks during repeated exposure to the traumatic memory in posttraumatic stress disorder: an exploratory fMRI study," *Journal of Psychiatric Research,* vol. 48, no. 1, pp. 47-55, 2014.

[44] Deshpande.G, LaConte.S, Peltier.S and Hu.X, "Connectivity Analysis of Human Functional MRI Data:From Linear to Nonlinear and Static to Dynamic," *Lecture Notes in Computer Science,* vol. 4091, pp. 17-24, 2006.

[45] Majeed.W, Magnuson.M, Hasenkamp.W and et.al, "Spatiotemporal dynamics of low frequency BOLD fluctuations in rats and humans," *NeuroImage,* vol. 54, pp. 1140-1150, 2011.

[46] Keilholz.S.D, Magnuson.M.E, Pan.W.J and et.al, "Dynamic properties of functional connectivity in the rodent.," *Brain Connectivity,* vol. 3, no. 1, pp. 31-40, 2013.

[47] Li.X, ZhuD, Jiang.X and et.al, "Dynamic functional connectomics signatures for characterization and differentiation of PTSD patients.," *Human Brain Mapping,* vol. 35, no. 4, pp. 1761-78, 2014.

[48] Thompson.G.J, Magnuson.M.E, Merritt.M.D and et.al, "Short-time windows of correlation between large-scale functional brain networks predict vigilance intraindividually and interindividually.," *Human Brain Mapping (in press),* 2012.

[49] Hutchison.R.M, Womelsdorf.T, Allen.E.A and et.al, "Dynamic functional connectivity: promise, issues, and interpretations.," *Neuroimage,* vol. 80, pp. 360-378, 2013.

[50] Sakoğlu.U, Pearlson.G.D, Kiehl.K.A and et.al, "A method for evaluating dynamic functional network connectivity and task-modulation: application to schizophrenia.," *MAGMA,* vol. 23, no. 5-6, pp. 351-366, 2010.

[51] Jia.H, Hu.X and Deshpande.G, "Behavioral relevance of the dynamics of the functional brain connectome," *Brain Connectivity,* vol. 4, no. 9, pp. 741-59, 2014.

[52] Greiser.K.H, Kluttig.A, Schumann.B and et.al, "Cardiovascular diseases, risk factors and short-term heart rate variability in an elderly general population: the CARLA study 2002-2006," *European Journal of Epidemiology,* vol. 24, no. 3, pp. 123-42, 2009.

[53] Harsan.L.A., Poulet.P, Guignard.B and et.al, "Brain dysmyelination and recovery assessment by noninvasive in vivo diffusion tensor magnetic resonance imaging," *Journal of Neuroscience Research,* vol. 83, no. 3, pp. 392-402, 2006.

[54] Henry.R.G, Oh.J, Nelson.S.J and Pelletier.D., "Directional diffusion in relapsing-remitting multiple sclerosis: a possible in vivo signature of Wallerian degeneration," *Journal of Magnetic Resonance Imaging,* vol. 18, no. 4, pp. 420-6, 2003.

[55] Morey.R.A, Haswell.C.C, Selgrade.E.S and et.al, "Effects of chronic mild traumatic brain injury on white matter integrity in Iraq and Afghanistan war veterans," *Human Brain Mapping,* vol. 34, no. 11, pp. 2986-99, 2013.

[56] Brodersen.K.H, Deserno.L, Schlagenhauf.F and et.al, "Dissecting psychiatric spectrum disorders by generative embedding," *Neuroimage Clinical,* vol. 16, no. 4, pp. 98-111, 2013.

[57] Deshpande.G, Li.Z, Santhanam.P and et.al, "Recursive cluster elimination based support vector machine for disease state prediction using resting state functional and effective brain connectivity," *PLoS One,* vol. 5, no. 12, p. e14277, 2010.

[58] Deshpande.G, James.G, Craddock.R and et.al, "Predicting Treatment in Patients with Major Depression Using Granger-Based Connectivity and Support Vector Machines," in *Proceedings of ISMRM 17th Scientific Meeting*, Honolulu, HI, 2009.

[59] Marquand.A.F, Filippone.M, Ashburner.J and et.al, "Automated, High Accuracy Classification of Parkinsonian Disorders: A Pattern Recognition Approach," *PLoS One,* vol. 8, no. 7, p. e69237, 2013.

[60] Liu.F, Xie.B, Wang.Y and et.al, "Characterization of post-traumatic stress disorder using resting-state fMRI with a multi-level parametric classification approach," *Brain Topography,* vol. 28, no. 2, pp. 221-37, 2015.

[61] Chen.G, Ward.D, Xie.C and et.al, "Classification of Alzheimer disease, mild cognitive impairment, and normal cognitive status with large-scale network analysis based on resting-state functional MR imaging," *Radiology,* vol. 259, pp. 213-221, 2011.

[62] Deshpande.G, Libero.L.E, S. R and et.al, "Identification of neural connectivity signatures of autism using machine learning," *Frontiers in Human Neuroscience,* vol. 17, p. 7:670, 2013.

[63] U. Sakoğlu, G. Pearlson, K. Kiehl, Y. Wang, A. Michael and V. Calhoun, "A method for evaluating dynamic functional network connectivity and task-modulation: application to schizophrenia.," *MAGMA,* vol. 23, no. 5-6, pp. 351-366, 2010.

[64] R. Hutchison, T. Womelsdorf, E. Allen, P. Bandettini, V. Calhoun, M. Corbetta, P. S. Della, J. Duyn, G. Glover, J. Gonzalez-Castillo and e. al., "Dynamic functional connectivity: promise, issues, and interpretations.," *Neuroimage,* vol. 80, pp. 360-378, 2013.

[65] J. D. Power, K. A. Barnes, A. Z. Snyder, B. L. Schlaggar and S. E. Petersen, "Spurious but systematic correlations in functional connectivity MRI networks arise from subject motion," *Neuroimage,* vol. 59, no. 3, pp. 2142-54, 2012.

[66] G. Deshpande, Z. Li, P. Santhanam, C. D. L. M. E. Coles, S. Hamann and X. Hu, "Recursive cluster elimination based support vector machine for disease state prediction using resting state functional and effective brain connectivity," *PLoS One,* vol. 5, no. 12, p. e14277, 2010.

[67] R. Craddock, P. Holtzheimer III, X. Hu and H. Mayberg, "Disease State Prediction From Resting State Functional Connectivity," *Magnetic Resonance in Medicine,* p. in press, 2009.

[68] V. Vapnik, The nature of statistical learning theory, New York: Springer, 1995.

[69] L. Wang, Support Vector Machines: Theory and Applications, New York: Springer, 2005.

[70] N. Kriegeskorte, W. Simmons, P. Bellgowan and C. Baker, "Circular analysis in systems neuroscience: the dangers of double dipping," *Nature Neuroscience,* vol. 12, no. 5, p. 535–540, 2009.

[71] M. Yousef, S. Jung, L. Showe and M. Showe, "Recursive Cluster Elimination (RCE) for classification and feature selection from gene expression data," *BMC Bioinformatics,* vol. 8, p. 144, 2007.

[72] F. Pereira, T. Mitchell and M. Botvinick, "Machine learning classifiers and fMRI: a tutorial overview," *Neuroimage,* vol. 45, p. S199–S209, 2009.

[73] T. E. Behrens, H. Johansen-Berg, M. W. Woolrich, S. M. Smith, C. A. Wheeler-Kingshott, P. A. Boulby, G. J. Barker, E. L. Sillery, K. Sheehan, O. Ciccarelli, A. J. Thompson, J. M. Brady and P. M. Matthews, "Non-invasive mapping of connections between human thalamus and cortex using diffusion imaging," *Nature Neuroscience,* vol. 6, no. 7, pp. 750-757, 2003.

[74] H. Johansen-Berg, T. E. Behrens, E. Sillery, O. Ciccarelli, A. J. Thompson, S. M. Smith and P. M. Matthews, "Functional–anatomical validation and individual variation of diffusion tractography-based segmentation of the human thalamus," *Cerebral Cortex,* vol. 15, no. 1, pp. 31-39, 2005.

[75] D. A. Handwerker, J. M. Ollinger and M. D'Esposito, "Variation of BOLD hemodynamic responses across subjects and brain regions and their effects on statistical analyses," *Neuroimage,* vol. 21, no. 4, pp. 1639-51, 2004.

[76] J. Hayes, M. Vanelzakker and L. Shin, "Emotion and cognition interactions in PTSD: a review of neurocognitive and neuroimaging studies," *Frontiers in Integrated Neuroscience,* vol. 6, p. 89, 2012.

[77] J. M. Cisler, J. S. Steele, J. K. Lenow, S. Smitherman, B. Everett, E. Messias and C. D. Kilts, "Functional reorganization of neural networks during repeated exposure to the traumatic memory in posttraumatic stress disorder: an exploratory fMRI study," *Journal of Psychiatric Research,* vol. 48, no. 1, pp. 47-55, 2014.

[78] Pereira.F, Mitchell.T and Botvinick.M, "Machine learning classifiers and fMRI: a tutorial overview," *Neuroimage,* vol. 45, p. S199–S209, 2009.

[79] Yeh.P, Liu.W, Ollinger.J and et.al, "White Matter Microstructural Change and Deep Subcortical Iron Level in Traumatic Brain Injury," in *Proceedings of the Annual Meeting of Organization for Human Brain Mapping*, Honolulu, Hawaii, 2015.

[80] Goodman.J, Leong.K.C and Packard.M.G., "Emotional modulation of multiple memory systems: implications for the neurobiology of post-traumatic stress disorder," *Reviews in the Neurosciences,* vol. 23, no. 5-6, pp. 627-43, 2012.

[81] Packard.M.G, "Anxiety, cognition, and habit: a multiple memory systems perspective," *Brain Research,* vol. 1293, pp. 121-8, 2009.

[82] Schwabe.L, Tegenthoff.M, Höffken.O and Wolf.O.T., "Mineralocorticoid receptor blockade prevents stress-induced modulation of multiple memory systems in the human brain," *Biological Psychiatry,* vol. 74, no. 11, pp. 801-8, 2013.

[83] Boccia.M, D'Amico.S, Bianchini.F and et.al., "Different neural modifications underpin PTSD after different traumatic events: an fMRI meta-analytic study," *Brain Imaging and Behavior,* 2015 (in press).

[84] Ghiglieri.V, Sgobio.C, Costa.C and et.al, "Striatum-hippocampus balance: from physiological behavior to interneuronal pathology," *Progress in Neurobiology,* vol. 94, no. 2, pp. 102-14, 2011.

[85] Favaro.A, Manara.R, Pievani.M and et.al, "Neural signatures of the interaction between the 5-HTTLPR genotype and stressful life events in healthy women," *Psychiatry Research,* vol. 223, no. 2, pp. 157-63, 2014.

[86] A. T. Mattfeld and C. E. Stark, "Striatal and medial temporal lobe functional interactions during visuomotor associative learning," *Cerebral Cortex,* vol. 21, no. 3, pp. 647-58, 2011.

[87] Mattfeld.A.T and Stark.C.E, "Functional contributions and interactions between the human hippocampus and subregions of the striatum during arbitrary associative learning and memory," *Hippocampus,* 2015.

[88] Woo.C.W and Wager.T.D., "Neuroimaging-based biomarker discovery and validation," *Pain,* vol. 156, no. 8, pp. 1379-81, 2015.

[89] M. Kennis, A. R. Rademaker, S. J. van Rooij, R. S. Kahn and E. Geuze, "Resting state functional connectivity of the anterior cingulate cortex in veterans with and without post-traumatic stress disorder," *Human Brain Mapping,* vol. 36, no. 1, pp. 99-109, 2015.

[90] K. Foerde, B. J. Knowlton and R. A. Poldrack, "Modulation of competing memory systems by distraction," *Proceedings of the National Academy of Sciences USA,* vol. 103, pp. 11778-11783, 2006.

[91] L. Schwabe and O. T. Wolf, "Stress modulates the engagement of multiple memory systems in classification learning," *The Journal of Neuroscience,* vol. 32, pp. 11042-11049, 2012.

[92] C. W. Hoge, H. M. Goldberg and C. A. Castro, "Care of war veterans with mild traumatic brain injury: Flawed perspectives," *The New England Journal of Medicine,* vol. 360, no. 16, p. 1588−1591, 2009.

[93] A. N. Simmons and S. C. Matthews, "Neural circuitry of PTSD with or without mild traumatic brain injury: a meta-analysis," *Neuropharmacology,* vol. 62, no. 2, pp. 598-606, 2012.

[94] G. Deshpande and X. Hu, "Investigating effective brain connectivity from fMRI data: past findings and current issues with reference to Granger causality analysis," *Brain Connectivity,* vol. 2, no. 5, pp. 235-45, 2012.

[95] G. Deshpande, K. Sathian and X. Hu, "Assessing and compensating for zero-lag correlation effects in time-lagged Granger causality analysis of FMRI," *IEEE Transactions on Biomedical Engineering,* vol. 57, no. 6, pp. 1446-56, 2010.

[96] G. Kirchgässner, J. Wolters and U. Hassler, Introduction to Modern Time Series Analysis, New York: Springer, 2012.

[97] P. Illari, F. Russo and J. Williamson, Causality in the Sciences, New York: Oxford University Press, 2011.

[98] G. Deshpande, K. Sathian, X. Hu and J. A. Buckhalt, "A rigorous approach for testing the constructionist hypotheses of brain function," *The Behavioral and Brain Sciences,* vol. 35, no. 3, pp. 148-9, 2012.

[99] K. J. Friston, L. Harrison and W. Penny, "Dynamic causal modelling," *Neuroimage,* vol. 19, no. 4, pp. 1273-302, 20013.

[100] A. Roebroeck, E. Formisano and R. Goebel, "Mapping directed influence over the brain using Granger causality and fMRI," *Neuroimage,* vol. 25, no. 1, pp. 230-242, 2005.

[101] G. Lohmann, K. Erfurth, K. Müller and R. Turner, "Critical comments on dynamic causal modelling," *Neuroimage,* vol. 59, no. 3, pp. 2322-9, 2012.

[102] X. Wen, G. Rangarajan and M. Ding, "Is Granger causality a viable technique for analyzing fMRI data?," *PLoS One,* vol. 8, no. 7, p. e67428, 2013.

[103] S. Ryali, K. Supekar, T. Chen and V. Menon, "Multivariate dynamical systems models for estimating causal interactions in fMRI," *Neuroimage,* vol. 54, no. 2, pp. 807-23, 2011.

[104] S. B. Katwal, J. C. Gore, J. C. Gatenby and B. P. Rogers, "Measuring relative timings of brain activities using fMRI," *Neuroimage,* vol. 66, pp. 436-48, 2013.

[105] S. Ryali, Y. Shih, T. Chen, J. Kochalka, D. Albaugh, Z. Fang, K. Supekar, J. Lee and V. Menon, "Combining optogenetic stimulation and fMRI to validate a multivariate dynamical systems model for estimating causal brain interactions," *Neuroimage,* vol. 132, pp. 398-405, 2016.

[106] M. D. Wheelock, K. R. Sreenivasan, K. H. Wood, L. W. Ver Hoef, G. Deshpande and D. C. Knight, "Threat-related learning relies on distinct dorsal prefrontal cortex network connectivity," *Neuroimage,* vol. 102, no. 2, pp. 904-12, 2014.

[107] G. Deshpande, L. E. Libero, K. R. Sreenivasan, H. D. Deshpande and R. K. Kana, "Identification of neural connectivity signatures of autism using machine learning," *Frontiers in Human Neuroscience,* vol. 17, p. 7:670, 2013.

[108] N. L. Hutcheson, K. R. Sreenivasan, G. Deshpande, M. A. Reid, J. Hadley, D. M. White, L. Ver Hoef and A. C. Lahti, "Effective connectivity during episodic memory retrieval in schizophrenia participants before and after antipsychotic medication," *Human Brain Mapping,* vol. 36, no. 4, pp. 1442-57, 2015.

[109] M. Grant, D. White, J. Hadley, N. Hutcheson, R. Shelton, K. Sreenivasan and G. Deshpande, "Early life trauma and directional brain connectivity within major depression," *Human Brain Mapping,* vol. 35, no. 9, pp. 4815-26, 2014.

[110] K. Sathian, G. Deshpande and R. Stilla, "Neural changes with tactile learning reflect decision level reweighting of perceptual readout," *Journal of Neuroscience,* vol. 33, no. 12, pp. 5387-98, 2013.

[111] S. Lacey, R. Stilla, K. Sreenivasan, G. Deshpande and K. Sathian, "Spatial imagery in haptic shape perception," *Neuropsychologia,* vol. 60, pp. 144-158, 2014.

[112] M. Grant, K. Wood, K. Sreenivasan, M. Wheelock, D. White, J. Thomas, D. Knight and G. Deshpande, "Influence of early life stress on intra- and extra-amygdaloid causal connectivity," *Neuropsychopharmacology,* vol. 40, no. 7, pp. 1782-93, 2015.

[113] C. Feng, G. Deshpande, C. Liu, R. Gu, Y.-J. Luo and F. Krueger, "Diffusion of responsibility attenuates altruistic punishment: A functional magnetic resonance imaging effective connectivity study," *Human Brain Mapping,* vol. 37, no. 2, pp. 663-77, 2015.

[114] G. Bellucci, S. Chernyak, M. Hoffman, G. Deshpande, O. Monte, K. Knutson, J. Grafman and F. Krueger, "Effective connectivity of brain regions underlying third party punishment: functional MRI and Granger causality evidence," *Social Neuroscience,* 2016 (in press).

[115] R. Hutchison, T. Womelsdorf, E. Allen, P. Bandettini, V. Calhoun, M. Corbetta, P. S. Della, J. Duyn, G. Glover, J. Gonzalez-Castillo and e. al., "Dynamic functional connectivity: promise, issues, and interpretations.," *Neuroimage,* vol. 80, pp. 360-378, 2013.

[116] H. Jia, X. Hu and G. Deshpande, "Behavioral relevance of the dynamics of the functional brain connectome," *Brain Connectivity,* p. (in press), 2014.

[117] A. Venkataraman, M. Kubicki and P. Golland, "From connectivity models to region labels: identifying foci of a neurological disorder," *IEEE Transactions on Medical Imaging,* vol. 32, no. 11, pp. 2078-98, 2013.

[118] R. Miller, M. Yaesoubi, J. Turner, D. Mathalon, A. Preda, G. Pearlson and e. al., "Higher Dimensional Meta-State Analysis Reveals Reduced Resting fMRI Connectivity Dynamism in Schizophrenia Patients," *PLoS One,* vol. 11, no. 3, p. e0149849, 2016.

[119] D. Garrett, G. Samanez-Larkin, S. MacDonald, U. Lindenberger, A. McIntosh and C. Grady, "Moment-to-moment brain signal variability: a next frontier in human brain mapping?," *Neuroscience and Biobehavioral Reviews,* vol. 37, no. 4, pp. 610-24, 2013.

[120] B. Rashid, M. Arbabshirani, E. Damaraju, M. Cetin, R. Miller, G. Pearlson and V. Calhoun, "Classification of schizophrenia and bipolar patients using static and dynamic resting-state fMRI brain connectivity," *NeuroImage,* vol. 134, pp. 645-657, 2016.

[121] K. H. Greiser, A. Kluttig, B. Schumann, C. A. Swenne, J. A. Kors, O. Kuss, J. Haerting, H. Schmidt, J. Thiery and K. Werdan, "Cardiovascular diseases, risk factors and short-term heart rate variability in an elderly general population: the CARLA study 2002-2006," *European Journal of Epidemiology,* vol. 24, no. 3, pp. 123-42, 2009.

[122] D. Rangaprakash, G. Deshpande, T. Daniel, A. Goodman, J. Katz, N. Salibi, T. Denney and M. Dretsch, "Static and Dynamic Functional Connectivity Impairments in Concussed Soldiers with and without PTSD," *Proceedings of the Annual Meeting of the International Society for Magnetic Resonance in Medicine,* vol. 23, p. 4402, 2015.

[123] J. J. Vasterling, M. Verfaellie and K. D. Sullivan, "Mild traumatic brain injury and posttraumatic stress disorder in returning veterans: Perspectives from cognitive neuroscience," *Clinical Psychology Review,* vol. 29, no. 8, pp. 674-84, 2009.

[124] G. C.W.J., "Investigating causal relations by econometric models and cross-spectral methods," *Econometrica,* vol. 37, pp. 424-438, 1969.

[125] M. Kaminski, M. Ding, W. Truccolo and S. Bressler, "Evaluating causal relations in neural systems: Granger causality, directed transfer function and statistical assessment of significance," *Biological Cybernetics,* vol. 85, pp. 145-157, 2001.

[126] G. Deshpande, P. Santhanam and X. Hu, "Instantaneous and causal connectivity in resting state brain networks derived from functional MRI data," *Neuroimage,* vol. 54, no. 2, pp. 1043-52, 2011.

[127] G. Deshpande, P. Wang, D. Rangaprakash and B. M. Wilamowski, "Fully Connected Cascade Artificial Neural Network Architecture for Attention Deficit Hyperactivity Disorder Classification from Functional Magnetic Resonance Imaging Data," *IEEE Transactions on Cybernetics,* 2015 (in press).

[128] C. Büchel and K. Friston, "Dynamic changes in effective connectivity characterized by variable parameter regression and Kalman filtering.," *Human Brain Mapping,* vol. 6, no. 5-6, pp. 403-408, 1998.

[129] A. Krishnan, L. Williams, A. McIntosh and H. Abdi, "Partial Least Squares (PLS) methods for neuroimaging: a tutorial and review," *Neuroimage,* vol. 56, no. 2, pp. 455-75, 2011.

[130] K. Emmert, R. Kopel, J. Sulzer, A. B. Brühl, B. D. Berman and et al., "Meta-analysis of real-time fMRI neurofeedback studies using individual participant data: How is brain regulation mediated?," *Neuroimage,* vol. 124, no. Pt A, pp. 806-12, 2016.

[131] S. F. White, M. E. Costanzo, J. R. Blair and M. J. Roy, "PTSD symptom severity is associated with increased recruitment of top-down attentional control in a trauma-exposed sample," *Neuroimage Clinical,* vol. 7, pp. 19-27, 2014.

[132] M. T. Berlim and F. Van Den Eynde, "Repetitive transcranial magnetic stimulation over the dorsolateral prefrontal cortex for treating posttraumatic stress disorder: an exploratory meta-analysis of randomized, double-blind and sham-controlled trials," *Canadian Journal of Psychiatry,* vol. 59, no. 9, pp. 487-96, 2014.

[133] J. F. Thayer and R. D. Lane, "A model of neurovisceral integration in emotion regulation and dysregulation," *Journal of Affective Disorders,* vol. 61, no. 3, p. 201–16, 2000.

[134] K. Oishi, A. Faria, J. Hsu, D. Tippett, S. Mori and A. Hillis, "Critical role of the right uncinate fasciculus in emotional empathy," *Annals of Neurology,* vol. 77, no. 1, pp. 68-74, 2015.

[135] K. H. Rosen, Discrete mathematics and its applications, New York: McGraw-Hill, 2012.

[136] G. E. Doucet, R. Rider, N. Taylor, C. Skidmore, A. Sharan, M. Sperling and J. Tracy, "Presurgery resting-state local graph-theory measures predict neurocognitive outcomes after brain surgery in temporal lobe epilepsy," *Epilepsia,* vol. 56, no. 4, pp. 517-26, 2015.

[137] J. S. Crone, A. Soddu, Y. Höller, A. Vanhaudenhuyse, M. Schurz, J. Bergmann, E. Schmid, E. Trinka, S. Laureys and M. Kronbichler, "Altered network properties of the fronto-parietal network and the thalamus in impaired consciousness," *Neuroimage Clinical,* vol. 4, pp. 240-8, 2013.

[138] P. Lin, J. Sun, G. Yu, Y. Wu, Y. Yang, M. Liang and X. Liu, "Global and local brain network reorganization in attention-deficit/hyperactivity disorder," *Brain Imaging and Behavior,* vol. 8, no. 4, pp. 558-69, 2014.

[139] M. A. Rocca, P. Valsasina, A. Meani, A. Falini, G. Comi and M. Filippi, "Impaired functional integration in multiple sclerosis: a graph theory study," *Brain Structure and Function,* p. (in press), Sept 2014.

[140] Q. Yu, J. Sui, K. A. Kiehl, G. Pearlson and V. D. Calhoun, "State-related functional integration and functional segregation brain networks in schizophrenia," *Schizophrenia Research,* vol. 150, no. 2-3, pp. 450-8, 2013.

[141] P. Hellyer, G. Scott, M. Shanahan, D. Sharp and R. Leech, "Cognitive Flexibility through Metastable Neural Dynamics Is Disrupted by Damage to the Structural Connectome," *The Journal of Neuroscience,* vol. 35, no. 24, pp. 9050-63, 2015.

[142] B. Abler, A. Roebroeck, R. Goebel, A. Höse, C. Schönfeldt-Lecuona, G. Hole and H. Walter, "Investigating directed influences between activated brain areas in a motor-response task using fMRI," *Magnetic Resonance Imaging,* vol. 24, no. 2, pp. 181-5, 2006.

[143] G. Deshpande, P. Wang, D. Rangaprakash and B. Wilamowski, "Fully Connected Cascade Artificial Neural Network Architecture for Attention Deficit Hyperactivity Disorder Classification From Functional Magnetic Resonance Imaging Data," *IEEE Transactions on Cybernatics,* vol. 45, no. 12, pp. 2668-79, 2015.

[144] W. L. Thompson, S. D. Slotnick, M. S. Burrage and S. M. Kosslyn, "Two forms of spatial imagery: neuroimaging evidence," *Psychological Science,* vol. 20, no. 10, pp. 1245-53, 2009.

[145] P. A. Carpenter, M. A. Just, T. A. Keller, W. Eddy and K. Thulborn, "Graded functional activation in the visuospatial system with the amount of task demand," *Journal of Cognitive Neuroscience,* vol. 11, no. 1, pp. 9-24, 1999.

[146] G. K. Aguirre, E. Zarahn and M. D'esposito, "The variability of human, BOLD hemodynamic responses," *Neuroimage,* vol. 8, no. 4, pp. 360-9, 1998.

[147] R. A. Poldrack, J. A. Mumford and T. E. Nichols, Handbook of Functional MRI Data Analysis, New York: Cambridge University Press, 2011.

[148] G. Deshpande, K. Sathian and X. Hu, "Effect of hemodynamic variability on Granger causality analysis of fMRI," *Neuroimage,* vol. 52, no. 3, pp. 884-96, 2010.

[149] T. K. Len and J. P. Neary, "Cerebrovascular pathophysiology following mild traumatic brain injury," *Clinical Psychology and Functional Imaging,* vol. 31, no. 2, pp. 85-93, 2011.

[150] S. M. Southwick, S. Paige, C. A. Morgan, J. D. Bremner, J. H. Krystal and D. S. Charney, "Neurotransmitter alterations in PTSD: catecholamines and serotonin," *Seminars in Clinical Neuropsychiatry,* vol. 4, no. 4, pp. 242-8, 1999.

[151] A. R. Mayer, T. Toulouse, S. Klimaj, J. M. Ling, A. Pena and P. S. Bellgowan, "Investigating the properties of the hemodynamic response function after mild traumatic brain injury," *Journal of Neurotrauma,* vol. 31, no. 2, pp. 189-97, 2014.

[152] T. Arichi, G. Fagiolo, M. Varela, A. Melendez-Calderon, A. Allievi, N. Merchant, N. Tusor, S. J. Counsell, E. Burdet, C. F. Beckmann and A. D. Edwards, "Development of BOLD signal hemodynamic responses in the human brain," *Neuroimage,* vol. 63, no. 2, pp. 663-73, 2012.

[153] S. K. Thompson, S. A. Engel and C. A. Olman, "Larger neural responses produce BOLD signals that begin earlier in time," *Frontiers in Neuroscience,* p. 8:159, 2014.

[154] K. Mifflin, C. Benson, B. Kerr, F. Aricioglu, M. Cetin, S. Dursun and G. Baker, "Involvement of Neuroactive Steroids in Pain, Depression and Anxiety," *Modern Trends in Pharmacopsychiatry,* vol. 30, pp. 94-102, 2015.

[155] G. Buzsáki, K. Kaila and M. Raichle, "Inhibition and brain work," *Neuron,* vol. 56, no. 5, pp. 771-83, 2007.

[156] G. G. Brown, L. T. Eyler Zorrilla, B. Georgy, S. S. Kindermann, E. C. Wong and R. B. Buxton, "BOLD and perfusion response to finger-thumb apposition after acetazolamide administration:

differential relationship to global perfusion," *Journal of Cerebral Blood Flow and Metabolism,* vol. 23, no. 7, pp. 829-37, 2003.

[157] D. W. Busija, F. Bari, F. Domoki and T. Louis, "Mechanisms involved in the cerebrovascular dilator effects of N-methyl-d-aspartate in cerebral cortex," *Brain Research Reviews,* vol. 56, no. 1, p. 89–100, 2007.

[158] S. D. Muthukumaraswamy, C. J. Evans, R. A. Edden, R. G. Wise and K. D. Singh, "Individual variability in the shape and amplitude of the BOLD-HRF correlates with endogenous GABAergic inhibition," *Human Brain Mapping,* vol. 33, no. 2, pp. 455-65, 2012.

[159] B. H. Cohen, "The Neural Substrate of the Subjective Experience of Anxiety," in *The Annual Meeting of the Social and Affective Neuroscience Society*, October 2009.

[160] S. Nikolaus, C. Antke, M. Beu and H. W. Müller, "Cortical GABA, striatal dopamine and midbrain serotonin as the key players in compulsive and anxiety disorders--results from in vivo imaging studies," *Reviews in the Neurosciences,* vol. 21, no. 2, pp. 119-39, 2010.

[161] Z. Cohen, G. Bonvento, P. Lacombe and E. Hamel, "Serotonin in the regulation of brain microcirculation," *Progress in Neurobiology,* vol. 50, no. 4, pp. 335-62, 1996.

[162] A. E. Ramage, B. T. Litz, P. A. Resick, M. D. Woolsey, K. A. Dondanville and e. al., "Regional cerebral glucose metabolism differentiates danger- and non-danger-based traumas in post-traumatic stress disorder," *Social Cognitive and Affective Neuroscience,* p. in press, Sept 2015.

[163] I. M. Rosso, M. R. Weiner, D. J. Crowley, M. M. Silveri, S. L. Rauch and J. E. Jensen, "Insula and anterior cingulate GABA levels in posttraumatic stress disorder: preliminary findings using magnetic resonance spectroscopy," *Depression and Anxiety,* vol. 31, no. 2, pp. 115-23, 2014.

[164] M. E. Costanzo, Y. Y. Chou, S. Leaman, D. L. Pham, D. Keyser, D. E. Nathan, M. Coughlin, P. Rapp and M. J. Roy, "Connecting combat-related mild traumatic brain injury with posttraumatic stress disorder symptoms through brain imaging," *Neuroscience Letters,* vol. 577, pp. 11-15, 2014.

[165] O. David, I. Guillemain, S. Saillet, S. Reyt, C. Deransart, C. Segebarth and A. Depaulis, "Identifying neural drivers with functional MRI: an electrophysiological validation," *PLoS Biology,* vol. 23, no. 6, pp. 2683-97, 2008.

[166] M. Havlicek, K. J. Friston, J. Jan, M. Brazdil and V. D. Calhoun, "Dynamic modeling of neuronal responses in fMRI using cubature Kalman filtering," *Neuroimage,* vol. 56, no. 4, pp. 2109-28, 2011.

[167] K. R. Sreenivasan, M. Havlicek and G. Deshpande, "Nonparametric hemodynamic deconvolution of FMRI using homomorphic filtering," *IEEE Transactions on Medical Imaging,* vol. 34, no. 5, pp. 1155-63, 2015.

[168] A. Zilverstand, M. Parvaz and R. Goldstein, "Neuroimaging cognitive reappraisal in clinical populations to define neural targets for enhancing emotion regulation. A systematic review," *Neuroimage,* p. (in press), 2016 June 7.

[169] M. Goodkind, S. Eickhoff, D. Oathes, Y. Jiang, A. Chang, L. Jones-Hagata and e. al., "Identification of a common neurobiological substrate for mental illness," *JAMA Psychiatry,* vol. 72, no. 4, pp. 305-15, 2015.

[170] J. Radua, M. Phillips, T. Russell, N. Lawrence, N. Marshall, S. Kalidindi and e. al., "Neural response to specific components of fearful faces in healthy and schizophrenic adults," *Neuroimage,* vol. 49, no. 1, pp. 939-46, 2010.

[171] D. Rangaprakash, G. Deshpande, A. Venkataraman, J. Katz, T. Denney and M. Dretsch, "Identifying Foci of Brain Disorders from Effective Connectivity Networks," *Proceedings of the Annual Meeting of the International Society for Magnetic Resonance in Medicine,* vol. 24, p. 3740, 2016.

A1. Inter-Group HRF Differences

We presented the group differences in HRF parameters in the Chapter 6 (Figs 6.2 through 6.6). Here we provide further details on those results (Tables A1 through A5).

Table A1. *Significantly altered response height (RH) in hemodynamic response function, HRF, which were significant for PTSD > Control and PCS+PTSD > Control comparisons. Thalamus, midbrain, insula, visual and default-mode network regions were altered. Table corresponds to Fig.6.2 in Chapter 6.*

Cluster no.	No. of Voxels	Peak MNI Coordinates			AAL Region Name	T-statistic
1	405	-6	-8	14	Thalamus_L	5.70
2	373	-4	-32	-12	Midbrain	5.91
3	129	4	-60	12	Calcarine_R	5.53
4	158	-40	-12	-12	Temporal_Sup_L	4.32
5	113	-2	-52	28	Cingulum_Post_L	5.29
6	96	40	20	-12	Insula_R	4.21
7	84	2	-68	22	Precuneus_R	5.33

Table A2. *Significantly altered time-to-peak in HRF. They were significant for Control > PTSD and Control > PCS+PTSD comparisons. Visual and default-mode network regions were altered. Table corresponds to Fig.6.3 in Chapter 6.*

Cluster no.	No. of Voxels	Peak MNI Coordinates			AAL Region Name	T-statistic
1	180	2	-60	22	Precuneus_R	6.03
2	124	-10	-74	10	Calcarine_L	5.55
3	113	-2	-62	18	PCC_L	6.09
4	51	18	-70	12	Calcarine_R	3.26
5	34	-2	56	26	Frontal_Sup_Medial_R	3.38

Table A3. *Significantly altered full-width at half-max (FWHM) in HRF, which were significant for Control > PTSD and Control > PCS+PTSD comparisons. Visual and default-mode network regions were altered. Table corresponds to Fig.6.4 in Chapter 6.*

Cluster no.	No. of Voxels	Peak MNI Coordinates			AAL Region Name	T-statistic
1	180	-4	-60	20	PCC_L	5.94
2	174	-10	-74	10	Calcarine_L	4.71
3	118	2	-60	22	Precuneus_R	5.88
4	90	16	-76	12	Calcarine_R	3.33
5	39	56	-60	20	Temporal_Mid_R	3.80

Table A4. *Significant alterations in all three HRF parameters, which were significant for Control > PTSD and Control > PCS+PTSD comparisons. Table corresponds to Fig.6.5 in Chapter 6.*

Cluster no.	No. of Voxels	Peak MNI Coordinates			AAL Region Name
1	34	-2	-64	26	PCC_L
2	34	2	-66	30	Precuneus_R

Table A5. *Significant differences between all three groups, which represent alterations caused in both PTSD and mTBI. This difference was observed only with FWHM. Table corresponds to Fig.6.6 in Chapter 6.*

Cluster no.	No. of Voxels	Peak MNI Coordinates			AAL Region Name
1	34	-2	-62	26	PCC_L
2	34	2	-65	30	Precuneus_R

A2. Seed-Based Functional Connectivity Analysis

We presented the functional connectivity maps obtained with the L_PCC seed in the Chapter 6 (Figs 6.7 through 6.10). Here we provide further details on those results (Tables A6 through A9).

Table A6. *Brain regions whose functional connectivity with the left posterior cingulate (**L_PCC**) seed ROI was significantly different between the groups for data **without hemodynamic deconvolution.** Table corresponds to Fig.6.7 in Chapter 6.*

Cluster no.	No. of Voxels	Peak MNI Coordinates			AAL Region Name	T-statistic
1	4831	30	-72	-42	Cerebelum_Crus2_R	6.79
2	4798	12	-64	36	Precuneus_R	6.98
3	1209	-40	-48	-24	Fusiform_L	5.97
4	760	-26	48	-4	Frontal_Mid_L	5.45

Table A7. *Brain regions whose functional connectivity with the left posterior cingulate (**L_PCC**) seed ROI was significantly different between the groups for data **with hemodynamic deconvolution.** Table corresponds to Fig.6.8 in Chapter 6.*

Cluster no.	No. of Voxels	Peak MNI Coordinates			AAL Region Name	T-statistic
1	1347	4	-62	34	Precuneus_R	4.78
2	790	-12	22	-10	Caudate_L	4.87
3	671	-14	72	-4	Frontal_Sup_L	5.87
4	637	-46	-54	-24	Temporal_Inf_L	4.41
5	586	-32	-54	48	Parietal_Inf_L	4.71
6	582	44	46	28	Frontal_Mid_R	6.31
7	526	-16	-14	-26	Parahippocampal_L	4.82

Table A8. *Functional connectivity group differences which were greater (i.e. higher T-value) in data without deconvolution as compared to that with deconvolution performed (**pseudo-positives**) (for the left posterior cingulate [**L_PCC**] seed ROI). Table corresponds to Fig.6.9 in Chapter 6.*

Cluster no.	No. of Voxels	Peak MNI Coordinates			AAL Region Name	T-statistic
1	4456	30	-72	-42	Cerebelum_Crus2_R	6.52
2	3886	-14	-54	20	Precuneus_L	6.33
3	939	-44	-46	-30	Fusiform_L	4.39
4	399	-24	48	-4	Frontal_Mid_L	3.20

Table A9. *Functional connectivity group differences which were smaller (i.e. lower T-value) in data without deconvolution as compared to that with deconvolution performed (**pseudo-negatives**) (for the left posterior cingulate [**L_PCC**] seed ROI). Table corresponds to Fig.6.10 in Chapter 6.*

Cluster no.	No. of Voxels	Peak MNI Coordinates			AAL Region Name	T-statistic
1	666	-12	22	-10	Caudate_L	4.29
2	582	44	46	28	Frontal_Mid_R	6.31
3	183	-14	72	-4	Frontal_Sup_L	5.52
4	163	-14	-8	-26	Parahippocampal_L	4.46
5	124	-32	46	-6	Frontal_Mid_Orb_L	3.67

Results for the PCC ROI were presented in the Chapter 6. Here we present results for the right precuneus ROI (Figs A1 through A4 and Tables A10 through A13). As with the PCC ROI, we observe that significant alterations in PTSD and mTBI differ appreciably between the two analysis pipelines. Also we noticed more number of pseudo-positives than pseudo-negatives, as in the PCC ROI case. These results lead to the same conclusion reached with the PCC ROI.
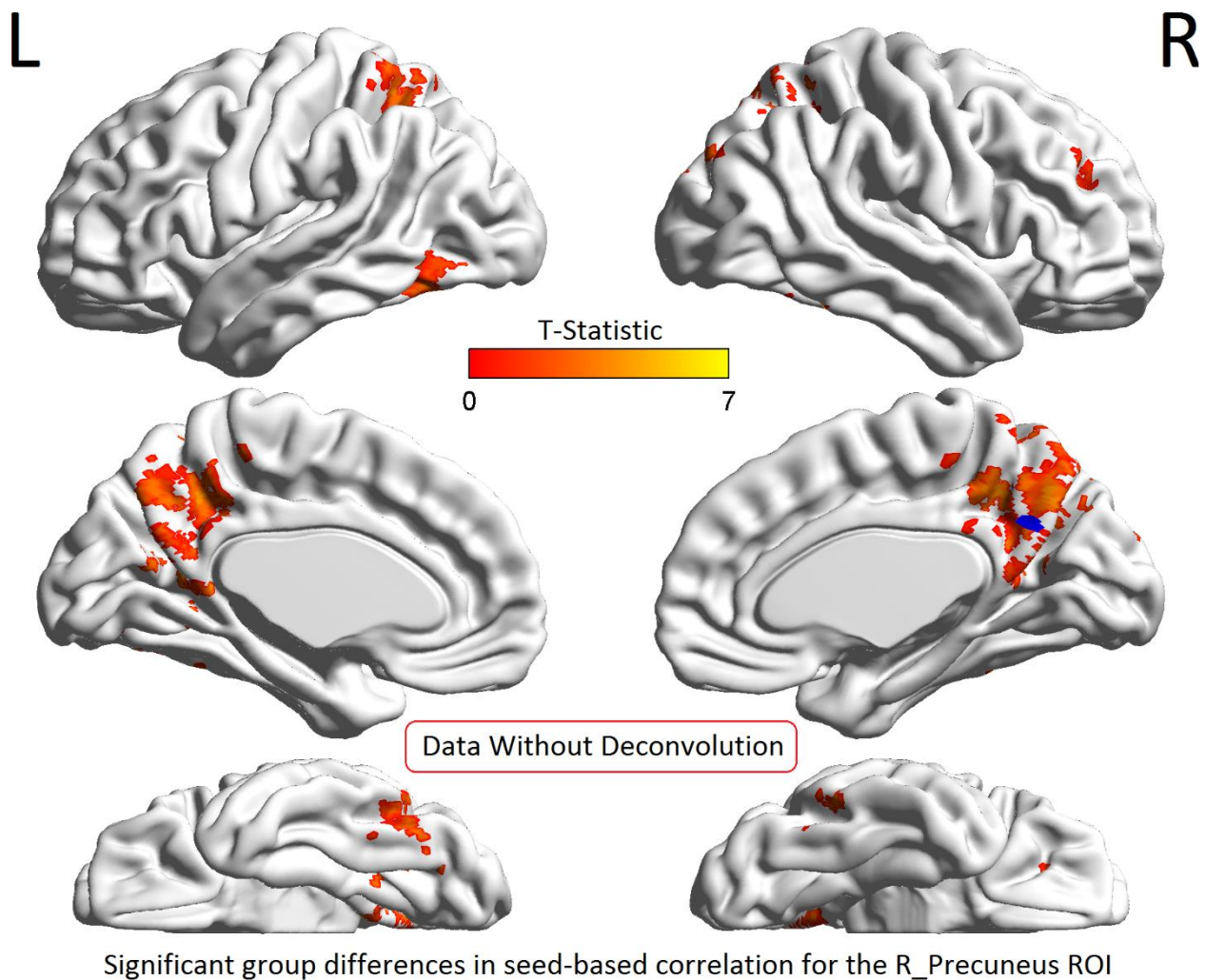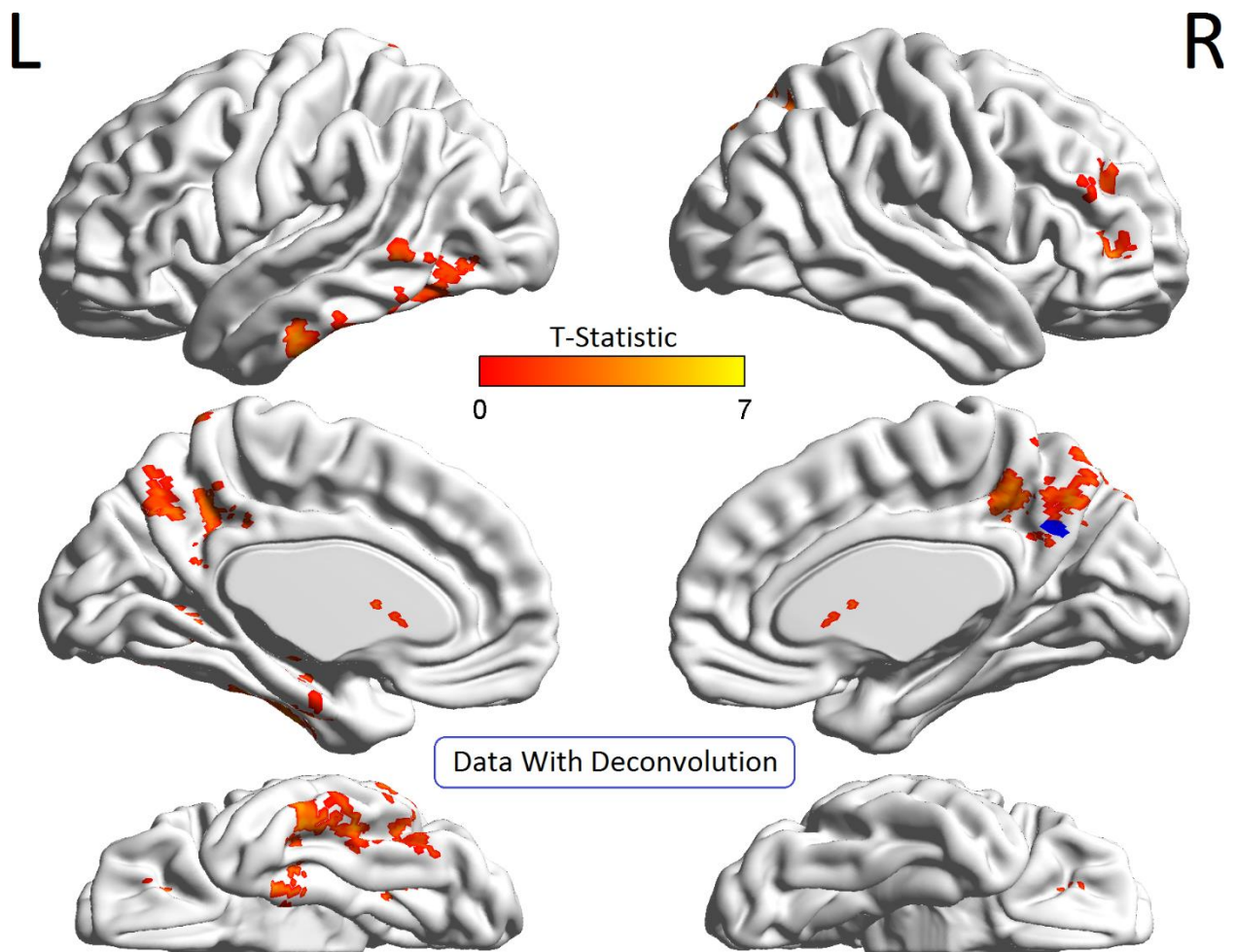

Significant group differences in seed-based correlation for the R_Precuneus ROI

Fig.A1. *Brain regions whose functional connectivity with the right Precuneus (R_Prec) seed ROI (marked blue region) was significantly different between the groups for data **without** hemodynamic deconvolution.*

Significant group differences in seed-based correlation for the R_Precuneus ROI
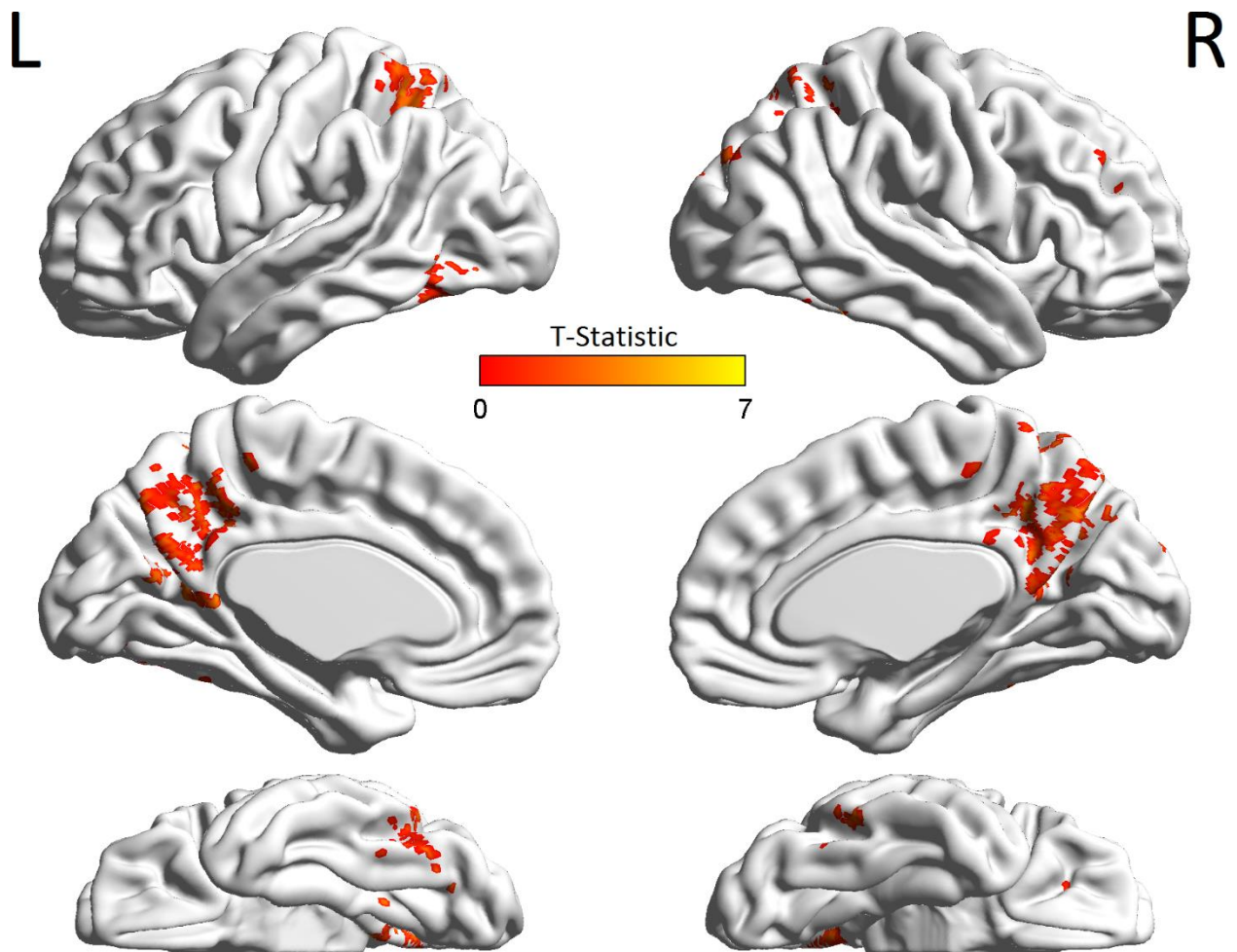
Fig.A2. *Brain regions whose functional connectivity with the right Precuneus (R_Prec) seed ROI (marked blue region) was significantly different between the groups for data **with** hemodynamic deconvolution.*
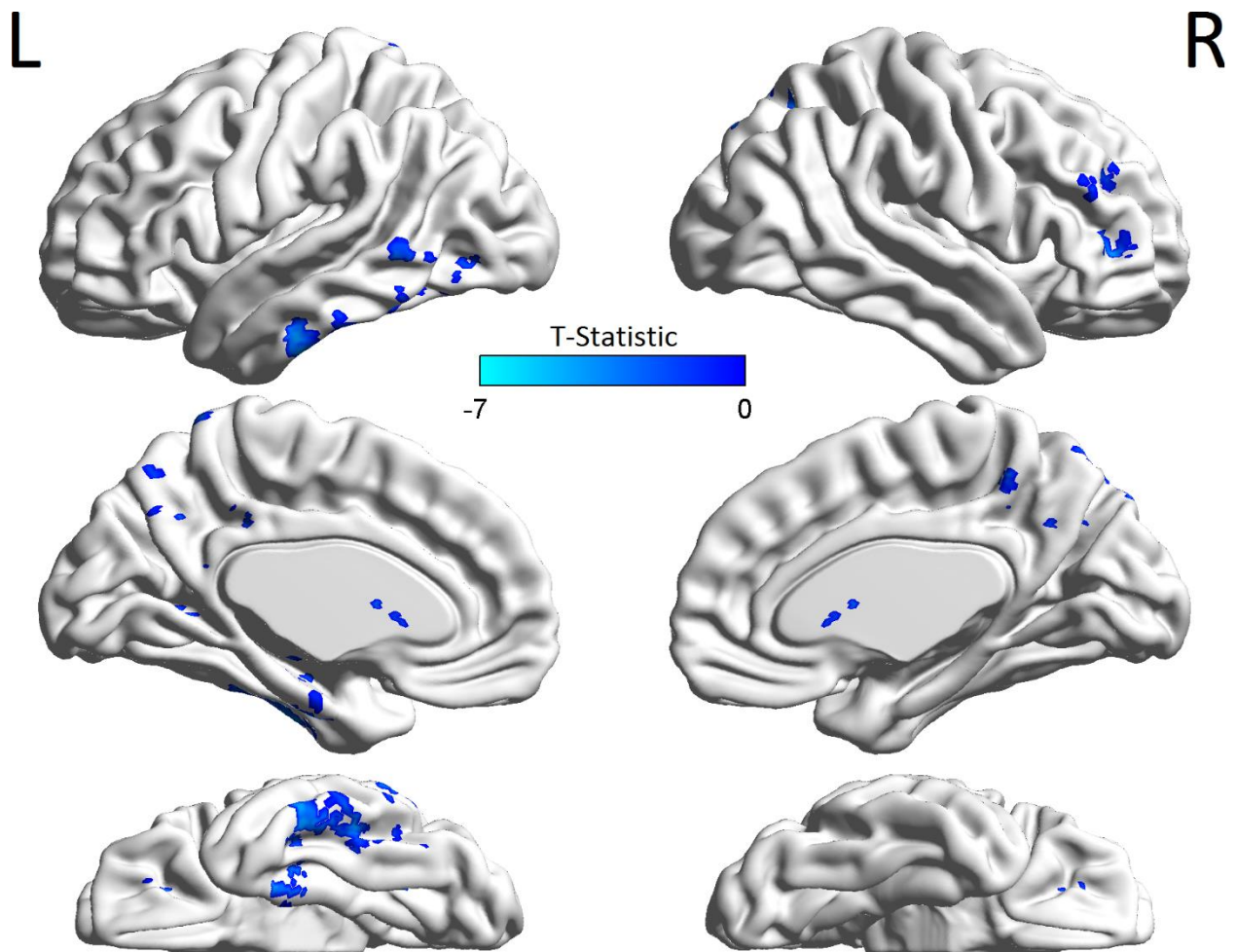
R_Precuneus ROI T-Statistic Map: Without Deconvolution > With Deconvolution

Fig.A3. *Pseudo-positives, that is, functional connectivity group differences which were greater (higher T-value) in data without deconvolution as compared to that with deconvolution performed (for the right precuneus [R_Prec] seed ROI)*

R_Precuneus ROI T-Statistic Map: With Deconvolution > Without Deconvolution

Fig.A4. *Pseudo-negatives, that is, functional connectivity group differences which were smaller (lower T-value) in data without deconvolution as compared to that with deconvolution performed (for the right precuneus [R_Prec] seed ROI)*

Table A10. *Brain regions whose functional connectivity with the right precuneus (**R_Prec**) seed ROI was significantly different between the groups for data **without hemodynamic deconvolution.** Table corresponds to Fig.A1.*

Cluster no.	No. of Voxels	Peak MNI Coordinates			AAL Region Name	T-statistic
1	3236	-12	-44	-10	Lingual_L	5.55
2	1015	40	-56	-48	Cerebelum_7b_R	5.66
3	849	22	34	16	Frontal_Mid_R	5.93
4	711	-46	-50	-26	Temporal_Inf_L	4.80
5	595	-36	-54	58	Parietal_Sup_L	4.78

Table A11. *Brain regions whose functional connectivity with the right precuneus (**R_Prec**) seed ROI was significantly different between the groups for data **with hemodynamic deconvolution.** Table corresponds to Fig.A2.*

Cluster no.	No. of Voxels	Peak MNI Coordinates			AAL Region Name	T-statistic
1	1813	34	44	2	Frontal_Mid_R	5.70
2	1364	8	-40	42	Cingulum_Mid_R	5.02
3	890	-16	-14	-26	Parahippocampal_L	5.05
4	599	26	-78	-40	Cerebelum_Crus2_R	5.47
5	583	-42	-48	-26	Fusiform_L	4.79
6	576	-58	-62	-16	Temporal_Inf_L	4.63

Table A12. *Functional connectivity group differences which were greater (i.e. higher T-value) in data without deconvolution as compared to that with deconvolution performed (**pseudo-positives**) (for the right precuneus [**R_Prec**] seed ROI). Table corresponds to Fig.A3.*

Cluster no.	No. of Voxels	Peak MNI Coordinates			AAL Region Name	T-statistic
1	2415	-10	-44	-10	Lingual_L	5.18
2	785	42	-56	-50	Cerebelum_7b_R	4.31
3	595	-36	-54	58	Parietal_Sup_L	4.78
4	350	22	36	16	Frontal_Mid_R	4.52
5	300	-46	-48	-30	Temporal_Inf_L	4.26

Table A13. *Functional connectivity group differences which were smaller (i.e. lower T-value) in data without deconvolution as compared to that with deconvolution performed (**pseudo-negatives**) (for the right precuneus [**R_Prec**] seed ROI). Table corresponds to Fig.A4.*

Cluster no.	No. of Voxels	Peak MNI Coordinates			AAL Region Name	T-statistic
1	267	36	56	20	Frontal_Mid_R	3.84
2	827	-12	24	-6	Caudate_L	4.85
3	890	-16	-14	-26	Parahippocampal_L	4.47
4	103	26	-78	-40	Cerebelum_Crus2_R	4.52
5	348	-50	-20	-22	Fusiform_L	4.29
6	175	-58	-62	-16	Temporal_Inf_L	3.81
7	215	-8	-52	74	Precuneus_L	4.73